



Peloutier, Vincent (1998) *Flume study of the deposition of fine sediment into river gravel*. PhD thesis.

<http://theses.gla.ac.uk/8485/>

Copyright and moral rights for this thesis are retained by the author

A copy can be downloaded for personal non-commercial research or study, without prior permission or charge

This thesis cannot be reproduced or quoted extensively from without first obtaining permission in writing from the Author

The content must not be changed in any way or sold commercially in any format or medium without the formal permission of the Author

When referring to this work, full bibliographic details including the author, title, awarding institution and date of the thesis must be given

# **Flume study of the deposition of fine sediment into river gravel**

A thesis submitted in partial fulfilment of the  
requirements for the degree of Doctor of Philosophy

Vincent Peloutier

Department of Civil Engineering, University of Glasgow  
October 1998

# Abstract

Increased land erosion and drainage, combined with larger impoundments for water consumption needs, result in increased levels of sediments infiltrating into gravel river beds. This can cause a threat to the ecology of rivers and to fish populations. However, the mechanisms by which transported fine sediments deposit, i.e. pass through the surface layer of gravel before infiltrating into the bed pores, are poorly researched. Several investigators have highlighted the needs for further explorations in that field, as it also has direct implications in phenomena such as flood hydraulics sediment transport, armouring and downstream fining.

Previous studies have indicated that deposition rates are proportional to sediment concentrations and fall velocities in still water. A preliminary series of experiments was conducted in an 8m-long flume to compare deposition rates of sand through single layers of gravel to transport rates measured 25mm above the bed surface. It was found that the deposition rates  $\Delta$  are proportional to the near-bed concentration of fine particles  $C_b$ . The constant of proportionality has the dimension of a velocity, and represents an average fall velocity through the bed surface layer, or deposition velocity  $w_d$ . The ratio between the deposition velocity  $w_d$  and the fall velocity in still water  $w_s$ , referred to as the dimensionless deposition velocity  $w_d^*$ , gives an indication of the effects of the gravel bed surface on the settling behaviour of the sediment particles.

Following the preliminary series of experiments, the main series of experiments was aimed at measuring deposition velocities in different hydraulic and sediment conditions to study the physical mechanisms controlling the deposition process. It was found that the deposition velocity generally increases with grain size, but tends to stabilise in the upper size range (i.e. particles transported by saltation). Deposition velocities tend to decrease as bed shear stress and turbulence level increase, particularly in the case of medium-size sand ( $\sim 300\text{-}350\mu\text{m}$ ). Gravel size does not appear to have a significant influence on the deposition velocity of particles coarser than  $\sim 200\mu\text{m}$ .

The deposition velocity results of experiments using medium-size sand were, in general, larger than the fall velocity  $w_s$  for particles finer than  $\sim 200\mu\text{m}$  in diameter, indicating a phenomenon of enhanced deposition. This phenomenon has already been

observed in previous studies (e.g. Jobson and Sayre, 1970). It was not detected in experiments using very fine sand, but the deposition velocity results in this case followed similar variations with grain size to that observed with medium sand.

The experimental results suggested a distinction between three ranges of fine sediment: (1) the Stokes' range includes very fine particles, the diffusion coefficient of which is nearly equal to that of the fluid. The depositional behaviour of these particles is directly influenced by the structure of near-bed turbulence. A bursting-based analysis showed that the so-called deposition parameter  $w_d^+ = w_d u^* / (g d)$  is in this case related to near-bed turbulence and bed roughness parameters, but not to the grain size; (2) the intermediate range, which is influenced by both turbulence and gravity. A dimensional analysis indicated that, under these circumstances,  $w_d^+$  increases with grain size; and (3) the upper range, which corresponds to the range of particles transported by saltation. Deposition is, in this case, mainly influenced by the landing angle of the fine particles and the bed surface topography.

The experiments also indicated that the deposition process is influenced by turbulence damping, a phenomenon which consists in the reduction of the eddy diffusivity of the fluid by increasing sediment transport concentration and grain size. This phenomenon can be described using van Rijn's  $\phi$  coefficient. It was observed that the deposition velocity  $w_d$  tends to increase with increasing turbulence damping.

The experimental results were applied to model downstream sorting of fine particles in gravel-bed rivers in 2-D uniform flow conditions. Methods of computation and examples of applications are described.

# Acknowledgements

I would like to express my sincere thanks to all those who assisted me during these three years, including:

**Dr J. Graham Herbertson** and **Dr. Trevor B. Hoey**, my supervisors, for their help and advice throughout the course of this work.

**Prof. D. Alan Ervine** and **Dr. Gary Pender** for their suggestions on some of the experimental aspects of the project.

**Prof. Nenad Bicanic** for his encouragement in computational modelling.

**Prof. Raoul Caruba** of the IRIM, University of Nice-Sophia Antipolis and **Dr. Edward Evans** of Halcrow Ltd, for allowing me to use some of their facilities to complete the writing of the thesis.

**Willy Henderson** and **Tim Montgomery**, the laboratory technicians, for their many hours of laborious work and discussions about Scottish football.

**Alan Cuthbertson** and **Okko Heinrich** for their useful cooperation on a particle-tracking flume study.

**Breac McLeod**, **Andy McAuley**, and **Chris Fuller**, for their advice and suggestions, particularly on some experimental aspects of the study.

**Ken McCall** for sorting the IT problems.

**Dan Lee** and **Vijay Kumar** for our invaluable discussions at 76 Oakfield Avenue.

**Marc Buisson** for our memorable conversations at the **Research Club**, which I must also thank for providing ‘bottomless’ coffee mugs, the malt of the month and ‘Le Monde’.

“...a pool of the river suddenly boiled up in my face in a little fountain.  
It was in a very dreary, marshy part among dilapidated trees that you see  
through holes in the trunk of;  
and if any kind of beast or elf or devil had come out of that sudden silver ebullition  
I declare I do not think I should have been surprised.  
It was perhaps a thing as curious – a fish, with which  
these head waters of the stream are alive.”

Robert Louis Stevenson, Letter to Sydney Colvin, Dec. 1891.

# Table of contents

Abstract.....	ii
Acknowledgements.....	iv
Quotation.....	v
Table of contents.....	vi
List of Figures.....	ix
List of Tables.....	xii
Notations.....	xiii

## Chapter I: Introduction

1.1 General remarks.....	1
1.2 Origin and implications of the matrix infiltration problem .....	4
1.2.1 Sources of fine sediment.....	4
1.2.2 Implications of matrix accumulation for fisheries .....	5
1.2.3 Other implications.....	6
1.3 Basis of the study.....	7
1.4 Summary of the main points/Aims of the study .....	9

## Chapter II: Literature review

2.1 Sedimentation niches .....	11
2.1.1 In-bank settling .....	11
2.1.2 Over-bank sedimentation .....	14
2.1.3 Summary and conclusion.....	14
2.2 Fine sediment deposition .....	14
2.2.1 Physical parameters.....	14
2.2.1.1 Introduction.....	14
2.2.1.2 Relative grain size distributions.....	15
2.2.1.3 Gravity .....	17
2.2.1.4 Near-bed turbulence.....	18
2.2.1.5 Summary and conclusion.....	22
2.2.2 Relative influence of gravity and turbulence .....	23
2.2.2.1 Introduction.....	23
2.2.2.2 Deposition dominated by gravity.....	23
2.2.2.3 Deposition influenced by both gravity and turbulence .....	24
2.2.2.3.a Probability of deposition .....	24
2.2.2.3.b Influence of diffusion.....	26
2.2.2.3.c Spatial deposition .....	28
2.2.2.4 Deposition dominated by turbulence .....	29
2.2.3 Hydraulics, sediment transport and deposition .....	30
2.2.3.1 Transport mode and size selectivity.....	30
2.2.3.2 Hydraulic controls.....	31
2.2.4 Summary .....	32
2.3 Fine sediment infiltration and re-suspension .....	33
2.3.1 Introduction.....	33
2.3.2 Infiltration patterns.....	34
2.3.2.1 General remarks .....	34
2.3.2.2 Siltation .....	34
2.3.2.3 Clogging.....	35

2.3.3 Influence of interstitial flow on deposition and infiltration .....	36
2.3.4 Influence of high flow events.....	37
2.3.5 Summary and conclusion .....	38
2.4 Summary of the main points / Extended aims .....	39

**Chapter III: Preliminary experiments**

3.1 Introduction.....	41
3.2 Preliminary experiments on infiltration .....	41
3.2.1 Introduction.....	41
3.2.2 Experimental observations of infiltration processes .....	45
3.2.2.1 Introduction.....	45
3.2.2.2 Infiltration of LB-775 .....	45
3.2.2.3 Infiltration of LA-260 .....	47
3.2.3 Infiltration within pools .....	49
3.2.3.1 Spatial deposition patterns .....	49
3.2.3.2 Influence of interstitial flows .....	50
3.2.4 Conclusion .....	51
3.3 Preliminary experiments on deposition .....	52
3.3.1 Background.....	52
3.3.2 Materials and method.....	54
3.3.2.1 Flume channel set-up .....	54
3.3.2.2 Sediment feeder .....	56
3.3.2.3 Sand separator.....	57
3.3.2.4 Experimental method .....	59
3.3.3 Results.....	61
3.4 Conclusion .....	67

**Chapter IV: Main series of experiments**

4.1 Introduction.....	69
4.2 Background.....	69
4.3 Material and methods.....	71
4.3.1 Sediment .....	71
4.3.2 Flow measurements.....	73
4.3.2.1 ADV probe.....	73
4.3.2.2 Shear velocity calculation methods.....	75
4.3.3 Experimental set-up .....	79
4.3.4 Range of data in the experiments .....	82
4.4 Results.....	83
4.4.1 Velocity measurements.....	84
4.4.2 Near-bed concentrations and deposition rates.....	85
4.4.3 Median size of near-bed and deposited fine sediment .....	88
4.4.4 Deposition velocity results.....	91
4.4.5 Dimensionless deposition velocity results .....	93
4.5 Conclusion .....	100

**Chapter V: Analysis**

5.1 Introduction.....	102
5.2 Dimensional analysis .....	103
5.2.1 Theory.....	103
5.2.2 Application .....	105
5.3 Deposition of suspended load .....	107
5.3.1 Suspension criterion.....	107

5.3.2 Physical model .....	108
5.4 Deposition of saltating load .....	111
5.4.1 Description .....	111
5.4.2 Theoretical model .....	112
5.5 Influence of turbulence damping .....	116
5.6 Conclusion .....	120

**Chapter VI: Application: downstream deposition rates**

6.1 Introduction.....	122
6.2 Deposition from a point source.....	123
6.2.1 Theoretical analysis.....	123
6.2.2 Application: computation of the coefficients ( $r_i$ ) .....	127
6.3 Case of a continuous source.....	131
6.3.1 Uniform source .....	131
6.3.1.1 Concentration equation .....	132
6.3.1.2 Example of application .....	136
6.3.2 Non-uniform sources in uniform flow .....	139
6.3.2.1 Method .....	139
6.3.2.2 Example of application .....	139
6.3.3 Real-life applications and model sensitivity .....	142
6.3.3.1 Example 1 .....	142
6.3.3.2 Example 2 .....	143
6.4 Conclusion .....	144

**Chapter VII: Conclusion**

7.1 Summary of the main points.....	146
7.2 Discussion .....	149

<b>References</b> .....	155
-------------------------	-----

**Appendices**

Appendix 1.....	166
Appendix 3.1.....	167
Appendix 3.2.....	171
Appendix 3.3.....	173
Appendix 3.4.....	176
Appendix 4.1.....	179
Appendix 4.2.....	184
Appendix 4.3.....	190
Appendix 4.4.....	192
Appendix 4.5.....	194
Appendix 4.6.....	195
Appendix 4.7.....	197
Appendix 5.1.....	219
Appendix 5.2.....	221
Appendix 6.....	222

# List of Figures

FIGURE 1.1: typical arrangements of fluvial gravels .....	2
FIGURE 1.2: ten-week old salmon alevin .....	6
FIGURE 1.3: four-stage cycle followed by fine sediment transported in gravel-bed rivers .....	8
FIGURE 2.1: sand deposit at the downstream end of a gravel bar .....	12
FIGURE 2.2: main areas of fine sediment deposition in gravel-bed rivers .....	12
FIGURE 2.3: tightly-packed and loosely-packed bed configurations. ....	15
FIGURE 2.4: fall velocities computed from Stokes' law and Cheng's formula .....	17
FIGURE 2.5: schematic model of typical hairpin-shape vortex configurations.....	19
FIGURE 2.6: spatial structure of turbulent shear flows.....	19
FIGURE 2.7: sequences of a burst cycle .....	20
FIGURE 2.8: sequence of images of particle/shear layer interaction.....	21
FIGURE 3.1: Armfield C4 tilting flume.....	42
FIGURE 3.2: experimental set-up and sand deposition areas in the C4 flume .....	42
FIGURE 3.3: grading curves of sand and gravel used in the experiments on infiltration.....	43
FIGURE 3.4: deposition of LB-775 coarse sand into EN-20 gravel (Experiment PE1) .....	46
FIGURE 3.5: infiltration of LA-260 into EN-20 gravel (Experiment PE2) .....	47
FIGURE 3.6: infiltration of LA-260 into EN-13 gravel (Experiment PE5).....	48
FIGURE 3.7: fine sediment deposition and flow patterns in pools .....	50
FIGURE 3.8: main flume set-up for funnel-trap experiments .....	55
FIGURE 3.9: funnel-shaped trap .....	56
FIGURE 3.10: fine sediment feeder .....	57
FIGURE 3.11: sand separator .....	58
FIGURE 3.12a: example of plot of the average deposition rate $\langle \Delta_0 \rangle$ against initial sediment concentration $C_0$ (Experiment B1).....	63
FIGURE 3.12b: example of the variations of the suspended solid monitor readings against time (Experiment B1) .....	63
FIGURE 3.12c: example of the calibration of the suspended solids monitor readings (Experiment B1).....	64
FIGURE 3.12d: example of plot of the instantaneous deposition rate against the estimated near-bed sediment concentration $C_b$ (Experiment B1).....	64
FIGURE 3.13: deposition velocity measured in the funnel-shaped trap $w_d$ against the median size of the bed surface gravel .....	65
FIGURE 3.14: deposition velocity measured in the funnel-shaped trap $w_d$ against shear velocity $u^*$ .....	65
FIGURE 3.15: spatial distribution of the deposition rates for three experiments of the preliminary series .....	67
FIGURE 4.1: flume set-up for the main series of experiments .....	70
FIGURE 4.2: sand and gravel grading curves .....	72
FIGURE 4.3a: ADV probe and support mechanism .....	73

FIGURE 4.3b: detail of the velocity measurement system of the ADV probe.....	74
FIGURE 4.4: near-bed sediment sampling procedure.....	80
FIGURE 4.5: transverse velocity profile .....	81
FIGURE 4.6: deposition rate measured for Experiment E5 and average deposition rate over all the experiments of the main series (except E6) against distance downstream from source.....	85
FIGURE 4.7: plot of the estimated decay rate $a$ of the deposition rate $\Delta$ (computed as $a = -\ln(\Delta_7/\Delta_{3.1})/\ln(2.62/0.9)$ ) against shear velocity $u^*$ for all experiments with LA-260 (except E6) .....	86
FIGURE 4.8: near-bed sediment concentration measured during Experiment E5 and average near-bed concentration for all experiments of the main series (except E6) against distance downstream from source .....	86
FIGURE 4.9a: variations of the near-bed fine sediment composition along the six sediment traps for experiment G3 .....	87
FIGURE 4.9b: variations of the deposited sediment composition along the six sediment traps for experiment G3 .....	87
FIGURE 4.10: average medium size $\langle d_{50} \rangle$ of both deposited and near-bed sediment against longitudinal distance.....	88
FIGURE 4.11: influence of $u^*$ on the difference in mean size between deposited and transported sediment (LA-260) .....	90
FIGURE 4.12: comparison between the average deposition velocity $\langle w_d \rangle$ and Cheng's fall velocity.....	92
FIGURE 4.13: average deposition velocity $\overline{w_d}$ against shear velocity for LA- 260 sand.....	93
FIGURE 4.14: average dimensionless deposition velocity $\langle w_d^* \rangle$ against grain size, for experiments with LA-260 and B3-100 sands .....	94
FIGURE 4.15: average dimensionless deposition velocity $\overline{w_d^*}$ against shear velocity for LA-260 sand.....	94
FIGURE 4.16: plots of the dimensionless deposition velocity against grain size for different gravel sizes, illustrating the influence of the shear velocity $u^*$ on $w_d^*$ .....	96
FIGURE 4.17: plots of the dimensionless deposition velocity against grain size for different classes of shear velocity, illustrating the influence of the gravel size on $w_d^*$ .....	97-98
FIGURE 4.18: dimensionless deposition velocity against grain size for experiments E5, E6 and E7, illustrating the influence of the composition and the input rate of sediment on $w_d^*$ .....	99
FIGURE 5.1a: deposition parameter $w_d^+ = w_d u^* / (gd)$ against dimensionless grain size $d^*$ for all experiments carried out with LA-260 sand ( $d^* < 10$ ). .....	106
FIGURE 5.1b: deposition parameter $w_d^+ = w_d u^* / (gd)$ against dimensionless grain size $d^*$ for all experiments carried out with sand B3-100. ....	106
FIGURE 5.2: model for the deposition and re-suspension of saltating load .....	112
FIGURE 5.3: average landing angles over five size fractions $\bar{\beta}$ against shear velocity $u^*$ .....	115
FIGURE 5.4: dimensionless deposition velocity $w_d^*$ against van Rijn's damping coefficient $\phi$ .....	118

FIGURE 5.5: factor $k_2$ and exponent $n_2$ ( $w_d^*=k_2\phi^{n_2}$ ) against dimensionless grain size $d^*$ .....	118
FIGURE 6.1.a: semi-log plot of the deposition rate $\Delta$ against distance downstream for seven experiments of the main series and for the average over the whole series.....	128
FIGURE 6.1.b: semi-log plot of the deposition rate $\Delta$ against distance downstream for eight experiments of the main series.....	128
FIGURE 6.2: coefficient ( $r_i$ ) against grain size .....	130
FIGURE 6.3: uniform continuous source ( $i_{0j}$ ), settling of the different size fractions in the main flow and initial near-bed concentrations per unit length $c_{b0j}$ .....	131
FIGURE 6.4: computation of the near-bed concentration $C_{bj}(x)$ for $x \leq x_1 + \ell_j$ : graphic representation .....	132
FIGURE 6.5: computation of the near-bed concentration $C_{bj}(x)$ for $x > x_1 + \ell_j$ : graphic representation .....	134
FIGURE 6.6: computation of the longitudinal distribution of the deposition rate $\Delta$ in the case of a uniform continuous source .....	137
FIGURE 6.7: (non-uniform) input function, 9-section mesh and result from the model described in §6.3.2.1.....	141
FIGURE 6.8: (non-uniform) input function, 18-section mesh and result from the model described in §6.3.2.1.....	141
FIGURE 6.9: application of the model described in §6.3.1 to Example 1 .....	142
FIGURE 6.10: application of the model described in §6.3.2 to Example 2 .....	143

# List of Tables

TABLE 3.1: main characteristics of the preliminary series of experiments on infiltration.....	44
TABLE 3.2: main characteristics and results of the funnel-trap series of experiments .....	61
TABLE 3.3: median size of the sand collected in the funnel trap for five experiments.....	62
TABLE 3.4: median size of the sand collected at several locations along the flume in Experiment A0. ....	67
TABLE 4.1: results of flow and friction parameters .....	77
TABLE 4.2: comparison of data from previous and present studies.....	82
TABLE 4.3: main characteristics of the eighteen experiments of the main series .....	83
TABLE 4.4: average results of zero-plane displacement, roughness length and equivalent roughness size for the three types of gravel used .....	84
TABLE 4.5: ratio between the deposited fines and the near-bed fines mean size ( $d_{50dep} / d_{50tp}$ ), averaged over the six traps, and shear velocity $u^*$ .....	90
TABLE 4.6: average deposition velocity obtained for all experiments with LA-260 and B3-100 against grain size.....	91
TABLE 4.7: average dimensionless deposition velocity $\langle w_d^* \rangle$ obtained for all experiments with LA-260 and B3-100 against grain size. ....	93
TABLE 5.1: landing angles $\beta$ obtained from Equation [5.20], against size fraction and experiment label. ....	114
TABLE 5.2: Van Rijn's damping factors and dimensionless deposition velocities for experiments E5, E6 and E7. ....	117
TABLE 5.3: Variations of the factor $k_2$ and the exponent $n_2$ (of the formula $w_d^* = k_2 \phi^{n_2}$ ) against dimensionless grain size for the experiments E5, E6 and E7. ....	118
TABLE 6.1: results of the coefficients ( $r_i$ ), ratio of the near-bed and depth-averaged concentrations for the size fraction $i$ , for the experiments of the main series with LA-260. ....	130
TABLE 6.2: non-uniform source, application of the method described in §6.3.2.1. ....	140
TABLE 6.3: model sensitivity assessment on the value of the coordinate $x_{max}$ , i.e. the maximum coordinate at which $\Delta \geq 10^{-3} \text{kg.m}^{-2} \cdot \text{s}^{-1}$ . ....	143

# Notations

## 1 Alphanumeric characters

a	decay rate of the deposition rate ( $m^{-1}$ )
$A_s$	horizontal area occupied by a 'sweep event' ( $m^2$ )
B	flume breadth (m)
c	sediment concentration ( $kg.m^{-3}$ )
C	depth-averaged sediment concentration ( $kg.m^{-3}$ )
$C_0$	initial depth-averaged sediment concentration ( $kg.m^{-3}$ )
$C_0'$	initial sediment concentration gradient ( $kg.m^{-4}$ )
$C_a$	reference near-bed volume concentration
$C_b$	near-bed sediment concentration ( $kg.m^{-3}$ )
$C_d$	width of deposition corridor (m)
$C_r$	width of re-suspension corridor (m)
$C_s$	average sediment concentration within the bed surface layer ( $kg.m^{-3}$ )
d	median fine sediment size ( $\mu m$ or mm)
$d^*$	dimensionless particle diameter ( $= (\rho_s g v^{-2})^{1/3} d$ )
D	median framework sediment size (mm)
$D_d$	longitudinal dispersion coefficient of fine sediment particles ( $m^2.s^{-1}$ )
$D_m$	clay particles molecular diffusion ( $m^2.s^{-1}$ )
E	entrainment rate of sediment ( $kg.m^{-2}.s^{-1}$ )
$E_s$	dimensionless entrainment rate of fine sediment
Fr	Froude number ( $= U (g h)^{-1/2}$ )
g	gravitational acceleration ( $m.s^{-2}$ )
$g_L$	longitudinal mass transport rate of fines ( $kg.m^{-3}.s^{-1}$ )
$g_v$	vertical mass transport rate of fines ( $kg.m^{-3}.s^{-1}$ )
h	flow depth measured from the bed interface (m)
H	bed surface level (m)
$I_0$	input rate of fine sediment ( $kg.s^{-1}$ or $g.s^{-1}$ )
$i_0$	input rate per unit width ( $kg.m^{-1}.s^{-1}$ )
$i_1$	size fraction interval
k	vertical dimension of roughness elements (m)
$k_1, k_2$	constants
$k_f$	parameter related to the flocculation rate of cohesive sediment
$k_{ref}$	reference vertical dimension of the roughness elements (m)
$k_s$	equivalent roughness size (m)
$\ell_i$	distance required by fine particles released at the water surface (size fraction i) to reach the bed surface (m)
L	distance between two consecutive discs in 2D saltating particles deposition model (m)
M	sediment entrainment parameter ( $kg.m^{-2}.s^{-1}$ )
$n_f$	flocculation parameter
$n_1, n_2$	exponents
N	number of particles per unit bed area per time ( $m^{-2}.s^{-1}$ )
p	fraction of the available pore space of the gravel that is occupied by sand

$p_a$ .....	average value of $p$ in the active layer
$p_{ab}$ .....	effective value of $p$ near the bottom of the active layer.
$p_{at}$ .....	an effective value of $p$ near the top of the active layer
$p_e$ .....	an "exchange value of $p$ ".
$p'$ .....	coefficient of probability of deposition
$P_d$ .....	probability of deposition
$Pe_s$ .....	sedimentation Peclet number ( $= w_s h / 2\varepsilon$ )
$Q$ .....	fluid discharge ( $m^3 \cdot s^{-1}$ )
$q$ .....	unit fluid discharge ( $m^2 \cdot s^{-1}$ )
$r$ .....	coefficient such that $rC$ is equal to $C_b$
$r_s$ .....	coefficient such that $r_s C$ is equal to $C_s$
$R$ .....	disc radius in 2D saltating particles deposition model (m)
$Re$ .....	Reynolds number based on the grain fall velocity ( $= w_s l / \nu$ , where $l$ is a characteristic distance)
$Re^*$ .....	particle Reynolds number ( $= u^* d / \nu$ )
$S$ .....	bed slope
$Sc$ .....	Schmidt number ( $= \nu / D_m$ )
$Sps$ .....	spacing between sweep events (m)
$t$ .....	time (s)
$t^\circ$ .....	temperature ( $^\circ C$ )
$T_s$ .....	average turbulent sweep period (s)
$u$ .....	longitudinal flow velocity ( $m \cdot s^{-1}$ )
$u'$ .....	fluctuating component of the longitudinal flow velocity ( $m \cdot s^{-1}$ )
$u^*$ .....	shear velocity ( $m \cdot s^{-1}$ )
$U$ .....	depth-averaged longitudinal flow velocity ( $m \cdot s^{-1}$ )
$U_{cd}$ .....	critical flow velocity for sediment deposition ( $m \cdot s^{-1}$ )
$v$ .....	lateral flow velocity ( $m \cdot s^{-1}$ )
$v'$ .....	fluctuating component of the lateral flow velocity ( $m \cdot s^{-1}$ )
$w$ .....	vertical flow velocity ( $m \cdot s^{-1}$ )
$w'$ .....	fluctuating component of the vertical flow velocity ( $m \cdot s^{-1}$ )
$w^*$ .....	parameter accounting for the relative influence of gravity against turbulence ( $= w_s / u^*$ )
$w_d$ .....	deposition velocity ( $m \cdot s^{-1}$ )
$w_d^*$ .....	dimensionless deposition velocity ( $= w_d / w_s$ )
$w_d^+$ .....	deposition parameter ( $= w_d u^* / (g d)$ )
$w_s$ .....	sediment fall velocity ( $m \cdot s^{-1}$ )
$w_s'$ .....	average exchange velocity through the zero-velocity plane ( $m \cdot s^{-1}$ )
$x$ .....	longitudinal distance measured from the sediment release point (m)
$x'$ .....	longitudinal distance measured from the beginning of the test section (m)
$x^+$ .....	longitudinal wall-unit distance
$y$ .....	lateral distance (m)
$Z$ .....	elevation above the zero-velocity level (m)
$Z^+$ .....	vertical wall-unit distance
$Z_{ADV}$ .....	height between the sampling volume and the bed surface (m)
$Z_b$ .....	height between the ADV probe and the bed surface (m)
$Z_d$ .....	height between the ADV probe and the flume bed (m)
$Z_0$ .....	roughness length (m)
$Z$ .....	elevation above the bed interface (m)
$Z_s$ .....	suspension number ( $= w_s / \beta_d \kappa u^*$ )

## 2 Greek characters

$\alpha$ .....	parameter related to the average spacing between sweep events
$\beta$ .....	landing angle of particles transported by saltation ( $^{\circ}$ )
$\beta_d$ .....	ratio of sediment diffusion and fluid diffusion coefficients
$\chi_i^j$ .....	coefficient used to compute the fractional near-bed concentration of the size fraction $i$ over trap $j$ ( $= C_{bi}^j / C_b^j$ )
$\delta$ .....	deposition rate per unit length ( $\text{kg.m}^{-3}.\text{s}^{-1}$ )
$\partial x$ .....	short longitudinal distance (m)
$\Delta$ .....	deposition rate ( $\text{kg.m}^{-2}.\text{s}^{-1}$ )
$\Delta_b$ .....	near-bed deposition rate ( $\text{kg.m}^{-2}.\text{s}^{-1}$ )
$\Delta_{ts}$ .....	average deposition rate measured over a given test section ( $\text{kg.m}^{-2}.\text{s}^{-1}$ )
$\Delta_0$ .....	deposition rate measured in the funnel-shaped trap ( $\text{kg.m}^{-2}.\text{s}^{-1}$ )
$\Delta z$ .....	zero-plane displacement (m)
$\varepsilon$ .....	eddy diffusivity ( $\text{m}^2.\text{s}^{-1}$ )
$\varepsilon_z$ .....	vertical fluid turbulent diffusion coefficient ( $\text{m}^2.\text{s}^{-1}$ )
$E$ .....	entrainment rate ( $\text{kg.m}^{-2}.\text{s}^{-1}$ )
$\Phi$ .....	critical diameter ratio
$\gamma$ .....	specific weight of fluid ( $\text{kg.m}^{-2}.\text{s}^{-2}$ )
$\gamma_s$ .....	specific weight of sediment ( $\text{kg.m}^{-2}.\text{s}^{-2}$ )
$\gamma_s^*$ .....	immersed specific weight ( $\text{kg.m}^{-2}.\text{s}^{-2}$ ) ( $= \gamma_s - \gamma$ )
$\Gamma_s$ .....	sediment diffusion coefficient ( $\text{m}^2.\text{s}^{-1}$ )
$\Gamma_{sz}$ .....	vertical sediment diffusion coefficient ( $\text{m}^2.\text{s}^{-1}$ )
$\eta$ .....	bed surface layer thickness (m)
$\phi$ .....	van Rijn's turbulence damping coefficient
$\kappa$ .....	Von Karman's constant ( $\sim 0.4$ )
$\lambda$ .....	porosity
$\lambda_s$ .....	average area of sweep events per unit bed area
$\mu$ .....	dynamic viscosity (Pa.s)
$\nu$ .....	fluid kinematic viscosity ( $\text{m}^2.\text{s}^{-1}$ )
$\rho_w$ .....	density of fluid ( $\text{kg.m}^{-3}$ )
$\rho_s$ .....	density of sediment ( $\text{kg.m}^{-3}$ )
$\rho_s^*$ .....	submerged specific density of sediment ( $= (\rho_s - \rho_w) / \rho_w$ )
$\sigma$ .....	sediment sorting index ( $= \sqrt{(d_{84} / d_{16})}$ )
$\Sigma_i^j$ .....	coefficient used to compute the fractional deposition rate of the size fraction $i$ into trap $j$ ( $= \Delta_{bi}^j / \Delta_b^j$ )
$\tau_b$ .....	bed shear stress (Pa)
$\tau_c$ .....	critical shear stress for sediment transport (Pa)
$\tau_{cd}$ .....	critical shear stress for sediment deposition (Pa)
$\tau_{ce}$ .....	critical shear stress for sediment entrainment (Pa)
$\tau^*$ .....	Shields parameter ( $= \tau / (\gamma \rho_s^* d)$ )
$\zeta$ .....	relative depth ( $= z / (h + \Delta z)$ )

### 3 Subscripts

b..... near-bed  
c..... critical value  
calc ..... data calculated from model  
dep..... deposited sediment  
e..... entrainment  
exp..... experimental data  
i ..... size fraction index  
s ..... bed surface layer  
tpt ..... transported sediment  
0..... initial data  
 $d_{16}$ ,  $d_{50}$ ,  $d_{84}$  .... 16<sup>th</sup>, 50<sup>th</sup> and 84<sup>th</sup> percentile fine sediment size ( $\mu\text{m}$  or mm)  
 $D_{50}$ ,  $D_{84}$ ,  $D_{90}$ .. 50<sup>th</sup>, 84<sup>th</sup> and 90<sup>th</sup> percentile bed sediment size (mm)  
min ..... minimum value  
max..... maximum value

### 4 Superscripts

j ..... trap index  
n..... series rank

### 5 Specific notations

$\langle x \rangle$  ..... average per size fraction (i.e. average of all the data obtained in all the experiments for a given size fraction)  
 $\bar{x}$  ..... average per experiment (i.e. average of all the data obtained for all the size fractions of a given experiment)  
 $\sim$  ..... approximate value

# Chapter I

## Introduction

### 1.1 General remarks

Rivers are the landscape's self-formed gutter system that carry rainfall and snow-melt towards topographic sinks. By way of momentum transfers from the flow to the alluvium, rivers are also both the means and the routes by which the products of continental weathering are carried to lakes and oceans. Over periods of geological time, this erosional activity is responsible for major landscape modifications (Leopold *et al.*, 1964).

Because of their relatively steep slope and high variability in discharge (or 'flashy' regime), gravel-bed rivers are particularly dynamic river environments, continuously reworked by the erosion and deposition of coarse and fine sediments. Fluvial gravels tend to be poorly sorted, with a geometric standard deviation normally ranging between 2 to 4 (where 1 would indicate uniform sizes). The dominant gravel mode is often associated with a secondary fine sediment mode (Pettijohn, 1975; Sambrook-Smith, 1996), which includes particles up to 2mm in diameter. Because of the relatively large difference in size between the modes, fine particles that are transported near the bed have the opportunity to pass through the bed surface pores (i.e. to deposit) and to settle within the gravel framework (i.e. to infiltrate). The fine particles are then generally referred to as *matrix* particles. They remain within the bed until being re-entrained by a flow of sufficient magnitude.

In general, the interstitial spaces are only partially filled by matrix fines (Carling and Reader, 1982). The gravel bed is then referred to as *framework-supported* (or clast-supported), i.e. its coarser elements are in grain-to-grain contact and the fine elements do not bear any part of the bed fabric (Figure 1.1a). In contrast to this is a *matrix-supported* bed, which contains a large proportion of sand (~50%) and gravel elements that are not in overall contact (Figure 1.1d). The latter results either from simultaneous deposition of

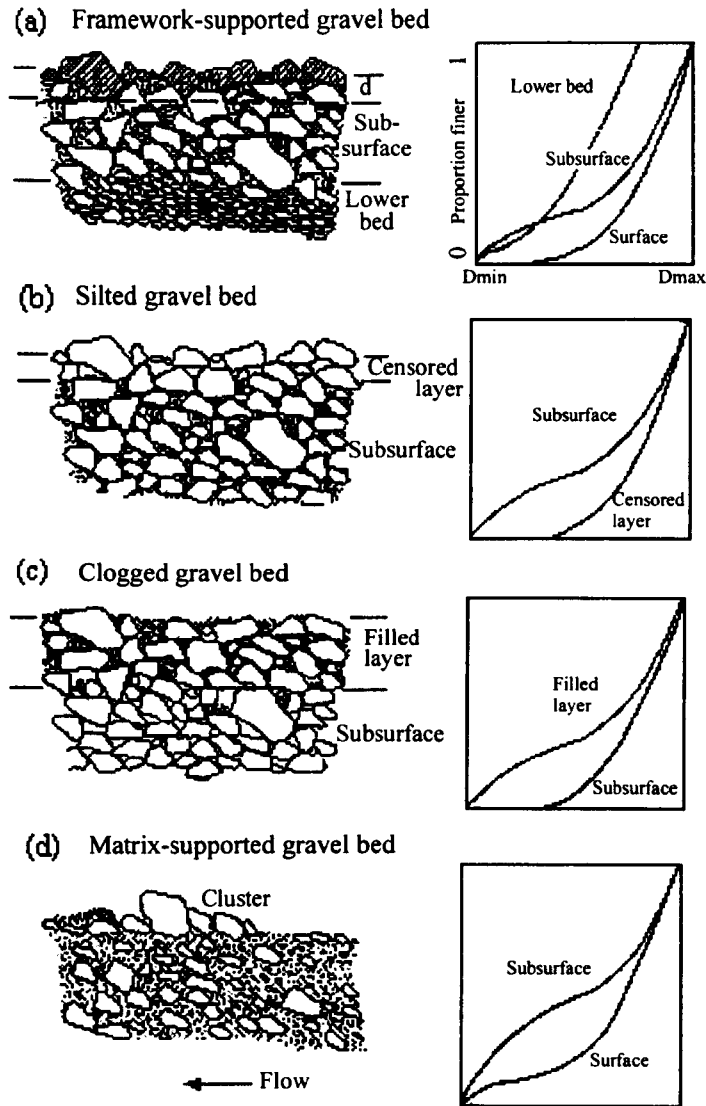


FIGURE 1.1: typical arrangements of fluvial gravels, with type cumulative grain size curves on the right (after Church *et al.*, 1987)

sand and gravel, or by gravel particles being incorporated into a sand bed (Petts, 1988a). It can be found in rivers undergoing debris flows or very high sediment transport rates, and is common in semi-arid rivers. Fine sediment can deposit in framework-supported gravel either by filling the subsurface voids and leaving only the top of the bed free of fines (Figure 1.1b), or conversely by filling the top layers of gravel and preventing any deeper infiltration (Figure 1.1c).

Fine particles are transported in the main flow either as bedload, suspended load or by saltation. These particles have the opportunity to deposit into the bed only when reaching the near-bed region. Similarly, particles deposited near the bed surface are the

most likely to be re-entrained into the flow. The balance between deposition and entrainment of fine sediment particles has a direct effect on the composition of the bed. For example, the selective entrainment of the finest particles can lead to the formation of a bed surface layer that is considerably coarser than the subsurface, or *armouring* (Parker *et al.*, 1982). This coarser layer is generally referred as an *armour layer* when it is static, and a *pavement* (or sometimes *mobile armour*) when it is active. The equilibrium between deposition and entrainment has also a direct effect on sediment transport: if large quantities of matrix fines are present within the riverbed (for example after long, low-flow periods), the transport rates during large flow events are larger than when the bed is free of fines.

The river bed forms the boundary between the river and the substrate. It is in particular the habitat of various aquatic species, and also a filter layer which controls the exchanges between surface and ground water. The accumulation of matrix particles can affect these functions of the river bed. It represents a significant threat to the reproduction of salmon species and to the ecology of the river in general (A.S.C.E. Task Committee on Sediment Transport and Aquatic Habitats, 1992), and it can impede seepage and groundwater recharge (Schälchli, 1995).

Many researchers have examined various aspects of the deposition/infiltration process, but no method is currently available that allows the making of quantitative or even qualitative predictions of sediment accumulation in given conditions. This is partly due to the complexity of the phenomenon of sediment transport, which is only partially understood and a major subject of research in hydraulics. This may also have resulted from the fact that the major part of the studies on sediment transport in gravel-bed rivers over the past thirty years have focussed on the question of sediment entrainment, whereas less consideration has been given to the question of sediment deposition. However, because of the abundance of potential depositional niches at the surface of and within gravel beds, better knowledge of this subject is necessary to improve our understanding of phenomena including bedload transport, suspended sediment transport, armouring and downstream fining. In gravel bed rivers, sediment transport and deposition are intimately connected processes: the sediment transport rate during a flood event for example depends to a large extent on the quantity of fine sediment stored within the bed pores. Conversely, the way fine particles are transported has a direct influence on the deposition process: there is more deposition when more particles are

transported near the bed. The relationship between near-bed transport and deposition is precisely the main subject of the following pages.

## **1.2 Origin and implications of the matrix infiltration problem**

### **1.2.1 Sources of fine sediment**

Increasing the input of fine sediment to a river system can lead to higher accumulation of fines within the pores of gravel beds. Geological erosion caused by climatic and biological processes, as well as stream bed and bank erosion are natural causes of fine sediment input into rivers. However, anthropogenic sources due to logging and mining operations, road construction, and agricultural activities can induce erosion rates as high as one hundred times the normal rate (Julien, 1995). Drainage works and poor land management also produce higher levels of fines. Similarly, physical modifications to the river system, including channelisation, excess gravel extraction, or dam construction may alter the equilibrium conditions in a river resulting in a fine-sediment overload, and subsequent deposition. Such increases in the quantity of matrix sediment may however be only temporary if sufficiently high flows occur to flush the gravel (Adams and Beschta, 1980).

River regulation, in the form of impoundment and water transfer schemes, usually results in prescribed minimum discharges and the elimination of high discharges (Carling, 1987; Sear, 1993). This reduces the overall channel competence, causing higher deposition and infiltration, and lower ability for the river to flush fine sediment out of the bed. Sear (1993) observed that regulation caused a reduction in the average size of matrix particles, leading to deeper infiltration and larger accumulations. Petts (1988a) found higher matrix content downstream from tributary sources (>20% by weight) compared to non-regulated sites (<5%) in two UK regulated rivers. In addition to direct regulation, decreases in rainfall due to climate changes may also cause larger fines infiltration rates.

### 1.2.2 Implications of matrix accumulation for fisheries

High quantities of matrix fines in gravel beds can adversely affect *salmonidae* populations. This represents an important loss in terms of commercial value for the salmon fisheries industry, and in terms of sporting and recreational value (Milner *et al.* 1981).

Due to human intervention, a significant reduction in the quantity of high quality gravel-bed habitat has been reported in recent years (Brookes, 1988; Petts, 1988b). Salmon species stocks tend to be very sensitive to such changes as one important requirement for these migratory fish to survive in freshwater is a suitable spawning and egg incubation environment (Maitland and Campbell, 1992). Salmon and trout lay their eggs in a pit (referred to as a redd) excavated upstream of riffle crests, and bury them under 100 to 400mm of bed material. The stream bottom at the riffle head gradually assumes a convex shape, which causes a downwelling of the current into the substrate (Stuart, 1953; Thibodeaux and Boyle, 1987). This movement of water provides a constant supply of oxygen and effectively removes carbon dioxide and metabolic waste materials produced by the eggs (also called ova). The preferred range of gravel sizes is between 10 to 100mm. The choice of location of the redd and the initial winnowing of fines during the excavation enhances gravel permeability, hence interstitial flow and fry emergence. However, the ova and the alevins are vulnerable to sediment deposition and scour for some two to six months after laying. That period usually coincides with the autumn or winter seasons, i.e. periods of high flows.

Sediment infiltration causes a reduction in the bed's permeability and interstitial flow. Laboratory observations have shown that a layer of very fine sand less than 10mm thick can reduce by more than a thousand times the permeability of normally highly-permeable gravel. (Van't Woudt and Nicolle, 1978). Such reduction in bed permeability and interstitial flow can lead to: (1) intoxication of the ova by its own metabolic waste (Bailey *et al.*, 1980); and (2) low levels of oxygenation, which increase the rates of malformation and vulnerability of the alevins (Turnpenny and Williams, 1980). Fine sediment infiltration can also cause: (1) ova injury by abrasion; (2) a further reduction in the oxygen levels because of the organic matter carried by the fines; and (3) reduced emergence of alevins as fine gravel and coarse sand form a barrier near the surface (Phillips *et al.*, 1975) (Figure 1.2). Further, the filling of gravel pores affects some

populations of macroinvertebrates, which, in turn, lowers the food resources for fish in the river. Increases in matrix sediment content as low as 5 to 10% in volume can be detrimental to aquatic resources (Cordone and Kelley, 1961).



FIGURE 1.2: ten-week old salmon alevin, with its characteristic yolk sac. Matrix fine sediment can block the emergence of the alevins from the gravel. (Photo by B. Lavies; in Lee, 1981)

### 1.2.3 Other implications

The processes of deposition and infiltration of fines have other important implications. These include:

(1) predictions of sediment transport rates in gravel-bed rivers. Gravel beds act like a source and sink of fine sediment, depending on the flow rate. A large scatter in the transported sediment rate/water discharge ( $Q_b$  vs  $Q$ ) relation can be sometimes observed as a result of variations in the amount of fines present in the bed (Frostick *et al.*, 1984). Better knowledge on the deposition-infiltration process can lead to improvements in the prediction of sediment transport rates in gravel-bed rivers.

(2) groundwater recharge. Infiltration of fines, and in particular of cohesive sediment, can reduce dramatically interstitial flow circulation and consolidate the bed, rendering bed flushing by high flows difficult. Exchanges between the river and the

underlying aquifer can subsequently be reduced, which can put groundwater resources for water supply at risk (Schälchli, 1995).

(3) the exploitation of gravel deposits. Ancient gravel deposits may serve as water, oil or gas reservoirs (Ashworth *et al.*, 1994; Frostick *et al.*, 1984). Lowland deposits of gravel-bed streams often provide an exploitable gravel resource (Frostick *et al.*, 1984), and may contain placers (Allan and Frostick, 1997). There is thus a geological and economic interest in the study of the history and the structure of fluvial deposits.

(4) the infiltration of toxic material in coarse beds, e.g. in urban areas. The valleys of mountainous areas provide abundant resources in freshwater, which are used notably by heavy and pollutant industries. Fine sediments tend to concentrate some of the pollution released into river systems, and their infiltration can lead to a long-term contamination of the bed (Thoms, 1987).

### 1.3 Basis of the study

The active bed is that part of the gravel-bed that can be set in motion by the largest flows. Bed mobilisation is generally described as a necessary condition for the re-entrainment of matrix particles. Fine sediments that do not infiltrate deeper than the active bed tend to follow a four-stage cycle, i.e. (1) transport/settling within the flow; (2) deposition; (3) infiltration; and (4) flushing and re-entrainment (Figure 1.3). Deposition refers to the passage of the particles through the surface layer pores while infiltration designates their further movement through the subsurface layer voids.

Once settling particles have reached the top of the bed surface, they become available for deposition. This complex process involves such parameters as the diameters of the fine and coarse sediment and the level of turbulence, and is described in more detail below. Once they have deposited, fine particles can infiltrate through the sub-surface. This process is influenced principally by the ratio between matrix size and pore size. In the absence of significant fluid movement within the subsurface voids, grains fall until reaching a pore too small to allow passage (Frostick *et al.*, 1984). This process is mainly related to granular mechanics and is relatively well documented and understood (§2).

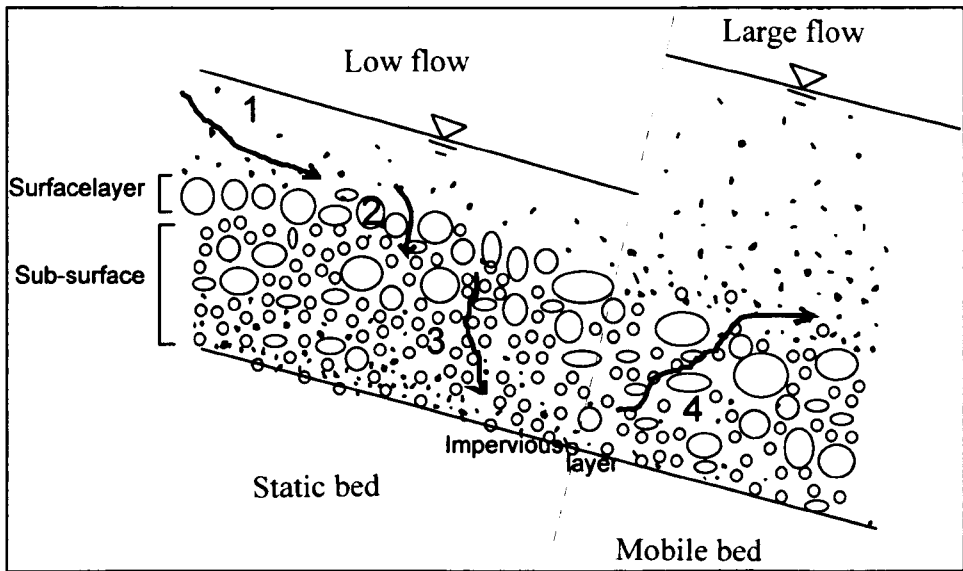


FIGURE 1.3: four-stage cycle followed by fine sediment transported in gravel-bed rivers

Matrix particles can remain within gravel interstices over long periods, until they are flushed out of the bed. Different magnitudes of high flow events result in fine sediment being flushed from different levels of the bed, the highest flows reaching the deepest particles. This in turn has a direct effect on the sediment transport rate. However, sediments flushed out tend to re-deposit during receding flows, which generates a balance between infiltration and flushing of sediment. Thus, the average fines content tends to remain relatively constant (Milhous, 1973) unless a marked source of fines is added to the system. The flushing process is complex and it is only recently that scientists have pioneered its analysis (Wilcock *et al.*, 1996; Kondolf and Wilcock, 1996).

Deposition is the process by which fine particles pass from the turbulent, open-channel flow medium to the more tranquil porous flow medium through a filter layer, i.e. the bed surface layer. It is a key area for the knowledge of the mechanics of sediment fluxes in gravel-bed rivers. The detailed physics of this process are still, however, poorly researched. It has often been indicated that deposition criteria, like entrainment criteria, depend on parameters such as the sediment concentration and the fall velocity (e.g. Einstein, 1968; Carling, 1984; §2.2.2.3). Other parameters have also been related to the deposition process (e.g. Froude number in Beschta and Jackson, 1979), but no general formulation has been proposed to describe this influence. This is due to the complexity of the phenomena involved. The bed surface forms a physical barrier against the

penetration of settling particles, the influence of which is difficult to determine mathematically. The near-bed region is also the subject to complex and intense turbulent activity, but the structure of near-bed turbulence in gravel-bed rivers is not yet well understood.

Several researchers have nevertheless highlighted the need for further investigations in this direction. Carling (1984) recommends the study of detailed flow and suspended sediment data very close to the bed, using both experimental and field studies. Following a review on the development of sedimentation science since the 1930s, Vanoni (1984) suggests that the first order problem for transport and sedimentation processes lies in and near the river bed. Einstein (1968) concludes from flume observations that the separation between deposition and continued transport occurs at the surface of the bed, within the first one or two layers of gravel. Toro-Escobar *et al.* (1996), in their study of streambed aggradation, note the importance of the sieving mechanisms by which the surface layer filters the deposit that is released to the substrate.

Several field studies have been conducted on the subject of sediment deposition and infiltration in gravel-bed rivers (e.g. Frostick *et al.*, 1984; Lisle, 1989). This type of study has brought interesting results in terms of qualitative observations, particularly for infiltration (e.g. from the analysis of freeze-core samples). Several numerical methods and models have also been proposed. These have focussed on particular aspects of deposition/infiltration, e.g. on the lodging of matrix particles within stratified beds (Wu and Shen, 1993; Lauck *et al.*, 1993) or on the effect of matrix infiltration on interstitial oxygen transport within salmon redds (Alonso *et al.*, 1994). In the present study, an experimental approach has been adopted in order to investigate the basic physical properties of the deposition process. The experiments were carried out in an open-channel flume, under controlled hydraulic, fine sediment input and bed composition conditions.

#### **1.4 Summary of the main points / aims of the study**

Increased fine sediment inputs in rivers, combined with lower flows can result in increased levels of matrix sediments depositing into gravel beds. This can cause a threat to the ecology of rivers and to fish populations. However, the processes by which

transported fine sediments deposit, i.e. pass through the surface layer of gravel before infiltrating through the subsurface, are still poorly researched. Better knowledge of sediment deposition has direct implications for phenomena such as sediment transport, bed armouring and downstream fining.

Three series of flume experiments were carried out to study the process of fine sediment deposition through porous beds (two preliminary series and one main series). In these experiments, the deposition of sand and silt particles through medium to very-coarse pebbled, flat beds was tested (size-class specifications are indicated in Appendix 1). The aims of this study were: (1) to identify some of the main parameters involved in the deposition-infiltration process. The deposition velocity  $w_d$  was defined as the ratio between the near-bed concentration and the deposition rate of fine sediment. It was used to measure the effect of several parameters, like bed sediment size and shear velocity, on deposition; (2) to get a better understanding of the physical mechanisms involved in the deposition process. Different types of depositional behaviour were identified for different sediment size fractions and transport modes. The experimental results were analysed using methods based on the dimensional analysis, the properties of near-bed turbulence, and the landing angles of particles transported by saltation; and (3) to apply the results in a real-life context. Downstream sorting of fine sediment released at the water surface was modelled in 2D using the results of the study. Two examples of application of the model were considered.

After the review of some of the relevant literature (Chapter 2), two series of preliminary experiments are described (Chapter 3), followed by the description of the main body of the experimental work (Chapter 4). The implications of the results are subsequently discussed (Chapter 5), as well as some of their possible applications (Chapter 6).

## Chapter II

# Literature review

### 2.1 Sedimentation niches

Due to the diversity in channel morphology and the large variety of hydraulic conditions encountered in gravel-bed rivers, fine sediment deposition is not geographically uniform and tends to occur in specific areas. At the macroscale, areas of high infiltration are generally associated with areas with high input and transport rates of fines e.g. in highly erodible areas, or close to mining or forestry activities. Petts (1988a) and Klein (1993) have also highlighted the strong dependence of fine intrusion on the proximity to upstream tributary inputs. At the mesoscale, there are two main, nearly opposite, types of river environments that receive the highest quantity of infiltrated fines: the slack water areas and the highest flow velocity regions. As a general rule, the coarser elements (gravel, coarse sand) are mainly deposited in the deeper parts of the channel, most of the finer sands accumulate along the sides of the channel while silts and clays deposit in areas of shallow overflow on the floodplains (Happ, 1950). At the microscale, interactions between the bed's geometry and the flow induce a segregation in the deposition of the different sizes of sediment entrained by the river. This results in sediment of a particular size being systematically and repeatedly placed in similar parts of the gravel-bed river (Bluck, 1971).

#### 2.1.1 In-bank settling

In the meandering River Endrick, Bluck (1971) noted six major fines sedimentation areas (Figure 2.2): (1) pools; (2) inner accretionary banks (i.e. junctions between floodplains and bars); (3) bar tails; (4) lees behind gravel bars; (5) riffle tails;

and (6) cross-over reaches of meanders (Figures 2.1 and 2.2). Sand and clay were sometimes found below the surface of riffle heads, while thin sands occasionally deposited at bar heads. Ashworth *et al.*'s experimental work (1994) also indicated confluence scours, abandoned channels and lees behind obstructions and behind bank discontinuities to be privileged areas of sedimentation.



FIGURE 2.1: sand deposit at the downstream end of a gravel bar (Photo T.B. Hoey)

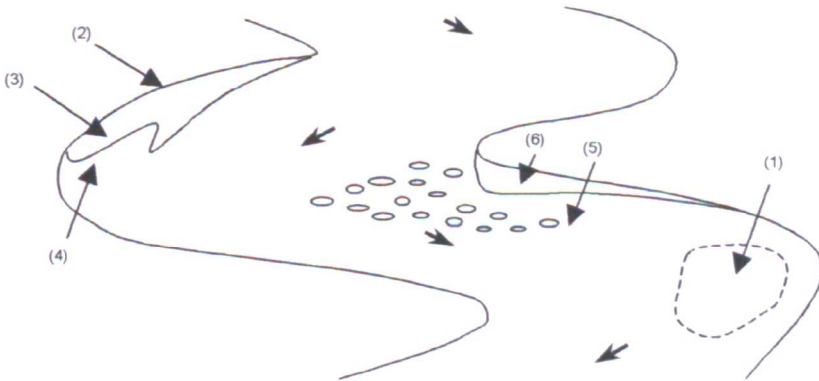


FIGURE 2.2: main areas of fine sediment deposition in gravel-bed rivers, according to Bluck (1971)

In-bank deposits are commonly associated with recirculating flows. Studying the deposition of clay and silt particles within an area of stagnant water located behind a

gravel bar of the River Severn, Tipping *et al.* (1993) found that fine particles accumulation takes place mainly during the longest periods of low flow, particularly during spring and summer, whereas autumn and winter see short periods of accumulation ended by flood events where all deposited fines are flushed away. Simulations carried out on the basis of field measurements showed that a particle-segregation phenomenon induced a preferential accumulation of aggregates of much larger size (30 $\mu\text{m}$  to 240 $\mu\text{m}$ ) than the average suspended sediment particle size (9 $\mu\text{m}$ ). Schmidt *et al.* (1993) conducted flume experiments to study the processes of sedimentation in a lateral eddy at a channel expansion. A bar formed within the zone of recirculating current, with highest deposition rates occurring at its downstream end, near the reattachment zone between the main flow and the flume wall. Unlike in the previous example, sediment sorting resulted in a generally finer deposit (~300 $\mu\text{m}$ ) than the transport by the main channel (~800 $\mu\text{m}$ ), with the coarsest elements (~650 $\mu\text{m}$ ) settling near the reattachment point and the finest (~130 $\mu\text{m}$ ) in the lee of the obstruction corresponding to the beginning of the flow expansion. The rate of deposition was roughly proportional to the transport rate of sediment in the main flow, and the capture rate of the eddy gradually decreased as the sand filled the recirculation zone. These last two examples represent cases where deposition is associated with size selective processes. On the contrary, Carling and Reader (1982) found that the grain size composition of the very fine particles transported at low concentrations during base flows in upland British rivers was similar to the material infilling bed pores. Size selectivity is thus not systematically observed.

Laboratory work has also shown that the presence of vegetation on the streambed significantly enhances deposition, with larger amounts of fine sediment accumulating as the grass blade is shorter (Abt *et al.*, 1994). On the other hand, unstable obstructions, such as large woody debris or boulders, can maintain one part of a gravel-bed clear of fines by setting up strong secondary currents (Wesche, 1985).

Finally, local bed topography in relation to river stage determines the time that fine sediment is supplied to any single part of the bed. Bar tops, for example, receive less sediment than pools during low flow periods in summer because they are not permanently submerged, and are thus less subjected to sediment deposition and infiltration (Frostick *et al.*, 1984).

### **2.1.2 Over-bank sedimentation**

Over-bank flows cause sedimentation on the flood plains of most rivers. Flood plain deposits are almost exclusively composed of sediment carried by suspension, with sand depositing first, as a result of the increased friction caused by the banks, and building natural sandy levees that border the channels (Happ *et al.*, 1940). Finer sediment is carried farther and deposits as a thinner layer over the entire surface of the floodplain. Flood plain deposits are generally not well sorted and tend to vary in grain size and thickness from place to place (Trask, 1950). Bluck (1971) observed on the flood plains of the River Endrick larger accumulations of silt, fine sand and clay in swales between meander scrolls and in ox-bow lakes.

### **2.1.3 Summary and conclusion**

Size selective processes generate preferential depositional areas of fines in rivers, building specific bed forms and sediment grading patterns. Within the river banks, fines sedimentation occurs mainly at low flow, in pools and in recirculating-flow areas, e.g. behind bars, but it also occurs at higher flows in deeper parts of the river. Particles that settle onto the bed surface become available for deposition and infiltration. Whether or not a settling particle is deposited into the bed depends on how it interacts with the gravel surface and near-bed turbulence.

## **2.2 Fine sediment deposition**

### **2.2.1 Physical parameters**

#### **2.2.1.1 Introduction**

The bed interface separates the open-channel flow medium from the bed's porous medium. Fine particles transported within the main flow can only deposit into the bed by passing through a zone, which can be called the near-bed area, and which comprises: (1)

above the bed interface, the inner zone, which is this lower part of the main flow dominated by shear forces and turbulence; and (2) below the bed interface, the buffer zone, which is the zone located between the bed interface and the level where the mean longitudinal velocity becomes zero (zero-velocity level). Within this zone, the trajectory of any given transported particle is mainly affected by three physical processes: its natural settling behaviour, the displacement of the surrounding fluid and the contacts with the bed surface.

### 2.2.1.2 Relative grain size distributions

The first condition for deposition to take place is that the pores formed by the gravel framework are sufficiently large to allow the passage of the finer elements. This condition relies mainly on the relative mean size of the gravel compared to that of the fine sediment ( $D/d$ ), and to a lesser extent on the degree of sorting of both mixtures.



FIGURE 2.3: tightly-packed and loosely-packed bed configurations. The dark-coloured disc indicates the size of the largest sphere that can deposit through each type of uniform bed.

In the case of tightly-packed uniform spheres, the critical threshold of deposition  $\Phi$  corresponds to a diameter ratio  $D/d$  of  $3+2\sqrt{3}$  (referred to as the Apollonian ratio,  $\sim 6.5$ ), realised when a small sphere can just pass through an equilateral triangle of larger spheres (Jullien and Meakin, 1988) (Figure 2.3). This implies that when the diameter ratio  $D/d$  is above 6.5, fine particles can deposit. Below the critical value, the coarse layer forms a barrier against the passage of the particles, which get clogged. This critical ratio falls to  $\Phi=1+\sqrt{2}$  ( $\sim 2.4$ ) if the bed is loosely packed (Carling, 1984), i.e. when the centres of adjacent large spheres form squares (Figure 2.3).

In the case of several uniform fine particles being released steadily above a uniform bed surface, Sakthivadivel and Einstein (1970) observe that when the diameter ratio  $D/d$  is between  $\Phi$  and  $2\Phi$ , pairs of matrix particles can bridge gaps within the bed surface, which gradually blocks the passage of the fines. When  $D/d$  is greater than  $2\Phi$ , the fine particles can pass freely through.

Whereas only one situation tends to occur (deposition or clogging) in the case of uniform or very well sorted coarse and fine sediment, the problem becomes more complex with non-uniform sediment mixtures as those found in natural rivers. Indeed, the non-uniformity of the gravel implies the non-uniformity of the bed surface pores. The size distribution of the pore diameters depends upon the size distribution, shape and packing of the framework material. Using vertical photographs, Frostick *et al.* (1984) derived the size distribution of the pores of a 27mm, well-sorted surface layer of sub-rounded flint pebbles, by taking the diameter of the maximum inscribed circle as a measure of size. It was moderately sorted with an average size of 4.1mm, corresponding to a ratio between average bed size and average pore diameter of 6.6, well in agreement with the Apollonian ratio (i.e. with the case of uniform spheres). However, the largest pore diameters measured were approximately 11mm in size, i.e. a ratio of 2.44, which would allow even the largest fines to penetrate the bed. The lowest pore diameters were close to 0mm, probably causing the clogging of fine particles. A wide range of bed surface pore sizes implies that any situation can occur. This is all the more true in the case where fine particles are poorly graded.

Lisle (1989) defined an average potential of infiltration as the ratio between the average framework size and fine sediment size, and a least potential as the ratio between the minimum framework sediment size and the maximum fine sediment size. Compilation of data from work by Beschta and Jackson (1979), Diplas and Parker (1985), Dhamotharan *et al.* (1980), Carling (1984) and Einstein (1968) shows a threshold in terms of average potential between 30 and 75, and in terms of least potential between 6.5 and 17. Lisle suggested that the average potential threshold is close to 60. This suggests that fine sediments have a higher probability of infiltrating when: (1) transported and framework sediments are both well sorted; and (2) there is little overlap between both grain size distributions.

## 2.2.1.3 Gravity

Sediment particles tend to settle naturally by gravity. In still water, drag forces tend to resist gravity forces and limit the settling velocity to a maximum, the fall velocity. Several formulae exist that can be used to compute the settling velocity of a particle of given size in a given fluid (two examples in Figure 2.4). Stokes (1851) derived the expression of the drag resistance of flow past a sphere using a simplified version of the Navier-Stokes equation. From this solution, it is possible to derive the following expression for the fall velocity of spherical particles (known as Stokes' law):

$$w_s = \frac{1}{18} \frac{\rho_s^* g d^2}{\nu} \quad [2.1]$$

where,  $\rho_s^* = (\rho_s - \rho_w) / \rho_w$ ,  $\rho_w$  is the density of the fluid,  $\rho_s$  the density of the sediment,  $d$  the particle diameter,  $g$  the gravitational acceleration and  $\nu$  the kinematic viscosity of the fluid. Equation [2.1] is only valid for spherical particles and Reynolds numbers ( $Re = w_s d / \nu$ ) lower than 1.

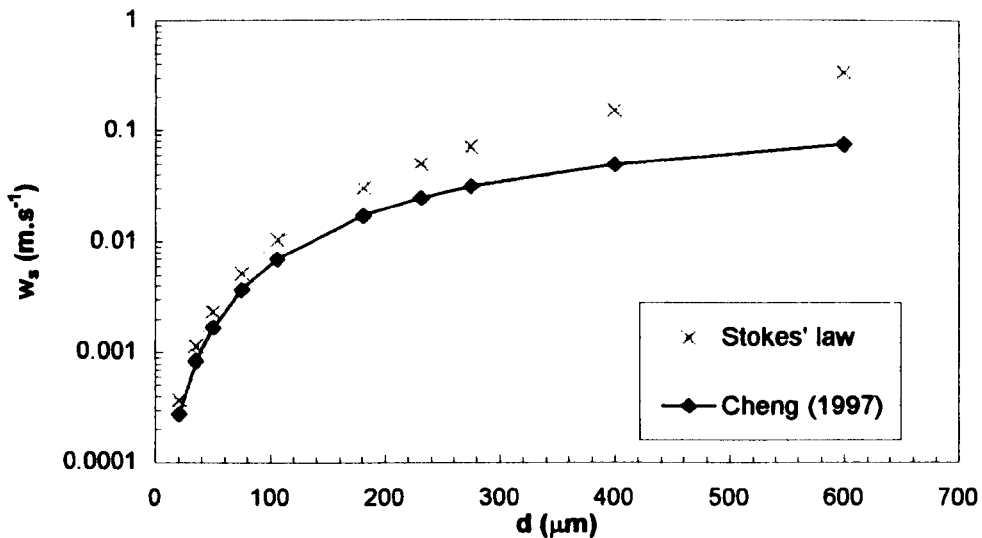


FIGURE 2.4: fall velocities computed from Stokes' law and Cheng's formula.

However, natural sediment is in general non-spherical, a characteristic which tends to generate more resistance against flow. It has in fact been found that the fall velocities of natural sand particles tend to be in average 25% less than predicted by [2.1]

(from Cheng, 1997). In addition, flow conditions in rivers always correspond to Reynolds numbers much larger than 1. Several semi-theoretical and empirical formulas have thus been developed to extend Stokes' law to a wider range of flow and sediment shape conditions (e.g. Raudkivi, 1990). Based on some of this work and on experimental data for quartz sand particles, Cheng (1997) has derived the following formula:

$$w_s = \frac{v}{d} \left( \sqrt{25 + 1.2d_*^2} - 5 \right)^{1.5} \quad [2.2]$$

where  $d_*$  is the dimensionless particle parameter defined as:

$$d_* = \left( \frac{\rho_s * g}{\nu^2} \right)^{\frac{1}{3}} d \quad [2.3]$$

Equation [2.2] applies to natural sand particles. It is valid over a wide range of flow conditions, i.e from Stokes-type conditions ( $Re \leq 1$ ) to high Reynolds numbers ( $Re = 10^3 \sim 10^5$ ). Because of these characteristics, it has been used to compute the reference settling velocities in the present study.

#### 2.2.1.4 Near-bed turbulence

Turbulence is due to eddies of various sizes, starting from the micro-turbulent dimensions, close to  $\nu/u^*$ , to the macro-turbulent ones, nearly equal to the flow depth  $h$ . Because of friction, flows along smooth solid boundaries generate a zone of turbulence, laid upon a relatively thin viscous sublayer containing fluid in laminar condition. The intensity of turbulence increases with the Reynolds number and is inversely related to the relative depth  $\xi$  (Nowell and Church, 1978).

Studies on the turbulence generated by smooth walls have indicated that turbulent eddies combine in vortex-like structures of varying size and strength within the inner zone. Some typical vortex structures have been described in the literature; e.g. hairpin-shape vortices, which form an arch with the open end trailing upstream and the closed end raised downstream (Robinson, 1991) (Figure 2.5).

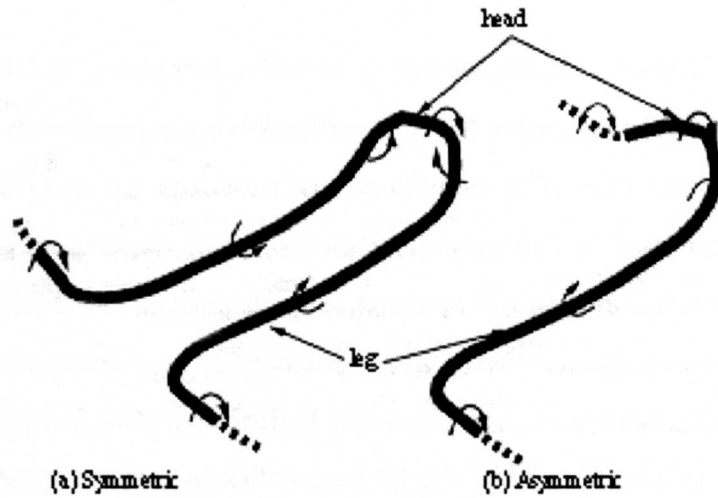


FIGURE 2.5: schematic model of typical hairpin-shape vortex configurations. The sense of vorticity is indicated by the arrows (after Smith, 1996)

The alignment in the stream-wise direction of counter-rotating pairs of vortices results in a succession of: (1) high-speed regions where the flow is directed towards the wall and laterally outwards, and (2) low-speed regions, or *streaks*, where the current is directed away from the wall and the streamflow velocity is retarded (Kline *et al.*, 1967). Yalin (1992) has suggested that these series of large-scale high-speed and low-speed regions can also be detected at a higher scale, and follow a chessboard-like arrangement in plan (Figure 2.6) which extends throughout the entire flow depth (also Nakagawa and Nezu, 1981).

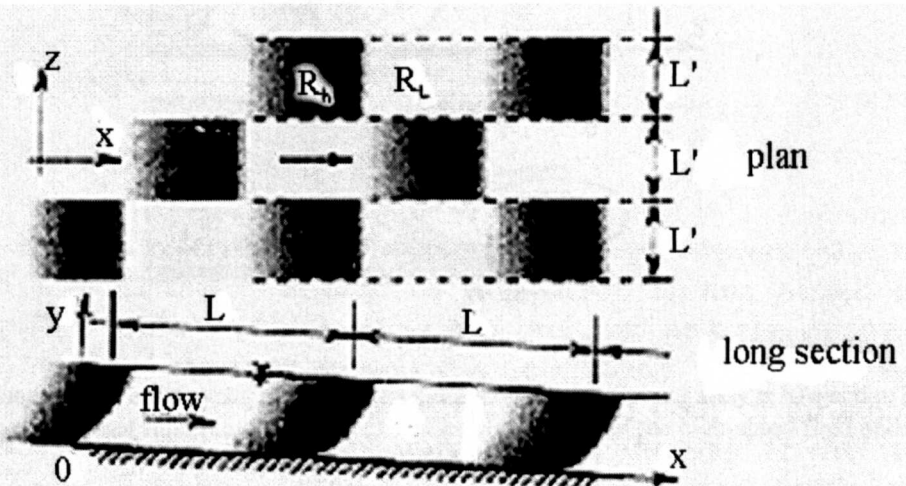


FIGURE 2.6: spatial structure of turbulent shear flows.  $R_h$  and  $R_l$  are respectively the high-speed and low speed regions. The large-scale lengths  $L$  and  $L'$  are of several flow depths (after Yalin, 1992)

If the velocity gradient that forms at the boundary between two consecutive regions is sufficiently large, a burst-forming eddy ( $e$ ) is generated near the wall, and is subsequently ejected in the upward direction (Figure 2.7). This displacement of fluid generates circulatory motions in the low-speed region ( $e'$ ,  $e''$ ), while the high-speed fluid overtakes the eddy  $e$  through the area between the eddy and the free-surface. The eddy  $e$  gradually increases in volume and slows as it moves away from the wall. Finally, an inrush of high-speed fluid is propelled below the eddy as a result of the 'obstruction' and the subsequent pressure gradient caused by the eddy  $e$ . Turbulent boundary layers near smooth walls thus display deterministic structures of irregular, but persistent flow patterns in the shape of rapid short duration inflows (i.e. *sweeps*) and slower long duration outflows (i.e. *ejections*) (Smith, 1996).

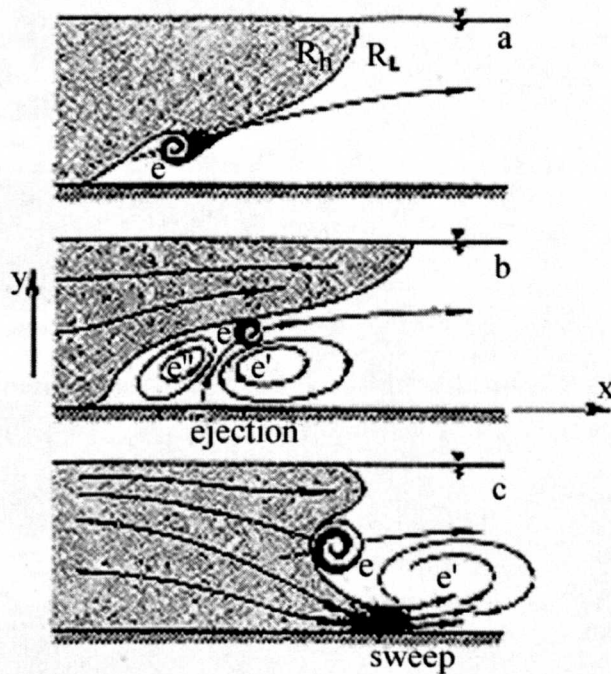


FIGURE 2.7: sequences of a burst cycle, with: a) development of a burst-forming eddy  $e$ ; b) ejection of the eddy  $e$  within the low-speed fluid region  $R_L$ ; and c) sudden acceleration of the high-speed fluid under the eddy  $e$ , or 'sweep' (after Yalin, 1992)

In the case of rough-wall boundary layers, there is evidence that the 'burst-sweep' process occurs with similar characteristics (Grass, 1971), at scales determined by

the mean size of the roughness elements  $k_s$ . Increased levels of momentum exchange caused by larger roughness elements tend to accentuate the amplitude of sweeps and ejections near the bed surface, and hence the overall degree of turbulence. The presence of the coarse bed elements causes trapping of lateral flows within the gaps between the protruding elements, and thus alter the coherence of the wall-streak structure, yet without eradicating it completely (Grass *et al.*, 1991). Flow separation behind roughness elements results in the destruction of the viscous sublayer. As a result, log-velocity profiles are not valid close to the rough boundary ( $\xi < 0.35$ ) (Nowell and Church, 1978). One can thus distinguish between a near-bed region, dominated by obstacle-derived vortices, and an outer region of mean unidirectional flow. In addition to the burst process, the interactions between these two layers result in an intermittent shedding of vortices from the lee of obstacle clasts into the outer zone (Kirkbride, 1993).

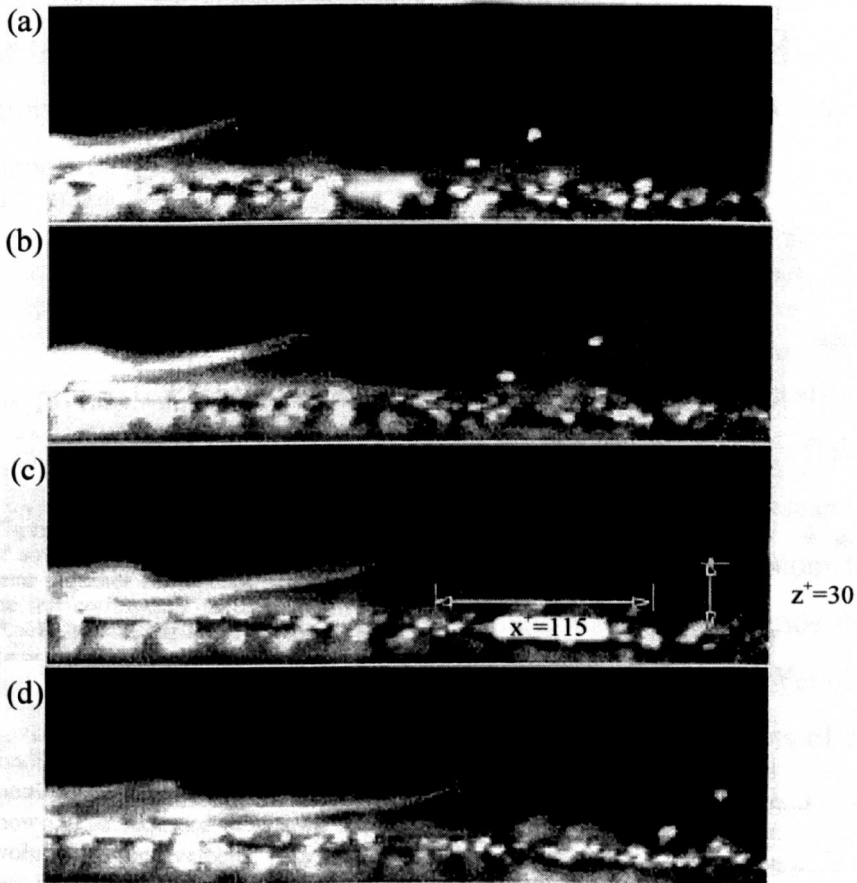


FIGURE 2.8: sequence of images of particle-shear layer interaction. Sand particles ( $220\mu\text{m}$ ) are ejected at a distance of about 100 to 200 wall units ( $x^+=x u^*/\nu$ ,  $z^+=z u^*/\nu$ ) downstream from the shear layer (from García *et al.*, 1996).

Laboratory observations of particle entrainment using flow visualisation and turbulent measurement techniques have yielded information on the role of the coherent turbulent structures on sediment transport. On smooth surfaces, particles immersed within the viscous sublayer tend to be sorted in the spanwise direction, and collect along low-speed streaks of the flow (Niño and García, 1996). In the near-wall region, intermittent shear layers lift particles lying on the channel bottom into the flow (García *et al.*, 1996) (Figure 2.8). Within rough beds, hiding effects between grains tend to prevent the entrainment of particles with sizes finer than that of the roughness elements. The roughness elements also tend to retard the motion of the shear layers. As a result, the ability of the flow to entrain particles is reduced; and hence the ability of particles to deposit is increased.

Fine particles tend to move within the interstices of the roughness elements, and their trajectory is mainly controlled by the geometry of the bed protrusions. Some fines are entrapped within the lee-side of coarse grains (Carling, 1984), and are intermittently introduced into the gravel void space by turbulent sweeps, as well as gravitational settling. Einstein (1968) reported that pore size does not influence the quantity of particles deposited into the bed per unit bed surface.

#### 2.2.1.5 Summary and conclusion

The process of deposition is mainly controlled by gravity, near-bed hydraulics and grain mechanics. Fine particles of density larger than that of the fluid tend to fall towards the bed at velocities that depend on particle density and shape, and on the surrounding fluid's viscosity. Shear forces generate eddies and random fluid motions which can interact with the fine particles motions and counterbalance fall velocities. Transported fines can collide against the bed and be re-entrained or get clogged within bed pores. The level of influence of these phenomena on the process of fine sediment deposition depends mainly on the size of the fine particles.

## 2.2.2 Relative influence of gravity and turbulence.

### 2.2.2.1 Introduction

When fine particles are too coarse to pass through the bed surface, there is no possible deposition. Considering the situation where fine particles can freely deposit through a gravel bed surface, the relative effects of gravity and turbulence determines whether a fine particle deposits into the bed or not.

Fine sediment particles can be divided into three groups in terms of their response to fluid turbulence. The first group includes the heaviest particles, for which transport and deposition is dominated by gravity. These particles are practically not affected by turbulence. Second is the so-called Stokes range, where particles have a turbulent diffusion coefficient  $\Gamma$ , nearly equal to that of the fluid  $\epsilon$ . These particles follow almost exactly turbulent fluctuations, and the effects of gravity on the particles are negligible. The third, or intermediate, size group coincides more or less with the sand size range, and is the one that usually has been of primary concern in suspended sediment transport theories (Jobson and Sayre, 1970). It is affected significantly by both gravity and turbulence, thus its response in terms of entrainment, transport or deposition can vary significantly with local hydrodynamic conditions.

### 2.2.2.2 Deposition dominated by gravity

When the weight of a fine particle is sufficiently large compared to the level of turbulence that surrounds it, it is hardly affected by the turbulent flow fluctuations and its vertical velocity component is nearly the same as in still water. This condition can be characterised by the parameter  $w^*$ , ratio of the fall velocity  $w_s$  (i.e. maximum vertical velocity reached in still water at  $t^\circ=20^\circ\text{C}$ ) and the shear velocity  $u^*$ . The analysis of Camp's experimental data, concerned with sedimentation in settling tank, suggests that this group is composed of particles with fall velocities such that  $w^* > 5$  (Owen, 1969). From the results a random walk model, Hoyal *et al.* (1995) have proposed  $w^* > 1$ .

The deposition rate of sediment is usually represented by a vertical flux of discrete elements, defined as the mass of solids passing through or settling on a unit

surface, per unit time. In the case of gravity-dominated deposition (and open-work gravel), it is given by:

$$\Delta = C_s w_s \quad [2.4]$$

where  $\Delta$  is the deposition rate ( $\text{kg}\cdot\text{m}^{-2}\cdot\text{s}^{-1}$ ) and  $C_s$  the average concentration of the material passing through a given surface area ( $\text{g}\cdot\ell^{-1}$ ).

Hazen (1904) has used [2.4] for describing sedimentation in a settling tank. In gravel-bed rivers, relatively large fines undergo little advection and deposit quickly after being released into the bed surface, provided their size is sufficiently small to pass through the bed surface pores. Under low-flow conditions, this can result in gravel-beds being filled and eventually covered by fines immediately downstream of a source (§3). However, most of the deposition of fines in real rivers occurs during large flows. These generate sufficient levels of turbulence to influence the settling behaviour of even the coarsest fines (sand or granules) and to produce high transport rates, which results in high deposition opportunities over large reaches of the river. Deposition is necessarily influenced by turbulence in these highly turbulent conditions. For finer particles (e.g. fine sand, silts), the degree of turbulence present in gravel-bed rivers, even at low flow, has an important effect on the depositional behaviour.

### 2.2.2.3 Deposition influenced by both gravity and turbulence

#### 2.2.2.3.a Probability of deposition

Several authors have found a linear correlation between the near-bed suspended sediment concentration of fine particles  $C_b$  (or alternatively the average concentration  $C$ ), and the deposition rate  $\Delta$  (e.g. Carling, 1984; Alonso *et al.*, 1988; Fletcher *et al.*, 1995). This has often been written in the following form:

$$\Delta = C_b w_s P_d \quad [2.5]$$

where  $w_s$  is the average terminal fall velocity of the fine particles ( $m.s^{-1}$ ) and  $P_d$  is a dimensionless factor accounting for the probability of deposition (e.g. Einstein and Krone, 1962; McCave and Swift, 1976).

Einstein (1968) studied the deposition of silt particles in coarse beds. He assumed the existence of a theoretical plane of demarcation near the surface of the bed below which particles cannot be affected by near-bed turbulence. If the near-bed concentration  $C_b$  is measured at this level, then the probability  $P_d$  has to be 1 as the fall velocity of the fine particles is by definition no longer affected at this plane's level. This theory has the advantage of making sure that re-suspension can not affect the results, as it cannot happen once particles has passed through the plane of demarcation. However, velocity profiles over porous beds extend into the surface layer by a certain distance  $\Delta z$ , that can reach up to 0.7 times the equivalent roughness height of the bed (Bayazit, 1976). Thus, in practice, the application of Einstein's theory poses experimental and practical problems, as it requires measurement of sediment concentrations: (1) within bed surface pores; and (2) at a level which is in general difficult to determine because of the turbulent instabilities.

Carling and McCahon (1987) measured a coefficient  $P_d$  close to 0.6 with particles finer than 2mm in a 4 to 11m-wide cobble-bedded river ( $d_{50}=83mm$ ). Other authors have proposed general expressions for the parameter  $P_d$ . In the context of smooth beds, Krone (1962) studied shoaling processes in estuaries and proposed that the probability of deposition  $P$  be given by:

$$P_d = 1 - \frac{\tau_b}{\tau_{cd}} \quad \text{for } \tau_b < \tau_{cd} \quad [2.6]$$

where  $\tau_b$  is the bed shear stress and  $\tau_{cd}$  the critical shear stress for deposition ( $P=0$  when  $\tau_b \geq \tau_{cd}$ ). Critical shear stress for deposition was described as equal to that for erosion. McCave and Swift (1976) adopted a similar view for the deposition of fine-grained sediments in the deep sea, but included other effects than that of shear in the expression of  $P_d$ , i.e. organic resuspension, irregularities on the bed and occasional erosion by large eddies (a phenomenon characteristic of sediment transport in the deep sea). However, no explicit formula was given for any of these three parameters. Another study concerned

with deposition in estuaries (Uncles *et al.*, 1985) proposed an expression based this time on flow velocities i.e.:

$$P_d = 1 - \frac{U^2}{U_{cd}^2} \quad \text{for } U < U_{cd} \quad [2.7]$$

where  $U$  is the mean flow velocity and  $U_{cd}$ , the threshold current velocity for deposition, which can be determined from Hjulström's curves for example.

In the case of rough beds, Carling (1984) examined the siltation of a gravel-bed test section in a flume. Proportionality was found between the mean deposition rate over the test section  $\Delta_{ts}$ , measured as the difference between the input and the output of fine sediment, and the initial (upstream) sediment concentration  $C_0$  ( $0.01 \text{g} \cdot \ell^{-1} < C_0 < 10 \text{g} \cdot \ell^{-1}$ ). It was proposed that the constant of proportionality represents an average exchange velocity  $w_s'$  across the 'zero' velocity plane between the flow and the gravel void space, i.e.:

$$\Delta_{ts} = C_0 w_s' \quad [2.8]$$

The probability  $P_d$ , defined as the ratio between  $w_s'$  and  $w_s$  was close to 0.6. However, this analysis was not extended to local near-bed sediment concentrations and deposition rates.

#### 2.2.2.3.b Influence of diffusion

The suspended load can be defined as the group of transported particles which remain within the flow, having no contact with the bed for significant fractions of time. Turbulence has a diffusive effect on suspended particles. This effect can be quantified by means of an eddy viscosity (or turbulent diffusion) coefficient, which allows to relate sediment fluxes to local concentration gradients (i.e. Boussinesq's assumption, 1896). Camp (1943) proposed that the variations of sediment concentrations due to deposition can be expressed at time  $t$  as a function of the ratio  $w^*$  and a Peclet number for

sedimentation  $Pe_s = w_s h / 2 \varepsilon$ . Deposition rates were inversely related to  $Pe_s$ , i.e. deposition decreases with increased turbulence.

Dobbins (1943) in his study on sedimentation in settling tanks, suggested that the deposition rate at the bottom of the tank is equal to difference between the flux due to the fall velocity and the pickup rate of fine material from the bottom by turbulence i.e.:

$$\Delta = w_s C_{(y=0)} + \varepsilon_z \left( \frac{\partial C}{\partial y} \right)_{(y=0)} \quad [2.9]$$

where  $\varepsilon_z$  is the vertical diffusion coefficient, assumed equal to that of the fluid ( $\beta_d=1$ ). For a given type of sediment, the pickup rate depends only on the characteristics of the flow and is thus constant in steady uniform flow conditions.

Jobson and Sayre (1970) combined the previous idea to that of the probability of deposition described in 2.2.2 and proposed that the rate of transfer from suspension to the bed be given by:

$$\Delta = C w_s P_d + \Gamma_{sz} \frac{\partial C}{\partial y} \quad [2.10]$$

where  $\Gamma_{sz}$  is the turbulent mass transfer coefficient of the fine sediment at the distance  $z$  above the bed.

Lastly, Sayre (1968) added an entrainment term  $E$  to the second term of the latter equation in his study on silt dispersion.  $E$  was defined as an average local entrainment rate, product of the amount of fines in local storage per unit area of bed surface and an entrainment rate coefficient. Similar approaches were used by Ouillon and Le Guennec (1996) for a 2D suspended sediment transport model and by Teisson (1997) for a cohesive sediment transport equation. Ouillon and Le Guennec defined the entrainment rate as the product of the fall velocity and an equilibrium reference concentration, as that defined by van Rijn (1984). Teisson indicated that entrainment formulae generally take the following form:

$$E = M \left( \frac{\tau_b}{\tau_{ce}} - 1 \right) \quad \text{for } \tau_b > \tau_{ce} \quad [2.11]$$

where  $M$  is a parameter depending on the bed properties, and  $\tau_{ce}$  the critical shear stress for sediment entrainment.

### 2.2.2.3.c Spatial deposition

Deposition rates into porous beds are related to the concentrations of sediment transported above the bed. Mass balance constraints imply that as fines particles deposit, the concentration decreases with distance downstream, which in turn implies that deposition rates also decrease with distance downstream. Downstream sorting of sediment has commonly been described as an exponential function of distance from a point source.

Einstein (1968) established both analytically and experimentally that the concentration of silt particles depositing into a gravel mixture in a recirculating flume follows an exponential decay against time. It was found that the decay rate depends on the fall velocity of the particles  $w_s$ , the water depth  $h$  and the ratio between near-bed and average concentrations  $r$ . This implies that the concentration decays with distance from a point source in a river channel. Applying Equations [2.5] and [2.6] to Einstein's formula, Stow and Bowen (1980) derived the following sedimentation formula, which gives the deposition rate as a function of distance:

$$\frac{\Delta}{C_0 p'} = f(D) \exp(-Xf(D)) \quad [2.12]$$

where  $C_0$  is the sediment concentration at the source ( $\text{kg.m}^{-3}$ ),  $p'$  is a factor that accounts for other influences than that of shear on deposition ( $P_d = p'(1 - \tau/\tau_c)$ ),  $f$  is the function defined as  $f(D) = w_s(1 - \tau/\tau_c)$  and  $X = p'x/(hU)$ . Carling (1984) studied some of the properties of the probability of deposition  $P_d$  by comparing experimental data to an expression similar to [2.12].

## 2.2.2.4 Deposition dominated by turbulence

The Stokes range includes the particles for which gravitational effects are negligible on transport and deposition. These particles are typically finer than 50 to 100 $\mu\text{m}$ . Above 1  $\mu\text{m}$ , inertial effects are still significant and molecular diffusion is negligible. The dominant mechanism is the flow field fluctuations in the vertical direction. On smooth walls, particles are propelled by eddies from the main flow to the wall, through the viscous sublayer. A similar, eddy-based approach can be used for rough surfaces, or a two-stage method combining turbulent diffusion to the roughness layer and deposition processes inside it (Oron and Gutfinger, 1986).

Inertial effects become negligible approximately below 0.3 $\mu\text{m}$ , i.e. in the clay size range, and particles are then transported and deposited mainly by turbulence and molecular (or Brownian) diffusion. The latter is influenced by the particle molecular diffusivity  $D_m$ . For rough surfaces, the particle settling velocity is proportional to  $u^*$  and to the Schmidt number  $Sc = \nu / D_m$  to the power  $-2/3$  (Fernandez de la Mora and Friedlander, 1982). Electrostatic forces can also influence the deposition of very fine particles (Tien, 1989).

Very fine material like silts and clays often have cohesive properties. As cohesive material is transported, the characteristics of the particles, including their settling velocity, change. This is mainly due to processes of aggregation of particles, or flocculation. The rate at which flocculation takes place is influenced by the nature of the flow. It is usually computed indirectly through the dependency of the settling velocity on concentration (Teisson, 1997), i.e.:

$$w_s = k_f c^{n_f} \quad [2.13]$$

where  $k_f$  and  $n_f$  are two characteristic parameters. Mixing enhances contacts between individual particles, and hence the speed of flocculation. Shear stresses induced by velocity gradients tend to limit the size to which particles can grow.

The deposition of particles of the Stokes range is inhibited by infrequent contacts with the bed surface (Lisle, 1989). At the surface of the rough wall, the fluid flows

around the individual protrusions, but significant quantities can pass into the bed through turbulent diffusion or as a result of local hydraulic conditions. The lagrangian model of Hoyal *et al.* (1995) indicates that particles of the order of tens of microns in size tend to settle faster than predicted by Stokes' law. The infiltration of important quantities of cohesive sediment can stick together the individual components of a gravel bed, and increase the value of the critical shear for bed mobilisation and sediment flushing (Schälchli, 1995).

### **2.2.3 Hydraulics, sediment transport and deposition**

#### **2.2.3.1 Transport mode and size selectivity**

Deposition is to a large extent related to sediment transport. Bedload and suspended load particles deposit into gravel-beds in different ways as their behaviour in relation to the bed surface and near-bed turbulence is different.

Several authors have reported high deposition rates of bedload particles in gravel beds (Sear, 1993; Lisle, 1989). Even if it represents a short-lived supply, the fact that the bedload is transported close to the bed and that it comes regularly into contact with the bed surface gives it a great probability of deposition. In three streams of northern California, Lisle measured that bedload particles, which were in the size range 0.25mm-2mm, accounted for 70 to 78% of infiltrated sediments. The finest fractions of bedload, i.e. medium sand in this case, deposited in priority (also Beschta and Jackson, 1979; Frostick *et al.*, 1984). The accumulation efficiency, i.e. the ratio between accumulation and transport was also highest for medium sand in two out of three rivers. Lisle argued that this occurred because fine sand was abundant in the sediment load and large enough to be in intermittent contact with the bed, and yet small enough to pass through small interstices. Similarly, Beschta and Jackson's (1979) flume experiments indicated that particles transported 10mm above the bed had an average size of 0.5mm, whereas matrix fines had a mean diameter lower than 0.3mm, suggesting size selectivity towards medium sand.

Deposition of substantial amounts of suspended sediments into gravel beds have been reported from laboratory investigations (e.g. Einstein, 1968), even at low

concentrations (Carling, 1984). However, suspended sediment tend to deposit less than bedload because of its lower mass, and hence its lower fall velocity. Large eddies that form in the outer layer of shear flows prevent suspended particles from reaching the near-bed area. The fact that the suspended load is always present within the water body unlike bedload which is transported over a certain threshold, and that it may account for 80 to 95% of the total solid load transported during storms in disturbed watersheds, does not compensate for this difference (Lisle, 1989).

Parker (1995) proposed an equation of mass conservation of suspended load relatively to dispersion, infiltration and resuspension of uniform sand in a uniform gravel bed, which reads:

$$\frac{\partial}{\partial t}(hC) + \frac{\partial}{\partial x}(hUC) = w_s[p_a \rho E_s - (1 - p_{at})rC] + HD_d \frac{\partial^2 C}{\partial x^2} \quad [2.14]$$

where  $C$  is the depth-averaged concentration of sand ( $\text{kg.m}^{-3}$ ),  $h$  the flow depth,  $U$  the depth-averaged flow velocity,  $p$  the fraction of the available pore space of the gravel that is occupied by sand ( $p=0$  for open-work gravel and  $p=1$  for complete pore filling),  $p_{at}$  an effective value of  $p$  near the top of the active layer,  $E_s$  a dimensionless entrainment rate of sand into suspension that would prevail if the bed was completely covered by sand,  $r$  a coefficient such that  $rC$  is the near-bed sand concentration (related to  $w_s/u^*$ ) and  $D_d$  the longitudinal dispersion coefficient of the suspended sediment.

Equation [2.14] considers that the variation of the quantity of sand present in a given volume of the water column is equal to the rate of downstream advection of suspended sediment, plus the mass of sand entrained from the active layer minus the rate of deposition of sand and the rate of longitudinal dispersion. This is similar to the approaches developed by Dobbins (1943) and Jobson and Sayre (1970) ([2.9] and [2.10]).

### 2.2.3.2 Hydraulic controls

Different point of views have been raised regarding the effect of bed shear stress and turbulence on depositional processes through porous beds.

Formulations by Krone (1962), McCave and Swift (1976) and Uncles *et al.* (1985) support the idea that bed shear stress exerts a negative influence on deposition (§2.2.2.3). This is confirmed by Sear's (1992, 1993) field measurements at three spawning riffle sites of the North Tyne river in Northern England, which indicate that suspended sediment infiltration rates correlate negatively with local shear stress for relatively low discharges. It is argued that high shear stresses keep the suspension clear of the streambed by resuspension. Similarly in non-permeable traps installed on the bed of Turkey Brook, Frostick *et al.* (1984) have measured significantly lower deposition rates on one part of the channel where a gravel bar concentrated the flow near the left-bank, resulting in higher shear velocities. Lastly, Beschta and Jackson (1979) note on the base of two experiments a decrease in deposition rates (25 to 15%) with increasing Froude number (0.8 to 1.05), caused by increasing winnowing taking place as turbulence penetrates deeper into the bed in supercritical conditions.

Other researchers have argued that hydraulic controls are of secondary importance. Carling (1984) found no correlation between shear stress and deposition rates. The deposition rates measured for individual classes of grain size, as the difference between input and output of sand in the flume, varied insignificantly with water depth, bed shear stress, particle Reynolds number ( $Re^* = u^* d / \nu$ ) and Froude number. Schälchli (1995) found that increasing Shields stresses (i.e. bed shear stress non-dimensionlised by the immersed specific weight  $\gamma_s^*$  and the sediment size) and subsequent higher turbulent fluctuations increased deposition slightly. This influence, however, was described as small compared to other parameters like sediment concentration, bed material size distribution, hydraulic gradient or water temperature. Einstein's experiments (1968) in a re-circulating flume found almost no influence of the mean flow velocity on the temporal decay rate of silica flour particles (between  $3.5\mu$  and  $30\mu$ ) over a coarse bed.

#### **2.2.4 Summary**

The ability of fine particles to deposit through a bed surface depends mainly on the relative size and sorting of sediments. The presence of a coarse and well-sorted bed surface allows in general the fines to penetrate freely into the bed. In that case,

deposition is primarily related to the fine sediment concentration as, all other parameters being equal, the concentration increases the quantity of fines moving into positions that make it eligible for deposition. The fines settling behaviour is also influenced by the relative influence of gravity and turbulence, which can be represented by the parameter  $w^* = w_s / u^*$ . Three ranges of particle size can be defined using  $w^*$ , i.e. gravity-dominated, intermediate and Stokes range. For the first two ranges, the fines deposition rate  $\Delta$  depends on the type of sediment transport, the reach morphology, local hydraulics and other parameters, which are in general grouped in one single factor  $P_d$ .  $P_d$  has been argued by several researchers to depend mainly on bed shear stress. Bedload particles, for which gravitational influence dominates, tend to undergo size-selective deposition towards finer particles when transported over porous beds. Deposition of particles of the Stokes' range, which are more sensitive to fluid displacements, is hindered by comparatively lower fall velocities. However, some particles get trapped in lee eddies between roughness elements, and are propelled into the bed by turbulent sweeps. Very fine particles get deposited through turbulent diffusion or mass transfer processes.

After being deposited, fines reaching the interface between the bottom of the surface layer and the top of the substrate become available either for suspension at high flow rate, or for infiltration (Milhous, 1973). As the influence of the main flow becomes secondary, the relative size of the fine particles and the bed pores and the influence of intergravel flow determine where infiltrating fine particles get temporarily immobilised within the bed.

## **2.3 Fine sediment infiltration and re-suspension**

### **2.3.1 Introduction**

Processes of deposition, infiltration, re-suspension and transport of fines form a continuum. Each of them represents one aspect of the interactions of a gravel-bed river with its fine sediment load. These phenomena interact with each other: the quantity of fine sediment transported influences directly the deposition rate, and the depth at which fines infiltrate has an effect on the amount of particles re-suspended, etc... Therefore, although these subjects are not directly related to the present study, the description of the

processes of infiltration and re-suspension forms a necessary complement to investigations on deposition.

### 2.3.2 Infiltration patterns

#### 2.3.2.1 General remarks

Infiltration refers to the downward movement of fine particles through the bed's subsurface. This process concerns particles that have previously deposited in the bed. These particles are referred to as matrix sediments. Matrix sediment is normally derived from both suspended and bedload, in proportions that vary from one river to another. Two main types of infiltration patterns tend to occur:

(1) The finest sediments (clay, silt or very fine sand for example) tends to seep through the gravel and deposit at the base of the permeable layer, filling the pores from the bottom up and leaving the upper layers of gravel relatively clean (Einstein, 1968): this is generally referred to as *siltation*.

(2) Coarser sediments (medium or coarse sand for example) tend to remain close to the surface forming a seal, thus preventing any further siltation until it is flushed during a flood event (Beschta and Jackson, 1979): this phenomenon is called *bed clogging* or *sealing*.

The relative size and sorting between framework and matrix sediments (§2.2.1.2) has thus a key role in the infiltration process. Frostick *et al.* (1984) have established that there is an inverse relation between the mean diameter of the sub-surface and that of the infiltrated fines. Additional processes, like *interstitial flows*, which are commonly observed in pool-riffle sequences, and bed surface *winnowing*, where near-bed turbulence maintains the bed surface clear of fines over a certain depth, can also have a significant influence (§2.3.3).

#### 2.3.2.2 Siltation

Siltation describes the process whereby fines can freely infiltrate through the bed pores. Matrices deposit at the base of the bed, filling most of the pore space and leaving

only the bed surface free of sand. The filling of a porous bed by siltation is generally a rapid process, and it typically occurs in rivers featuring well-graded framework gravel and fine sands or silt (Carling, 1984). Siltation is often associated with low flows and small storm events (Lisle, 1992), or with receding flows if the bed is not clogged. Most silting particles are derived from suspended load scoured from upstream pools and recirculation zones (§2.1), and from bank erosion and drainage ditches (Frostick *et al.*, 1984). Clay particles (1µm-diameter or less) are more likely to deposit in the top layers of the bed rather than at the bottom because of their cohesive properties (Einstein, 1970).

The siltation rate is equal to the deposition rate as long as the bed is not already filled with matrices. Several authors have found a direct relationship between the siltation rate and the suspended sediment concentration (Einstein, 1968; Alonso *et al.*, 1994). Once the bed is filled, the siltation rate falls to zero as incoming particles get winnowed away from the bed surface. Winnowing tends to prevent the deposition of suspendible fractions over a depth of approximately  $0.5D_{90}$  (Lisle, 1989; Carling, 1984; Beschta and Jackson, 1979) ( $D_{90}$  refers to the 90<sup>th</sup> percentile gravel sediment size). In cases of coarse and well-sorted bed armour layers, sub-surface matrices can also be winnowed away (Lisle, 1989).

Siltation represents an important threat to *salmonidae* ova and alevins (Adams and Beschta, 1980; Frostick *et al.*, 1984). This threat is increased as the interval between high flows is greater, because more silts and very fine sands accumulate in the bed during the long low-flow periods.

### 2.3.2.3 Clogging

Gravel-bed rivers normally exhibit a coarser surface layer than the sub-surface gravel, which can impede particles that have deposited from infiltrating further. Bed clogging occurs as a result of infiltrating particles being caught in bed pores close to the top of the subsurface. This process in turn impedes further infiltration and thus reduces the rate of accumulation of fines.

Bed clogging tends to occur when the overlap between the grain size distributions of bed and matrix particles is sufficiently important (§2.2.1.2). Alonso *et al.* (1994) attribute the clogging process to the formation of drapes, i.e. the accumulation of

small groups of matrix particles too large to seep through bed pores in the near-surface layers of the bed (also Frostick *et al.*, 1984). Once coarser fines are filtered out by gravel, they in turn filter out smaller fines, which eventually, after sufficient accumulation, leads to the formation of a bed seal.

Bed seals typically form after large flows that can entrain the bed surface layer. The material leading to the formation of bed seals is usually derived from bedload particles, like coarse sand, but granules and small pebbles can also be found. The maximum depth of infiltration of a bed seal ranges typically between  $2.5D_{90}$  and  $5D_{90}$  (Beschta and Jackson, 1979; Diplas and Parker, 1992). In general, the seal penetrates deeper with finer matrix material and larger bed shear stresses. The later phenomenon is due to the fact that turbulence offers more opportunities for particles deposited near the surface-subsurface interface to infiltrate deeper into the bed, exactly like vibrations facilitate the passage of sediment particles through sieves. The thickness of the seal depends on the depth at which it is formed, on the matrix size, on the gravel composition and on the magnitude of the interstitial flow, should it exist (Alonso *et al.*, 1994). It is typically  $2.5D_{90}$ - to  $3.5D_{90}$ -thick (Beschta and Jackson, 1979; Lisle, 1989). The quantity of fine particles clogged into gravel beds increases with the Froude number at relatively high transport rates, but is not influenced by any other flow parameters such as average bed shear stress, unit stream power or Reynolds number (Beschta and Jackson, 1979; Diplas and Parker, 1992).

### **2.3.3 Influence of interstitial flow on deposition and infiltration.**

Interstitial flows are displacements of fluid occurring within the pores of the gravel framework. At the bed surface, these flows can significantly interfere with fine particles, and either enhance or inhibit deposition. Within the bed, they can dislodge matrix fines and cause deeper infiltration or, more rarely though, re-suspension.

The presence of an uneven bed geometry can create pressure differentials leading to the presence of interstitial flows referred to as convective currents. Flow convection is typical over a bedform as a result of the reduction in the main flow's cross-sectional area. Increased pressure directs the flow towards the bed and into the bed pores on the upstream face. This results in a downward interstitial flow, which tends to keep the bed

clear of fines in an area where *salmonidae* commonly spawn (Lisle, 1989). However, this flow can also entrain air into the bed, resulting in unsaturated conditions and air accumulation in large pores. This can possibly have a negative effect on *salmonidae* ova and alevins (van't Woudt and Nicolle, 1978)

This downward interstitial flow is subsequently upwelled. It converges towards an area located between the crest and the trough on the downstream face of the bedform as a result of the cross-sectional expansion and subsequent water suction. Carling and Glaister (1987) have argued that this upwelling is responsible for inhibited fines penetration over the top of river bedforms. Under certain conditions, this can change the infiltration pattern (e.g. from siltation to clogging).

#### **2.3.4 Influence of high flow events**

Large flows tend to obliterate the arrangements of particles consecutive to low flow, depositional periods (Diplas and Parker, 1992) and have a major influence on the composition of gravel beds (Adams and Beschta, 1980).

Increased turbulence levels can entrain matrix fines out of the gravel framework. Fines flushing can only occur with flows that cause bedload transport or disturb the channel bed (Beschta and Jackson, 1979), and only 'suspendible' fractions tend to be flushed out. The flushing rates are largest in areas of highest shear stresses (Sear, 1993). As a result, re-suspension occurs in priority within the top layers of the bed. In terms of its impact on the bed's permeability, Schälchli (1992) distinguishes between three phases, i.e. transitional phase, flushing phase and mobile-bed phase. These phases correspond to increasing depths over which fines are flushed out of the gravel framework as bed shear stress increases.

Fine sediment deposition also occurs during and following large flow events. The large quantities of fine particles entrained provide the largest opportunities for the passage of sediment into the bed, hence the highest deposition rates (Sear, 1993). As a result, major floods generate much of the coarser, sand sized, material which accumulates within the interstitial spaces (Frostick *et al.*, 1984). Another consequence is that the size of the matrix which accumulates in winter, when most floods occur, is coarser than in summer, low-flow period.

Lisle (1989) reports that flows capable of transporting enough bedload to cause deleterious amounts of deposition of fines in cleaned gravel-beds occur only between zero and six times a year. Mobilisation of the top layers causes the infiltration of significant amounts of particles, including gravel sized, within the exposed and mobile subsurface (Sear, 1993). Areas of streambeds are commonly scoured or filled by several centimetres or more during this type of flows, although cross-sections normally maintain their same general shape and mean elevation (Lisle, 1989). Scour-and-fill is likely to affect gravel beds' composition as much or more so than the infiltration process. For example, bed scour exposes deep levels of the bed to infiltration, and as the bed subsequently fills, different levels of the bed can be filled with matrices, resulting in the constitution of deep bed seals.

Scour-and-fill poses the larger threat to *salmonidae* ova (Lisle, 1989). Bed scour exposes the eggs to the current or to matrix fines. Bed fill can reduce oxygenation and obstruct the emergence of the alevins. The danger tends to be more limited in small streams, where the effect of floods on the bed material is less than in larger rivers.

### **2.3.5 Summary and conclusion**

Fine sediment infiltration in gravel-bed rivers is characterised by two main processes i.e. siltation and clogging. Siltation represents the situation where deposited particles pass directly to the bottom of the bed. It is typical with relatively fine particles and well-sorted beds, and tends to occur in low flow conditions and over extended periods. Clogging consists of the accumulation of relatively large matrix particles during high flow conditions near the top of the sub-surface. The threshold between siltation and clogging depends mainly on the relative size and sorting coefficients of framework and matrix particles.

The accumulation of matrices within a porous bed can cause a drastic reduction in the bed's permeability. However, interstitial flows can affect significantly the infiltration patterns, for example by inhibiting the formation of bed seals. Convection currents tend to keep the bed pores relatively free of fines at the upstream side of riffles, which has important implications for the reproduction of *salmonidae*.

The occurrence of large flows has a major impact on the composition of gravel beds: large deposition rates of fines occur as a result of large transport rates, while large quantities of sediment are picked-up by turbulence and re-entrained into the main flow. This generally results in significant infiltration of the finest fractions of bedload and the re-entrainment of suspendible matrix particles. However, scour and fill processes can also affect bed composition, for example by exposing low levels of the bed directly to the flow.

## 2.4 Summary of the main points / Extended aims

Transported particles tend to settle in specific areas of gravel-bed rivers. If the particles are sufficiently fine, they become available for deposition and subsequently for infiltration. Clogging occurs if particles are caught at the top of the sub-surface, while siltation refers to an accumulation of fines from the bottom of the bed, up. Relative sediment size and interstitial flows are the main parameters which control the infiltration pattern. However, the distribution of fine particles in the bed is also influenced by major flows, which generate the largest deposition and re-suspension rates of fines, and by scour-and-fill processes.

Similar rules apply to the concept of deposition, except that these are combined with an additional element, i.e. the influence of flow velocity and turbulence. The relative influence of turbulence and gravity on a given particle decides which type of depositional behaviour it follows. Three ranges of particle size can be defined, i.e. gravity-dominated, intermediate and Stokes range. For the first two ranges, the fines deposition rate  $\Delta$  depends mainly on the near-bed sediment transport rate  $C_b$ , but also on the type of sediment transport, the reach morphology, local hydraulics and other parameters, which are in general grouped in one factor  $P_d$ . It has been argued that  $P_d$  depends mainly on the bed shear stress, but also on other parameters. Bedload particles, for which gravitational influence dominates, tend to undergo size-selective deposition towards finer particles when transported over porous beds. Deposition of suspended load particles, which are more sensitive to fluid displacements, is hindered by their comparatively lower fall velocity. However, some particles get trapped in lee eddies

between roughness elements, and are propelled into the bed by turbulent sweeps. Very fine particles get deposited through turbulent diffusion or mass transfer processes.

Overall, this review has shown that sediment deposition can take place in a wide range of situations and is influenced by a large number of parameters. However, the generally-agreed concepts that deposition is proportional to the fines concentration and the fall velocity, and that it is strongly related to shear stress, provide a good basis for research. In addition, the reported links with the type of transport (bedload, suspended load), with the structure of near-bed turbulence and with hydraulic parameters like the Froude or the Reynolds numbers, represent other possible directions for investigation.

## Chapter III

# Preliminary experiments

### 3.1 Introduction

The preliminary experiments consisted of two series of respectively five and nine tests. The general objective of these series was to prepare the main series of experiments in terms of technique used and of program of experiments. Different techniques were tested to represent the gravel framework, to release fine sediment into the flume, to measure deposition and transport rates, to catch the sediment entrained out of the flume and to measure flow velocities. In parallel, the deposition process was visually monitored, and the concept of deposition velocity was defined in order to be able to measure deposition. Some measurements were carried out to analyse the effect of two parameters, i.e. the gravel bed surface composition and the shear velocity.

### 3.2 Experiments on infiltration

#### 3.2.1 Introduction

Five preliminary tests on the process of fine sediment infiltration were conducted in an Armfield™ C4 tilting flume (Figure 3.1). The aims were: (1) to reproduce some of the main features described in previous studies on the deposition/infiltration process; (2) to observe directly the transport, deposition and infiltration of fine particles in order to get a better understanding of the mechanisms involved; and (3) to practice fine sediment infiltration modelling in a laboratory flume, test some of the equipment, and prepare the main series of experiments. The information collected was mainly qualitative, i.e. observation of the trajectory of particles and of the areas of deposition.

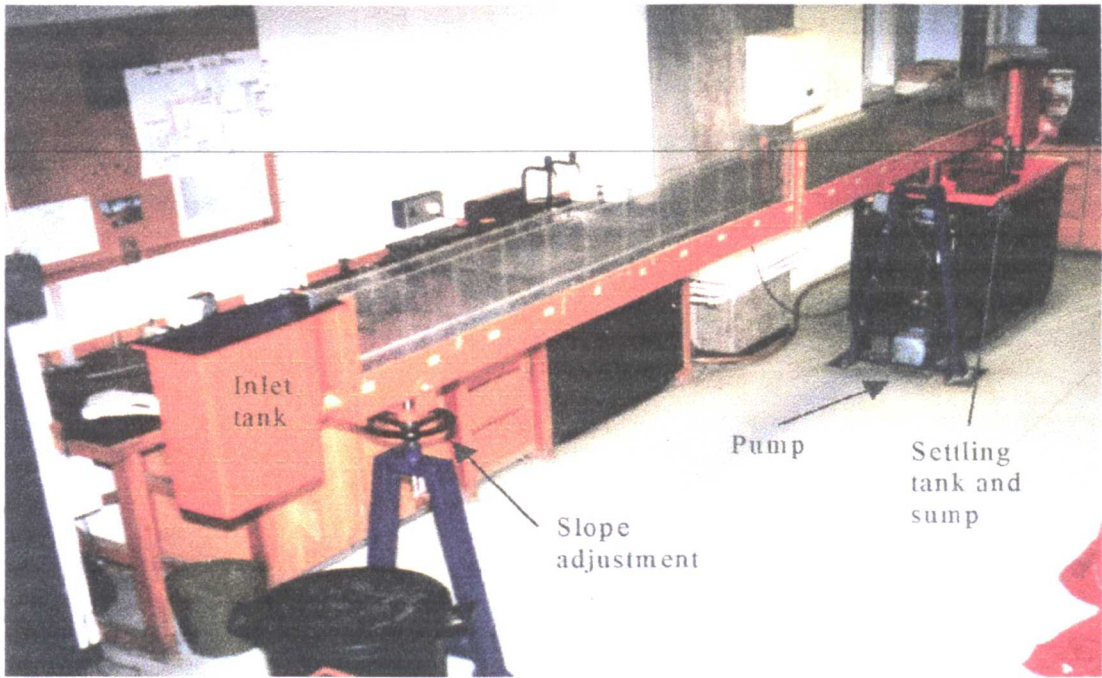


FIGURE 3.1: Armfield C4 tilting flume.

The Armfield™ C4 tilting flume is 80mm wide, 250mm deep, 5m long. The bed slope can be modified by adjusting the height of the upstream support (Figure 3.1). Transparent walls allow observations of fine sediment motion near the walls. The flume operates as a water-recirculating, sediment-feeding system. Sand is released to the water surface from an upstream tank (Figure 3.2). The sediment that is transported out of the flume is collected in a small settling tank. This tank is fitted with a V-notch outlet which allows discharge measurement. Water subsequently falls into the sump.

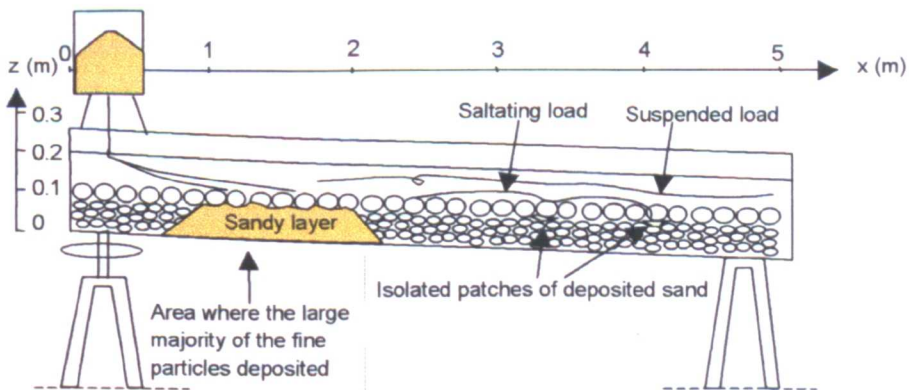


FIGURE 3.2: experimental set-up and sand deposition areas in the C4 flume

Two types of sand were tested: (1) Loch Aline sand, generally referred to as *LA-260*: a white, very well-sorted sand of mainly fine and medium grain sizes, with a median grain size  $d_{50}=260\mu\text{m}$ , and a sorting index  $\sigma=1.21$  ( $\sigma = \sqrt{(d_{84} / d_{16})}$ ); and (2) Leighton Buzzard sand, or *LB-775*: a brown-coloured, coarse sand with  $d_{50}=775\mu\text{m}$  and a sorting index  $\sigma=1.23$  (Figure 3.3). The sand was released on to the water surface near the upstream end of the flume, using a sediment hopper.

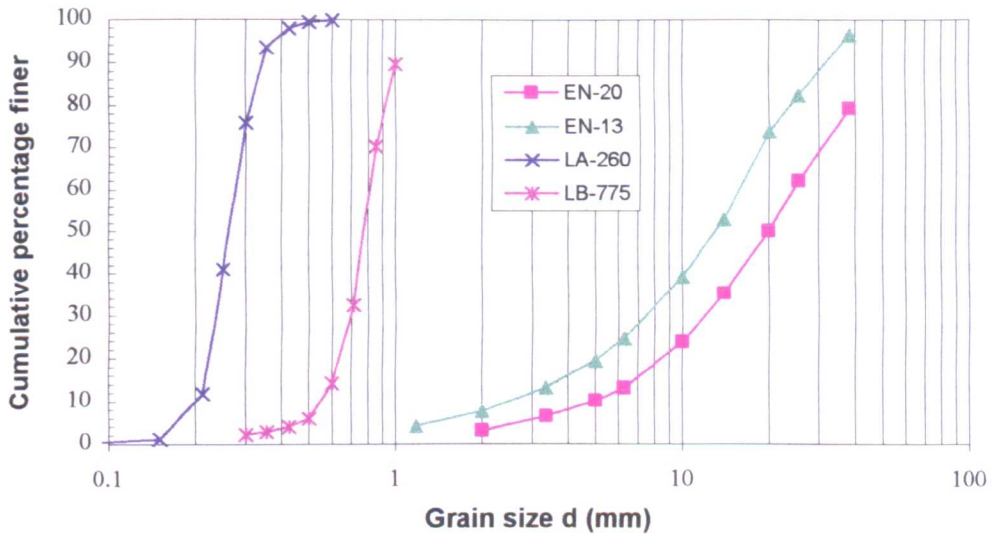


FIGURE 3.3: grading curves of sand and gravel used in the experiments on infiltration

The gravel used in this and in all the other series of experiments was natural gravel, in order to reproduce conditions as close to the prototype as possible. It was thought that the non-uniformity of the natural gravel, compared to the uniform shape of a bed surface composed of spherical particles for example, would introduce differences in the depositional behaviour of the fine particles. For example, the presence of non-uniform gaps, and in particular the exceptionally large ones, could possibly have an effect on the deposition process. The non-uniform bed surface could also affect the characteristics of near-bed turbulence.

The gravel was collected at three different locations along the River Endrick. The River Endrick is located approximately 40km N/NW of Glasgow. It is a 40km-long entrenched, meandering river, that drains an area of  $250\text{km}^2$ , mostly in the Campsie Fells, and flows into Loch Lomond (Bluck, 1971). The three locations selected (Killearn,

Ballochruin and Drymen) are located in easily accessible parts of the lower, flatter portion of the river, within a reach where the gravel bed is still quite coarse. To avoid the presence of large amounts of fine material in the gravel mixture, only material from the surface layer of gravel bars was collected.

Two types of gravel were tested (Figure 3.2). The first type (EN-20) was a combination of 50% of Drymen gravel, 28% of Ballochruin gravel and 22% of Killearn gravel. Its average size was 20mm (coarse pebbles), it was moderately sorted and slightly negatively skewed. The second type (EN-13) was only composed of Drymen gravel ( $d_{50}=13\text{mm}$  i.e. medium pebbles range). It was moderately to poorly sorted, and negatively skewed.

Experiment	Sand	Gravel	D/d	Slope	Bedforms
PE1	LB-775	EN-20	25	1/42	Flat bed
PE2	LA-260	EN-20	77	1/42	Flat bed
PE3	LA/LB mix	EN-20	33	1/83	Three pools
PE4	LA-260	EN-20	77	1/83	Three pools
PE5	LA-260	EN-13	51	1/58	Three pools

TABLE 3.1: Main characteristics of the preliminary series of experiments on infiltration.

When pouring the gravel mixtures onto the flume bed, differential settling of the finest gravel elements into the pores formed by the coarsest ones resulted in the formation of a coarser surface layer. The whole bed was 80mm thick. In all the experiments, the flow rates applied remained below the critical condition for entrainment of the finest gravel sizes.

Different ranges of parameters were tested (slope, coarse and fine sediment size, bed surface profile, input sediment) which have been summarised in Table 3.1.

## **3.2.2 Experimental observations of infiltration processes**

### **3.2.2.1 Introduction**

Most of the LA-260 and virtually all the LB-775 sand grains were too heavy to be transported over a significant distance by the flow. Only about 40% of the LA-260 sand released was transported by suspension or saltation. The rest of the fine particles settled rapidly through the main flow and were deposited into the bed, gradually filling the pores to the surface. Once one part of the bed was filled with matrix fines up to the surface, particles rolled over that part of the bed until reaching clear bed pores and depositing. Thus, the bed could be divided into two parts during the experiments: (1) an upstream part, with the surface layer (and sometimes the subsurface) filled with sand, which gradually expanded in the downstream direction; and (2) a downstream part, almost clear of fines, where only particles that had been transported by saltation or suspension could deposit (Figure 3.2). The experiments were run over a sufficiently long time to reach capacity infiltration, i.e. when the sandy layer reached the downstream end of the flume.

### **3.2.2.2 Infiltration of LB-775.**

Only one experiment (PE1) was conducted with the coarse LB-775 sand. The EN-20 gravel bed was used in this experiment. It was observed that while the sand particles penetrated through the coarser surface layer, most of them were too coarse to enter the sub-surface (Figure 3.4). When the front of the sandy layer reached a clean area of bed, a few particles infiltrated into the sub-surface, sometimes quite deeply (e.g. 40 to 60mm below the top of the 80mm-thick bed). Sand grains rapidly started to accumulate at the interface between the surface layer and the sub-surface. These grains gradually clogged the bed and reduced the opportunities for other particles to infiltrate deeply, leading to the formation of a sand seal, which acted as a barrier against further infiltration. Fine sediments sometimes accumulated above the surface, giving to the bed the appearance of a sandy bed (left part of Figure 3.4). However, protruding stones were usually not completely buried under sand (central part of Figure 3.4) and sometimes

shifted the sandy layer down (left part of Figure 3.4). In general, a large volume of unfilled pore space remained below the surface layer.



FIGURE 3.4: deposition of LB-775 coarse sand into EN-20 gravel (Experiment PE1)

The result in terms of infiltration pattern in this first preliminary experiment was consistent with previous work, as clogging occurred with a sediment size ratio  $D/d=25$ , below the minimum threshold of 30 obtained from the results of five different studies (§2.2.1.2).

During Experiment PE3 (where a mixture of LA-260 and LB-775 was released into the flume), a patch of LB-775 sand which had deposited within the surface layer 18 minutes after the beginning of the experiment began to infiltrate into the sub-surface after approximately one hour. This suggested that a newly formed sand seal could collapse soon after it had formed. Three possible phenomena were thought to cause the collapse: (1) the vibrations caused by the pump and the circulation of water in the flume; (2) the pressure caused by the weight of sand accumulating on top of the sandy layer, combined with the effect of turbulent fluctuations on this layer; or (3) the circulation of interstitial flow. Additional observations suggested that (1) and (2) were probably the dominant effects (dye tests showed no evidence of substantial interstitial flows).

This phenomenon, already studied by Frostick *et al.* (1997), supports the idea that, in real rivers, sand seals can be partially destroyed during intermediate flows (below the critical bed entrainment threshold) and on the rising limb of peak flow hydrographs, as the gravel bed particles are subjected to vibrations. This has important implications on the deposition/infiltration process, because many more fine particles can infiltrate the bed during or after these intermediate flow events as a result of the destruction of the fine sediment seal and the jostling of bed particles.

### 3.2.2.3 Infiltration of LA-260.

Four experiments were conducted with LA-260. Unlike LB-775, the finest fractions of LA-260 could be transported by saltation and suspension. Samples of transported sediment indicated average concentrations of  $2.20\text{g}\cdot\ell^{-1}$  one centimetre above the bed surface,  $1.20\text{g}\cdot\ell^{-1}$  three centimetres above the bed surface and  $0.08\text{g}\cdot\ell^{-1}$  six centimetres above the bed surface. Most of the LA-260 sand transported was transported as saltating load.



FIGURE 3.5: infiltration of LA-260 into EN-20 gravel (Experiment PE2), dominated by siltation and surface winnowing

The siltation pattern of infiltration (§2.3.2.2), where fine particles seep through the gravel and deposit at the base of the permeable layer, occurred during experiments carried out with both medium and coarse pebbles (EN-13 and EN-20). This was the main pattern of infiltration into EN-20 (Figure 3.5), as void filling reached 95% in

Experiment PE2. In this experiment, the sediment size ratio was  $D/d=77$ , above the maximum limit of 75 obtained from five studies (§2.2.1.2). However, only a few particles settled within the surface layer, where the flow velocity was sufficient to winnow the fines away. Isolated patches of sand deposited at the surface when the surface layer was locally sheltered from the flow, as in the lee of large pebbles (right-hand side of Figure 3.5). As in the case of LB-775 sand, large gravel elements protruding at the bed surface also caused the top of the infiltrated sandy layer to be locally shifted down into the sub-surface as a result of convective currents flowing underneath these obstacles. This resulted in the top of the sand layer developing a wave-shaped profile (Figure 3.5).

Experiment PE5 ( $D/d=51$ ) produced a wider variety of infiltration patterns than the other experiments. An intermediate pattern of infiltration between siltation and clogging was sometimes observed in areas where gravel was significantly finer than the average. In these areas, only a few isolated gaps would allow the fines to infiltrate into the bed. When LA-260 filled the available space located below one of these gaps, it generated a cone of deposition. If the base of this cone encountered another gap through which particles could infiltrate, another cone of deposition would be generated below the first one. Accordingly, fines should reach deep into the bed through a series of piled-up cones of infiltration (which appear at the centre-right of Figure 3.6 as a series of white oblique veins).



FIGURE 3.6: infiltration of LA-260 into EN-13 gravel (Experiment PE5). The highlighted area illustrates the phenomenon of cone-shaped infiltration.

Observations indicated that cone-shaped infiltration is typical of situations where the bed is composed of poorly-graded material and where the ratio  $D/d$  is intermediate between siltation and clogging (e.g.  $D/d \sim 40$ ).

The close observation of the movement of particles through inter-gravel voids indicated that, in siltation conditions, the grains settle rapidly and steadily along specific cascades, and can be locally diverted by coarse grains and interstitial currents, particularly within large voids. One small air bubble entrapped in a bed pore was also observed to divert the settling path of infiltrating LA-260 sand, and even to trap some of the grains. Van't Woudt and Nicolle (1978), who measured the entrapment of air within gravely mixtures resulting from water percolation, found that after 300 hours, 9% of the voids volume had been filled with air. Similar air intrusion is likely to occur in poorly graded gravel riverbeds where there is circulation of water e.g. within riffles. It is possible that where there is a significant concentration of air within the bed material, the air can act as a barrier against infiltration.

Finally, some isolated areas of the gravel bed remained totally free of fines. These areas were typically five to ten centimetres long, and separated by half a metre to a metre. This was usually due to the presence of a generally thin layer of finer gravel which prevented the fines from seeping through (e.g. centre of Figure 3.6).

### **3.2.3 Infiltration within pools.**

The settling behaviour of fine particles within a series of three artificially-created pools was observed in Experiments PE3, PE4 and PE5. The pools were 40 to 70mm deep and 0.5 to 1m long.

#### **3.2.3.1 Spatial deposition patterns.**

Deposition of LA-260 sand transported by suspension and saltation was observed in a series of three pools. The search for the main areas of deposition was complicated by the facts that little sediment was transported as far as the pools, and that most of the deposited sand silted to the bottom of the bed. However, it could be observed that more fine particles deposited in pools than elsewhere because of the lower flow velocities

encountered there. Evidence of re-circulation currents taking place within pool troughs was obtained using dye injections. Some of the transported fines deposited on the bed surface during Experiment PE5 because relatively fine gravel was used in this case (EN-13). It was observed on this occasion that pool heads were the main areas of deposition, whereas comparatively little deposition occurred over the flat sections between the pools (Figure 3.7).

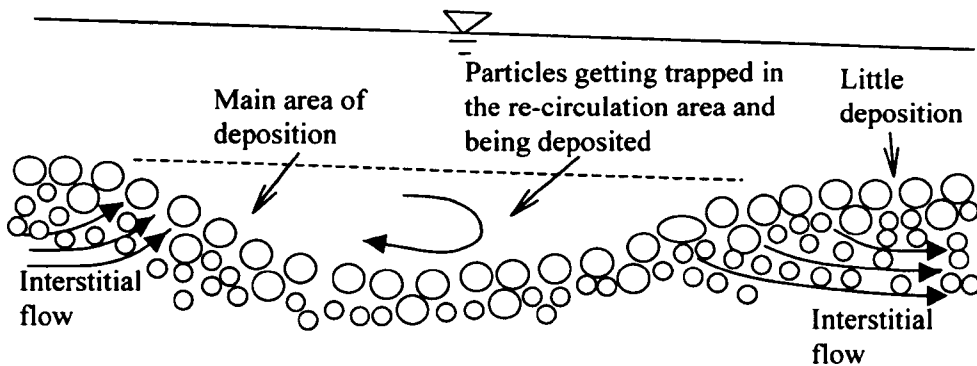


FIGURE 3.7: fine sediment deposition and flow patterns in pools

### 3.2.3.2 Influence of interstitial flows

Convective interstitial currents (§2.3.4.2) were observed between pools using dye tracers. These currents entered the porous medium at the tails of pools, and flowed back into the main water body at the head of the following pool (Figure 3.7). Some of the particles that deposited below pools were destabilised by these currents (§3.1.2.2) and infiltrated deeper into the bed. In particular, it was observed during Experiment PE3 that the bed remained free of matrix fines at the tail of a relatively deep pool, whereas other parts of the pool were filled with fine sediment. The relatively large depth of the pool induced the formation of a plunging current and resulted in a strong interstitial flow under the region located immediately downstream from the pool. Below the area of interstitial flow, 'cone-shaped' patterns of infiltration containing coarse LB-775 sand that had been dislodged from the surface layer were observed. At pool heads, deposited

fine particles were less affected by interstitial currents, possibly because of the upward orientation of the flow (Figure 3.7).

### **3.2.4 Conclusion**

The two 'classic' patterns of infiltration, i.e. siltation and sealing, have been observed in this preliminary series of experiments, as well as an intermediate one, specific to poorly graded gravel beds, where particles pass through isolated gaps through a series of piled-up cones of infiltration.

Bed clogging by sand particles occurred for a sediment size ratio of  $D/d=25$ , and was rapid. The shape of the sand seal is influenced by protruding gravel and by the bed surface geometry. Observations have confirmed that these structures are fragile, and may collapse as a result of vibrations within the gravel framework and pressure caused by the flow and the accumulation of sand. This suggests that, in rivers, sand seals can be destroyed even without bed entrainment, particularly if the relative sediment size conditions are close to the critical value between siltation and clogging.

Siltation has been observed for a ratio  $D/d=77$ . Eventually, the subsurface became almost completely filled in these conditions. Only the presence of layers of finer gravel or that of very coarse pebbles impeded siltation to occur. Air bubbles prevented a few particles from infiltrating. The surface layer remained almost free of fines, due to the winnowing of fines by turbulence.

A lot of fine particles deposited within pools as a result of the re-circulating flow taking place near the bed surface. Deposition was particularly noticeable at the pool's head. Interstitial flows taking place between consecutive pools facilitated the deeper infiltration of fines, particularly below pool tails, and impeded the formation of sand seals.

### 3.3 Preliminary experiments on deposition

#### 3.3.1 Background

This series of experiments was the first one concentrating on the deposition process i.e. the passage of the fine particles through the bed surface layer. It was carried out in an 8.60m-long flume. The aim was to study the relationship linking sediment transport and deposition through porous bed surfaces. The infiltration process, i.e the movement of deposited particles within the sub-surface, was not considered.

The initial concept of the experiments came from work by Carling (1984) (§2.2.2.3.a). Carling defined an exchange velocity of particles between the flow and the gravel void space  $w_s'$  as the ratio between the average deposition rate over the whole test section  $\Delta_{ts}$ , and the initial fine sediment concentration at the upstream end of the flume  $C_0$  (Equation [2.8]). This parameter was measured in different hydraulic and sediment size conditions. However, the association in this equation of two variables measured at different locations (between the upstream and downstream ends of the flume for  $\Delta_{ts}$ , at the upstream end of the flume for  $C_0$ ) renders difficult the physical interpretation of the parameter  $w_s'$  (Does it represent an exchange velocity of particles at the upstream end of the test section? For the whole test section?). A similar but slightly different concept was thus used in this study: the exchange velocity of fine particles was measured at any given position along the gravel bed, by considering the local near-bed concentration and deposition rate measured at this particular position.

Considering a flat and static section of an open-work porous bed, supporting uniform, 2-dimensional flow conditions, the parameter  $w_d$  ( $m.s^{-1}$ ) is defined as:

$$w_d = \frac{\Delta_b}{C_b} \quad [3.1]$$

where  $\Delta_b$  is the near bed deposition rate measured at a given point of coordinates  $x$ ,  $y$  and  $z=b$  ( $kg.m^{-2}.s^{-1}$ ), and  $C_b$  the corresponding near-bed concentration ( $g.l^{-1}$ ). In [3.1], the deposition rates and the sediment concentrations are considered near the bed simply

because a necessary condition for fine particles to deposit into the bed is to be transported in the vicinity of the bed surface. The parameter  $w_d$ , which is a ratio between a flux and a density, has the dimensions of a velocity. It represents the downward component of the velocity of the fine sediment at  $(x, y, b)$ , and is referred to in the following as the *deposition velocity*.

In practice, Equation [3.1] proves to be quite difficult to implement. On the one hand, deposition rates measured in sediment traps, like in the present study, represent the flux of particles  $\Delta$  measured at the zero-velocity level i.e. at  $z=0$ . Measurements of deposition rates at higher levels, within the non-uniform bed surface, where some of the particles are still influenced by turbulence are much more complicated, if not impossible, to carry out. On the other hand, measurements of sediment concentrations within a non-uniform bed surface are difficult because local flow conditions and constraints in terms of space for the measurement apparatus can bring a certain degree of error in the results. The measurements of  $C_b$  are thus best carried out at the bed interface. The difference in measurement level between both parameters  $\Delta$  and  $C_b$  introduces a shift in terms of near-bed concentration and deposition velocity. This shift has been approximated (Appendix 3.1) by considering the conservation of the mass transport rate of fines within the bed surface (i.e. between  $z=0$  and  $z=b$ ). It has been found that, in the present experimental conditions, it is typically three to four orders of magnitude lower than the main near-bed concentration term. Thus, the deposition velocity  $w_d$  can be expressed as:

$$w_d = \frac{\Delta}{C_b} \quad [3.2]$$

When measured over a certain surface area,  $w_d$  represents an average fall velocity of the fine particles through the bed surface over this area. It gives an indication on how easily fine particles can pass through a surface layer of gravel. If it is known for a given range of bed and flow and sediment size conditions, deposition rates can be computed directly from the near-bed concentrations and vice versa in any of these conditions.

Following a similar approach to that of Einstein (1968) (Appendix 3.1), the longitudinal variations of sediment concentration resulting from a deposition velocity  $w_d$ , can be expressed as:

$$C_{b(x)} = C_{b_0} e^{-\frac{w_d}{q} x} \quad [3.3]$$

where  $C_{b(x)}$  is the near-bed concentration measured at the distance  $x$  from the sediment release point ( $\text{kg.m}^{-3}$ ),  $q$  is the discharge per unit width ( $\text{m}^2.\text{s}^{-1}$ ) and  $r$  the constant of proportionality between depth averaged and near-bed concentrations. The combination of Equations [3.2] and [3.3] yields the equation for the spatial distribution of the deposition rate:

$$\Delta_{(x)} = C_{b_0} w_d e^{-\frac{w_d}{q} x} \quad [3.4]$$

An experimental study has been conducted to get some information on the variations of the deposition velocity against some of the parameters controlling the deposition process, e.g. the gravel bed surface composition or shear velocity. An experimental system was set up that would: (1) generate transport of fine sediment; (2) allow the fines to deposit through a surface layer of gravel; and (3) allow measurement of both transport and deposition rates.

### 3.3.2 Materials and method.

#### 3.3.2.1 Flume channel set-up

This series of experiments was conducted in a 0.75m-wide GRP tilting flume, and referred to herein as the main flume (Figures 3.8, 3.11, 4.4). The 8.60m-long main body of the flume is supported by eight transverse beams resting on a heavy jacking arrangement which allows changes in bed slope. Due to limitations in the maximum possible flow depth ( $h=130\text{mm}$ ), a relatively steep bed slope was required to reach an adequate transport capacity. The system originally allowed a maximum slope of  $\sim 1/160$  to be set, and was modified to allow slopes up to  $\sim 1/60$ .

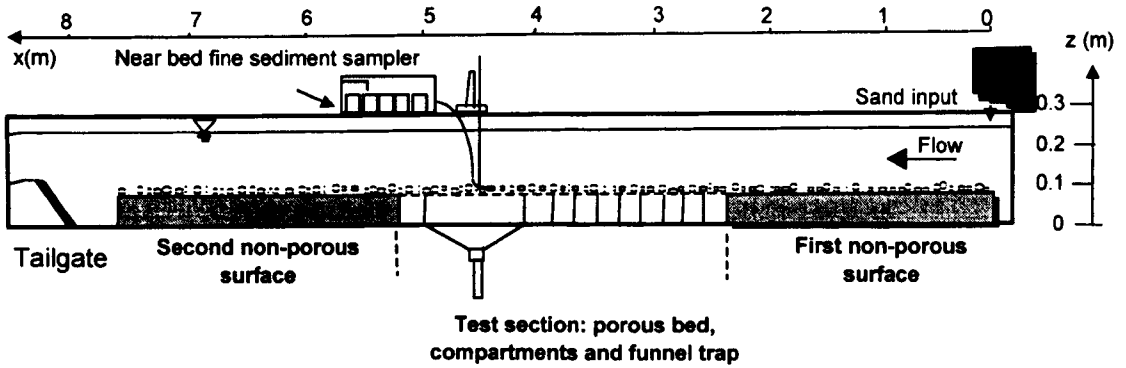


FIGURE 3.8: main flume set-up for funnel-trap experiments

The flume operates as a flow-recirculating system by way of a Myson™ MSK 150 centrifugal pump capable of delivering  $55\ell.s^{-1}$ . Water is pumped from the  $4.30\text{m}^3$  outlet sump, through a 152mm-diameter pipe, into the  $1.85\text{m}^3$  inlet tank from where it flows directly into the flume. An orifice plate fitted on the main pipe allows flow discharge measurements.

To improve the rigidity and regularity of the flume, it was lined on the base and sides with wood, resulting in a 7.75m-long, 270mm-deep and 770mm-wide channel. At the downstream and upstream ends, two large inserts of plywood ( $\sim 2.40\text{m}$  long) were fixed on the flume bed and supported a single layer of EN-20 gravel glued on their surface (Figure 3.8). Pieces of plywood were also fixed on the sides to prevent water from flowing below the inserts. These two sections acted as elements of continuity with the test section in terms of bed roughness and water depth.

Between these two sections, the test section contained a series of sediment compartments and the measurement section. The compartments were 770mm wide and consisted of 95mm-high plywood frames, overtopped by a mesh of 1mm aperture supporting a layer of gravel. The measurement section consisted of a funnel-shaped sediment trap, also covered by a 1mm-mesh supporting a single layer of gravel. The trap collected sediment depositing through the gravel surface over a  $600\times 600\text{mm}^2$  squared area. It was made of a funnel-shaped perspex base, fixed upon the underside of the flume with an aluminium frame, and leading to a graduated cylinder (Figure 3.9). Readings of

the volume of sand deposited in the cylinder were taken in general at one-minute intervals. The difference between two consecutive volume readings gave the vertical flux or deposition rate, i.e. the mass of fine sediment passing through the gravel surface per unit time and per unit surface area.

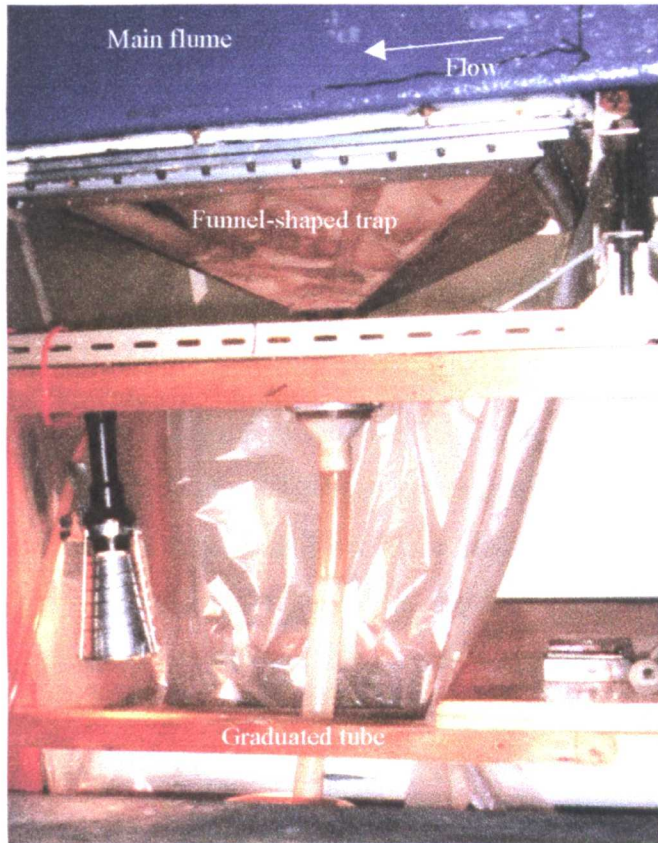


FIGURE 3.9: funnel-shaped trap and graduated tube used to measure instantaneous deposition rates of fine sediment through surface layers of gravel

### 3.3.2.2 Sediment feeder

The flume operated as a water-recirculating and sand-feeding system. A sediment feeder was installed over the inlet tank (Figure 3.10). It consisted of a 100-litre hopper, fitted with seven 50mm-diameter extractor screws operated by a variable speed drive unit. LA-260 sand was used for all experiments of this preliminary series (§3.2.1). The sand was released onto the water surface at the upstream end of the flume, over the whole flume width.

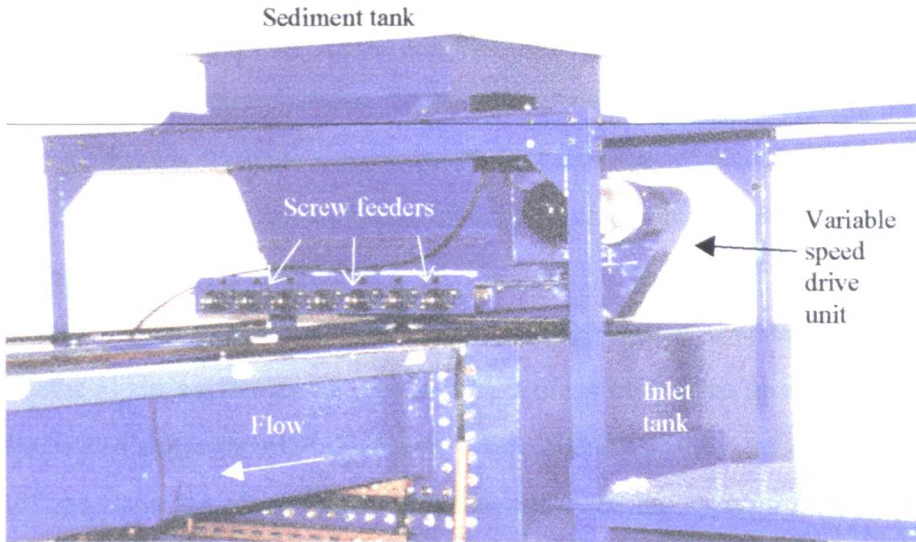


FIGURE 3.10: fine sediment feeder (upstream end of main flume)

This sediment input technique raised two questions in terms of particle settling velocities. Firstly, Jobson and Sayre (1970) suggested that the grouping effect resulting from the introduction of a concentrated jet of fine particles into water could have a significant influence of the settling behaviour of the fine particles. To minimise this effect, a series of seven cones was used to give a better spread of the fine particles across the width of the flume. Secondly, it was thought that dropping the fine particles on to the water surface could induce an additional downward velocity component, which could have an effect on the deposition velocity measurements. However, due to the length of the first impermeable bed section, the coarsest particles reached the bed well before the beginning of the test section. Thus, these particles were moving as bedload when sampled. For finer particles, the level of turbulence near the bed was sufficiently high to overcome the initial downward component. Overall, the release of the particles at the water surface is considered to have had an insignificant influence on the results.

### 3.3.2.3 Sand separator

In experimental conditions similar to that of the present study, Jobson and Sayre (1970) estimated that the length necessary to obtain equilibrium conditions of transport is  $x/h=100$ . The maximum value of  $x/h$  reached in the present study was  $\sim 75$ . A

substantial quantity of fines were thus carried through and out of the flume, into the sump. Unfortunately, the point where the sediment-laden flow plunged into the sump was located close to the pump intake. To prevent damage to the pump or clogging of the return pipe, a filtering system was designed to catch the sediment. Different systems were tested during the preliminary series of experiments, which showed that a two-stage separation process was required.

The system used operates as follows: the sediment-laden water leaving the flume is first directed against a flat frame, covered by a mesh of 100 $\mu\text{m}$  aperture (Figure 3.11). Most of the liquid seeps through the mesh, while a small amount of water and the great majority of the fines are ejected into the second part of the separator. This second part consists of a 300mm-deep mesh box and a ramp, over which the water/sediment mixture gains momentum and is projected against the mesh. As a result, all the water seeps through the mesh, and the fines accumulate on the bottom of the mesh box, below the ramp.

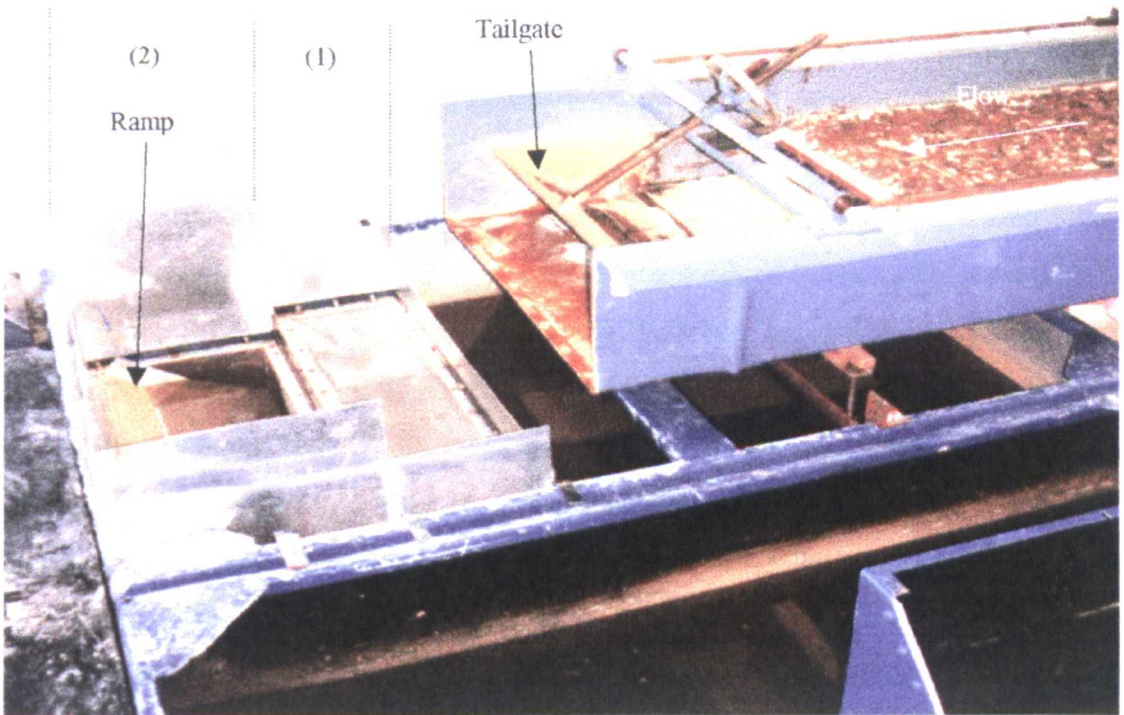


FIGURE 3.11: sand separator used to trap fine particles transported out of the main flume

The separator could accommodate up to 15kg of LA-260 sand, which was sufficient to allow releases up to 100kg of fines into the flume. After each experiment, the separator was emptied and cleaned using a high-pressure water-jet.

#### 3.3.2.4 Experimental method

A series of nine tests was conducted. The aim was to measure deposition velocities in different hydraulic and bed surface composition conditions. No distinction was made between the different size fractions present in the initial sand mixture. The flow rate was set to a maximum of  $54\ell.s^{-1}$  and bed slope at 1/142 (0.7%). Flow conditions were close to uniform 1.50m downstream of the release point. After settling through the flow, the majority of the LA-260 sand was transported by saltation (only the finest particles were continuously suspended).

Measurements were performed sufficiently far from the upstream end of the flume to allow the coarsest immobile fine particles to settle out, and to be left only with grains actively transported either by suspension or saltation. This was achieved by using a series of nine sediment compartments over a length of 1.90m before the measurement section. These compartments acted as reservoirs for the bulk of the deposited sandy layer (Figure 3.8).

To reproduce the conditions of the deposition process, a monogranular layer of natural gravel was used, which was supported by a mesh of 1-mm aperture on top of the test section. This method reduced considerably the labour required to carry the gravel in and out of the test section. There was empty space below the mesh, which raised the question of whether this would bring a different depositional behaviour that if a full gravel bed were used. In their study of fine sediment infiltration in the Turkey Brook, Frostick *et al.* (1984) found that, over a three-month period, the presence of a subsurface framework within sediment traps reduced the matrix infiltration rates to between 87% and 10% compared to control compartments which were not filled with gravel. The extent of this reduction was mainly related to the mean size of the subsurface grains, and to the formation of a clogged layer, impeding further infiltration of fine material.

However, when the subsurface gravel was large enough to let fine particles seep freely through the bed pores, its presence had hardly any effect on the accumulation rates.

In static bed conditions, almost all turbulent flow activity ceases below the top layer, which generally prevents any particle reaching this level from being re-entrained. In addition, the presence of the subsurface has only a minor influence on the pattern and intensity of turbulence taking place within the top layer. As a result, the use of a single surface layer of gravel was considered as sufficient to reproduce the process of fine sediment deposition into a (full-size) static bed.

The measurement section, where the deposition rate  $\Delta$  and the near-bed concentration  $C_b$  were measured, was located 4.60m downstream of the entrance of the flume channel. The input rate of fines was varied three to four times. This allowed study of the relation between  $\Delta$  and  $C_b$ , and of the variations of the deposition velocity  $w_d$ . Over the measurement section, a Rock&Taylor™ automatic sampler was used to measure  $C_b$ . In each experiment, about ten samples of 600ml of sediment-laden water were collected 25mm above the bed interface. Concentrations could not be measured closer to the bed because of the room required by the sampling nozzle. The samples were subsequently filtered through filter paper using a vacuum pump, oven-dried to destroy the filter paper and evaporate any remaining liquid, and finally weighed. In order to measure  $C_b$  continuously, readings were also taken at the same level using a turbidity-sensitive Partech™ - W.P.R.L. suspended solids monitor (s.s.m.). These readings were calibrated using the results of the concentrations obtained from the samples (Appendix 3.2).

The experiments were approximately 40 minutes long. Four different feed rates were tested (i.e.  $I_0 \sim 15, 30, 50$  and  $80 \text{g.s}^{-1}$ ), with  $\sim 10$  minutes spent on each feed rate. During this time, readings of the volume of deposited sediment and of the suspended solids monitor were taken every one or two minutes. Two to three samples of sediment were taken near the bed ( $z=25\text{mm}$ ), plus another three within the main flow ( $z=35, 55, 85\text{mm}$ ). As a result, about twenty-five measurements of the deposition velocity  $w_d$  could be made in every experiment.

At the end of the experiment, the volume of water retained in the test section was drained through a pipe connecting the funnel trap to the sump, the gravel surface and the sediment compartments were removed. The sand deposited in the compartments was

collected, placed in trays, oven-dried and weighed. The spatial variations of the deposition rate within the flume were derived from these results.

### 3.3.3 Results

Nine experiments were conducted (A5, A6, B1, B2, B3, C1, C2a, C2b, C3), testing eight different gravel surface compositions ranging from  $d_{50}=13\text{mm}$  to  $52\text{mm}$ . Mixtures of natural gravel from the River Endrick were used, varying from moderately to very well sorted, and having a majority of particles with a rounded shape. The main characteristics of each experiment have been summarised in Table 3.2.

The shear velocity was computed assuming a zero-plane displacement  $\Delta z$  (i.e. the distance below the bed surface at which  $U=0$ ) equal to  $0.7D_{84}$  (§4.4.1). It varied between  $0.083$  and  $0.091\text{m.s}^{-1}$ . Two of the experiments were run with the same bed and flow conditions: C2a where the gravel surface sediment was not mixed (the finest grains were placed first, followed by the largest which rested on top), and C2b where the same gravel mixture was well mixed. The aim of these two tests was to study how the size of the surface voids (larger in the case of C2a) would affect deposition for a given bed composition.

	A5	A6	B1	B2	B3	C1	C2a/C2b	C3
$D_{50}$ (m)	0.0180	0.0253	0.0182	0.0168	0.0197	0.0277	0.0131	0.0522
$D_{84}$ (m)	0.0267	0.0471	0.0279	0.0233	0.0324	0.0339	0.0210	0.0629
$\sigma$	1.54	2.07	1.54	1.46	1.63	1.24	1.68	1.22
$h$ (m)	0.106	0.106	0.119	0.119	0.120	0.121	0.119	0.120
$u^*$ ( $\text{m.s}^{-1}$ )	0.083	0.086	0.086	0.085	0.087	0.087	0.085	0.091
$w_d$ ( $\text{m.s}^{-1}$ )	0.0261	0.0206	0.0151	0.0215	0.0129	0.0259	0.0260/ 0.0245	0.0161

TABLE 3.2: main characteristics and results of the funnel-trap series of experiments (50th and 84th percentile gravel sizes, gravel sorting index, flow depth, shear velocity and deposition velocity).

In all of the experiments, a small amount of fines deposited on the initial impermeable-bed section, but the majority of the fine particles released deposited into the first four compartments of the test section. More than 80% of the fines were

deposited before the beginning of the measurement section. The particles collected in the funnel trap were 7 to 37 $\mu\text{m}$  finer than the original LA-260 sand (average 26 $\mu\text{m}$ ), as illustrated by Table 3.3.

Experiment	B4	C1	C2a	C2b	C3
$d_{50}$ deposit ( $\mu\text{m}$ )	236	228	253	231	223

TABLE 3.3: median size of the sand collected in the funnel trap during five experiments

Following Carling's (1984) method, the average deposition rates measured for a given input  $\langle \Delta_0 \rangle$  have been plotted against the initial sediment concentration  $C_0$  for each experiment. An example is shown on Figure 3.12a (all the plots can be found in Appendix 3.3). These plots confirm that the deposition rates of fines through gravel surfaces vary linearly with sediment concentration ( $r^2=0.97$  in average).

To measure the deposition velocity  $w_d$ , a measure of the instantaneous near-bed concentration  $C_b$  was required. This was obtained using a plot of the s.s.m. readings against time (Figures 3.12b), and the plot of the near-bed sediment concentrations obtained from samples against the s.s.m. readings (Figure 3.12c). The combination of the two best-fit equations obtained from these plots provided an equation relating time and near-bed concentration  $C_b$ , which was used to plot  $\Delta$  against  $C_b$  (example of computation and description in Appendix 3.2).

The results of the plots of the instantaneous deposition rates against near-bed concentrations  $C_b$  (Appendix 3.4, Figure 3.12b) indicate a linear correlation between these two variables ( $r^2=0.82$  in average). The slope of the best-fit line provides a measurement of the deposition velocity  $w_d$ . The comparatively poorer correlation between  $\Delta$  and  $C_b$  compared to that of  $\Delta_0$  and  $C_0$  case is due to the facts that: (1) the instantaneous deposition rates can be sometimes inaccurate because they are measured over relatively short periods (1 minute in general); (2) the instantaneous near-bed concentrations are measured indirectly (Figures 3.12b and 3.12c).

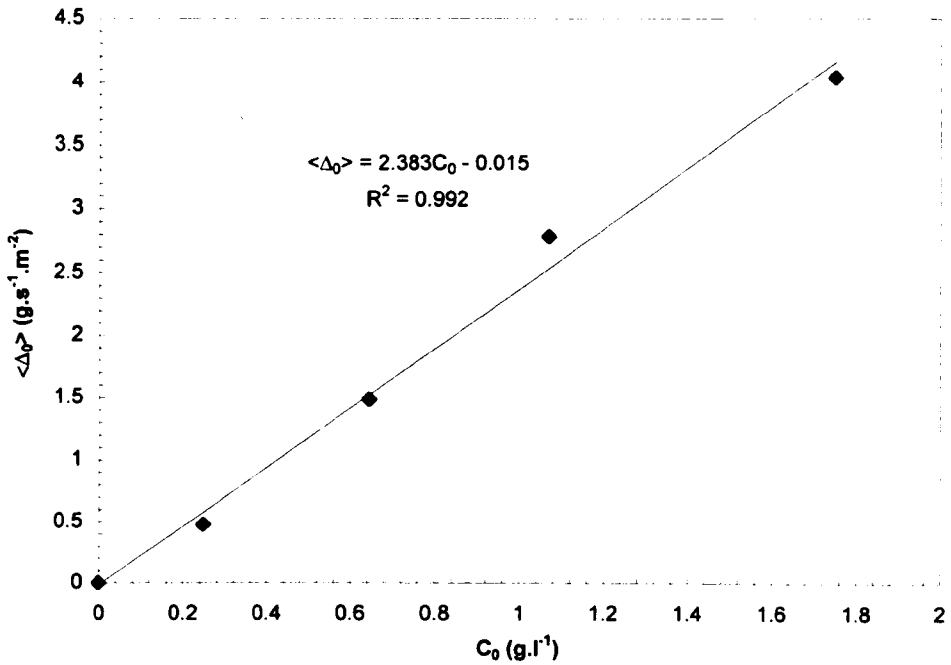


FIGURE 3.12a: example of plot of the deposition rate  $\langle \Delta_0 \rangle$  (average of all values obtained for a given input) against initial sediment concentration  $C_0$  (Experiment B1)

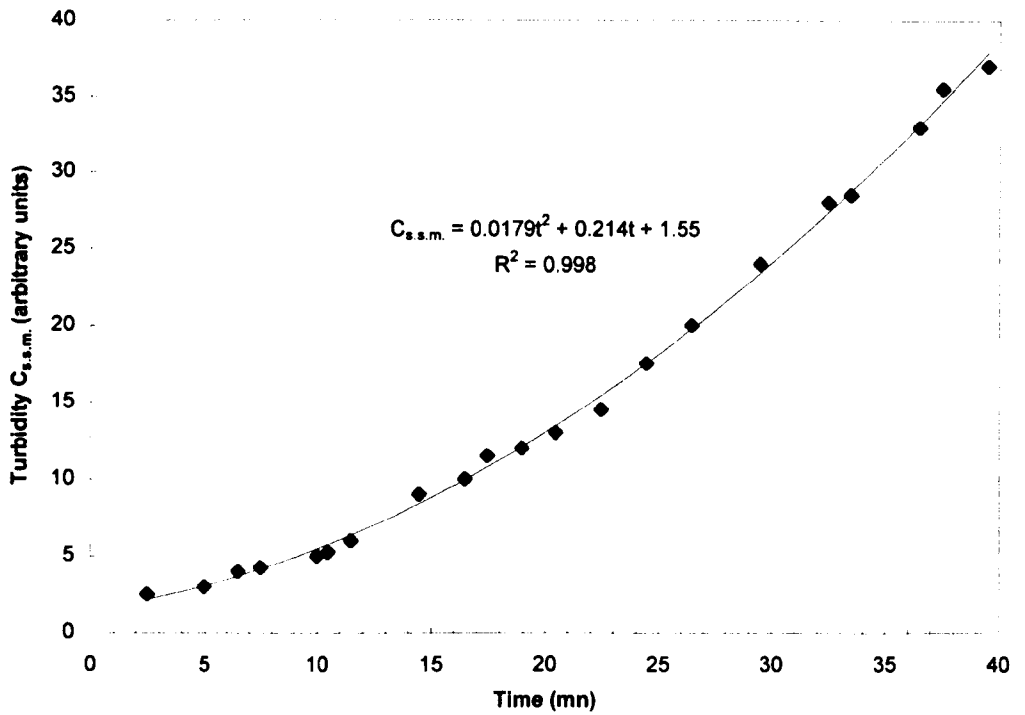


FIGURE 3.12b: example of the variations of the turbidity readings against time, and best-fit second-order polynomial curve (Experiment B1)

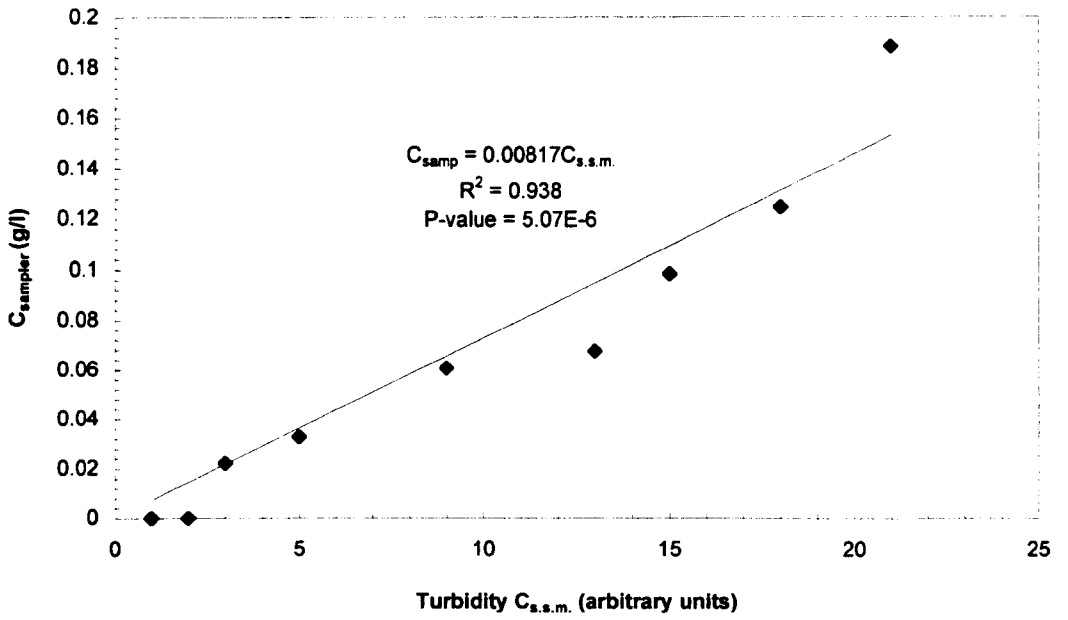


FIGURE 3.12c: example of the calibration of the s.s.m. readings using a plot of the near-bed concentration results obtained from the samples against the corresponding turbidity readings (Experiment B1)

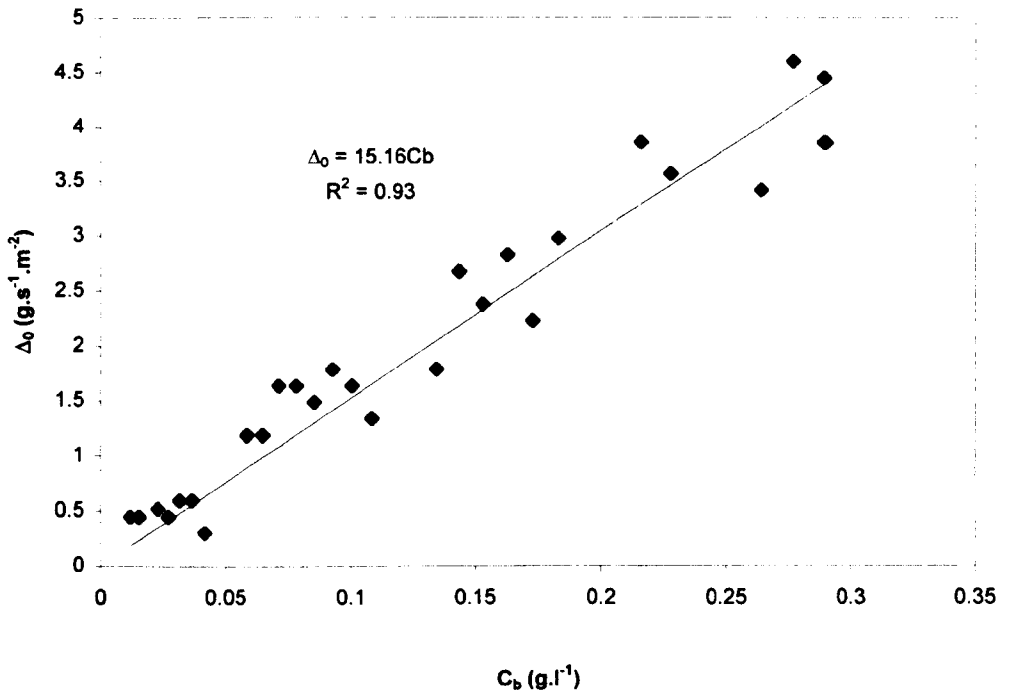


FIGURE 3.12d: example of plot of the instantaneous deposition rate against the near-bed sediment concentration  $C_b$  estimated from the s.s.m. data (Experiment B1)

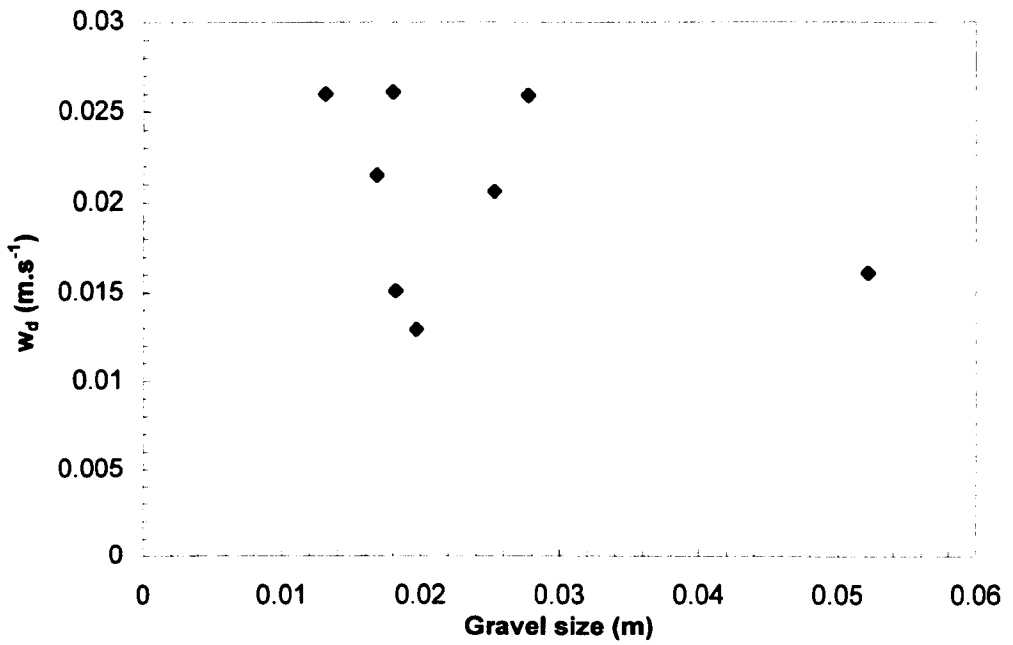


FIGURE 3.13: deposition velocity  $w_d$  measured in the funnel-shaped trap against the median size of the bed surface gravel

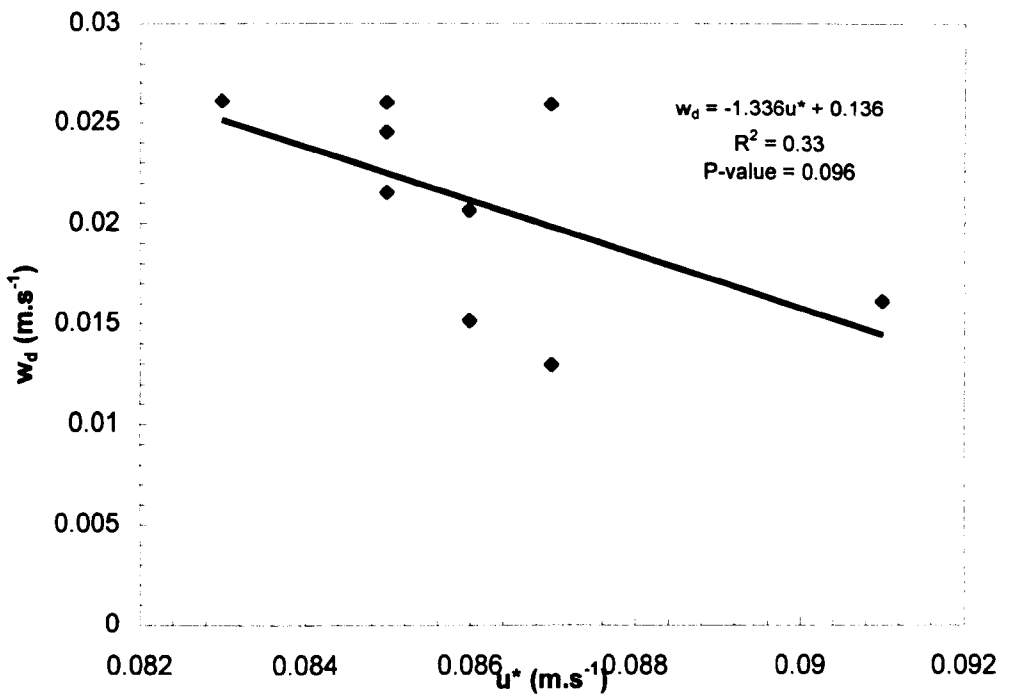


FIGURE 3.14: deposition velocity  $w_d$  measured in the funnel-shaped trap against shear velocity  $u^*$

The deposition velocity  $w_d$  was measured as the slope of the best-fit linear function between  $\Delta$  vs  $C_b$ . These results have been summarised at the bottom row of Table 3.2. The results do not indicate any specific relationship between gravel size and deposition velocity (Figure 3.13). No clear-cut trend emerges from the plot of the deposition velocities against shear velocity  $u^*$  (Figure 3.14). The best-fit line suggest that there is a poorly defined tendency for the deposition velocity to decrease with the shear velocity (and thus with the level of turbulence), but the overall relationship is not statistically significant ( $P\text{-value} > 0.05$ ).

The deposition velocity results of Experiments C2a and C2b are similar ( $0.0260$  and  $0.0245\text{m}\cdot\text{s}^{-1}$ ) which suggests that the arrangement of the particles below the bed interface does not influence deposition significantly. Given the fact that the top surface layers had a similar composition in both experiments (due to differential settling), this may in turn suggest that the most influential bed particles in terms of fine sediment deposition are the coarsest ones that protrude at the bed surface.

The deposition rates in the sediment compartments were computed by measuring the weight of sand deposited, and dividing it by the surface area of the compartment and the duration of the experiment. These were compared to the concentration decay equation derived previously ([3.3], Appendix 3.1). Considering that little sediment deposited over the first non-porous section,  $C_{b0}$  was approximated as  $C_{b0} = r I_0 / Q$ , where  $r$  is the ratio of near-bed to average concentrations (assumed equal to 2, a value close to the results obtained in §6.2.2),  $\langle I_0 \rangle$  the average sediment input rate for each experiment ( $\text{kg}\cdot\text{s}^{-1}$ ) and the flow rate  $Q$  ( $\text{m}^3\cdot\text{s}^{-1}$ ).

Most of the results (three examples in Figure 3.15) exhibited a concave curve shape, indicating the presence of a larger decay rate at the entrance of the test section than at its end. There was also a large difference between the experimental data and the spatial distribution predicted by Equation [3.3] (Figure 3.15). Although the model deposition rates were close to the experimental data near the beginning of the test section, [3.3] under-estimated the exponential decay rate, resulting in deposition rates about ten times as large as the experimental data just 2.5m downstream from the test section entrance. Changes in the concentration coefficient  $r$  did not significantly reduce this difference.

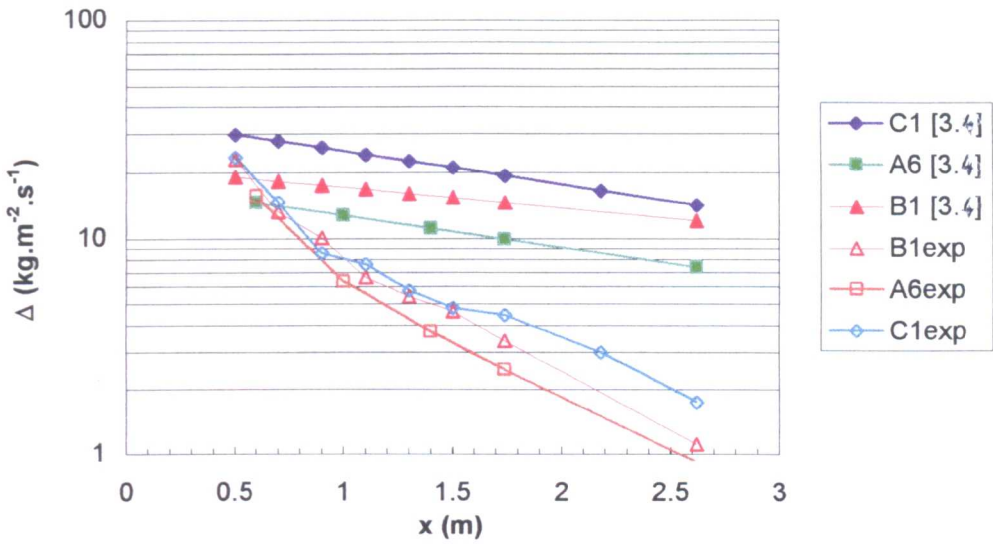


FIGURE 3.15: spatial distribution of the deposition rates for three experiments of the preliminary series and distributions predicted by Equation [3.3] ( $C_{b0}=rI_0/Q$ ,  $r=2$ )

Given that the decay rate depends only on the deposition velocity, the coefficient  $r$  and the unit discharge  $q$ , it was thought that the poor results obtained with [3.3] were mainly due to errors in the computation of the deposition velocity. The concave shape of the plots of the experimental deposition rates against distance suggested a change in the decay rate, thus a change in deposition velocity with distance. The fact that the size of deposited sediment decreased with distance downstream (Table 3.4) was thought to be one possible explanation for the reduction of the value of the deposition velocity along the flume.

Location	Trap 1	Trap 2	Trap 3	Trap 4	Trap 7	Separator
x (m)	2.60	3.00	3.40	3.80	5.16	>8
Size ( $\mu\text{m}$ )	262	255	250	243	220	205

TABLE 3.4: median size of the sand collected at several locations along the flume in experiment A0.

### 3.4 Conclusion

The ratio of the deposition rates through porous bed surfaces  $\Delta$  to the near-bed concentration of fine particles  $C_b$  has the dimension of a velocity, and is referred as the deposition velocity  $w_d$ . This parameter represents the downward velocity component of

the fine particles through the bed surface. Using a similar approach to that used by Einstein (1968), expressions of the spatial distribution of  $\Delta$  and  $C_b$  in the case of a point release were derived based on this parameter (Equations [3.3] and [3.4]).

A series of nine experiments was aimed at measuring this parameter for different hydraulic and bed gravel size conditions. These experiments were conducted in an 8.60m-long flume, where fine particles released at the water surface could settle and deposit through a 30-mm layer of gravel, into a series of sediment traps.

The instantaneous deposition rates, measured in a funnel-shaped trap, were found to be linearly correlated to the initial sediment concentration  $C_0$ , and to the concentration measured 25mm above the bed surface, on top of the trap.

The results indicated a possible (though non-statistically significant) negative influence of the turbulence intensity on the deposition velocities, while the gravel size did not appear to play a significant role on  $w_d$ . In terms of longitudinal distribution of the deposition rates, the results of Equation [3.3] did not agree with the experimental data, mainly because the model decay rate was too low. The model did not reproduce either the reduction in the decay rate with distance observed in the prototype. It was thought that this reduction could be due to changes in the deposition velocity  $w_d$  along the test section, as the composition of the near-bed sediment gradually changed. These problems highlighted the need for a more sophisticated experimental approach. In his analysis of the deposition process, Einstein (1968) noted that the different size fractions present within natural sand mixtures have different terminal fall velocities, and that it is therefore necessary to analyse these different fractions separately to determine how they are individually affected once they reach the bed surface. The main change between the main series and the preliminary series of experiments was thus to treat fine sediment size classes individually, each with their own mechanical specifications and response to flow turbulence, instead of considering fine sediment mixtures as a whole.

## Chapter IV

# Main series of experiments

### 4.1 Introduction

Two main conclusions have emerged from the preliminary series of experiments concerning the general experimental procedure for the study of fine sediment deposition: (1) it is not necessary to vary the input rate of fines during the experiments because, up to a certain concentration, the deposition rate is linearly correlated to the near-bed concentrations; and (2) different size classes have to be considered separately to study the deposition of non-uniform sediment. The main series of experiments was designed on this basis. Instead of varying the input of fines and monitoring continuously fine sediment concentrations and deposition rates, the fine sediments were released at a constant rate throughout the experiments and the near-bed concentrations  $C_b$  and deposition rates  $\Delta$  were measured after the runs. The granulometric compositions of the samples were computed in order to measure fractional concentrations  $C_b^i$  and deposition rates  $\Delta^i$  (where  $i$  is the size fraction index).

### 4.2 Background

The deposition velocity  $w_d$  obtained from Equation [3.2] ( $w_d = \Delta / C_b$ ) represents the settling velocity of fine sediments through the gravel bed surface. It can be compared to the terminal fall velocity of the particle in still water,  $w_s$ , using the so-called *dimensionless deposition velocity*  $w_d^*$  defined as:

$$w_d^* = \frac{w_d}{w_s} \quad [4.1]$$

The definition of the dimensionless deposition velocity is close to that of the probability  $P_d$  defined by Krone (1962) (§2.2.2.3a). However,  $w_d^*$  does not represent a probability of deposition because the latter depends directly on the value of the deposition velocity  $w_d$ , and not on a dimensionless parameter like  $w_d^*$ . Instead,  $w_d^*$  gives an indication of the mechanical effects of both the bed and the near-bed turbulence on the settling behaviour of the fine particles. It is a key parameter in the following analysis because it allows to compare the effects of different types of bed material or hydraulics conditions on the deposition process.

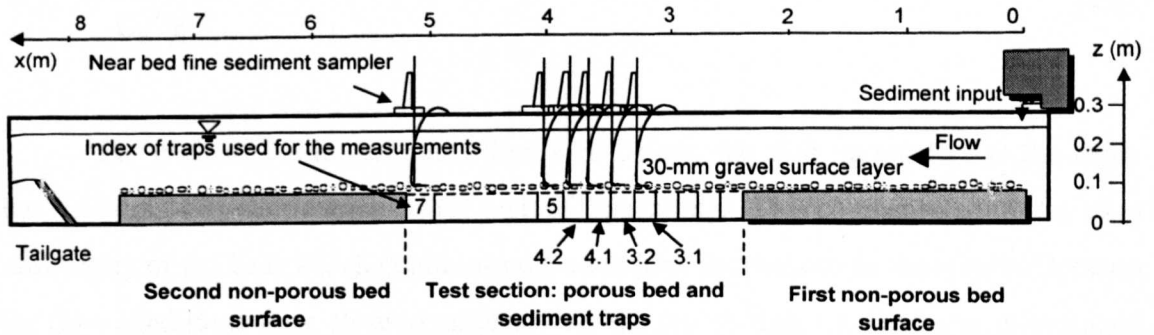


FIGURE 4.1: flume set-up for the main series of experiments

The experimental conditions in the present study are described in detail in the following section. In brief, sand is fed at the upstream end of a gravel-bedded flume while near-bed sediment and deposited sediment samples are collected halfway along in six sediment traps (Figure 4.1). Considering a series of size fraction intervals to analyse the results of these tests, let the subscript  $i$  represent one of these intervals, and the superscript  $j$  the trap index. If  $\Delta^j$  is the overall deposition rate measured in trap  $j$ , and  $\Sigma_i^j$  the proportion of size fraction  $i$  collected in trap  $j$ , then the deposition rate of the size fraction  $i$  in trap  $j$  is equal to:

$$\Delta_i^j = \Delta^j \Sigma_i^j \quad [4.2]$$

Similarly, if  $C_b^j$  is the near-bed sediment concentration over trap  $j$ , and  $\chi_i^j$  the proportion of this in size fraction  $i$ , then the corresponding near-bed concentration is:

$$C_{b_i}^j = C_b^j \chi_i^j \quad [4.3]$$

Combining equations [3.2], [4.2] and [4.3], the effective settling velocity of the size fraction  $i$  in trap  $j$  is given by:

$$w_{d_i}^j = \frac{\Delta^j \sum_i^j}{C_b^j \chi_i^j} \quad [4.4]$$

For each of the experiments described below, the four parameters at the right-hand side of [4.4] were measured for each of the six traps. This compensated for the non-uniformity of the bed, which could introduce random fluctuations in the results. Because the flow conditions were close to uniform over the test section, the results were averaged over the trap index  $j$  to yield overall effective fall velocities  $w_{d_i}$  through each type of gravel mixture.

### 4.3 Material and methods

#### 4.3.1 Sediment

Two types of sands were used for this series of tests. LA-260 sand, already used in the previous series of tests (§3.2.1), was re-used, together with the finer *B3-100* sand, a brown, well sorted, very fine sand, with a median grain size of  $100\mu\text{m}$ , and a sorting index  $\sigma=1.34$  (Figure 4.2).

Fractional deposition rates and near-bed concentrations were computed according to [4.2] and [4.3] by measuring the proportions of the different size fractions collected in the samples. These samples were sieved according to the following method:

the samples were first oven-dried at  $\sim 80\text{-}100^\circ\text{C}$ , and then sieved using 200mm-wide Endecotts BS410/1986 sieves. Different sieve sets were used for the samples obtained from LA-260 sand (63, 150, 212, 250, 300, 355, 425, 500, 600 $\mu\text{m}$ ) and those obtained from B3-100 sand (38, 45, 53, 63, 75, 90, 106, 125, 150, 180, 212, 250, 300 $\mu\text{m}$ ). The samples were sieved for 10 minutes using the Wykeham Farrance 62020 vibrator. A maximum quantity of 50g of each sample was used, not to get too much interaction between the grains during the sieving process which could block the passage of some of the particles. The fractions of sediment were weighed using a Sartorius SS2254 balance (accurate to a centigram), or alternatively a Mettler B4C1000 electric balance (accurate to a milligram) when the mass of sediment was less than 5mg.

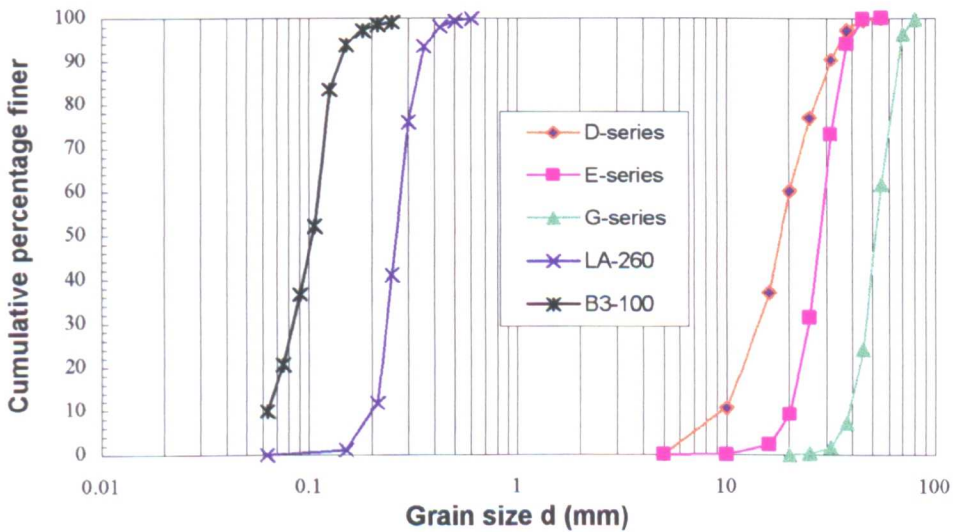


FIGURE 4.2: sand and gravel grading curves

Three types of gravel mixture were used for the tests (Figure 4.2), which were those already used in experiments B1, C1 and C3 of the funnel-trap series of experiments (§3.3.3). These were moderately-well to well sorted natural gravel, mainly composed of well rounded particles. Their median size (18.1, 27.7 and 52.2mm) ranged from the coarse pebble to the very coarse pebble range. The series of experiments were named according to the type of gravel used, i.e. respectively the D-, E- and G-series. The largest size material, the size of which is somewhat disproportionately large compared to the water depth ( $1.35 < h/D < 2.30$ ), was tested to analyse the effects on

infiltration of large eddies taking place within its large voids. All gravel particles finer than 5mm were removed from the mixtures to enable the fines to seep freely through the gravel pores. The porosity  $\lambda$  of the gravel mixtures was nearly constant for the three different types (0.42, 0.45 and 0.46 for D, E and G). Bulk volumes of 65 litres of gravel were used for the bed surface and placed over the 2.80m-long test section, resulting in an average bed thickness of 30mm.

#### 4.3.2 Flow measurements

##### 4.3.2.1 ADV probe

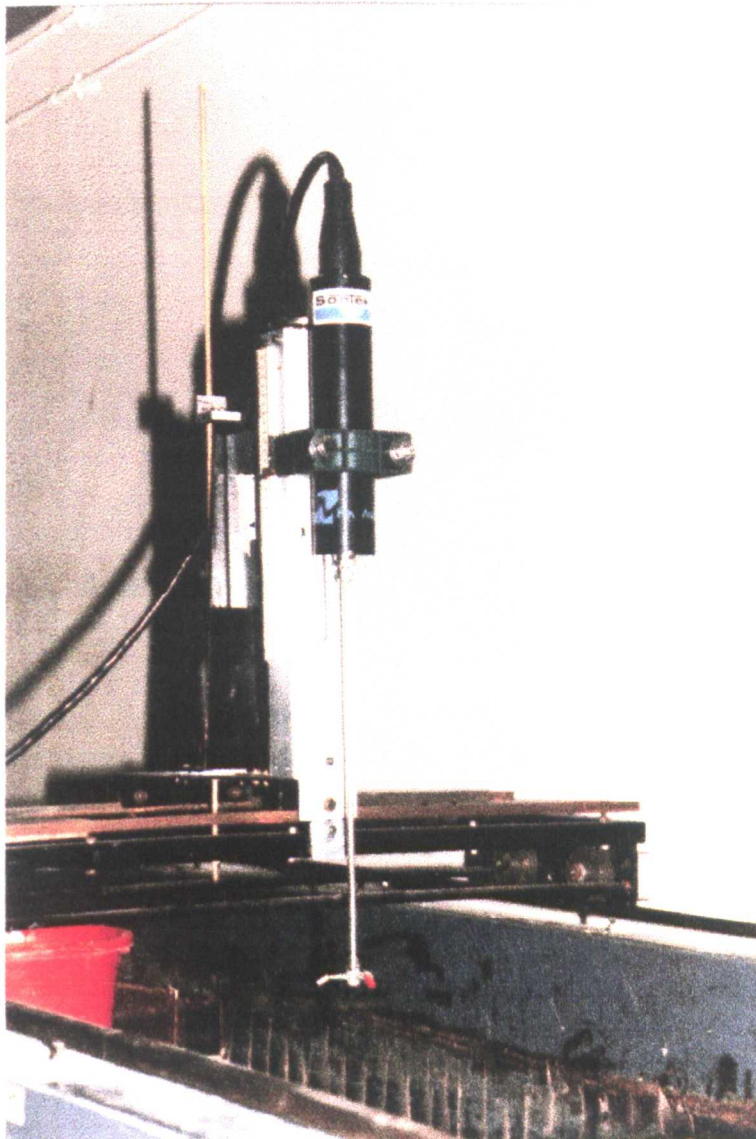


FIGURE 4.3a: ADV probe and support mechanism

Accurate measurement of flow parameters was an important issue in this study to get the best possible basis for comparison between the deposition results of the different experiments. These parameters were measured using a Sontek™ Acoustic Doppler Velocimeter (ADV) (Figures 4.3a and 4.3b). These probes operate as follows: short acoustic pulses are periodically produced by the transmitting transducer. While travelling through the water column, these pulses are reflected by scatterers, i.e. small particles like micro bubbles or particles in suspension. The receiving transducers detect the resulting acoustic echoes only if they originate from within the sampling volume (Figure 4.3b). The velocities are computed from the Doppler shift in frequency caused by the movement of the scatterers in the flow (assumed to be travelling at the same velocity as the flow).

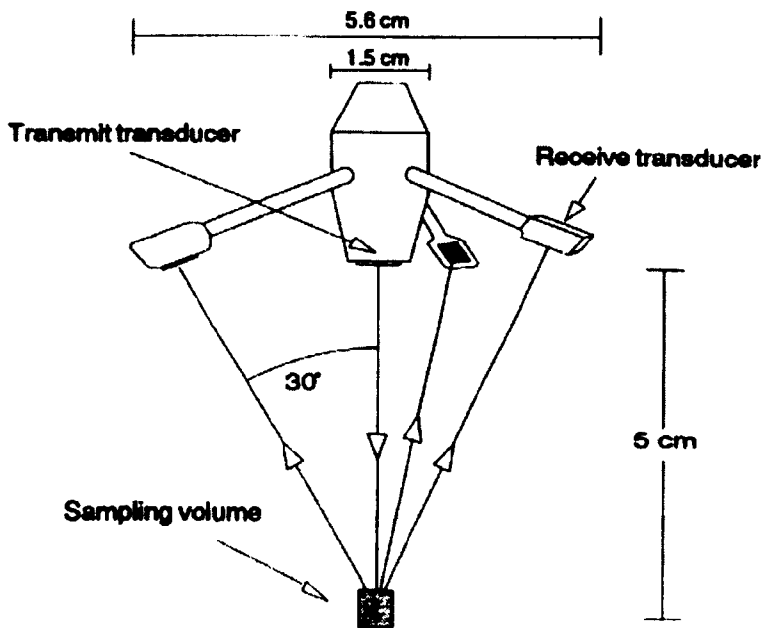


FIGURE 4.3b: detail of velocity measurement system of ADV probe

The probe is capable of measuring up to 25 flow velocities in each of the three dimensions every second. This information is logged on a PC, and statistical information regarding flow velocities and turbulence characteristics can be obtained using the WinADV software.

The sampling volume (i.e. the volume where the velocities are measured) is located approximately 50 to 70mm below the tip of the probe, therefore no velocity

measurements can be carried out in the upper 50 to 70mm of the water column. This represented an inconvenience in the particular conditions of these experiments as flow depth varied between about 70 to 120mm. As a result, flow velocities could only be measured in the immediate vicinity of the bed. There were cases where the probe could not be 'focussed' even when the flow was sufficiently deep. Its position above the bed had to be changed until a suitable signal could be read. It was thought that this particular problem was caused by the porosity of the bed, as further discussed in Chapter VII.

The method used to work out the velocity profiles from the ADV results and the resulting plots (relative depth  $\zeta = z / (h + \Delta z)$  against  $u(\zeta)$ ) are indicated in Appendix 4.1. Average flow velocities  $U$  were computed by interpolation of the velocity profiles. The mean velocity was taken at the level  $z = 0.37 (h + \Delta z)$ . When no velocity measurements were available at this depth, flow discharge measurements from the orifice plate were used to measure  $U$ , according to  $U = Q / [B (h + \Delta z)]$ . The results are indicated in Table 4.3. Near-bed flow velocities were also measured by interpolation, at  $z = \Delta z$ , and the results are indicated in Appendix 5.1.

#### 4.3.2.2 Shear velocity calculation methods

Two methods have been used to measure shear velocities: the first one is derived from the law of the wall, and the other one is based on Reynolds stress profiles.

One of the main problems when measuring velocity profiles over coarse, porous beds is to define the level where the apparent velocity becomes zero. This zero-velocity level is conceptual because in reality, the non-uniformity of the bed and the flow turbulence make it vary with space and time. In the present case, due to the relatively large grain size to flow depth ratio, the zero-plane displacement  $\Delta z$  (i.e. the difference between the bed surface level and the zero-velocity level) had to be included in the computation of the hydraulic radius  $R$  when using the classic shear velocity formula:

$$u^* = \sqrt{gRS} \quad [4.5]$$

which can be re-written (including the zero-plane displacement):

$$u^* = \sqrt{g \frac{B(h + \Delta z)}{B + 2(h + \Delta z)} S} \quad [4.6]$$

Several formulas have been proposed to compute directly  $\Delta z$  as a function of the roughness length  $z_0$  (Kamphuis, 1974; Bayazit, 1976).  $\Delta z$  can also be computed using the law of the wall, which requires an estimate of the equivalent sand roughness  $k_s$ . Several authors have proposed formulas relating the equivalent grain roughness  $k_s$  to various percentile grain sizes (e.g Ackers and White, 1973; Hey, 1979; van Rijn, 1982). The differences between the different formulae is mainly caused by differences in the conditions in which they have been obtained. Due to the specificity of the conditions of the present series of experiments (relatively shallow flow and coarse gravel), separate runs were carried out to measure  $\Delta z$  and  $z_0$  directly. These parameters were computed using a combination of two equations i.e. the law of the wall and equation [4.6]. The law of the wall can be expressed as:

$$u(z) = \frac{u^*}{\kappa} \ln\left(\frac{z}{z_0}\right) \quad [4.7]$$

or, including the zero-plane displacement  $\Delta z$ , as:

$$u(Z) = \frac{u^*}{\kappa} \ln(\zeta) + \frac{u^*}{\kappa} \ln\left(\frac{h + \Delta z}{z_0}\right) \quad [4.8]$$

where  $\zeta$  is the relative depth ( $= z / (h + \Delta z)$ ) and  $z_0$  the roughness length (m).

An initial zero-plane displacement was assumed in the first place. Near-bed velocity measurements obtained with the ADV probe were used to plot  $u(Z)$  against  $\ln(\zeta)$ . The slope  $m$  and the intercept  $b$  of the linear function that best-fitted this series of points were computed (using the least-squares method). The shear velocity could then be computed as  $u^* = \kappa m$ .  $\Delta z$  was determined by iteration, until this measurement of  $u^*$  and

Run	Law of the wall					Reynolds stress			
	$\Delta z$	$u^*$	$z_0$	$k_{s1}$	$k_s$	$u^*_1$	$u^*_1/u^*$	$u^*_2$	$u^*_2/u^*$
D3_1	0.0174	0.080	0.0043	0.129	0.099	0.038		0.050	
D3_2	0.0225	0.081	0.0054	0.163	0.112	0.035		0.048	
<D3>	0.0200	0.081	0.0049	0.146	0.106	0.037	0.45	0.049	0.61
D4	0.0252	0.077	0.0056	0.169	0.114	0.021	0.27	0.047	0.61
D5_1	0.0293	0.089	0.0072	0.215	0.129	0.030		0.047	
D5_2	0.0299	0.089	0.0072	0.216	0.129	0.039		0.044	
D5_3	0.0058	0.084	0.0033	0.098	0.086	n/a		n/a	
D5_4	0.0039	0.083	0.0030	0.089	0.082	n/a		n/a	
D5_5	0.0506	0.093	0.0079	0.237	0.135	0.040		0.053	
D5_6	0.0353	0.090	0.0056	0.168	0.113	0.063		0.064	
D5_7	0.0345	0.090	0.0058	0.175	0.116	0.057		0.052	
D5_8	0.0298	0.089	0.0049	0.147	0.106	n/a		0.057	
<D5>	0.0274	0.088	0.0056	0.168	0.112	0.046	0.52	0.053	0.60
D6_1	0.0060	0.100	0.0087	0.260	0.142	n/a		n/a	
D6_2	-0.0045	0.094	0.0008	0.024	0.042	n/a		n/a	
<D6>	0.0008	0.097	0.0047	0.142	0.092	n/a	n/a	n/a	n/a
E2_1	0.0380	0.091	0.0082	0.247	0.138	n/a		0.058	
E2_2	0.0417	0.092	0.0082	0.247	0.138	n/a		0.062	
E2_3	0.0410	0.091	0.0079	0.236	0.135	0.035		0.058	
E2_4	0.0309	0.090	0.0072	0.217	0.129	n/a		0.067	
<E2>	0.0379	0.091	0.0079	0.237	0.135	0.035	0.38	0.061	0.67
E3b_1	0.0139	0.079	0.0043	0.128	0.099	0.048		0.049	
E3b_2	0.0202	0.081	0.0052	0.157	0.110	n/a		0.053	
<E3b>	0.0171	0.080	0.0047	0.142	0.104	0.048	0.60	0.051	0.64
E4	0.0140	0.073	0.0039	0.118	0.095	0.053	0.73	0.062	0.85
E5_1	0.0210	0.108	0.0181	0.542	0.207	n/a		n/a	
E5_2	-0.0002	0.097	0.0015	0.044	0.057	n/a		n/a	
<E5>	0.0104	0.102	0.0098	0.293	0.132	n/a	n/a	n/a	n/a
G1_1	0.0216	0.087	0.0082	0.245	0.138	0.014		0.072	
G1_2	0.0710	0.096	0.0224	0.671	0.231	n/a		0.056	
<G1>	0.0463	0.092	0.0153	0.458	0.184	0.014	0.15	0.064	0.70
G2_1	0.0530	0.088	0.0141	0.424	0.182	0.021		0.056	
G2_2	0.0360	0.084	0.0116	0.348	0.165	0.024		0.054	
<G2>	0.0445	0.086	0.0129	0.386	0.174	0.023	0.26	0.055	0.64
G3_1	0.0390	0.080	0.0133	0.399	0.177	n/a		0.048	
G3_2	0.0620	0.086	0.0188	0.563	0.211	n/a		0.050	
<G3>	0.0505	0.083	0.0160	0.481	0.194	n/a	n/a	0.049	n/a
G4_1	0.0127	0.114	0.0042	0.127	0.098	n/a		n/a	
G4_2	0.0297	0.121	0.0040	0.119	0.095	n/a		n/a	
G4_3	0.0463	0.127	0.0059	0.177	0.117	n/a		n/a	
<G4>	0.0296	0.121	0.0047	0.141	0.103	n/a	n/a	n/a	n/a
G5,G7	0.0029	0.097	0.0017	0.050	0.061	n/a	n/a	n/a	n/a
	<z <sub>0</sub> > (D)		0.0052	<k <sub>s</sub> >(D)	0.106	<u <sup>*</sup> <sub>1</sub> /u <sup>*</sup> >:	0.42	<u <sup>*</sup> <sub>2</sub> /u <sup>*</sup> >	0.66
	<z <sub>0</sub> > (E)		0.0086	<k <sub>s</sub> >(E)	0.134				
	<z <sub>0</sub> > (G)		0.0096	<k <sub>s</sub> >(G)	0.142				

$\Delta z$ =zero-plane displacement,  $u^*$ =shear velocity,  $z_0$ =roughness length  
 $k_{s1}$ =equivalent roughness size computed from Nikuradze's rough law  
 $k_s$ =equivalent roughness size computed from Meland and Normann (1969) ([4.10])  
 $u^*_1=u^*$  computed by estimation of the Reynolds stress profile at  $z=0$   
 $u^*_2=u^*$  computed by estimation of the Reynolds stress profile at  $z=\Delta z$   
 $\langle x \rangle (Y)$ =average value of the parameter x for the series Y

When several velocity profiles have been made for one given experimental condition (e.g. results for the two measurements for D3: rows D3\_1 and D3\_2), the average values over all the measurements have been indicated (e.g row <D3>).

TABLE 4.1: results of flow and friction parameters

that given by equation [4.6] were equal (which also set the value of the shear velocity). Finally, the roughness length  $z_0$  was computed as  $z_0 = (h + \Delta z) / \exp(b / m)$ .

The second method to measure the shear velocity  $u^*$  used Reynolds stress profiles. The shear velocity can be computed by extrapolating the Reynolds stress measurements to the zero-velocity level, and by neglecting the viscous shear component of the total shear (Graf and Song, 1995), according to:

$$u^* = \left( \sqrt{v \frac{dU}{dy} - \overline{u'w'}} \right)_{z \rightarrow 0} \approx \left( \sqrt{-\overline{u'w'}} \right)_{z \rightarrow 0} \quad [4.9]$$

The sum  $\overline{u'w'}$  was computed directly using the WinADV package. Results for the Reynolds stress profiles have been summarised in Appendix 4.2.

The results in terms of flow and friction parameters are summarised in Table 4.1. The first five columns of Table 4.1 indicate the results obtained with the law-of-the-wall method. The accuracy of these results was poor when only a few measurements could be taken near the bed (i.e. experiments with flow depth  $h=0.07\text{m}$ , Table 4.1). This is particularly obvious for the zero-plane displacements obtained for experiments D6 and G5, which are very low compared to those obtained in deeper water. In these cases, this lower value of  $\Delta z$  resulted in an over-estimation of the shear velocity (e.g. D4, G3), but due to the method used (i.e. combination of two formulae), this effect was minimised and the values of  $u^*$  obtained were relatively consistent with the rest of the results. In the experiments using deeper water depths, the results obtained were generally of good quality, particularly so for the D- and G-series.

The results obtained with the Reynolds stress method are presented in the last four columns of Table 4.1. The zero-plane displacements computed by the law-of-the-wall method were used to determine the zero-velocity level. The intersection between this plane and the best-fit line of the Reynolds stresses provided the results called  $u^*_1$  in Table 4.1. Compared to the shear velocities obtained with the law-of-the-wall method, the values of  $u^*_1$  were on average 58% lower, and showed some inconsistency (e.g. E- and G-series: decrease in  $u^*_1$  with increase in flow depth). This was possibly due to the additional inaccuracy introduced by the use of the zero-plane displacement. As an

alternative, the shear velocities were computed using the Reynolds stress value at the bed surface level ( $z = \Delta z$ ) (see  $u^*_2$  in Table 4.1). These were more consistent (particularly for the D-series) and closer to the values obtained with the earlier method, but they were on average 34% lower.

Overall, the Reynolds stress profiles obtained were not linear in ~40% of the cases (Appendix 4.2), hence the larger scatter in the shear velocity results compared to the law-of-the-wall method. When the Reynolds stress profiles were linear, the results obtained from two different measurements were usually quite similar (e.g. D3, D5\_1 and D5\_2, G2). In addition, the profiles often exhibited a break near the bed with a steeper decrease in Reynolds stress in the lower part of the curve (e.g. D5\_3, E1\_1, E3\_2). This larger gradient resulted in an underestimation of the shear velocities, particularly at the zero-velocity level.

The non-uniformity of the bed and the relatively large roughness heights and turbulence intensities may have produced these inconsistencies in the Reynolds stress profile results. The equipment used is also a possible explanation. For example, it was noticed that the velocity measurement and Reynolds stress profile results were unstable when the ADV probe was placed above bed pores. The position of the probe had to be modified until the signal could be properly read by the receiving transducers. When the probe was placed above any large flat gravel of the largest gravel mixture (series G), the readings were of excellent quality. It is possible that the instability of the results was caused by additional signal reflections taking place from irregular bed surfaces, or from neighbouring gravel particles. These may have produced acoustic echoes that interfered with those recorded from the sampling volume.

Consequently, the parameters obtained from the law-of-the-wall method were used to analyse the experimental results. These parameters are summarised in Table 4.3.

### 4.3.3 Experimental set-up

The experimental set-up is sketched in Figure 4.1. The same flume as described in §3.3.2.1 was used (large flume). Four experiments were carried out to determine the appropriate experimental conditions for the experiments.

The deposition and near-bed concentration measurements were performed over a length of 1.94m in the test section, using six of the last eight compartments (the funnel-trap was not used in this series) (Figure 4.1). These compartments were the same as those used in the funnel-trap series to trap the heaviest sand particles. However, to avoid turbulence and re-circulation currents taking place within the sediment traps, the traps were filled with vertical tubular baffles, made of 85mm-long tubes of 14mm in diameter.



FIGURE 4.4: near-bed sediment sampling. Sediment traps 3.2 and 4.1 can be seen through the flume's side window, as well as the tubular baffles used to damp turbulence below the bed surface.

To measure the composition and the concentration of sediment transported near the bed, samples were siphoned out using flexible tubes of 6mm-external diameter. These were laid facing upstream upon the gravel surface halfway along each trap, and they were supported by a frame fixed onto a gauge. Due to the protrusion of the larger gravels and the width of the tubes, the near-bed sediment samples were effectively taken 7mm above the bed interface. This represented a significant improvement compared to 25mm of the preliminary series (§3.3.2.4), and it is comparable to the 10mm of Beschta and Jackson (1979). The samples were collected in 80-litre bins (Figure 4.4) in which the fine sediment was allowed to settle during several hours. After the end of the

experiment, the volume of water collected was measured and the sediment was retrieved for analysis.

LA-260 was mainly transported as saltating load, and B3-100 as suspended load. It was not possible to separate the finest fractions of B3-100 sediment from the flow due to the larger size of the separator's mesh (100 $\mu\text{m}$ ). Thus, the separator was not used in this case (the very fine B3-100 sand was unlikely to be a problem in terms of damage to the pump and accumulation of sand within the pipes), and some of the fine particles were re-circulated. The input of sand had thus to be carefully controlled not to have a gradual increase of the concentration of fines throughout the experiments. The Partech - W.P.R.L. probe was used to monitor that concentration, and the feed rate was regularly adjusted to keep it constant.

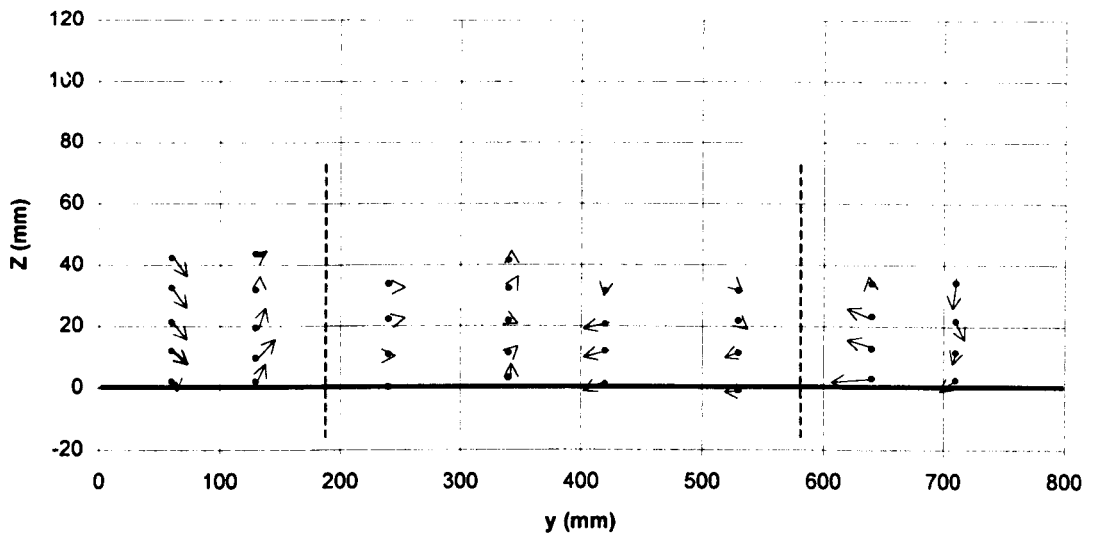


FIGURE 4.5: transverse velocity profile measured 3.23m d/s of the u/s end of the flume (i.e between traps 3.2 and 4.1) over an 18.1mm gravel bed.

The deposited sediment had to be sampled in an area of the flume where flow conditions are close to 2D and uniform near the bed, in order to collect fines deposited under similar flow conditions. In this series of experiments, the aspect ratio  $B / (h + \Delta z)$  varied between 4.6 and 11.0, which is larger than the 3.5 ratio found by Graf and Song (1995) in similar experimental conditions as a minimum requirement for 2D flow conditions. A series of flow measurements were carried out to work out the section of the flume where these conditions would occur. These measurements, carried out with

18.1mm gravel, indicated that flow conditions were close to two-dimensional near the bed within a section of the flume starting between ~130mm and ~220mm away from the flume walls (Figure 4.5), i.e at least within the central 40% of the flume width. It was assumed that a similar 2D behaviour would apply to the two other gravel mixtures. The deposited fines were thus sampled over the central third of the flume width.

The deposition rates in each trap were measured by dividing the mass of sand by the surface area over which the sample was collected and by the duration of the experiment. The grading analysis of the sand collected provided the  $\sigma_i^j$  coefficients. The sand obtained from the near-bed sediment samples was oven-dried, weighed and analysed to measure the near-bed concentration  $C_b^j$  and the  $\chi_i^j$  coefficients.

#### 4.3.4 Range of data in the experiments

The sediment size and the range of concentrations tested were at a 1:1 scale with that of the field. This method has been described as the most appropriate for laboratory experiments on sediment laden flows (Teisson, 1992), and it has been adopted by the majority of investigators working on fine infiltration processes. Only Diplas and Parker (1992) have worked at a reduced scale (~1:10) on this problem. In terms of shear stress, relatively low flow depths were compensated by relatively high slopes (1/62 and 1/135) to generate shear velocities and turbulence intensities comparable to those of prototype streams. Several other flume studies on sediment transport and deposition have been carried out using this method (Table 4.2),

	Diplas and Parker (1992) (scale 1:10)	Beschta and Jackson (1979)	Carling (1984)	Schälchli (1995)	Main series of experiments
S (min/max) (%)	1.2/1.7	~1/~3	~1/~2	~1/~3	0.7/1.6
h (min/max) (mm)	24/44	60/140	60/170	20/220	70/120
Q (min/max) ( $\ell.s^{-1}$ )	6/15	44/96	19/117	15/135	23/54
$u^*$ (min/max) ( $m.s^{-1}$ )	0.063/0.086	~0.08/~0.125	0.02/0.21	~0.07/~0.18	0.07/0.12
$C_0$ (min/max) ( $mg. \ell^{-1}$ )	150/500	150/4000	38/9110	Recirculating	750/8200

TABLE 4.2: comparison of data from previous and present studies

The fine material feed rate was set at  $I_0 \sim 40 \text{g.s}^{-1}$  for all experiments but one, where the effect of a large input rate was tested. Mean flow velocity varied between  $U=0.25 \text{m.s}^{-1}$  and  $U=0.64 \text{m.s}^{-1}$  (Table 4.3). The flow rate ranged between  $Q=23 \text{l.s}^{-1}$  and  $Q=54 \text{l.s}^{-1}$  and the bed surface supported a hydraulically rough regime. In general, the flow depth became close to uniform  $\sim 1.50 \text{m}$  downstream of the release point. Mean flow depth, measured from the average bed surface level, varied between  $h=70 \text{mm}$  and  $h=120 \text{mm}$  and grain Reynolds numbers  $Re^*$  ranged between 2.8 and 72.

#### 4.4 Results

The results of 18 experiments (D3, D4, D5, D6, D7, E2, E3b, E4, E5, E6, E7, G1, G2b, G3, G4, G5, G6, G7) are reported and commented upon in this section. The main parameters of the experiments are summarised in Table 4.3. The implications of the results are discussed in the following chapter.

Run	Matrix		Framework			Flow							
	$I_0$ ( $\text{g.s}^{-1}$ )	$d$ ( $\mu\text{m}$ )	$D$ (mm)	$\sigma$	$S$	$Q$ ( $\text{m}^3\text{s}^{-1}$ )	$h$ (m)	$u^*$ ( $\text{m.s}^{-1}$ )	$\Delta z$ (m)	$U$ ( $\text{m.s}^{-1}$ )	$z_0$ (m)	$k_s$ (m)	$\nu$ ( $\text{m}^2\text{s}^{-1}$ )
D3	43	260	18.1	1.54	0.007	0.041	0.10	0.08	0.020	0.44	0.0049	0.106	1.05E-06
D4	43	260	18.1	1.54	0.007	0.028	0.08	0.08	0.025	0.35	0.0057	0.114	1.02E-06
D5	43	260	18.1	1.54	0.007	0.054	0.12	0.09	0.027	0.48	0.0056	0.112	1.08E-06
D6	40	260	18.1	1.54	0.016	0.046	0.07	0.10	0.001	0.64	0.0047	0.092	1.03E-06
D7	35	100	18.1	1.54	0.016	0.046	0.07	0.10	0.001	0.64	0.0047	0.092	9.98E-07
E2	43	260	27.7	1.24	0.007	0.054	0.12	0.09	0.038	0.44	0.0079	0.135	1.05E-06
E3b	44	260	27.7	1.24	0.007	0.042	0.10	0.08	0.017	0.47	0.0048	0.104	1.02E-06
E4	43	260	27.7	1.24	0.007	0.026	0.08	0.07	0.014	0.36	0.0039	0.095	1.02E-06
E5	47	260	27.7	1.24	0.016	0.039	0.07	0.10	0.010	0.56	0.0098	0.132	1.02E-06
E6	438	260	27.7	1.24	0.016	0.039	0.07	0.10	0.010	0.56	0.0098	0.132	1.02E-06
E7	35	100	27.7	1.24	0.016	0.039	0.07	0.10	0.010	0.56	0.0098	0.132	1.00E-06
G1	42	260	52.2	1.22	0.007	0.054	0.12	0.09	0.046	0.42	0.0152	0.184	1.10E-06
G2b	44	260	52.2	1.22	0.007	0.040	0.10	0.09	0.045	0.36	0.0129	0.174	1.02E-06
G3	43	260	52.2	1.22	0.007	0.025	0.08	0.08	0.051	0.25	0.0160	0.194	1.05E-06
G4	43	260	52.2	1.22	0.016	0.054	0.09	0.12	0.030	0.51	0.0047	0.103	1.05E-06
G5	42	260	52.2	1.22	0.016	0.039	0.07	0.10	0.003	0.43	0.0017	0.061	1.01E-06
G6	36	100	52.2	1.22	0.016	0.054	0.09	0.12	0.030	0.51	0.0047	0.103	9.84E-07
G7	35	100	52.2	1.22	0.016	0.039	0.07	0.10	0.003	0.43	0.0017	0.061	9.84E-07

$I_0$ =input rate,  $d$ =median size of fines,  $D$ =median size of gravel,  $\sigma$ =sorting index of gravel,  $S$ =slope  
 $Q$ =discharge,  $h$ =flow depth,  $u^*$ =shear velocity,  $\Delta z$ =zero-plane displacement,  $U$ =mean velocity  
 $z_0$ =roughness length,  $k_s$ =equivalent roughness size,  $\nu$ =kinematic viscosity

TABLE 4.3: main characteristics of the eighteen experiments of the main series

## 4.4.1 Velocity measurements

In terms of bed roughness and shear, results obtained from all the velocity measurements have been summarised in Table 4.1, and the main results can be found in Table 4.3.

The average results for  $\Delta z$ ,  $z_0$  and  $k_s$  for each series of experiments are presented in Table 4.4, and some typical ratios (e.g.  $k_s/D_{84}$ ) are also indicated for comparison with previous work. The zero-plane displacements were close to  $0.7-0.8D_{84}$ . The computed roughness lengths  $z_0$  lay within the range of  $0.1D_{50}$  to  $0.2D_{50}$  found by Schack *et al.* (1985). In terms of equivalent grain roughness  $k_s$ , results obtained from Nikuradze's rough law (i.e.  $k_s=30z_0$ ) were scattered and could not be related satisfactorily to the grain size of the bed material (as was also found by Carling (1984)). According to Zagni and Smith (1976), this is due to the porous nature of the gravel bed, for which the zero-velocity level is located at a considerably greater distance below the bed surface level than in the case of an impermeable bed. Better results were obtained from Meland and Norrman's (1969; in Carling, 1984) formula for flow over rhombohedrally packed glass beads:

$$k_s = e^{\frac{\ln(z_0)+0.939}{1.951}} \quad [4.10]$$

	D-series (D=18mm)	E-series (D=28mm)	G-series (D=52mm)
$\Delta z$ (m)	0.024	0.023	0.043
$\Delta z/D_{84}$	0.86	0.68	0.68
$z_0$ (m)	0.0052	0.0086	0.0096
$z_0/D_{50}$	0.288	0.311	0.185
$k_s$ (m)	0.106	0.135	0.142
$k_s/D_{84}$	3.79	3.97	2.26

TABLE 4.4: average results of zero-plane displacement, roughness length and equivalent roughness size for the three types of gravel used (results for D6, E5 and G5 excluded for the computation of  $\Delta z$ ).  $k_s$  calculated using [4.10].

The results (Table 4.4) were in close agreement with the frequently repeated value of  $3.5D_{84}$  (e.g. Hey, 1979) for the D- and E-series. For the larger gravel size, the result was significantly lower ( $\sim 2.3D_{84}$ ), probably as a result of the low ratio between water depth and bed roughness height, which caused a change in flow structure, as discussed by Bray and Davar (1987).

The shear velocities varied between  $u^*=0.073\text{m}\cdot\text{s}^{-1}$  and  $u^*=0.121\text{m}\cdot\text{s}^{-1}$  (Table 4.3). Quite similar results were obtained for the three gravel sizes with a constant water depth.

#### 4.4.2 Near-bed concentrations and deposition rates.

Variations of the near-bed concentrations and deposition rates with distance were monitored. The average deposition rates varied in average between  $0.0130\text{kg}\cdot\text{m}^{-2}\cdot\text{s}^{-1}$  in the first trap (0.90m downstream of the entrance of the test section), and  $0.0030\text{kg}\cdot\text{m}^{-2}\cdot\text{s}^{-1}$  in the last one (+2.60m) (Appendix 4.3, Figure 4.6). Although individual plots, like that of E5 and D4 on Figure 4.6, tend to have irregular contours, the average semi-log plot is close to linear with a slight concavity, which agrees with results obtained in §3.3.3 (Figure 3.15).

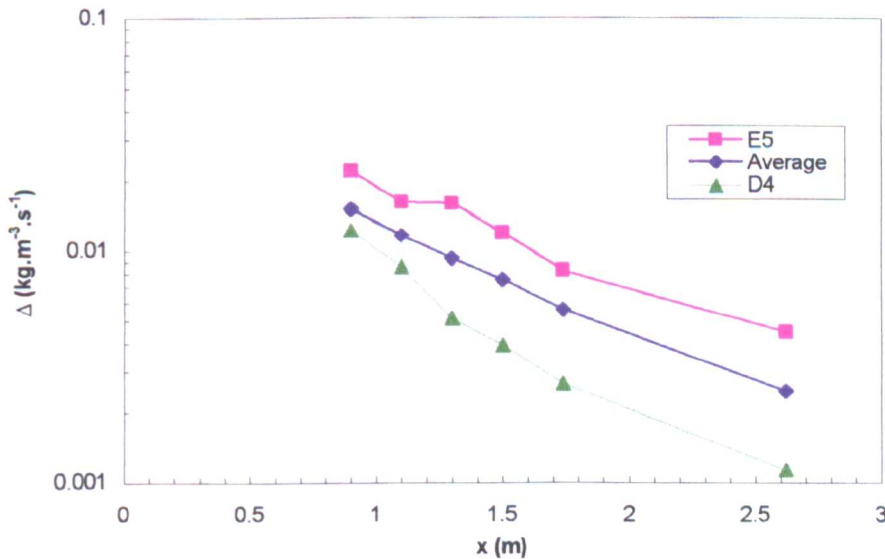


FIGURE 4.6: deposition rate measured for Experiments E5 and D4 (used as examples) and average deposition rate across all the experiments of the main series with LA-260 (except E6, which had a much larger input than the other experiments), plotted against distance downstream from source

All the graphs representing the variations of  $\Delta$  against  $x$  for experiments with LA-260 sand can be found in Figures 6.1a and 6.1b and all the numerical results in Appendix 4.3. The analysis of the results indicates that the deposition rates undergo a lower decay in experiments featuring the largest shear velocities (e.g. G4, E5, D6) compared to those where  $u^*$  is low (e.g. D3, E4, G3) (Figure 4.7).

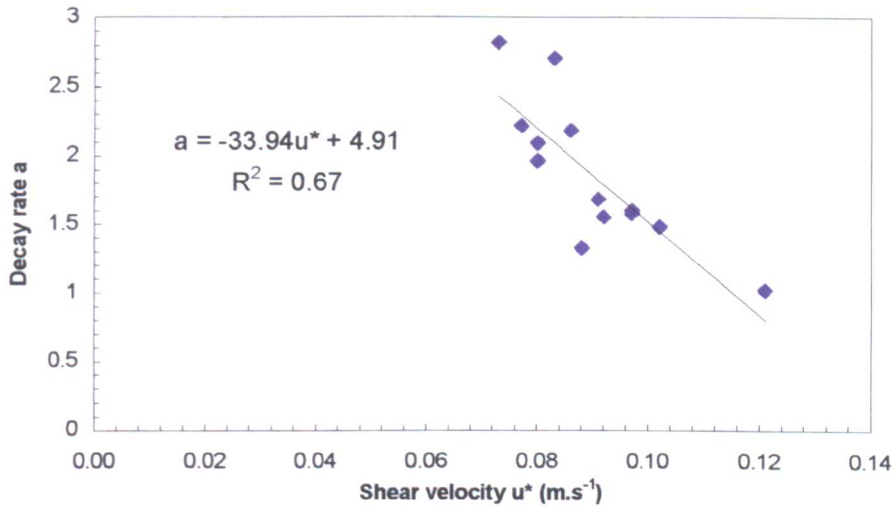


FIGURE 4.7: plot of the estimated decay rate  $a$  of the deposition rate  $\Delta$  (computed as  $a = -\ln(\Delta_7/\Delta_{3.1})/\ln(2.62/0.9)$ ) against shear velocity  $u^*$  for all experiments with LA-260 (except E6)

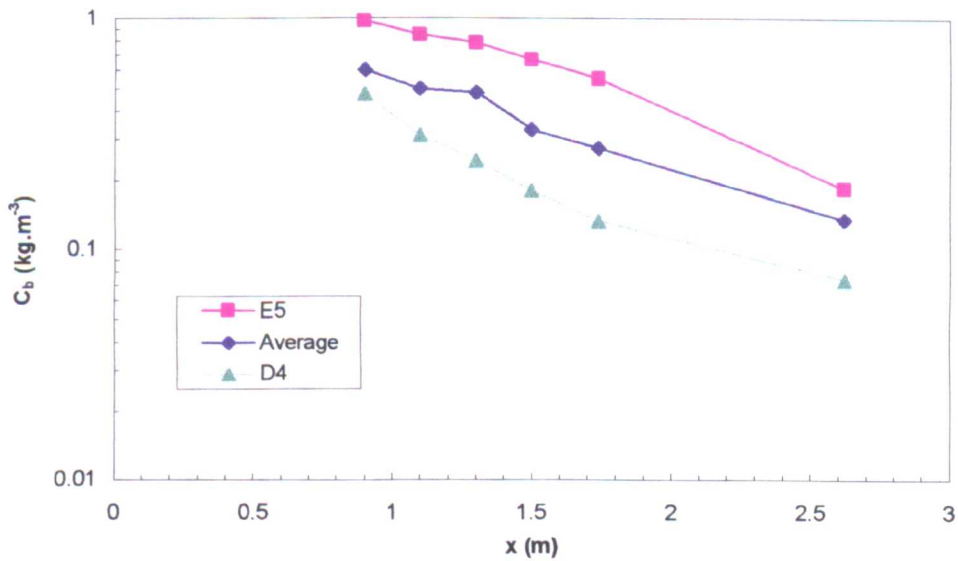


FIGURE 4.8: near-bed sediment concentration measured during Experiments E5 and D4 (used as examples) and average near-bed concentration for all experiments of the main series with LA-260 (except E6) against distance downstream from source

The near-bed concentrations from direct sampling were also found to decrease with distance, from  $\sim 0.890 \text{ kg.m}^{-3}$  in average to  $\sim 0.500 \text{ kg.m}^{-3}$  (volume concentrations:  $3.3 \times 10^{-4}$  to  $1.8 \times 10^{-4}$ ) (Appendix 4.3, Figure 4.8). Results were more scattered than those of  $\Delta$  because of the lower quantities of sediment collected and the sensitivity of the results to the location of the sampling tubes. On Figure 4.8, even if the result obtained from trap 4.1 is slightly offset, the semi-log plot of the average near-bed concentration against distance is close to linear (again with a slight concavity), suggesting an exponential decay of  $C_b$  with distance downstream.

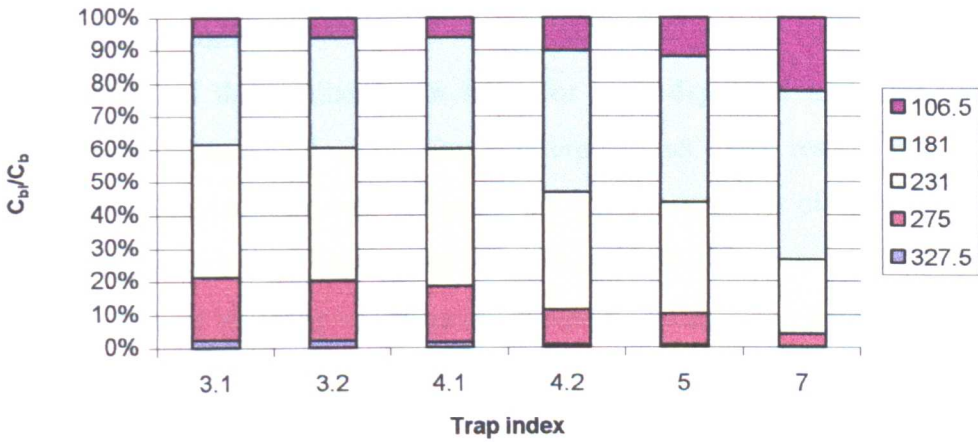


FIGURE 4.9a: variations of the near-bed fine sediment composition along the six sediment traps for experiment G3 (used as an example). The legend refers to the median size of each size class.

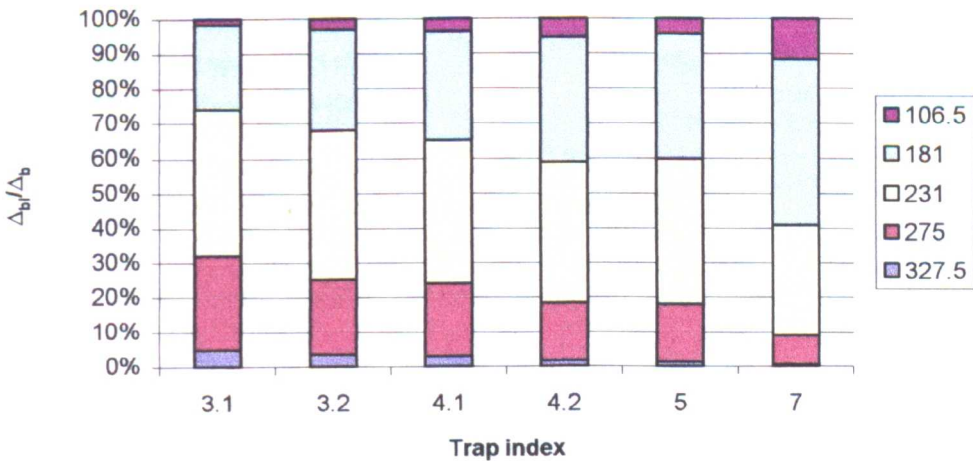


FIGURE 4.9b: variations of the deposited sediment composition along the six sediment traps for experiment G3 (used as an example). The legend refers to the median size of each size class.

### 4.4.3 Median size of near-bed and deposited fine sediment

The median size of the near-bed and deposited sediment samples decreased with distance downstream. This is illustrated by Figures 4.9a and 4.9b, which represent the proportions of the five main size fractions in the deposited and near-bed sediment samples (i.e.  $C_{bi}/C_b$  and  $\Delta_i/\Delta$  for 106.5, 181, 231 275 and 327.5 $\mu\text{m}$ ) collected during experiment G3 (similar plots were obtained in the other experiments). The proportion of the smaller size fractions (106.5 and 181 $\mu\text{m}$ ) increases in the downstream direction at the expense of the larger size fractions, reflecting an overall fall in median size with distance downstream.

Values of the median grain sizes for both deposited and near-bed sediment samples were determined using linear interpolations. The results are presented in Appendix 4.4, and summarised in Figure 4.10, which is a plot of the average deposited and near-bed sample size over all the experiments obtained from both LA-260 and B3-100 sand, against distance downstream. Several conclusions can be drawn from this figure:

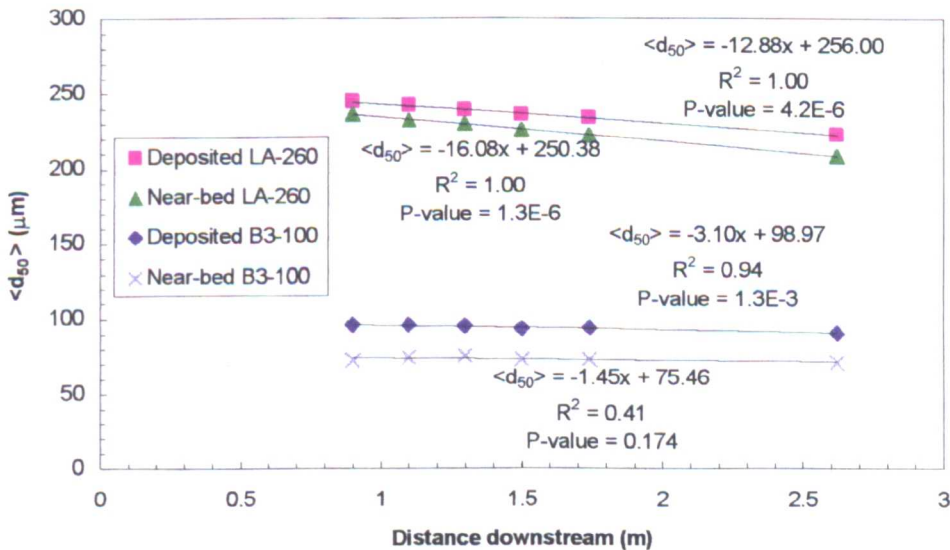


FIGURE 4.10: average medium size  $\langle d_{50} \rangle$  of both deposited and near-bed sediment against longitudinal distance. The value of  $\langle d_{50} \rangle$  corresponds to an average over all the experiments run with either LA-260 or B3-100 sands. The data for each individual experiment is presented in Appendix 4.4.

(1) in the case of LA-260 sand, the median size of the deposited and near-bed samples decreases with distance. This is because the coarser particles of the LA-260 mixture deposit faster than the finer ones, which results by continuity in a gradual decrease of the median size of the near-bed sediment, and thus also of the deposited sediment.

(2) in the case of B3-100 sand (D7, E7, G6, G7), median sizes tend to increase with distance over the first three traps. This is because the bulk of the fine particles reaches the near-bed zone close to trap 4.1. Upstream of trap 4.1, particles reach the bed surface mainly through diffusion processes, and these particles are relatively finer than the bulk. Downstream of trap 4.1, the coarser particles transported near the bed deposit faster (as with LA-260), but in addition particles finer than the average reach the near-bed area further downstream after having settled more slowly through the water column. This results in a decrease in size in both near-bed and deposited samples.

(3) the median size of the deposited samples is coarser than that of the corresponding near-bed samples. Again, this is the result of the faster deposition of the coarser particles compared to the finer ones.

(4) in the case of LA-260 sand, the median size of the samples (either near-bed or deposited) is always finer than that of the input (LA-260), except in the case of the large input (E6) where the first deposited sample has the same size as the input sand (Appendix 4.4). The finer catch is due to the deposition of the coarsest sand fractions in the first four traps (1.1, 1.2, 2.1, 2.2).

(5) the variations of sample sediment size against distance appear to be linear, particularly in the case of LA-260 sand. However, the distance over which the measurements are taken is short and not representative of the general trend. In addition, the fact that the grain size has to remain positive is in contradiction with a linear decrease. Considering a test section of infinite length, the fact that fine particles can only deposit and not be re-suspended implies that the sample sediment size can only converge towards zero.

The ratio between the mean size of the deposited fines and the near-bed fines ( $d_{50dep}/d_{50tp}$ ) has been computed for each experiment and for each trap (Appendix 4.5). These results have been summarised in Table 4.5, where the ratio  $d_{50dep}/d_{50tp}$  averaged over the six traps is indicated for increasing shear velocities.

Run	E4	D4	D3	E3b	G3	G2b	D5
$u^*$ (m.s <sup>-1</sup> )	0.068	0.072	0.076	0.076	0.078	0.08	0.084
$\frac{d_{50\ dep}}{d_{50\ tpt}}$ %	7.14	10.05	5.81	4.08	6.00	4.53	6.38
Run	E2	G1	G5	D6	E5	E6	G4
$u^*$ (m.s <sup>-1</sup> )	0.086	0.086	0.096	0.097	0.102	0.102	0.121
$\frac{d_{50\ dep}}{d_{50\ tpt}}$ %	4.18	3.44	2.41	3.38	3.23	3.97	2.88

TABLE 4.5: ratio between the deposited fines and the near-bed fines mean size ( $d_{50dep}/d_{50tpt}$ ), averaged over the six traps, and shear velocity  $u^*$  (in increasing order)

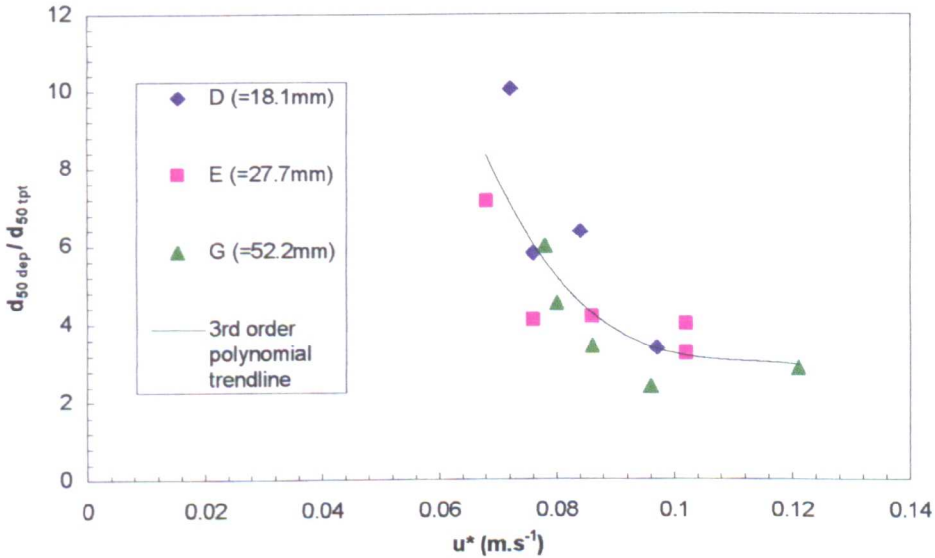


FIGURE 4.11: influence of  $u^*$  on the difference in median size between deposited and transported sediment (LA-260)

The plot of the percentages  $d_{50dep}/d_{50tpt}$  against  $u^*$  (Figure 4.11) shows a consistent trend, indicating that the gap in size between deposited and near-bed fines tends to decrease as the shear velocity increases. In the case of B3-100 sand (Appendix 4.5), the lower percentage  $d_{50dep}/d_{50tpt}$  corresponds also to the largest shear velocity.

In short, the median sizes of deposited and near-bed fines tend to decrease with longitudinal distance. This is due to the difference in deposition velocity between the coarse and the fine fractions of the near-bed sediment mixture. This also causes the deposited sediment to be coarser than the corresponding near-bed sediment. The gap

between deposited and near-bed fines in terms of  $d_{50}$  tends to decrease with increasing shear velocity.

#### 4.4.4 Deposition velocity results

The detailed results, experiment by experiment, sediment trap by sediment trap for  $\Delta_i$ ,  $C_{bi}$ , and  $w_{di}$  are presented in Appendix 4.7. The values of the average deposition velocities  $w_d$  (obtained by averaging the results of each of the six traps) for each experiment and each trap are summarised in Appendix 4.6. The average results  $\langle w_d \rangle$  obtained for all the experiments with LA-260 and B3-100 are presented for each size fraction in Table 4.6.

The deposition velocity represents the average settling velocity of fine particles through the bed surface. Just like the fall velocity in still water, this parameter tends to increase with grain size for both LA-260 and B3-100 sands. However, it can be seen that

Size ( $\mu\text{m}$ )	106	181	231	275	327	390	462	550			
$\langle w_d \rangle$ ( $\text{m.s}^{-1}$ )	0.009	0.018	0.024	0.031	0.040	0.044	0.047	0.041			
$w_s$ ( $\text{m.s}^{-1}$ )	0.007	0.017	0.024	0.031	0.039	0.047	0.057	0.068			
Size ( $\mu\text{m}$ )	49	58	69	82.5	98	115.5	137.5	165	196	231	275
$\langle w_d \rangle$ ( $\text{m.s}^{-1}$ )	0.001	0.002	0.002	0.003	0.004	0.005	0.007	0.009	0.013	0.018	0.020
$w_s$ ( $\text{m.s}^{-1}$ )	0.002	0.002	0.003	0.004	0.006	0.008	0.011	0.015	0.019	0.024	0.031

TABLE 4.6: average deposition velocity obtained for all experiments with LA-260 (upper part) and B3-100 (lower part), against grain size.

for the larger size fractions of LA-260,  $\langle w_d \rangle$  tends to stabilise, and even begins to decrease between 462.5 and 550 $\mu\text{m}$ . The comparison between the average deposition velocities of LA-260 sediment and the fall velocities at 20°C computed from Cheng (Figure 4.12) indicates the following general trends:

(1) between  $\sim 200$  and  $\sim 350\mu\text{m}$ , the average deposition velocity is close to the fall velocity.

(2) below  $\sim 200\mu\text{m}$ , the average deposition velocity is larger than the fall velocity.

In other words, a phenomenon of *enhanced deposition* is observed in the majority of the

experiments. The difference between deposition velocity and fall velocity appears to increase as sediment size decreases.

(3) for particles larger than approx.  $\sim 350\mu\text{m}$ , the deposition velocity is lower than the fall velocity.

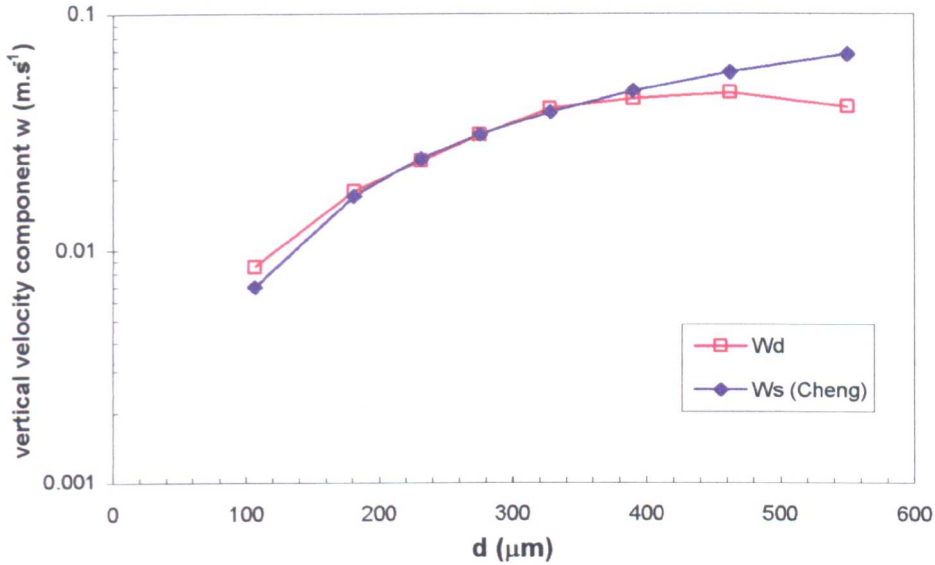


FIGURE 4.12: comparison between the average deposition velocity across all experiments with LA-260 sand  $\langle w_d \rangle$  and Cheng's fall velocity.

Overall, the effect of the bed surface gravel is thus to reduce the natural differences between the settling velocities of fine and coarse sand particles. This difference, which is 10-fold between  $100\mu\text{m}$  and  $550\mu\text{m}$  particles in still water, is reduced to five times in terms of deposition velocity.

Concerning the results of the average deposition velocity for each experiment, no clear distinction is found between the three groups of experiments (D, E, G), thus gravel size has no apparent effect of on  $w_d$ . However, the plot of  $\overline{w_d}$  (average over the results of all size fractions) against the shear velocity  $u^*$  (Figure 4.13) indicates that increasing shear velocity and turbulence intensity tend to reduce the deposition fluxes of fine particles through the bed pores (the results of the E-series are not, however, as conclusive as those of the other two series). This confirms the results of earlier studies on sediment settling velocities in water by Camp (1943) and Krone (1962) (§2.2.2.3).

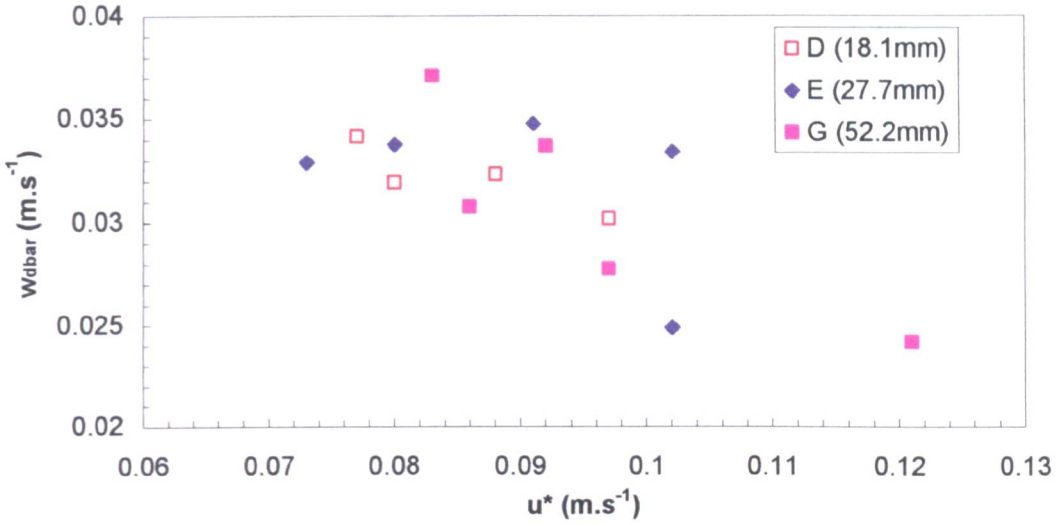


FIGURE 4.13: average deposition velocity across all size fractions  $\overline{w_d}$  against shear velocity for LA-260 sand

#### 4.4.5 Dimensionless deposition velocity results.

The dimensionless deposition velocity  $w_d^*$ , the ratio of the deposition velocity  $w_d$  to the fall velocity  $w_s$ , gives an indication of the mechanical effects of the bed surface and the turbulent flow on the particles. The detailed results ( $w_{di}^*$ ) are presented in Appendix 4.7 and a summary of the results for each experiment can be found in Appendix 4.6.

Size ( $\mu\text{m}$ )	106	181	231	275	327	390	462	550			
$\langle w_d^* \rangle$ ( $\text{m.s}^{-1}$ )	1.26	1.08	1.00	1.01	1.06	0.94	0.83	0.61			
Size ( $\mu\text{m}$ )	49	58	69	82.5	98	115.5	137.5	165	196	231	275
$\langle w_d^* \rangle$ ( $\text{m.s}^{-1}$ )	0.82	0.71	0.72	0.66	0.64	0.65	0.63	0.64	0.69	0.73	0.66

TABLE 4.7: average dimensionless deposition velocity  $\langle w_d^* \rangle$  obtained for all experiments with LA-260 (1<sup>st</sup> row) and B3-100 (2<sup>nd</sup> row), against grain size.

Again the average value over all the experiments with the same type of sand has been computed to show the general trend (Figure 4.14). For the coarser sand,  $\langle w_d^* \rangle$  is generally larger than 1 below 200 $\mu\text{m}$ , lower than 1 above 350 $\mu\text{m}$ , and close to 1 between 200 $\mu\text{m}$  and 350 $\mu\text{m}$  in the present experimental conditions. This is just another way of expressing the comparison made in the previous paragraph between  $\langle w_d \rangle$  and the fall velocity  $w_s$ . The curve decreases up to 220 $\mu\text{m}$ , increases between 220 $\mu\text{m}$  and 320 $\mu\text{m}$ ,

and decreases again above 320mm. A similar trend is observed for the experiments with B3-100 sand:  $\langle w_d^* \rangle$  tends to decrease up to 140mm, it increases between 140 and 230 $\mu\text{m}$  and it decreases thereafter (Figure 4.14). The values of  $\langle w_d^* \rangle$  are significantly lower compared to those obtained with LA-260.

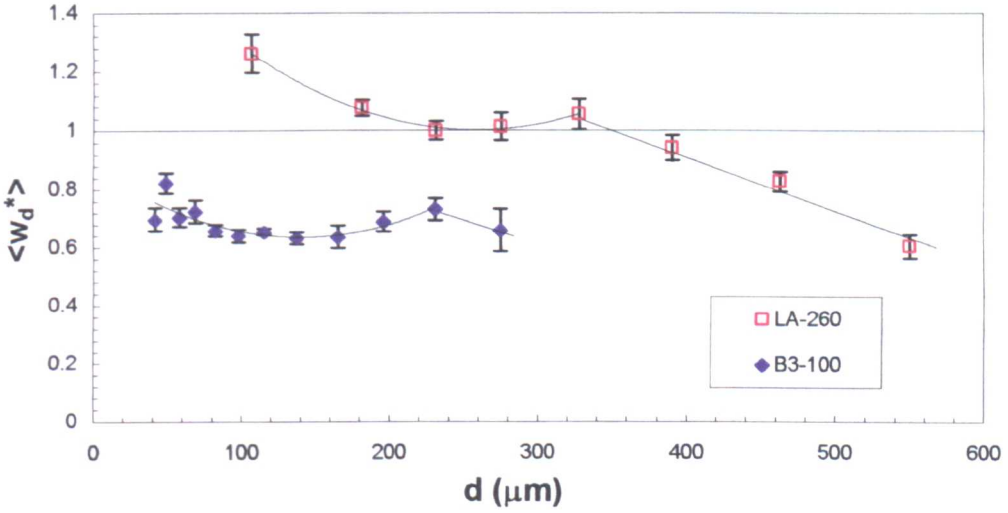


FIGURE 4.14: average dimensionless deposition velocity  $\langle w_d^* \rangle$  against grain size, for experiments with LA-260 and B3-100 sands.

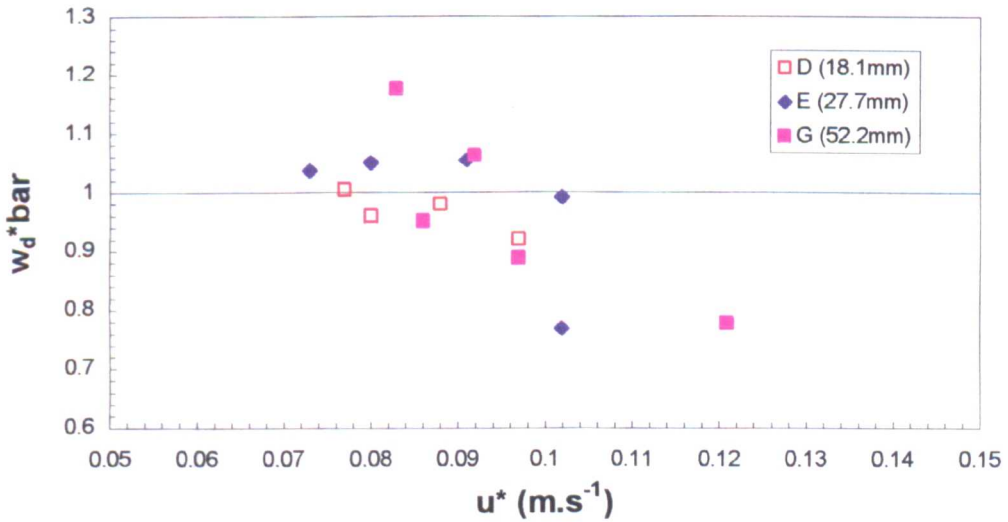


FIGURE 4.15: average dimensionless deposition velocity across all size fractions  $\overline{w_d^*}$  against shear velocity for LA-260 sand

In order to enable the comparison between the results of different experiments, the average dimensionless deposition velocity  $\overline{w_d^*}$  (measured over all size fractions

present in LA-260 sand) has been plotted in Figure 4.15 against shear velocity. The graph shows that, as could be expected from the previous results for  $w_d$ ,  $w_d^*$  generally decreases with the shear velocity  $u^*$ .

Figures 4.16a, 4.16b and 4.16c present three plots of dimensionless deposition velocities  $w_d^*$  against grain size for constant bed size conditions but varied shear velocities. Generally, these graphs also support the idea that higher shear velocities tend to impede sediment deposition. This is particularly noticeable in Figure 4.16c, which is the one concerned with the coarsest gravel ( $d_{50}=52.2\text{mm}$ ): all the points are arranged in descending order relatively to  $u^*$  for any size fraction between 231 and 462.5 $\mu\text{m}$ . The top curve (G3) represents the experiment featuring the lowest value of  $u^*$ , while the bottom curve (G4) is that with the largest  $u^*$ . The largest differences in  $w_d^*$  caused by changes in shear velocity are observed for the 327.5 $\mu\text{m}$  size fraction, and this difference tends to decrease away from this point. At  $d=181\mu\text{m}$  and  $d=550\mu\text{m}$ , the differences are quite small, while for the very fine range ( $d=106.5\mu\text{m}$ ), the curves tend to separate again, in a similar way than with  $d=327.5\mu\text{m}$  (inversely to  $u^*$ ).

The trends are less clear for the lower median gravel sizes. Figure 4.16a is the closest to Figure 4.16c, with the spacing between the curves characterized by two constrictions, here at 181 $\mu\text{m}$  and 462.5 $\mu\text{m}$ . Between these points, the curves are also arranged in descending order relatively to  $u^*$ , except in the cases of experiments D4 and D3 at  $d_m=327.5\mu\text{m}$  and 390 $\mu\text{m}$ . This may be the proximity of the shear velocities in the two experiments ( $u^* = 0.077$  and  $0.080\text{m}\cdot\text{s}^{-1}$ ). In Figure 4.16b, the dimensionless deposition velocities are arranged in descending order relatively to the shear velocity between 181 and 327.5 $\mu\text{m}$ , but above 327.5 $\mu\text{m}$ , the relative position of the points varies. However, the curve supporting the largest  $u^*$  (E5) always exhibits a lower  $w_d^*$  than the other experiments.

Overall, Figure 4.16 confirms that deposition rates decrease as the shear velocity increases, particularly from intermediate grain sizes ( $\sim 300\text{-}350\mu\text{m}$ ). Two graphs out of three suggest that this effect is less for finer and coarser sands ( $\sim 200$  and  $500\mu\text{m}$ ).

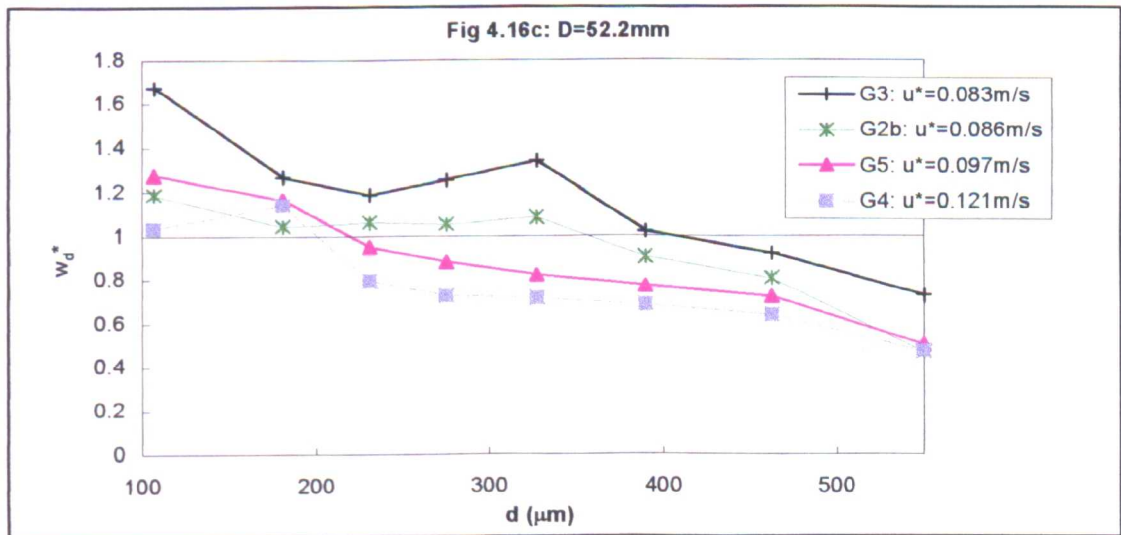
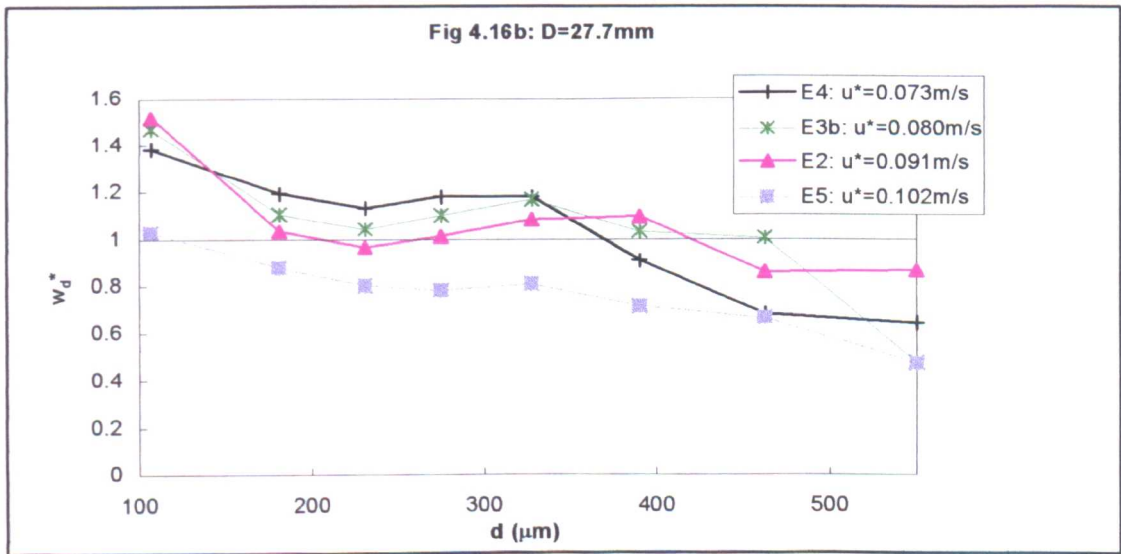
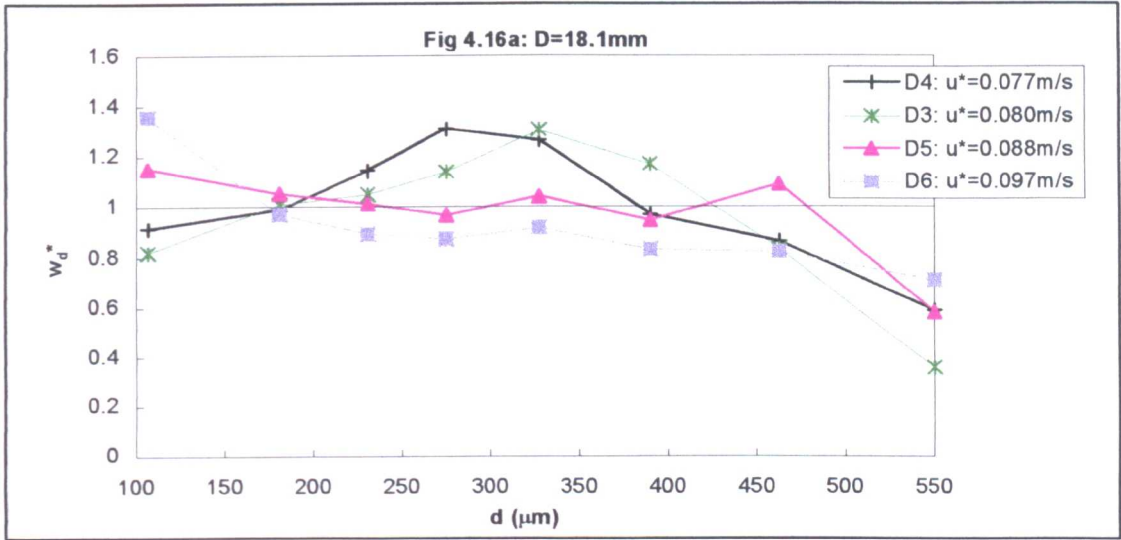


FIGURE 4.16: plots of the dimensionless deposition velocity against grain size for different gravel sizes, illustrating the influence of the shear velocity  $u^*$  on  $w_d^*$ .

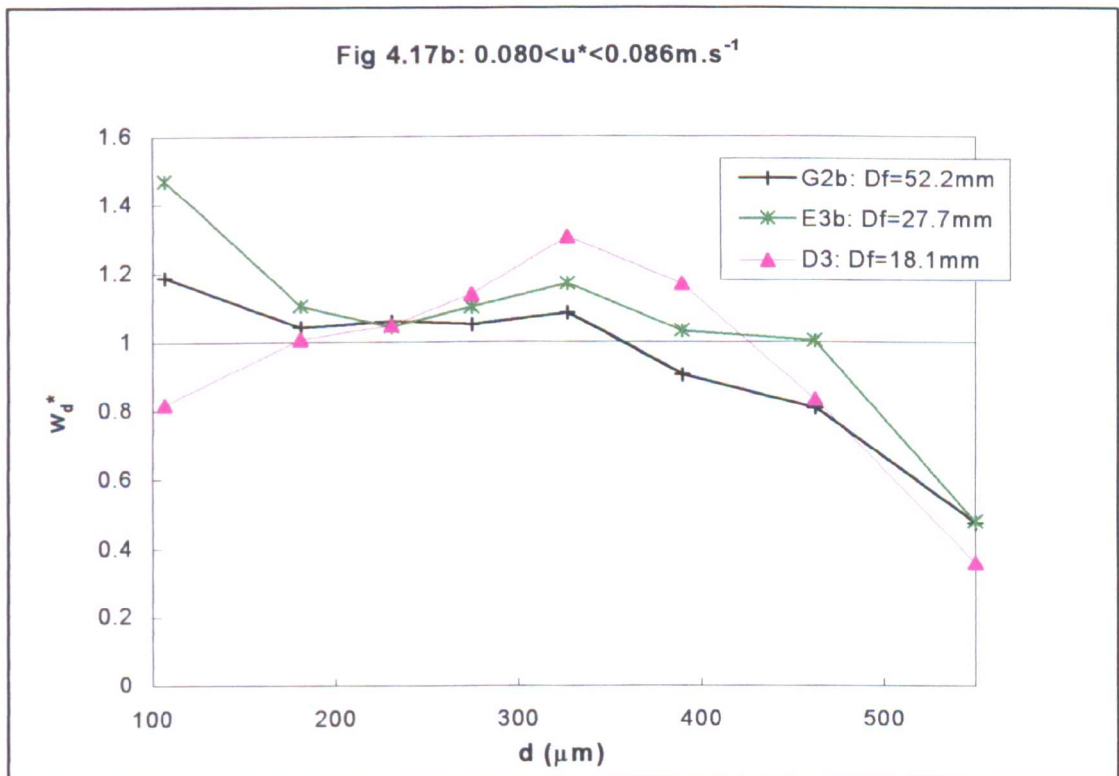
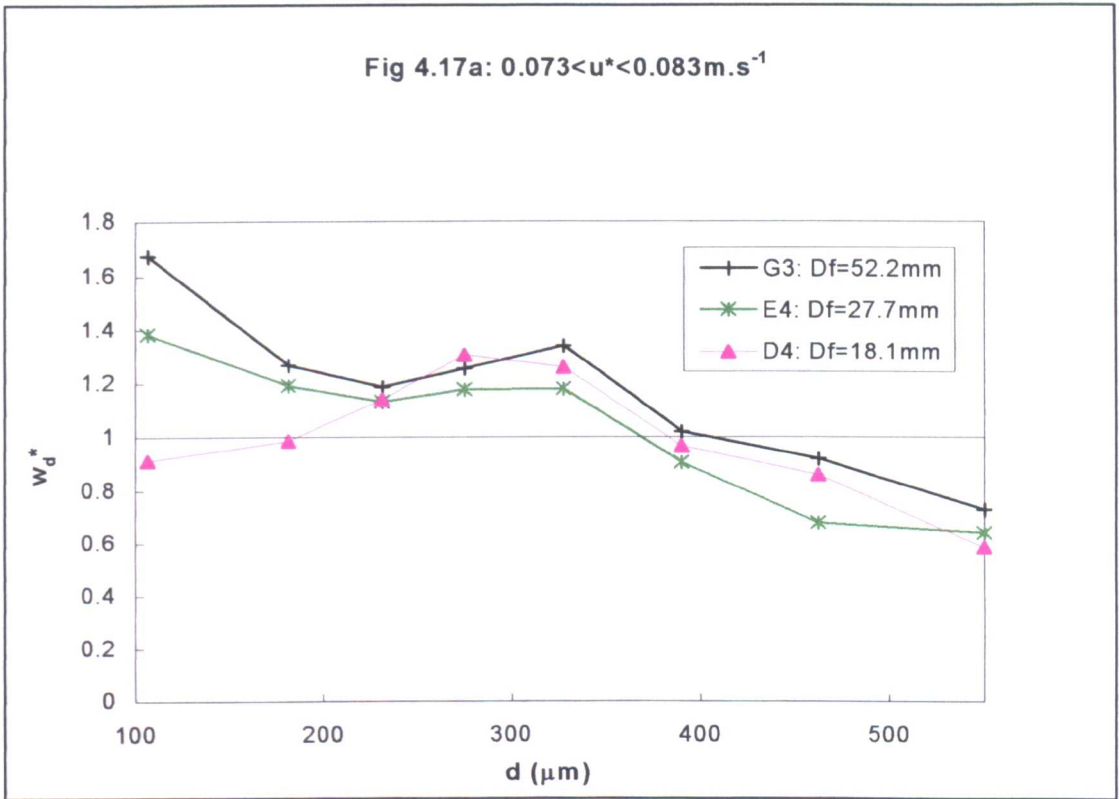


FIGURE 4.17a and 4.17b: plots of the dimensionless deposition velocity against grain size for different classes of shear velocity, illustrating the influence of the gravel size on  $w_d^*$ .

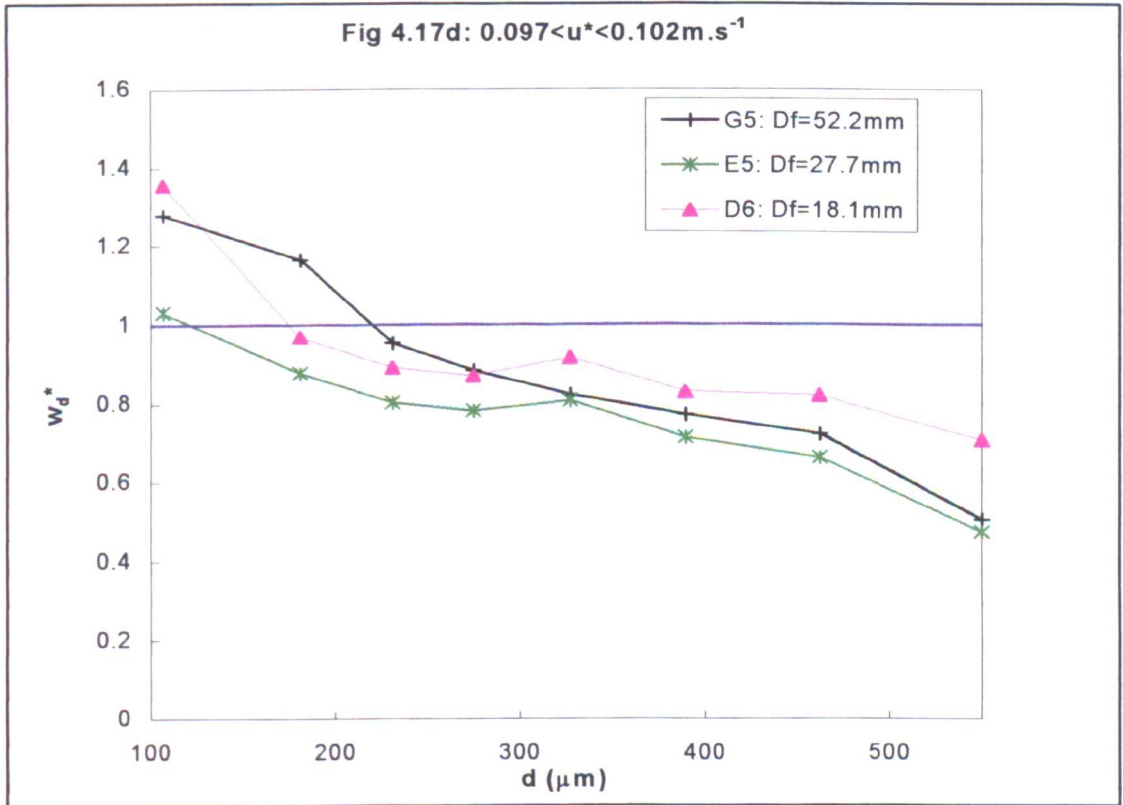
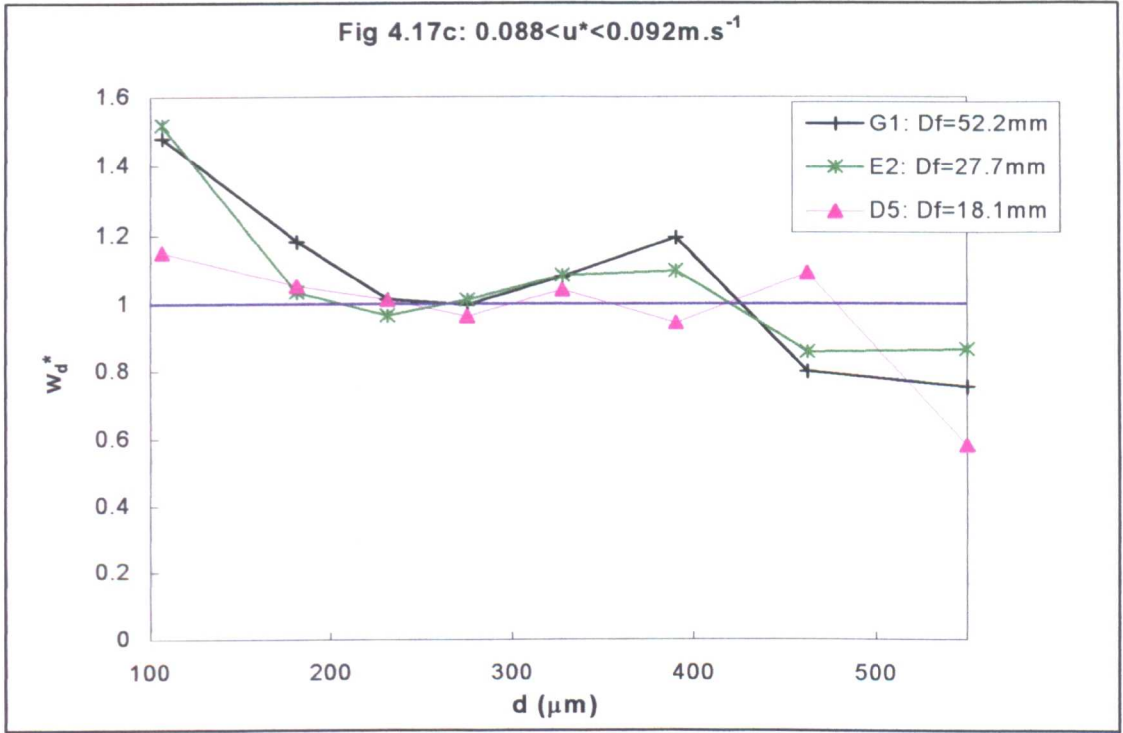


FIGURE 4.17c and 4.17d: plots of the dimensionless deposition velocity against grain size for different classes of shear velocity, illustrating the influence of the gravel size on  $w_d^*$ .

Another way to examine the data is to hold  $u^*$  constant and examine the effect of gravel size on  $w_d^*$ . Figures 4.17a, 4.17b, 4.17c and 4.17d show graphs of  $w_d^*$  against grain size for experiments featuring the same flow depth, and approximately the same values of  $u^*$ , but different types of gravel surfaces. In general, the curves tend to have similar shapes above  $\sim 200\mu\text{m}$ , and to be quite close to each other. Figure 4.17d, which features the largest shear velocities and the lowest flow depths, presents slightly larger gaps between the three curves. However, Figures 4.17a and 4.17b show remarkably consistent results, with little difference between the three cases.

Below  $200\mu\text{m}$ , the curves tend to diverge, particularly in Figures 4.17a and 4.17b, and to a lesser extent in Figures 4.17c and 4.17d. There is no clear influence of the gravel size on  $w_d^*$ , which confirms the results of the preliminary series of tests (§3.3.3) and that of Einstein (1968) on the deposition of silt-size, non-cohesive particles (§2.2.1.4). However, it can be noticed that the finest gravel ( $D_f=18.1\text{mm}$ ) tends to be associated with the lowest dimensionless deposition velocities below  $180\mu\text{m}$  (Figures 4.17a, 4.17b and 4.17c).

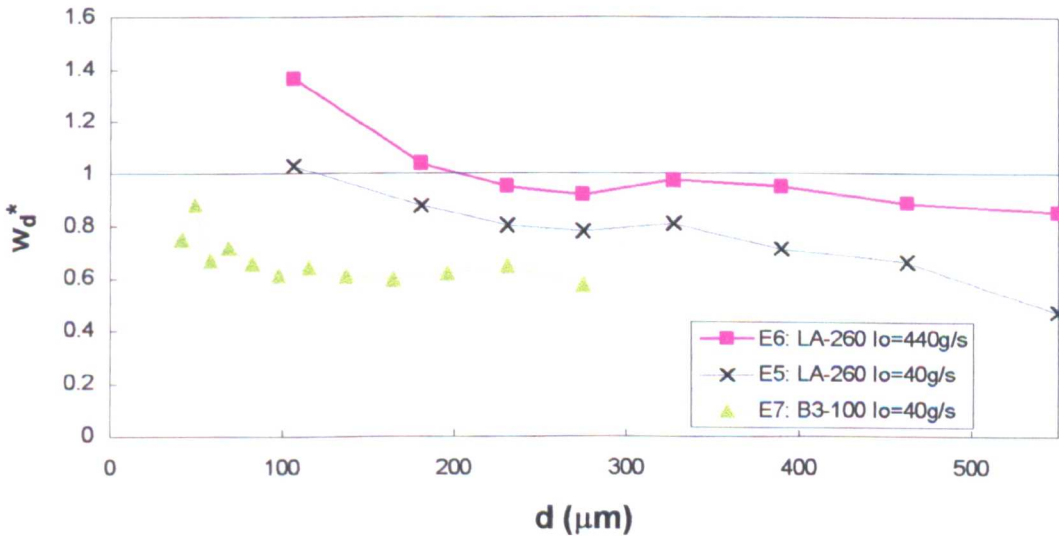


FIGURE 4.18: dimensionless deposition velocity against grain size for experiments E5, E6 and E7, illustrating the influence of the composition and the input rate of sediment on  $w_d^*$ .

Lastly, both shear velocity and gravel size were held constant to examine the possibility of the intervention of other parameters than  $u^*$  and  $D$  on the deposition process. Figure 4.18 presents the results of three experiments (E5, E6 and E7) featuring

the same bed material and shear velocity. Results from the intermediate (E5) and the lower curve (E7) were obtained with respectively LA-260 and B3-100 sands at an input rate of  $I_0=40\text{g}\cdot\text{s}^{-1}$ . The upper curve (E6) was obtained with LA-260 sand at an input of  $I_0=440\text{g}\cdot\text{s}^{-1}$ , i.e. eleven times larger than that of E5 and E7. These values of  $w_d^*$  were the largest obtained in the entire series of experiments.

Figure 4.18 reveals important differences in the dimensionless deposition velocities between  $\sim 100$  and  $\sim 275\mu\text{m}$ , where data is available in the three cases. These differences become increasingly large towards finer grain sizes. In these experiments, the near-bed concentrations varied between  $0.180\text{g}\cdot\ell^{-1} \leq C_b \leq 8.600\text{g}\cdot\ell^{-1}$  (Appendix 4.3), which is within the range over which Carling (1984) observed linear variations of the deposition rate against the concentration (§2.2.2.3a). However, changes in both near-bed concentration and composition of the gravel sediment mixture caused a significant variation in the dimensionless deposition velocity. This indicates that total near-bed fine sediment concentration and sediment size also exert a control on the deposition processes.

## 4.5 Conclusion

This is a summary of the main points presented in this chapter:

- (1) downstream from a point source, the average near-bed concentration and deposition rates follow an exponential decay. The decay rate decreases with increasing longitudinal distance and with increasing shear velocity.
- (2) the median size of near-bed and deposited sediment decreases with longitudinal distance. The sediment deposited is coarser than the corresponding near-bed sediment. The gap between deposited and near-bed sediment's  $d_{50}$  tends to decrease with increasing shear velocity.
- (3) the deposition velocity generally increases with grain size, but experiments with LA-260 suggest that it tends to stabilise and even decrease above  $450\mu\text{m}$ .

- (4) for the experiments with LA-260 sand, the dimensionless deposition velocity  $w_d^*$  generally decreases with grain size from a value larger than 1 below  $200\mu\text{m}$  to a value lower than 1 above  $350\mu\text{m}$ . A phenomenon of enhanced deposition is thus observed for the finest particles, whereas deposition of the largest particles tends to be retarded by the bed surface.
- (5) for B3-100 sand experiments, values of  $w_d^*$  are significantly lower than with LA-260 (no enhanced deposition), but similar trends are observed.
- (6) the deposition velocity of fine particles decreases with increasing shear velocity, particularly so for medium-size sand particles ( $\sim 300\text{-}350\mu\text{m}$ ).
- (7) gravel size does not have a significant influence on the deposition velocity of particles larger than  $200\mu\text{m}$ . Some observations suggest that deposition of particles finer than  $200\mu\text{m}$  may increase through larger gravel beds, but this contradicts the results of Einstein (1968) on silt particles.
- (8) the input rate and the composition of the fine sediment mixtures influence the deposition velocity, independently of gravel size and shear velocity.  $w_d$  tends to increase with the input rates and with the median size of the fine particles.

# Chapter V

## Analysis

### 5.1 Introduction

Very little theoretical formulation exists that can be used to study or predict the fines deposition/infiltration process (Einstein, 1968). The aim of this chapter is to: (1) find physical interpretations of the experimental results described previously; and (2) develop a theoretical description of these results.

As a start, two of the main findings from Chapter IV are recalled: (1) in the case of LA-260 sand, the finest particles ( $<200\mu\text{m}$ ) tend to undergo enhanced deposition, while coarsest fines ( $>350\mu\text{m}$ ) are deposited relatively slowly compared to their natural fall velocity; and (2) the bed surface size does not affect significantly the deposition of the coarser fines, but it may affect that of the finer particles. These two results suggest that there are variations in the nature of the depositional behaviour relatively to the transport mode and to the size of the fine particles.

Hoyal *et al.* (1995) reported a distinct change in the transport behaviour of fine sediment at a critical value  $w^*_c \sim 0.1$  ( $w^* = w_s / u^*$ ). This value corresponds in the present study to particles of  $\sim 130\mu\text{m}$  in diameter. Enhanced deposition ( $w_d^* > 1$ ) was reported for particle sizes such that  $w^* < w^*_c$ . Above  $w^*_c$ , the still water fall velocity was described as a good estimate of the mean deposition velocity.

Jobson and Sayre (1970, §2.2.2.1) differentiated between the Stokes range of particles, which has a dispersion coefficient nearly equal to that of the fluid, and the intermediate range. Sayre (1968) proposed that the critical threshold between these two ranges occurs for grain sizes approximately equal to  $100\mu\text{m}$ . Above this size, the depositional behaviour of the particles begins to be influenced by gravity. Due to the large difference in size between the bed and the transported particles, the fines that are

not suspended can only be transported by saltation, as rolling on the gravel bed is almost synonymous with immediate deposition. Clearly, a different process of deposition can be expected for particles transported by saltation, which collide periodically with the bed, compared to that of suspended particles, more influenced by near-bed turbulence. This is illustrated in Figure 4.12 by the break in the plot of  $w_d$  against grain size at  $\sim 330\mu\text{m}$ , which corresponds to a value of  $w^*$  close to 0.4.

These effects have led to the analysis of the experimental results being conducted by separating the processes of deposition of suspended particles from those of the saltating (bed) load. The key parameters involved in the deposition process have been identified by dimensional analysis. Following an analysis on the extent of the influence of these parameters, the results of experiments E5, E6 and E7 (§4.4.5) have led to the identification of an additional parameter involved in the process. Finally, an equation has been derived to summarise all these effects.

## 5.2 Dimensional analysis

### 5.2.1 Theory

Eleven variables can be considered to describe the process of fine sediment deposition into natural gravel-beds i.e. deposition rate  $\Delta$  ( $\text{kg}\cdot\text{m}^{-2}\cdot\text{s}^{-1}$ ), near-bed sediment concentration  $C_b$  ( $\text{kg}\cdot\text{m}^{-3}$ ), shear velocity  $u^*$  ( $\text{m}\cdot\text{s}^{-1}$ ), water depth  $h$  (m), dynamic viscosity  $\mu$  ( $\text{kg}\cdot\text{m}^{-1}\cdot\text{s}^{-1}$ ), fluid and sediment density (resp.  $\rho_w$  and  $\rho_s$ ,  $\text{kg}\cdot\text{m}^{-3}$ ), fine particle size  $d$  (m), mean bed sediment size  $D$  (m), bed porosity  $\lambda$  (dimensionless), and gravitational acceleration  $g$  ( $\text{m}\cdot\text{s}^{-2}$ ). Other parameters, such as bed sediment grading, coefficients of grain shape and coefficients related to the sub-surface composition are considered to have a second order influence and are ignored. Therefore, the initial equation reads:

$$\Delta = f(C_b, u^*, h, \mu, \rho_w, \rho_s, d, D, \lambda, g) \quad [5.1]$$

where  $f$  represents a given function.

These variables are combinations of three fundamental dimensions (i.e. mass M, time T and distance L). According to Buckingham's  $\Pi$  theorem, they can be rearranged into a series of  $11-3=8$  dimensionless parameters. Considering the fundamental dimensions as being represented by  $L = d$ ,  $M = \rho_w h^3$  and  $T = u^* g^{-1}$ , the dimensional analysis leads to:

$$\frac{\Delta u^*}{\rho_w g d} = f\left(\frac{d}{h}, \frac{D}{h}, \frac{C_b}{\rho_w}, \frac{\rho_s}{\rho_w}, \frac{u^{*2}}{g d}, \frac{g d^2}{\nu u^*}, \lambda\right) \quad [5.2]$$

The deposition rate  $\Delta$  is made dimensionless with the ratio between the shear velocity and the product of the fluid density, the gravity acceleration and the bed sediment median size. It is found to be related to: (1) the dimensionless fine sediment size  $d/h$ ; (2) the relative fine sediment grain size compared to the bed size  $d/D$ ; (3) the dimensionless sediment concentration  $C_b/\rho_w$  (4) the relative density of the particles  $\rho_s/\rho_w$ ; (5) a dimensionless gravity parameter, similar to the Froude number; (6) a flow parameter, similar to a Reynolds number when divided by (5); and (7) the bed porosity  $\lambda$ .

In the case of the present experimental work, several simplifications can be made to Equation [5.2] as some parameters were maintained constant or nearly constant throughout the whole series of experiments. This is the case for the relative sediment density, for the gravity and also to a certain extent for the kinematic viscosity. The influence of Term (4) of [5.2] can thus be omitted. Terms (5) and (6), which contain the parameters  $d$  and  $u^*$ , already accounted for in term (1) and in the dimensionless deposition rate, can also be considered as having a minor influence on the results of the experiments. Equation [5.2] reduces to:

$$\frac{\Delta u^*}{\rho_w g d} \approx f\left(\frac{d}{h}, \frac{D}{h}, \frac{C_b}{\rho_w}, \lambda\right) \quad [5.3]$$

In addition, if: (1) the near-bed concentration  $C_b$  is assumed to be sufficiently low for the deposition rate  $\Delta$  to be linearly related to  $C_b$ ; (2) the porosity  $\lambda$  is assumed to

remain constant; and (3) the parameter  $d^*$  ( $=d(\rho_s^*g/v^2)^{1/3}$ ) is used to represent the dimensionless grain size, then the relation becomes:

$$\frac{\Delta u^*}{C_b g d} = \frac{w_d u^*}{g d} \approx f\left(d^*, \frac{D}{h}\right) \quad [5.4]$$

The parameter  $d^*$  was used instead of  $d/h$  because it is a more general expression of the dimensionless grain size and because the influence of the water depth  $h$  was already accounted for in the second term  $D/h$ . Moreover, the analysis of the experimental data indicated a better correlation between  $w_d u^* / (g d)$  and  $d^*$  than with  $d/h$ . Once again, this assumption is specific to the present experimental conditions (i.e. relatively low flow depth and small variations in flow depth).

In these simplified conditions, the dimensionless parameter  $w_d u^* / (g d)$  has a first-order dependence on  $d^*$  and the ratio between bed particle size and water depth  $D/h$ . This parameter is referred in the following as the *deposition parameter*  $w_d^+$ . It is similar to a Froude number, which rejoins the analysis of Beschta and Jackson and the Fr-dependency of the deposition process.

### 5.2.2 Application.

Following the results of the dimensional analysis (Equation [5.4]), the deposition parameter  $w_d^+$  has been plotted against the dimensionless grain size  $d^*$ . The parameter  $D/h$  is indicated in brackets in the caption. The graphs are presented separately for the experiments conducted with LA-260 (Figure 5.1a), and with B3-100 (Figure 5.1b).

The graph in Figure 5.1a, which has the general shape of an arch, can be divided into two parts, separated by  $d^* \sim 8$  ( $d \sim 320 \mu\text{m}$ ). The peak of the parameter  $w_d^+$  is close to 1.10. The data tend to be more scattered at the limits of the dimensionless grain size interval than at the centre. The points are also less scattered in the rising part of the curve (i.e. below  $d^* \sim 8$ ), where the best-fit power function between  $w_d^+$  and  $d^*$  is:

$$w_d^+ = 0.50 \times d^{*0.37} \quad (70 \text{ data, } r^2=0.55) \quad [5.5]$$

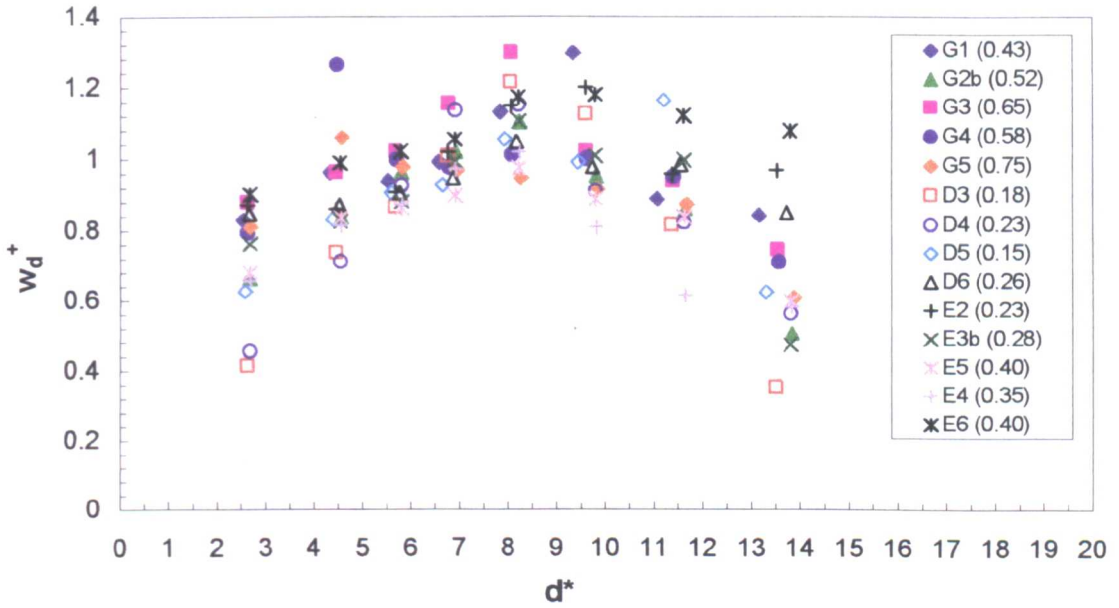


FIGURE 5.1a: deposition parameter  $w_d^+$  ( $=w_d u^*/(gd)$ ) against dimensionless grain size  $d^*$  ( $=d(g\rho_s^*/v^2)^{1/3}$ ) for all experiments carried out with sand LA-260. The ratio  $D/h$  is indicated in brackets.

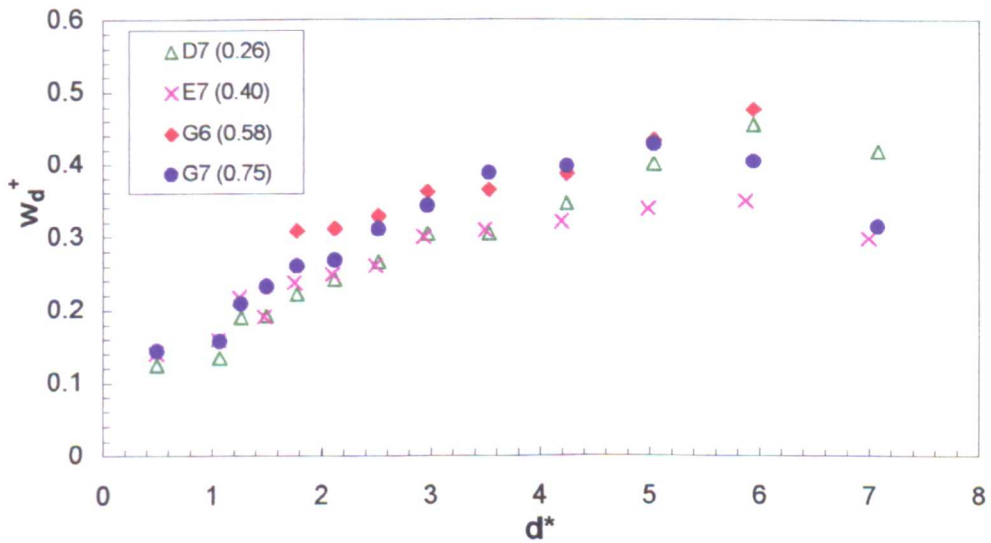


FIGURE 5.1b: deposition parameter  $w_d^+$  ( $=w_d u^*/(gd)$ ) against dimensionless grain size  $d^*$  ( $=d(g\rho_s^*/v^2)^{1/3}$ ) for all experiments carried out with sand B3-100. The ratio  $D/h$  is indicated in brackets.

For B3-100, Figure 5.1b indicates a similar trend than Figure 5.1a but with values of  $w_d^+$  significantly lower and a peak of  $w_d^+ \sim 0.4$  for  $d^* \sim 6$ . The scatter between the points tends to increase with grain size. The best-fit power function for this series of points is:

$$w_d^+ = 0.19 \times d^{*0.46} \quad (45 \text{ data, } r^2=0.78) \quad [5.6]$$

No significant influence of the parameter  $D/h$  on the deposition parameter  $w_d^+$  can be detected (Figures 5.1a and 5.1b). However, the fact that the peaks and the best-fit power function obtained in each case are different suggests that other parameters than those featuring in [5.4] have an effect on  $w_d^+$ .

Overall, the results from different bed and flow conditions tend to converge on a relation linking a dimensionless grain size parameter and a dimensionless deposition velocity for the suspended load, but there is at least one additional factor missing.

### 5.3 Deposition of suspended load

#### 5.3.1 Suspension criterion

Fine sediment can be suspended in a turbulent flow only if the velocity of upward directed fluid equals or exceeds the terminal fall velocity of the grains. The upward directed fluid stress required to balance the immersed weight of the suspended particles can only arise if turbulence is anisotropic, i.e. takes different values in different directions at any given point (Bagnold, 1966). Based on a theoretical analysis of vertical momentum flux in anisotropic turbulent shear flows by Bagnold (1966), Bridge and Bennett (1992) defined the following suspension criterion:

$$w_s \leq bu^* \quad [5.7]$$

where  $w_s$  is the terminal fall velocity and  $b$  a parameter such that  $b \sim 0.8$  for  $u^* y_D / \nu \geq 50$ , and  $b \approx 0.8 [(u^* y_D / \nu) / 50]$  for  $u^* y_D / \nu < 50$ , and  $y_D \approx 0.6 d_m$ . The threshold size can be determined by trial-and-error, by computing both parameters  $w_s$  and  $bu^*$  until they are equal. Using Cheng's method to compute the fall velocity, the results with  $\rho_s = 2700 \text{ kg.m}^{-3}$  and  $\nu = 10^{-6} \text{ m}^2.\text{s}^{-1}$  indicated maximum sizes in suspension of  $800 \mu\text{m}$  for  $u^* = 0.12 \text{ m.s}^{-1}$ ,  $188 \mu\text{m}$  for  $u^* = 0.10 \text{ m.s}^{-1}$ , and  $72 \mu\text{m}$  for  $u^* = 0.07 \text{ m.s}^{-1}$ .

### 5.3.2 Physical model

Observations reported by Carling (1984) (§2.2.1.4) suggest that suspended particles tend to be trapped in lee eddies before being entrained into the bed interstices by downward turbulent pressure pulses (equivalent to sweeps, §2.2.1.4). An analysis on the relationship between deposition and near-bed turbulence has thus been carried out, based on work by Cao (1995) on a bursting-based sediment entrainment function.

Considering a near-bed concentration  $C_b$  of fine particles over a porous bed, the number  $N$  of particles per unit bed area is given by (Shen and Ackermann, 1982; in Cao, 1995):

$$N = \frac{6 C_b}{\rho_s \pi d^2} \quad [5.8]$$

Raupach (1981) investigated the characteristics of turbulent events contributing to the Reynolds stress over smooth and rough surfaces. One of the main results of his study is that sweeps account for most of the shear stress close to rough surfaces, in a region defined as the roughness sublayer. If  $T_s$  is defined as the average period of the sweep events, it was also found that the parameter  $T_s u^* / \delta$ , where  $\delta$  is the boundary layer thickness, is invariant with changes in surface roughness and equal to  $\sim 0.15$  near the bed. Thus, the average turbulent sweep period was defined as:

$$T_s = 0.15 \frac{\delta}{u^*} \quad [5.9]$$

Various investigators (e.g. Kline *et al.*, 1967) have established from measurements that turbulent bursts in smooth wall cases extend on average over  $\sim 40v/u^*$  and  $\sim 25v/u^*$  respectively in the streamwise and transverse directions. In the case of rough bed surfaces, the length scale of these turbulent structures increases proportionally with the roughness scale (Smith, 1996). It has thus been assumed in the present study that the extent of the turbulent sweeps in both directions is directly related to  $k/k_{ref} \times$

$v/u^*$ , where  $k$  is the vertical dimension of the roughness elements, and  $k_{ref}$  a reference value of  $k$ . The area occupied by one sweep event is thus:

$$A_s = \frac{k^2 v^2}{k_{ref}^2 u^{*2}} \quad [5.10]$$

In terms of spacing between sweeps, Grass *et al.* (1991) have stated that the region above fixed roughness elements displays a somewhat organized spanwise pattern, with a spanwise spacing approximately equal to three times the vertical dimension of the roughness elements  $k$ . In the absence of any additional information, it has been assumed that both spanwise and longitudinal spacing of sweep events scale with  $k$ . Therefore, the average spacing between sweeps has been taken as:

$$Sp_s = \alpha k^2 \quad [5.11]$$

where  $\alpha$  is a parameter which depends on the flow and bed surface conditions.

Overall, the average area over which sweep events occur per unit bed area  $\lambda_s$  ( $= A_s / Sp_s$ ) can thus be estimated by:

$$\lambda_s = \frac{1}{\alpha} \frac{v^2}{k_{ref}^2 u^{*2}} \quad [5.12]$$

The deposition rate due to the action of the sweep events on the particles of diameter  $d$  and density  $\rho_s$  reads:

$$\Delta = \frac{\lambda_s N}{T_s} \rho_s \frac{\pi d_m^3}{6} \quad [5.13]$$

where the product  $\lambda_s N / T_s$  corresponds to the number of particles deposited per unit time and area. The combination of Equation [5.13] with [5.8], [5.9] and [5.12] leads to:

$$w_d = \frac{1}{0.15 \alpha k_{ref}^2} \frac{v^2 d}{u^* \delta} \quad [5.14]$$

or:

$$w_d^+ = \frac{1}{0.15 g \alpha k_{ref}^2} \frac{v^2}{\delta} \quad [5.15]$$

Equation [5.15] indicates that the dimensionless deposition parameter  $w_d^+$  depends on parameters related to near-bed turbulence ( $\alpha$ ,  $\delta$ ), on a reference roughness height  $k_{ref}$ , on the kinematic viscosity and on gravity. Thus, unlike in [5.5] and [5.6],  $w_d^+$  is related here to the bed surface characteristics. It does not depend on the sediment size. This is due to the conditions of derivation of [5.15], as fine particles are assumed to follow a Stokes'-range type of transport behaviour (i.e. dispersion coefficient nearly equal to that of the fluid and little influence of gravity, §5.1), and as sweep events characteristics are assumed to depend directly on the size of bed surface elements.

Assuming that the parameter  $\alpha$  is equal to 1 (i.e. the spacing between sweep events is equal to the roughness scale), it is possible to estimate the reference roughness scale  $k_{ref}$  from [5.15]. Given a boundary layer thickness of 0.1m (i.e. the average flow depth in the experiments), a kinematic viscosity of  $10^{-6} \text{m}^2 \cdot \text{s}^{-1}$  and a deposition parameter between 0.1 and 1.4 (§5.2.2), one obtains a value of  $k_{ref}$  close to  $5 \cdot 10^{-6} \text{m}$ . Considering that  $k$  is close to  $d_{50}$ , the ratio  $k/k_{ref}$  varies thus between 4000 and 10000 in the context of these experiments. This range is well above the values of 25 and 40 obtained by Kline *et al.* in the case of smooth walls. Considering a value of  $0.1 \text{m} \cdot \text{s}^{-1}$  for the shear velocity, one obtains values of 0.04m to 0.1m for the average extent of the sweep events ( $=k/k_{ref} \times v/u^*$ ), which is a reasonable range given the size of the roughness elements used in the experiments and the assumption made concerning  $\alpha$ .

Overall, an analysis based on the bursting theory has led to a different expression of the deposition parameter  $w_d^+$  ( $=w_d u^* / (g d)$ ) than that obtained in Equations [5.5] and [5.6]. This expression, which applies only to very fine particles (within the Stokes' range), indicates that the bed roughness and the conditions of turbulence are the main

parameters influencing  $w_d^+$ . The principal assumptions made were that both the horizontal distance occupied by a sweep event and the spacing between two of these events are related to the vertical dimension of the roughness elements  $k$ .

## 5.4 Deposition of saltating load

### 5.4.1 Description.

Figure 5.1a indicates differences in the depositional behaviour of the medium-size sand particles, compared to that of fine and very fine sand particles. For the largest sediment sizes ( $d^* > 10$  in the case of LA-260), it was not possible to relate the experimental results of deposition velocity directly to turbulence and grain size parameters. Another type of interpretation has thus to be sought, which begins by the study of the physical phenomena involved in the deposition of saltating particles.

Coarser fines are less influenced by near-bed turbulence (e.g. lee vortices) and by near-bed flow currents than finer particles because of their larger inertia. They are less likely to be 'caught' in a lee eddy or entrained by a turbulent sweep. Saltating particles reaching the bed surface tend to collide with protruding grains and to rebound away from the near-bed region or deposit. As a result, these particles are less often in the vicinity of the bed surface than the finer grains.

In the context of these experiments, near-bed sediment samples include: (1) particles that are going to be deposited (settling at  $\sim w_s$ ); (2) particles that are going to be re-suspended (settling at  $\sim w_s$ ); and (3) particles that are being re-suspended (upward vertical velocity component). There is an imbalance between the downward flux of particles that can be expected from the near-bed concentration  $C_b$ , and the deposition rate  $\Delta$ , because not all the particles that are sampled deposit (cf. categories (2) and (3) previously mentioned). This results in a deposition velocity  $w_d$  that is necessarily lower than  $w_s$ .

However, even if the dimensionless deposition velocity  $w_d^*$  of saltating particles tend to be lower than that of suspended particles, their actual deposition velocity  $w_d$  is larger (Figure 4.12). This implies that for equal concentrations, these particles still infiltrate much faster into a gravel bed than suspended fines.

## 5.4.2 Theoretical model.

A simple 2D model has been used to try to find a connection between the saltation mode of transport and the results of the experiments in terms of deposition. The basis of the model is represented in Figure 5.2. It is assumed that the bed surface can be represented in two dimensions by a series of uniform discs of diameter  $R$ , separated by a fixed distance  $L$ . Fine particles reach the bed surface area at a landing angle  $\beta$  and collide with the discs. It is assumed that if the axis of movement of one incident fine particle passes below the centre of the disc with which it collides, then the particle is deposited, and that conversely, if it passes above, the particle is re-suspended.

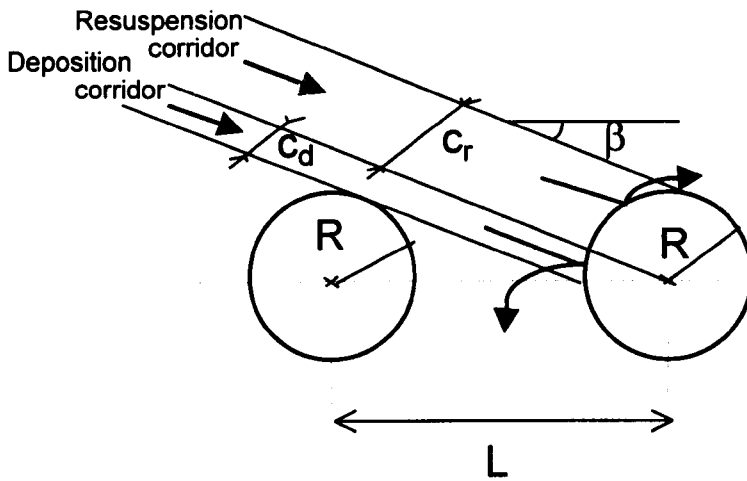


FIGURE 5.2: model for the deposition and re-suspension of saltating load

If  $C_r$  and  $C_d$  are defined as the widths of the corridors in which particles are respectively re-suspended/deposited (Figure 5.2), then these variables can be expressed from simple geometric considerations as:

$$C_r = R \quad [5.16]$$

$$C_d = L \sin(\beta) - R \quad [5.17]$$

Assuming a longitudinally uniform near-bed concentration of fines, the proportion of particles depositing  $P_d$  is:

$$P_d = \frac{C_d}{C_d + C_r} = \frac{\sin(\beta) - \frac{R}{L}}{\sin(\beta)} \quad [5.18]$$

The vertical settling velocity of the particles can be computed using the landing angle  $\beta$  and assuming that the longitudinal velocity of the particles near the bed surface is equal to the near-bed longitudinal flow velocity  $u_b$ . The deposition rate is then given by:

$$\Delta = P_d C_b u_b \tan(\beta) \quad [5.19]$$

Combining [5.18] and [5.19], and the general expression for  $w_d$  ( $= \Delta / C_b$ ), the following equation can be derived:

$$w_d = u_b \frac{\sin(\beta) - \frac{R}{L}}{\cos(\beta)} \quad [5.20a]$$

or, in terms of dimensionless deposition velocity:

$$w_d^* = \frac{u_b}{w_s} \frac{\sin(\beta) - \frac{R}{L}}{\cos(\beta)} \quad [5.20b]$$

The main difficulty in Equations [5.20a] and [5.20b] lies in the calculation of the landing angle  $\beta$ . This parameter depends on several variables including flow velocity, particle size and density, bed geometry, and turbulence intensity. Some data exists that has been derived from physical models (Wiberg and Smith, 1985) or from direct experimental measurements (Fernandez Luque and Van Beek, 1976), but the

experimental conditions of these studies did not match those of the present study and could not be used. As a result, an inverse method was used to obtain an estimate of  $\beta$ . The landing angle was derived from Equation [5.20b] by using the previously calculated dimensionless deposition velocities  $w_d^*$ . The results were compared with the literature data.

Details on these computations are presented in Appendix 5.1. Near-bed velocities were measured at the bed surface mean level using the ADV velocity profiles. The ratio between the spacing and the radius of the discs representing the bed was set at  $L/R=4$ , i.e. with the equivalent of one disc spacing between two consecutive discs. This choice, which corresponds to a relatively large spacing in 1-D, represents a lower spacing in 2D or 3D conditions. The submerged specific gravity of the fine particles was set at 1.7. The computed landing angles are summarised in Table 5.1. The average landing angle  $\bar{\beta}$  over the five different size fractions considered is indicated, as well as the shear velocity and the coefficient of variation of the results.

d ( $\mu\text{m}$ )	D3	D4	D5	D6	E2	E3b	E4	E5	E6	G1	G2b	G3	G4	G5	$\langle\beta\rangle$
550	19.1	22.3	20.4	19.9	23.7	21.2	24.9	19	22.5	22.9	21.2	26	17.6	18	21.34
462.5	23.4	24.1	23.7	19.8	22.2	26	23.6	19.7	21.4	21.9	24	26.6	17.9	18.8	22.36
390	24.8	23.4	21.2	18.9	22.6	24.4	24.6	19.2	20.7	23.7	23.3	25.6	17.5	18.3	22.01
327.5	23.9	24	20.5	18.5	21.1	23.6	25.2	18.8	19.7	21.2	23.1	26.3	17.1	17.75	21.48
275	21.1	22.3	18.9	17.5	19.4	21.4	23.1	17.8	18.4	19.5	21.2	23.4	16.6	17.3	19.85
$\bar{\beta}$	22.5	23.2	20.9	18.9	21.8	23.3	24.3	18.9	20.5	21.8	22.6	25.6	17.3	18.0	21.41
$u^*$ (m/s)	0.08	0.077	0.088	0.097	0.091	0.08	0.073	0.102	0.102	0.092	0.086	0.083	0.121	0.097	
c.v. (%)	10.3	3.8	8.4	5.2	7.5	8.7	3.7	3.7	7.7	7.4	5.7	5.0	2.9	3.1	5.9

TABLE 5.1: landing angles  $\beta$  obtained from Equation [5.20], against size fraction and experiment label.

Average landing angles  $\bar{\beta}$  over the five different size fractions, and  $\langle\beta\rangle$  over all experiments, shear velocity  $u^*$  and coefficient of variation c.v..

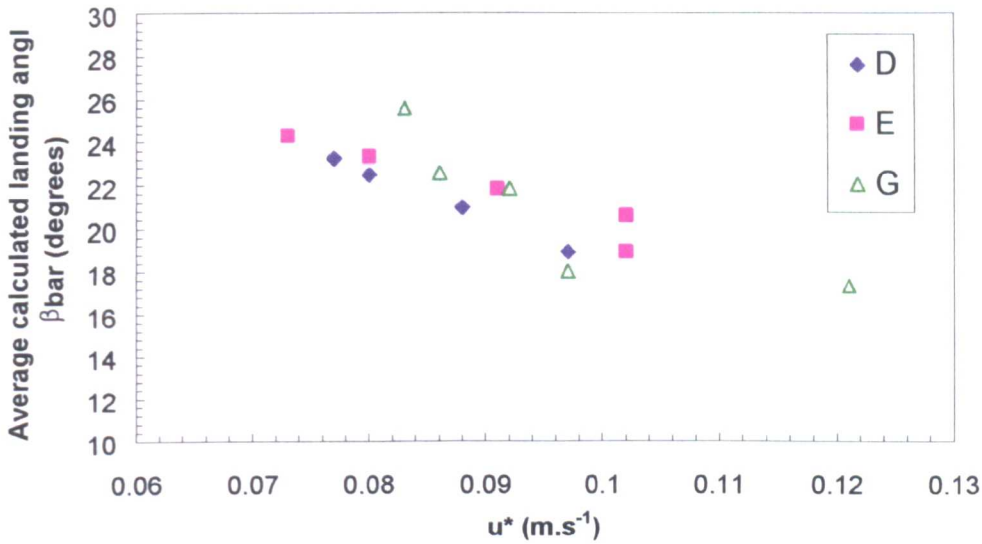


FIGURE 5.3: average landing angles over five size fractions  $\bar{\beta}$  (obtained from [5.20b]) against shear velocity  $u^*$

The results for all the experiments indicate a landing angle  $\beta$  which varies between a minimum of  $16.6^\circ$  (G4,  $275\mu m$ ) and a maximum of  $26.6^\circ$  (G3,  $462.5\mu m$ ), with an average of  $21.41^\circ$ . This is comparable to model data from Wiberg and Smith, who found a range of  $17^\circ$  to  $24^\circ$  for  $8.3mm$  particles. The coefficient of variation in each column is relatively small (between 2.9% and 10.3%) with an average of less than 6%, indicating a relatively low effect of grain size on  $\beta$ . However, the results for  $\langle \beta \rangle$  (average per size fraction) indicates that  $\beta$  tends to increase slightly with grain size up to  $500\mu m$ . Wiberg and Smith's model indicate a similar trend (for particles ranging between 0.5 and 5mm). The plot of  $\bar{\beta}$  (average per experiment) against  $u^*$  (Figure 5.3) indicates an inverse relationship between  $\beta$  and  $u^*$ . Again, these results are confirmed by Wiberg and Smith's results, whose model indicates a reduction in the landing angle of  $500\mu m$  quartz grains from  $15^\circ$  at  $\tau_b/\tau_{cr}=1.5$  to  $9^\circ$  at  $\tau_b/\tau_{cr}=8$ . Similar experimental results were obtained by Abbott and Francis (1977), who found that  $\beta$  decreased from  $17^\circ$  at  $\tau_b/\tau_{cr}=1.1$  to  $7^\circ$  at  $\tau_b/\tau_{cr}=6.3$ , and Niño *et al.* (1994), whose measured landing angles decreased from  $\sim 20^\circ$  to  $\sim 10^\circ$  between  $\tau^*=0.08$  to  $\tau^*=0.14$  (where  $\tau^*$  is Shields' parameter).

Therefore, the results of the landing angles  $\beta$  obtained from Equation [5.20] using the experimental data of  $w_d^*$ , are consistent with data obtained from the literature and follow similar trends. Clearly, this cannot prove that this data is correct nor that

Equation [5.20] describe exactly the physical phenomenon involved in the deposition of saltation particles, due to the simplicity of the model. However, it suggests that the concept of the model is correct and that the deposition of a saltating particle through a coarse bed surface can probably be described by particle saltation mechanics, i.e. using its landing angle and velocity characteristics, and a proper representation of the bed surface topography.

Finally, [5.20] supports the experimental result that gravel size does not significantly influence the deposition of the coarsest fines. It also suggests that bed porosity, which is a positive function of  $L/R$ , is a major parameter in that process. The fact that  $w_a^*$  increases with  $L/R$  in [5.20b] confirms what one would expect, i.e. that deposition rates and velocities increase with porosity.

### 5.5 Influence of turbulence damping.

Vanoni (1946) suggested that the presence of sediment tends to damp flow turbulence. Several investigators have subsequently observed and studied the influence of sediment on fluid velocity distributions. This was either expressed as a reduction in Von Karman's constant  $\kappa$  associated with logarithmic profiles (Einstein and Chien, 1955), or more recently, using an analogy with stratified shear flows and a wake component  $\Pi$  varying with suspension parameters (Coleman, 1981). Lau (1983) showed that in identical conditions, flow velocity in the longitudinal direction is lower near the bed and higher near the water surface for sediment-laden water compared to sediment-free water. Recent results (Teisson *et al.*, 1992) from a Reynolds stress model used to simulate sediment laden flows indicate that suspended sediments affect the characteristics of turbulence even at concentrations as low as  $1g/\ell$ . Similarly, the damping of fluid turbulence by sediment has an direct effect on the rates of deposition of fine particles into porous beds.

High suspended sediment concentrations reduce vertical eddy diffusivity and mixing, and therefore can affect the deposition of fine particles. Beschta and Jackson (1979) found that the Froude number affects deposition rates in a different way at low and high rates of sediment input, the latter corresponding to a concentration of  $12g.\ell^{-1}$

10mm above the bed surface. Carling (1984) on the other hand found no enhancement of deposition for concentrations even as high as  $10\text{g}\cdot\ell^{-1}$ .

Van Rijn (1984) introduced a method for predicting the effect of turbulence damping on suspended sediment, based on the suspension number  $Z_s (= w_s / (\beta_d \kappa u^*))$ . The modified suspension number is obtained by adding to  $Z_s$  a correction factor  $\phi$ . The factor  $\phi$ , which was computed by van Rijn using a trial-and-error method, was defined as:

$$\phi = 2.5 \left( \frac{w_s}{u^*} \right)^{0.8} \left( \frac{C_a}{C_0} \right)^{0.4} \quad \text{for } 0.01 \leq w_s / u^* \leq 1 \quad [5.21]$$

where  $C_a$  is a reference near-bed volume concentration ( $= C_b / \rho_s$ ) ( $C_a \geq 0.001$ ), and  $C_0$  is a reference concentration ( $= 0.65$ )

[5.21] has been used to analyse the results obtained in §4.4.5 (Figure 4.18). The damping factor  $\phi$  was computed for three experiments, i.e. E5, E6 and E7 using the average median size of the six near-bed samples to compute  $w_s$ , and the average near-bed concentration to compute  $C_a$ . The results are indicated in Table 5.2 and Figure 5.4, together with values of the dimensionless deposition velocity  $w_d^*$  for four grain sizes. Log-log plots of  $w_d^*$  against  $\phi$  are presented in Figure 5.4.

	E7	E5	E6
$\phi$	0.0108	0.0350	0.0819
$w_d^*(106\mu\text{m})$	$\sim 0.62$	1.029	1.365
$w_d^*(181\mu\text{m})$	$\sim 0.61$	0.877	1.038
$w_d^*(231\mu\text{m})$	0.646	0.802	0.949
$w_d^*(275\mu\text{m})$	0.577	0.78	0.918

TABLE 5.2: van Rijn's damping factors and dimensionless deposition velocities for experiments E5, E6 and E7.

The results indicate that the damping factor increases with the dimensionless deposition velocity for all the size fractions presented. Figure 5.4 suggests that a power relation may exist between  $w_d^*$  and  $\phi$ , but clearly this result has to be considered with

precautions due to the small number of data points available. However, to get an indication of what the effect of turbulence damping on deposition may be in these particular conditions, best-fit power functions have been computed for the four series of points. The coefficients  $k_2$  and  $n_2$  corresponding to the relation  $w_d^* = k_2 \phi^{n_2}$  are indicated in Table 5.3.

$d^*$	2.69	4.57	5.83	6.94
$k_2$	3.699	2.048	1.513	1.655
$n_2$	0.386	0.261	0.189	0.228
$r^2$	0.99	0.98	1.00	0.99

TABLE 5.3: Variations of the factor  $k_2$  and the exponent  $n_2$  (of the formula  $w_d^* = k_2 \phi^{n_2}$ ) against dimensionless grain size for the experiments E5, E6 and E7. The correlation coefficient  $r^2$  is indicated.

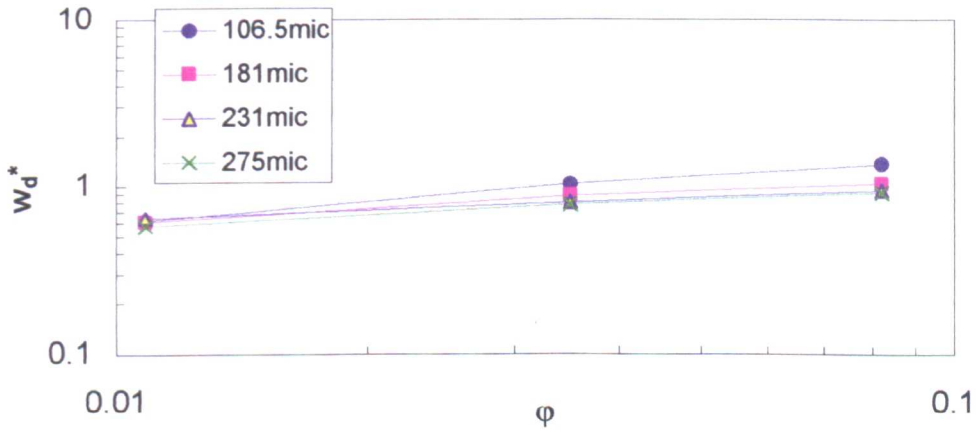


FIGURE 5.4: dimensionless deposition velocity  $w_d^*$  against van Rijn's damping coefficient  $\phi$  ( $=2.5(w_s/u^*)^{0.8}(C_b/0.65\rho_s)^{0.4}$ )

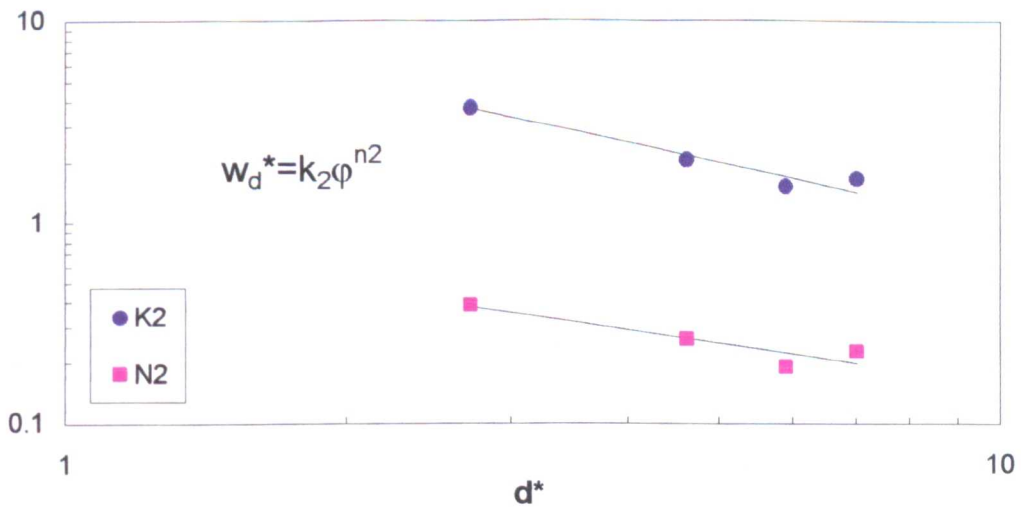


FIGURE 5.5: factor  $k_2$  and exponent  $n_2$  ( $w_d^* = k_2 \phi^{n_2}$ ) against dimensionless grain size  $d^*$

The variations of  $k_2$  and  $n_2$  with the dimensionless grain size  $d^*$  have been plotted on Figure 5.5. The graph indicates an inverse relation between  $k_2$  and  $d^*$ , which follows:

$$k_2 \approx \frac{10}{d^*} \quad (r^2=0.97) \quad [5.22]$$

and also between  $n_2$  and  $d^*$ , according to:

$$n_2 \approx \frac{0.75}{d^{0.68}} \quad (r^2=0.90) \quad [5.23]$$

Overall, the effect of sediment concentration and turbulence damping on the dimensionless deposition velocity for the series of experiments E5-E6-E7, can be described by the formula:

$$w_d^* \approx \frac{10}{d^*} \phi^{\frac{0.75}{d^{0.68}}} \quad [5.24]$$

From [5.24], the influence of turbulence damping relative to the dimensionless deposition velocity obtained in Experiment E5 (where  $\phi=0.035$ ) can be described by:

$$\frac{w_d^*}{w_d^*(E5)} \approx \left( \frac{\phi}{0.035} \right)^{\frac{0.75}{d^{0.68}}} \quad [5.25]$$

Experiment E5 is taken here as a reference because most experiments have been conducted in similar conditions in terms of damping coefficient  $\phi$ . Assuming that Equation [5.5] applies to the range of damping coefficients of these experiments ( $0.01 < \phi < 0.1$ ) and that turbulence damping has a similar influence to that described by Equation [5.25] in different shear velocity and bed composition conditions, then the combination of Equations [5.5] and [5.25] brings the general equation:

$$\frac{w_d u^*}{g d} \approx \frac{d^{*0.37}}{2} \left( \frac{\varphi}{\varphi_0} \right)^{\frac{0.75}{d^{*0.68}}} \quad [5.26]$$

which leads to the following equation in terms of deposition velocity:

$$w_d \approx d^{* \frac{4}{3}} \frac{g^{\frac{2}{3}}}{2 u^*} \left( \frac{v^2}{\rho_s^*} \right)^{\frac{1}{3}} \left( \frac{\varphi}{\varphi_0} \right)^{\frac{0.75}{d^{*0.68}}} \quad [5.27]$$

The range of application of [5.27] is:  $100\mu\text{m} < d < 275\mu\text{m}$ ,  $0.07\text{m.s}^{-1} \leq u^* \leq 0.12\text{m.s}^{-1}$ , and  $10^{-2} < \varphi < 10^{-1}$ .

Equation [5.27] was compared with the experimental results of the main series using the percentage of error  $e$  defined as:

$$e = \left| \frac{2(x_{\text{exp}} - x_{\text{calc}})}{x_{\text{exp}} + x_{\text{calc}}} \times 100 \right| \quad [5.28]$$

where  $x_{\text{exp}}$  is the experimental data and  $x_{\text{calc}}$  the model data. The results are indicated in Appendix 5.2. For LA-260 sand, it was found that the best agreement is achieved with a grain size of  $275\mu\text{m}$  (7% error), while less good results are obtained for  $106.5\mu\text{m}$  (27% error). Overall, [5.27] matched the LA-260 results within a margin of 16%. For B3-100, the results were best between 98 and  $196\mu\text{m}$ , and less good for the greatest grain size (i.e.  $275\mu\text{m}$ ), with an overall error of 11% compared to the experimental data.

## 5.6 Conclusion

The results of a dimensional analysis have indicated that the deposition parameter  $w_d^+ = w_d u^* / (g d)$  is a key variable in the deposition process. The plot of  $w_d^+$  against grain size for the experiments of the main series indicates that this parameter reaches a peak near  $d^*=7$ . This peak varies with the type of sediment used. The fact that the deposition velocity  $w_d$  is inversely related to  $u^*$  through  $w_d^+$  confirms that larger turbulence is generally synonymous with lower deposition.

On the one hand, the deposition of Stokes' range particles depends on the structure of near-bed turbulence, which leads to the phenomenon of enhanced deposition. A bursting-based analysis has indicated that the deposition parameter  $w_d^+$  depends only on the characteristics of the bed and of near-bed turbulence, but not on grain size. This suggests that the series of points on Figure 5.1a and 5.1b converge as  $d^*$  decreases.

On the other hand, saltating particles have a low dimensionless deposition velocity  $w_d^*$  because of their tendency to be re-entrained in the main flow by their contact with the bed surface. This transport mode corresponds to the decreasing part of Figure 5.1a. A model based on a simple description of the bed surface seems to support the validity of a mechanical interpretation of the phenomenon, but requires more precise knowledge of the landing angles of the particles.

Near-bed concentration and shear velocity are not the only two parameters controlling fine sediment deposition processes through bed pores. Turbulence damping, due to fine sediment size and concentration, also plays a role in the deposition of both suspended and saltating particles. This phenomenon can be described by van Rijn's  $\phi$  coefficient. The deposition velocity results of three experiments run with different coefficients  $\phi$  suggest that, all other parameters being equal, the more near-bed turbulence is damped, the larger the deposition rates.

A general expression for the deposition velocity, which combines the effects of suspended sediment deposition and turbulence damping, predicts the experimental results within an average margin of  $\pm 16\%$ . However, this equation has to be considered with precautions because of its restrictions in terms of range of application, and because its turbulence damping term is based on the results of only three experiments.

## Chapter VI

# Application: downstream deposition rates

### 6.1 Introduction

One possible application of the material presented in the previous chapters is to predict where along a gravel bed a given flow will deposit the various parts of its sediment load. From this information and from a knowledge of the rate, size and injection point of the incoming sediment, the civil engineer can forecast how fine sediments either washed into a coarse bed river from works areas, sewers, etc, or flushed out of reservoirs can affect sediment transport, flow turbidity, bed permeability and the aquatic environment. Further, this can also be used by the fisheries manager to predict how often a gravel bed of given thickness must be cleaned out to remain fully effective for salmon spawning. Lastly, the fluvial geomorphologist or the geologist may find it useful in the study of the evolution of the landscape, like for example the areas of deposition of placers (Allan and Frostick, 1997).

When fine particles released from a point source deposit into a riverbed, mass balance considerations imply that the near-bed concentration  $C_b$  and the deposition rate  $\Delta$  tend to decrease with distance downstream. As indicated by Equations [3.3] and [3.4], the downstream sorting of fine sediment over a porous bed can be described by a negative exponential function of the longitudinal coordinate  $x$ . The decay rate depends on the deposition velocity  $w_d$ , the coefficient  $r$  (ratio of the near-bed to the depth-averaged concentrations) and the inverse of the flow rate per unit width  $q$ . Results from the series of experiments on deposition (§3.3.3) have indicated that the decay rate of  $\Delta$  decreases with distance, resulting in a concave profile (using a single log-scale). This is due to changes in  $w_d$ , as the concentration and the average size of the fine sediment transported near the bed decrease in the downstream direction, thereby reducing

turbulence damping. These variations have to be taken into consideration in the calculations. The distinction between the different size fractions is also necessary as these are differently affected by turbulent flow environments and have distinct natural fall velocities.

Two cases are analysed in this chapter: (1) downstream deposition from a point source, i.e. uniform span-wise input at a given point of coordinate  $x_0$ . This case may be applied to situations where a small sediment-laden tributary or a sewer joins a gravel-bed river; (2) downstream deposition from an continuous uniform source, i.e. uniform input in both span-wise and downstream-wise directions between two points of coordinates  $x_0$  and  $x_1$ . This case applies for example to eroding reaches or to extended works along the banks of a river. In the former, results from the model have been compared with the experimental data of the main series of tests to estimate the coefficients ( $r_i = C_{b_i} / C_i$ ). The latter has been applied to the case of a non uniform input. In each case, the context of the study was in uniform and 2D flow conditions.

## 6.2 Deposition from a point source

### 6.2.1 Theoretical analysis.

From [3.3], the equation describing the longitudinal variations of near-bed sediment concentration of a given size fraction  $i$  with a deposition velocity  $w_{d_i}$  is:

$$C_{b_i} = C_{b0_i} \exp\left(-r_i \frac{w_{d_i}}{q} x\right) \quad [6.1]$$

where  $C_{b0_i}$  is the initial near-bed concentration measured at  $x=0$  and  $r_i$ , the ratio between the near-bed and the depth-averaged concentrations for the size fraction  $i$ .

On a 2D flow, clear water basis, sand particles are assumed to be released near the water surface, at the point with coordinate  $x_0$  and at a unit rate  $I_0$  ( $\text{kg}\cdot\text{s}^{-1}\cdot\text{m}^{-1}$ ). Only those size fractions that are not transported by suspension (i.e. particles that settle within the main flow until reaching the near-bed area) are considered. Their fall velocity is

assumed not to be affected by turbulence until reaching the bed surface. Neglecting longitudinal dispersion, the size fraction  $i$  of fall velocity  $w_{s_i}$  reaches the near-bed area after a distance  $\ell_i$  equal to:

$$\ell_i = \frac{Uh}{w_{s_i}} \quad [6.2]$$

At the point of coordinate  $x_0 + \ell_i$ , the initial near bed concentration of the size fraction  $i$  is approximately equal to the initial depth averaged concentration multiplied by the coefficient ( $r_i$ ), i.e.:

$$C_{b0_i} = r_i \frac{I_{0_i}}{q} \quad [6.3]$$

It has been found in §5.5 that the deposition velocity  $w_{d_i}$  depends on the degree of turbulence damping by fine particles, hence on  $C_{b_i}$ . But from the decay equation ([6.1]), the deposition velocity  $w_{d_i}$  is also required to compute the near-bed concentration  $C_{b_i}$ . Thus these two variables can not be computed independently, but only alternatively (by circular resolution). A mathematical series has thus to be used to solve the equations. Given initial conditions, the two variables are computed alternatively until both converge and give the final result. For each size fraction  $i$ , at coordinate  $x$ , the series is defined as follows:

$$C_{b_i}^n(x) = C_{b_i}^0 \exp \left\{ -r_i \frac{w_{d_i}^{n-1}}{q} [x - (x_0 + \ell_i)] \right\} \quad [6.4]$$

The overall concentration  $C_b^n$  is given by:

$$C_b^n(x) = \sum_{i=1}^{i=n} C_{b_i}^n(x) \quad [6.5]$$

The fractional components  $\chi_i^n$  are thus obtained using:

$$\chi_i^n = \frac{C_{b_i}^n(x)}{C_b^n(x)} \quad [6.6]$$

From Equation [6.6], it is possible to estimate the mean size of the near-bed sediment mixture at rank n as:

$$d^n = \sum_{i=1}^{i=n} \chi_i^n d_i \quad [6.7]$$

where  $d_i$  is the median size corresponding to the size fraction  $i$ . The dimensionless mean grain size is then obtained as (Equation [2.3]):

$$d_*^n = \left( \frac{\rho_s^* g}{v^2} \right)^{\frac{1}{3}} d^n \quad [6.8]$$

and the fall velocity, as proposed by Cheng (1997) ([2.2]), by:

$$w_s^n = \frac{v}{d^n} \left( \sqrt{25 + 1.2(d_*^n)^2} - 5 \right)^{\frac{3}{2}} \quad [6.9]$$

Van Rijn's damping coefficient ([5.20]) can then be computed according to:

$$\phi^n = 2.5 \left( \frac{w_s^n}{u^*} \right)^{0.8} \left( \frac{C_b^n}{0.65 \rho_s} \right)^{0.4} \quad [6.10]$$

As a result, the deposition velocities for each size fraction ( $w_{d_i}^n$ ) can be calculated as ([5.27]):

$$w_{d_i}^n = (d_n^*)^4 \frac{g^{\frac{2}{3}}}{2u^*} \left( \frac{v^2}{\rho_s^*} \right)^{\frac{1}{3}} \left( \frac{\varphi^n}{0.035} \right)^{\frac{0.75}{d_i^{*0.68}}} \quad [6.11]$$

Going back to Equation [6.4], the following term of the series ( $C_{b_i}^n$ ) (i.e.  $C_{b_i}^{n+1}$ ) can be computed from [6.11] and the result of  $w_{d_i}^n$ . The initial terms of the series are computed using Equations [6.7] to [6.11]. Given the initial concentration  $C_{b_0}$  of the near-bed sediment, the initial mean size of the sediment mixture can be approximated as:

$$d^{(n=0)} = \sum_{i=0}^{i=n} \chi_{0i} d_i \quad [6.12]$$

Following Equations [6.8] to [6.11], this result allows computation of the initial mean dimensionless grain size  $d_{50}^0$ , the corresponding fall velocity  $w_s^0$ , van Rijn's damping coefficient  $\varphi^0$  and the initial deposition velocity  $w_{d_i}^0$ .

The series is completely defined by its initial terms ( $C_{b_i}^0$ ,  $\chi_i^0$ ,  $d_{50}^0$ ,  $d_{50}^{*0}$ ,  $w_s^0$ ,  $\varphi^0$ ,  $w_{d_i}^0$ ) and Equations [6.4] to [6.11]. It converges and its limit gives the near-bed concentration at the coordinate  $x$ , i.e.  $C_{b_i}(x)$ . Following this computation, the deposition rates for each size fraction ( $\Delta_i$ ) can be computed as:

$$\Delta_i(x) = C_{b_i}(x) w_{d_i} \quad [6.13]$$

where  $w_{d_i}$  is the limit of the ( $w_{d_i}^n$ ) series. The 'overall' deposition rate is finally obtained as:

$$\Delta(x) = \sum_{i=1}^{i=n} \Delta_i(x) \quad [6.14]$$

### 6.2.2 Application: computation of the coefficients ( $r_i$ )

The previous method has been applied to the results of the main series of experiments to compute the coefficients ( $r_i$ ) (Equation [6.1]) corresponding to the different size fractions. These have been adjusted by iteration until there is the best agreement between the experimental and the model results.

The experimental set-up used in the main series of experiments did not allow infiltration to take place before the beginning of the test section, i.e. up to 2.40m downstream of the release point. However, some of the fine particles could reach the bed surface before that point. Thus, the method considering the start of the decay of  $C_{b_i}^n$  at the estimated point of contact of the particles with the bed (i.e.  $x_0 + \ell_i$ ), and represented by Equation [6.4], could not be used in that particular case. Instead, the results of the near-bed sediment samples over trap 3.1 were taken as the initial components of the near-bed concentration  $C_t^0$ . All the decay equations for the different size fractions were considered to originate at that point. To simplify the calculations, the notation  $x'$  was used to represent the longitudinal coordinate starting there (i.e.  $x' = x - 3.3$ ). The following, slightly modified version of Equation [6.4] was therefore used:

$$C_{b_i}^n(x') = C_{b_i}^0 \exp\left(-r_i \frac{w_{d_i}^{n-1}}{q} x'\right) \quad [6.15]$$

The experimental results in terms of deposition rates for the main series have been plotted on Figure 6.1a and 6.1b.

Only the experiments performed with LA-260 sand were taken into account, as B3-100 sand was mainly transported by suspension. The six longitudinal coordinates considered correspond to the six traps located downstream of  $x=3.3$ m (i.e. traps 3.1, 3.2, 4.1, 4.2, 5 and 7). The different results show a similar trend that confirms the results of §3.3.3, i.e. the negative exponential relationship between  $\Delta$  and  $x$ . Most curves also exhibit a concave shape on a semi-log plot as illustrated by the curve representing the average deposition rate over all the experiments (Figure 6.1a).

A spreadsheet has been used to carry out the computations of  $r_i$ . An example of the way the model has been implemented is shown in Appendix 6 for experiment D3. The computations of the different terms of the series for a given coordinate are shown on the first two pages. The last two illustrate the way the coefficients ( $r_i$ ) are determined. The areas highlighted in yellow correspond to the boxes where data can be entered by the user. These include the shear velocity  $u^*$ , the flow rate  $Q$ , the initial near-bed concentrations ( $C_{b0_i}$ ) and the experimental results  $\Delta_{exp_i}(x)$ .

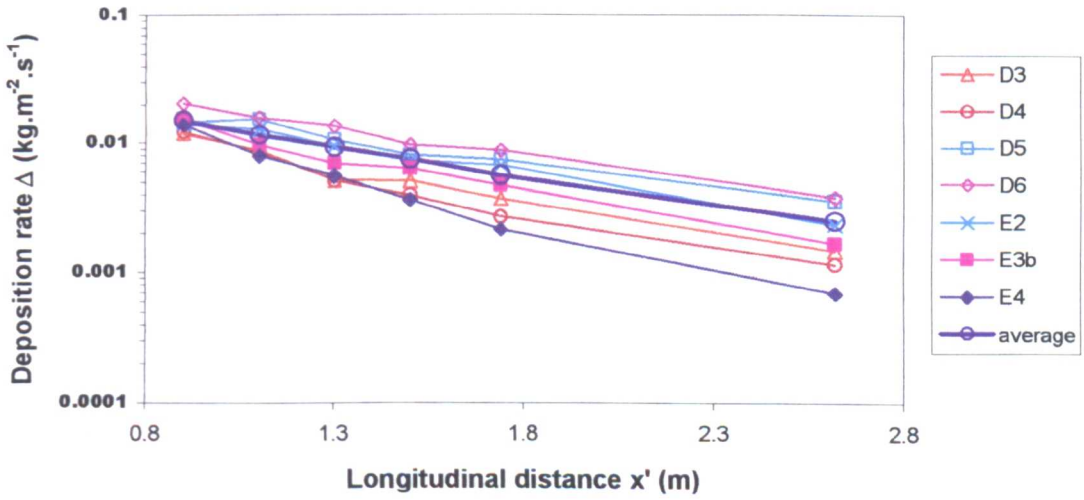


FIGURE 6.1.a: semi-log plot of the deposition rate  $\Delta$  against distance downstream for seven experiments of the main series and for the average over the whole series (LA-260).

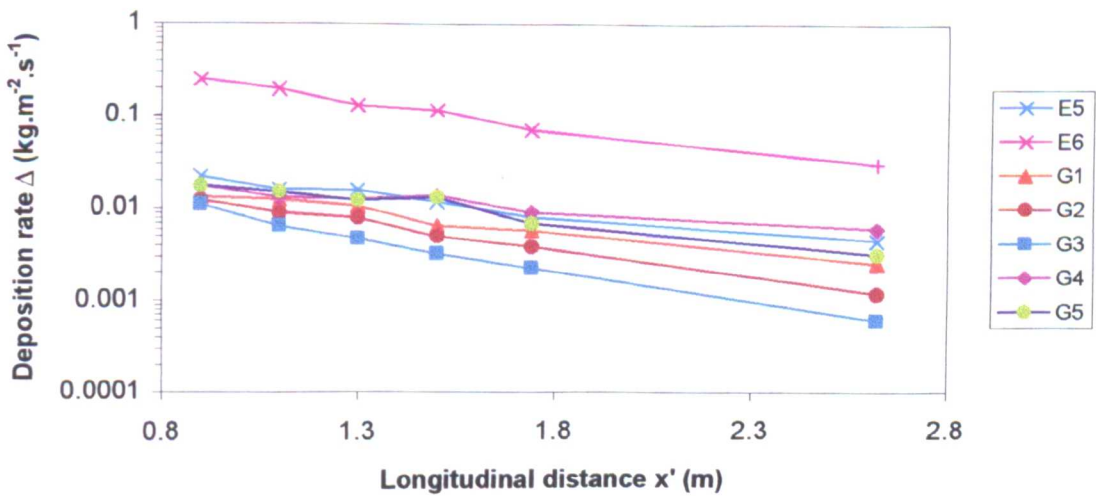


FIGURE 6.1.b: semi-log plot of the deposition rate  $\Delta$  against distance downstream for 8 experiments of the main series (LA-260).

The computations of the series corresponding to the coordinate  $x=1.72\text{m}$  (i.e. trap 7, used as an example) are presented on the first two pages of Appendix 6. Each column corresponds to a given size fraction, represented by its median size in row 15. The last column (column I) contains the results pertaining to the sediment mixture as a whole, notably  $C_b^n$  and  $\Delta^n$ . The estimated distance taken by the size fraction  $i$  to reach the bed surface from the release point, i.e.  $\ell_i$  (Equation [6.2]), is showed in row 18. In the case proposed, all particles reach the bed surface before trap 3.1 ( $x=3.3\text{m}$ ). Thus, all the size fractions contribute to the deposition that takes place into the six traps. The block delimited by rows 20 and 29 contains the computations corresponding to the initial conditions. The initial near-bed concentration  $C_{b_i}^{(n=0)}$  is set equal to  $C_{b0}^i$ . The initial terms of the series ( $\chi_i^0, d_{50}^0, d_{50^*}^0, w_s^0, \varphi^0, w_{d_i}^0$ ) and the initial deposition rate  $\Delta_i^0$  are subsequently computed. The series of blocks below, which begins at row 30, contains the data corresponding to increasing ranks in the series, i.e.  $n=1, 2, 3$ , etc. Similarly, all the different terms of the series ( $\chi_i^n, d_{50}^n, d_{50^*}^n, w_s^n, \varphi^n, w_{d_i}^n$ ) are computed using Equations [6.4] to [6.11]. The results for the whole sediment mixture, i.e.  $C_b^n$  and  $\Delta^n$ , are indicated in column I and the deposition rate results are summarised on top of the page, in column H. It can be observed that  $\Delta_{\text{model}}$  converges rapidly, as only 4 terms are required to get an accuracy to the fifth order. This convergence is even quicker for the other trap coordinates, which are lower than  $x'=1.72\text{m}$ . The computations for these coordinates have been carried out in other parts of the spreadsheet that are not represented in Appendix 6.

The last three pages of Appendix 6 illustrate the procedure used to determine the  $(r_i)$  coefficients. The yellow block on top of the first page contains the experimental data of  $\Delta$  for each coordinate and size fraction. The block below summarises the results obtained from the model. For example, in the first part of the Appendix, the results of the last row (i.e. row 103), which corresponds to the fractional deposition rates  $\Delta_i$  at  $x=1.72\text{m}$ , can also be found in column G of that block. For each size fraction, these experimental and model results are plotted on the graphs below. The coefficients  $(r_i)$  are determined by trial and error until both curves best match. The results are summarised at the bottom of the second page, where the plot of the overall deposition rates (experimental and model) is shown. This plot shows that, except in one case (Trap 4.1),

the model results match the experimental results closely. In particular, the decrease in decay rate with distance downstream (concave shape of curve) is reproduced. This is the result of the use of the mathematical series, which adjusts the damping coefficient, the deposition velocity and the near-bed concentration according to each other. It is a confirmation of the role played by turbulence damping on the deposition process.

All the results of ( $r_i$ ) for the experiments of the main series have been summarised in Table 6.1. Average values have been computed for each series (D, E and G) and for the whole series (last column), and plotted on Figure 6.2.

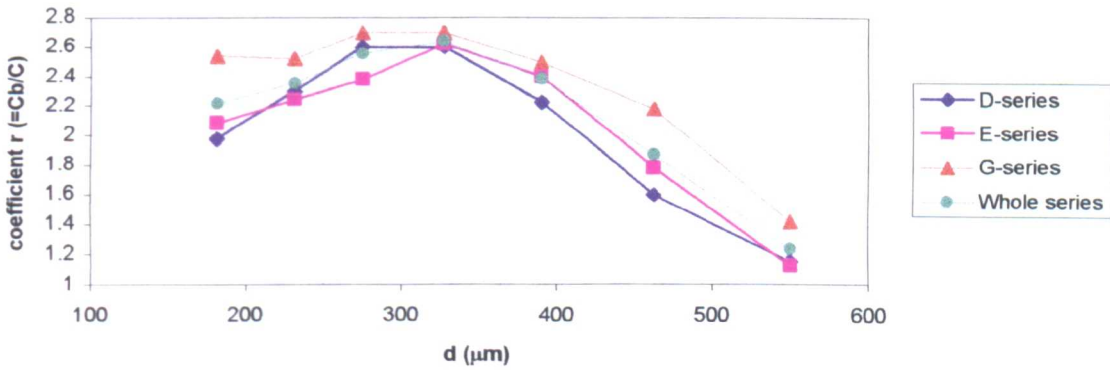


FIGURE 6.2: coefficient ( $r_i$ ) computed by adjustment of the results of the model described in §6.2.1 to experimental data from the main series.

$d_i$ ( $\mu\text{m}$ )	D3	D4	D5	D6	Avg	Overall averag	
550	1.3	0.8	0.8	1.7	1.15		
462.5	1.3	1.3	1.6	2.2	1.6		
390	2	2	2.5	2.4	2.22		
327.5	2.3	2.5	2.9	2.7	2.6		
275	2.4	2.5	3	2.5	2.6		
231	2.5	2.3	2.3	2.1	2.3		
181	2.5	2	1.6	1.8	1.97		
$d_i$ ( $\mu\text{m}$ )	E2	E3b	E4	E5	E6		Avg
550	1.1	1.3	0.5	1.2	1.5		1.12
462.5	2	2	1.2	1.7	2	1.78	1.87
390	2.5	2.4	2.3	2.4	2.4	2.4	2.39
327.5	2.7	2.7	2.6	2.6	2.5	2.62	2.64
275	2.5	2.6	2.5	2.3	2	2.38	2.56
231	2.2	2.4	2.3	2.2	2.1	2.24	2.36
181	2.3	2.2	2.2	1.8	1.9	2.08	2.21
$d_i$ ( $\mu\text{m}$ )	G1	G2b	G3	G4	G5	Avg	
550	1.4	0.9	0.9	1.6	2.3	1.42	
462.5	2.1	1.8	1.8	2.2	3	2.18	
390	2.8	2.6	1.9	2	3.2	2.5	
327.5	3.1	2.9	2.1	2.1	3.3	2.7	
275	3	3	2.3	1.9	3.3	2.7	
231	2.7	2.7	2.6	1.5	3.1	2.52	
181	3.1	3.1	2.6	2	2	2.54	

TABLE 6.1: results of the coefficients ( $r_i$ ), ratio of the near-bed and depth-averaged concentrations for the size fraction  $i$ , for the experiments of the main series with LA-260.

The results for the different series show similar trends, but it can be observed that the values of  $(r_i)$  for series G are always larger than the other two series. The average standard error is also larger for the G-series (0.25) than for the D- and E-series (respectively 0.16 and 0.09), indicating more variability in the results. The reason for these variations is probably related to the large size ( $d_{50}=52\text{mm}$ ) used in this series of experiments. In relatively shallow water, this may have introduced important changes in terms of turbulence and concentration profile equilibrium as depth and shear velocity were varied.

The three curves feature a maximum between 275 and 327.5 $\mu\text{m}$ , of the order of  $r=2.6$ , and a decline in  $r$  towards both extremes. In the case of suspended particles, the decrease of  $r$  with decreasing grain sizes occurs as finer particles get more uniformly distributed in the water column. The first part ( $d_i < 350\mu\text{m}$ ) of the curves for the D- and E-series illustrates this phenomenon.

Above  $d_i=327.5\text{mm}$ , the decrease in  $r$  may be caused by the transition towards the saltation mode of transport. It is thought that in this case, the fine particles are less and less often in contact with the bed surface (against which they rebound), but are most of the time transported slightly above, within the main flow.

### 6.3 Case of a continuous source

#### 6.3.1 Uniform source

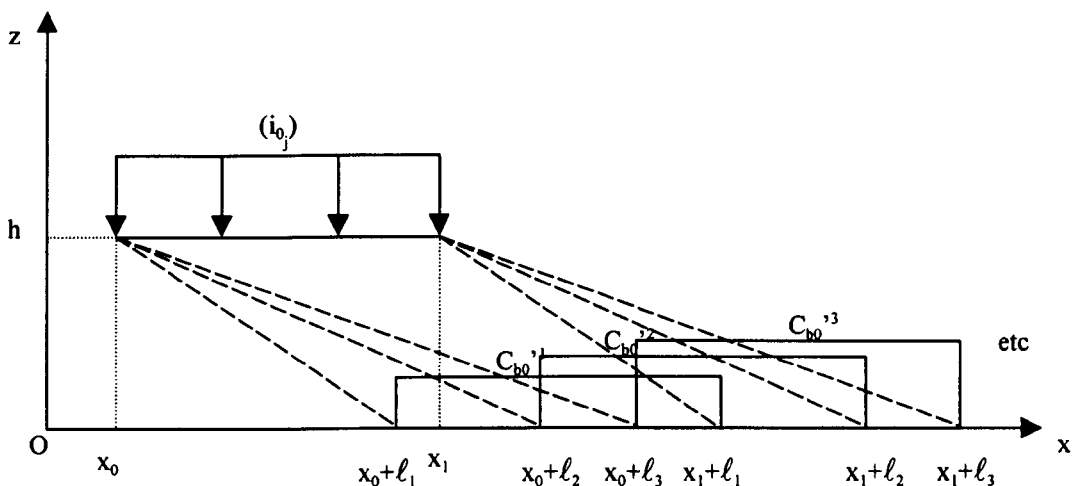


FIGURE 6.3: uniform continuous source  $(i_0)$ , settling of the different size fractions in the main flow and initial near-bed concentrations gradient  $C_{b0}^j$ .  $h$  is the flow depth

Assume that fine sediment of a given composition is released at a constant rate per unit width and length  $i_0$  ( $\text{kg}\cdot\text{s}^{-1}\cdot\text{m}^{-2}$ ) between two points with coordinates  $x_0$  and  $x_1$  in 2-D, uniform flow conditions (Figure 6.3). Outside this interval, there is no input of sediment.

As in §6.2, the size fractions that can be entrained into suspension are not considered. It is assumed that the fine particles disperse very little while settling through the main flow. The sediment input per unit length  $i_0$  results in a concentration gradient  $C_0'$  (unit= $\text{kg}\cdot\text{m}^{-4}$ ). Its depth-averaged value is equal to  $C_0' = i_0 / q$ . It is also assumed that when the fine particles reach the bed surface, the fines are already in equilibrium conditions and the relation  $C_{bo_j}' = r C_0'$  applies. As a result, the following initial conditions are considered for each size fraction  $j$ : (1) a constant near-bed concentration gradient  $C_{bo_j}' = r_j i_0 / q$  between the points of coordinates  $x_0 + \ell_j$  and  $x_1 + \ell_j$  ( $\ell_j$  as defined in Equation [6.4]); and (2) null concentration elsewhere for that particular size fraction (Figure 6.3).

### 6.3.1.1 Concentration equation.

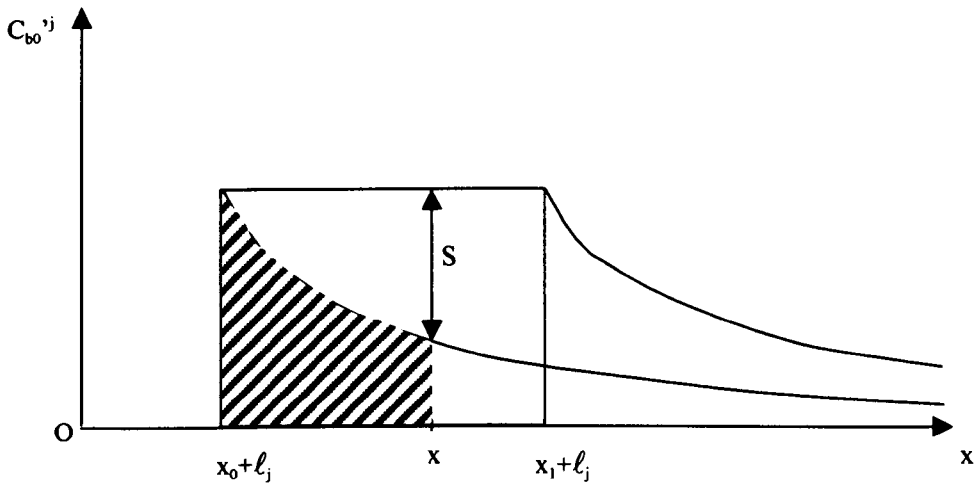


FIGURE 6.4: computation of the near-bed concentration  $C_b(x)$  for  $x \leq x_1 + \ell_j$ ; graphic representation

Considering the above initial condition, the concentration corresponding to each small volume of sediment laden fluid of length  $dx$  located between  $x_0 + \ell_j$  and  $x_1 + \ell_j$  (i.e.  $C_{b0_j} dx$ ) is going to decay in the same way as in the case of the point-source release, according to Equation [6.1]. In equilibrium conditions, the near-bed concentration  $C_{b_j}$  remains equal to zero upstream of the point of coordinate  $x_0 + \ell_j$ . For a given  $x$  such that  $x_0 + \ell_j < x < x_1 + \ell_j$ ,  $C_{b_j}(x)$  is equal to the sum of the remaining components of near-bed concentration due to the initial  $C_{b0_j}$  between  $x_0 + \ell_j$  and  $x$ .

On Figure 6.4, the segment S represents the range of concentrations that are to be summed to obtain  $C_{b_j}(x)$ . In terms of integration, this segment corresponds to the area highlighted, the expression for which is:

$$C_{b_j}(x) = \int_{\xi=x_0+\ell_j}^{\xi=x} C_{b0_j} \exp\left[-\frac{r_j w_{d_j}}{q} (\xi - (x_0 + \ell_j))\right] d\xi \quad \text{for } x_0 + \ell_j \leq x \leq x_1 + \ell_j \quad [6.16]$$

which results in:

$$C_{b_j}(x) = -\frac{q}{r_j w_{d_j}} C_{b0_j} \left\{ \exp\left[-\frac{r_j w_{d_j}}{q} (x - (x_0 + \ell_j))\right] - 1 \right\} \quad \text{for } x_0 + \ell_j \leq x \leq x_1 + \ell_j \quad [6.17]$$

Given the definition of the near-bed concentration gradient  $C_{b0_j}$  ( $= i_{0j} / q$ ), this leads to the following expression:

$$C_{b_j}(x) = -\frac{i_{0j}}{r_j B w_{d_j}} \left\{ \exp\left[-\frac{r_j w_{d_j}}{q} (x - (x_0 + \ell_j))\right] - 1 \right\} \quad \text{for } x_0 + \ell_j \leq x \leq x_1 + \ell_j \quad [6.18]$$

For  $x$  larger than  $x_1 + \ell_j$ , the near-bed concentration at equilibrium corresponds to the sum of the remaining components of  $C_b$  derived from the entire source over the range between  $x_0 + \ell_j$  and  $x_1 + \ell_j$ . This sum can be represented on Figure 6.5 by the segment S, and corresponds to the area highlighted. The expression for  $C_{b_j}(x)$  is thus:

$$C_{b_j}(x) = \int_{\xi=x_0+x-x_1}^{\xi=x} C_{b_{0j}}' \exp\left[-\frac{r_j w_{d_j}}{q} (\xi - (x_0 + \ell_j))\right] d\xi \quad \text{for } x \geq x_1 + \ell_j \quad [6.19]$$

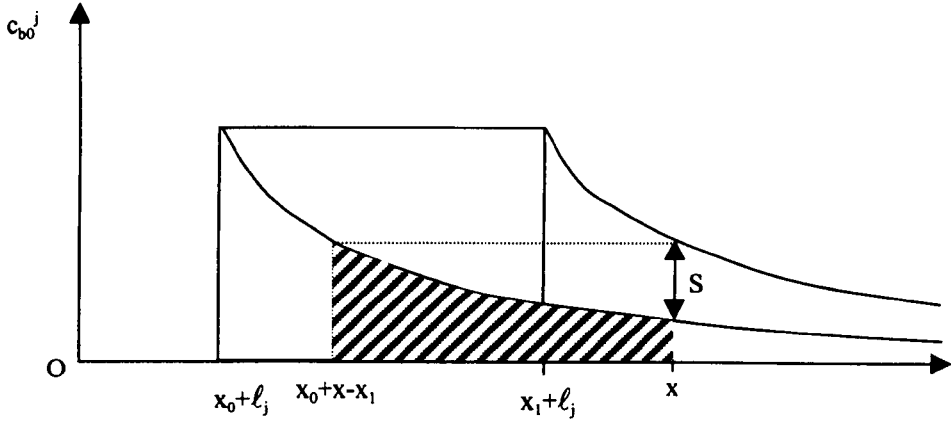


FIGURE 6.5: computation of the near-bed concentration  $C_{b_j}(x)$  for  $x > x_1 + \ell_j$ ; graphic representation

which results in the following equation:

$$C_{b_j}(x) = -\frac{i_{0j}}{r_j B w_{d_j}} \left\{ \exp\left[-\frac{r_j w_{d_j}}{q} (x - (x_0 + \ell_j))\right] - \exp\left[-\frac{r_j w_{d_j}}{q} (x - (x_1 + \ell_j))\right] \right\} \quad [6.20]$$

for  $x \geq x_1 + \ell_j$

The values of the near-bed concentration given by [6.18] and [6.20] are consistent in terms of initial conditions and continuity: (1) at  $x_0 + \ell_j$ , the value obtained from Equation [6.18] is  $C_{b_{0j}}'$ , which is what one might expect; and (2) both equations coincide at  $x_1 + \ell_j$ , with a value of  $C_{b_j}$  equal to:

$$C_{b_j}(x_1 + \ell_j) = \frac{i_{0j}}{r_j B w_{d_j}} \left\{ \exp\left[-\frac{r_j w_{d_j}}{q} (x_1 - x_0)\right] - 1 \right\} \quad [6.21]$$

The application of these equations causes the same problem as found in §6.2, i.e. the inter-dependence between the deposition velocity and the near-bed concentration.

The same method is used to solve this problem (see Equations [6.4] to [6.11]), except that Equation [6.4] is replaced by the new equations. Three cases have to be considered: (1) if  $x < x_0 + \ell_j$ , then  $C_{b_j}(x)=0$ ; (2) for  $x_0 + \ell_j < x < x_1 + \ell_j$ , the following equation (derived directly from [6.18]) is used:

$$C_{b_j}^n(x) = \frac{i_{0j}}{r_j B w_{d_j}^{n-1}} \left\{ \exp \left[ -\frac{r_j w_{d_j}^{n-1}}{q} (x - (x_0 + \ell_j)) \right] - 1 \right\} \quad [6.22]$$

Equation [6.22] converges towards  $C_{b_j}^\infty = i_{0j}/w_{d_j}^\infty$  where  $w_{d_j}^\infty$  is the limit of convergence of the deposition velocity. As a result, the limit in terms of deposition rate is  $\Delta_j^\infty = i_{0j}$ , i.e. deposition rate equal to input rate per unit area. This is consistent in terms of units and mass balance. Finally, (3) if  $x > x_1 + \ell_j$ , then from [6.20]:

$$C_{b_j}^n(x) = -\frac{i_{0j}}{r B w_{d_j}^{n-1}} \left\{ \exp \left[ -\frac{r w_{d_j}^{n-1}}{q} (x - (x_0 + \ell_j)) \right] - \exp \left[ -\frac{r w_{d_j}^{n-1}}{q} (x - (x_1 + \ell_j)) \right] \right\} \quad [6.23]$$

In this case,  $C_{b_j}^n$  converges towards  $C_{b_j}^\infty = 0$ . The limit of convergence of  $\Delta_j$  is thus also 0.

As far as the initial conditions are concerned, it is not possible to directly compute the initial deposition velocity  $w_{d_j}^0$  because the computation of the initial damping coefficient  $\varphi^0$  requires an initial volumetric concentration, which can not be computed from  $c_{b_j}^0$  or  $i_{0j}$  without a value of the deposition velocity (in other words, there is another circular resolution problem). An assumption has thus to be made regarding this initial deposition velocity: the fall velocity in still water  $w_{s_j}$  can be chosen for example. This choice does not affect the convergence of the series. Let thus the initial near-bed concentration be equal to:

$$C_{b_j}^0 = \frac{i_{0j}}{w_{s_j}} \quad [6.24]$$

The other initial terms (i.e.  $\chi_i^0$ ,  $d_{50}^0$ ,  $d_{50*}^0$ ,  $w_s^0$ ,  $\phi^0$ ,  $w_{d_i}^0$ ) are subsequently derived using the same equations as in §6.2.

### 6.3.1.2 Example of application

For illustration, the previous method is applied to one particular example. As before, the calculations have been conducted on a spreadsheet (Figure 6.6), with a general layout that is similar to that of the first page of Appendix 6. The same conditions as those of experiment D3 have been selected (in order to re-use the coefficients ( $r_i$ ) computed in §6.2.2), i.e. identical flow rate  $Q$  (box B8), shear velocity  $u^*$  (box B3), and coefficients ( $r_i$ ) (column D16 to D22). It has been assumed that the fines were originally released between the points of coordinate  $x_0=0\text{m}$  and  $x_1=5\text{m}$  (boxes B12 and B13). The input rate has been set at  $0.05\text{kg}\cdot\text{s}^{-1}\cdot\text{m}^{-2}$  (box B14), with a composition equal to that of LA-260 sand (column B16 to B22). A series of 16 coordinates between  $x=1\text{m}$  and  $x=15\text{m}$  has been selected (columns E4 to E11 and G4 to G11) to represent the downstream deposition pattern.

The series of large boxes below row 30 correspond to the computation of the deposition rate at the coordinate  $x=1\text{m}$  (used as an example). The initial conditions are indicated between rows 31 and 39, while the computations for ranks 1, 2, 3, etc are shown in the series of blocks starting from row 40. The results obtained at each rank of the series are summarised between boxes J4 to J13. The final results for all the different coordinates (i.e. the limits of the series) can be found in columns F4 to F11 and H4 to H11. For example, the limit of convergence found for  $x=1\text{m}$  (column J) is indicated in box F4. These results are plotted against longitudinal distance on the graph located below.

Rows 27 and 28 indicate the values of both  $x_0+l_j$  and  $x_1+l_j$  for each size fraction. For  $x=1\text{m}$ , it can be seen in row 27 that only the two largest size fractions have reached the bed surface, thus the initial near-bed concentration  $C_{b_0}$  is equal to 0 for all the finer size fractions (row 31). The computation of  $C_{b_j}$  in the following steps ( $n=1,2,3..$ ) is carried out using Equation [6.22], as the coordinate  $x=1\text{m}$  is lower than  $x_1+l_j$ .

	A	B	C	D	E	F	G	H	I	J
1	Longitudinal distribution of $\Delta$ : case of an extended finite uniform source									
2						(kg.s <sup>-1</sup> .m <sup>-2</sup> )		(kg.s <sup>-1</sup> .m <sup>-2</sup> )		x (m)
3	u* (m.s <sup>-1</sup> )	0.08			x (m)	$\Delta_{model}$	x (m)	$\Delta_{model}$	n	$\Delta_{model}$
4	$\rho_w$ (kg.m <sup>-3</sup> )	1000			1	0.0001699	8	0.0124349	0	0.0012872
5	$\rho_s$ (kg.m <sup>-3</sup> )	2700			1.5	0.0040067	9	0.0045163	1	0.0001675
6	v (m <sup>2</sup> .s <sup>-1</sup> )	0.000001			2	0.0166249	10	0.0018744	2	0.0001699
7	g (m.s <sup>-2</sup> )	9.8			3	0.0386413	11	0.0008863	3	0.0001699
8	Q (m <sup>3</sup> .s <sup>-1</sup> )	0.041			4	0.046832	12	0.0004607	4	0.0001699
9	B (m)	0.77			5	0.0491123	13	0.0002569	5	0.0001699
10	q (m <sup>2</sup> .s <sup>-1</sup> )	0.0532468			6	0.0495315	14	0.0001509	6	0.0001699
11					7	0.0330659	15	9.215E-05	7	0.0001699
12	x <sub>0</sub> (m)	0							8	0.0001699
13	x <sub>1</sub> (m)	5							9	0.0001699
14	i <sub>0</sub> (kg.s <sup>-1</sup> .m <sup>-2</sup> )	0.05								
15	d (μm)	c <sub>0j</sub> (%)	i <sub>0j</sub> (kg.s <sup>-1</sup> .m <sup>-2</sup> )	r <sub>j</sub>						
16		550	0.49	0.000245	1.3					
17		462.5	1.38	0.00069	1.3					
18		390	4.52	0.00226	2					
19		327.5	17.75	0.008875	2.3					
20		275	35.45	0.017725	2.4					
21		231	29.6	0.0148	2.5					
22		181	10.81	0.005405	2.5					
23										
24	d <sub>j</sub> (mic)	550	462.5	390	327.5	275	231	181		
25	d <sub>j</sub> <sup>0</sup>	14.047133	11.812362	9.9606942	8.3644291	7.0235664	5.8997958	4.6227837		
26	w <sub>sj</sub> (m.s-1)	0.0679656	0.0571395	0.0475127	0.0387234	0.0310304	0.0244473	0.0170114		
27	x <sub>0</sub> +l <sub>j</sub> (m)	0.7834369	0.9318736	1.1206857	1.375053	1.7159532	2.1780214	3.1300647		
28	x <sub>1</sub> +l <sub>j</sub> (m)	5.7834369	5.9318736	6.1206857	6.375053	6.7159532	7.1780214	8.1300647		
29										
30	x (m)	1	1	1	1	1	1	1	Overall	
31	C <sub>bj</sub> <sup>0</sup> (g.l <sup>-1</sup> )	0.0036048	0.0120757	0	0	0	0	0	0.0156805	
32	χ <sub>j</sub> <sup>0</sup>	0.2298887	0.7701113	0	0	0	0	0	482.61526	
33	χ <sub>j</sub> <sup>0</sup> .d <sub>j</sub> (mic)	126.43877	356.17649	0	0	0	0	0	12.32611	
34	d <sub>50</sub> <sup>0</sup> (mic)								0.0597026	
35	d <sub>50</sub> <sup>0</sup>								0.0190521	
36	w <sub>s</sub> <sup>0</sup> (m.s <sup>-1</sup> )									
37	φ <sub>0</sub>									
38	w <sub>dj</sub> <sup>0</sup> (m.s <sup>-1</sup> )	0.1001548	0.076697	0.0589292	0.0449379	0.0342219	0.0260385	0.0177154		
39	Δ <sub>j</sub> <sup>0</sup> (kg.m <sup>-2</sup> .s)	0.000361	0.0009262	0	0	0	0	0	0.0012872	
40	C <sub>bj</sub> <sup>0</sup> (g.l <sup>-1</sup> )	0.0010057	0.0010775	0	0	0	0	0	0.0020832	
41	χ <sub>j</sub> <sup>0</sup>	0.4827749	0.5172251	0	0	0	0	0		
42	χ <sub>j</sub> <sup>0</sup> .d <sub>j</sub> (mic)	265.52618	239.21662	0	0	0	0	0		
43	d <sub>50</sub> <sup>0</sup> (mic)								504.7428	
44	d <sub>50</sub> <sup>0</sup>								12.891253	
45	w <sub>s</sub> <sup>0</sup> (m.s <sup>-1</sup> )								0.06247	
46	φ <sub>0</sub>								0.0088112	
47	w <sub>dj</sub> <sup>0</sup> (m.s <sup>-1</sup> )	0.0919911	0.0696191	0.0527891	0.0396404	0.0296622	0.0221227	0.0145669		
48	Δ <sub>j</sub> <sup>0</sup> (kg.m <sup>-2</sup> .s)	9.252E-05	7.501E-05	0	0	0	0	0	0.0001675	
49	C <sub>bj</sub> <sup>0</sup> (g.l <sup>-1</sup> )	0.0010258	0.0010837	0	0	0	0	0	0.0021095	
50	χ <sub>j</sub> <sup>0</sup>	0.4862704	0.5137296	0	0	0	0	0		
51	χ <sub>j</sub> <sup>0</sup> .d <sub>j</sub> (mic)	267.44872	237.59994	0	0	0	0	0		
52	d <sub>50</sub> <sup>0</sup> (mic)								505.04866	
53	d <sub>50</sub> <sup>0</sup>								12.899065	
54	w <sub>s</sub> <sup>0</sup> (m.s <sup>-1</sup> )								0.0625078	
55	φ <sub>0</sub>								0.0088598	
56	w <sub>dj</sub> <sup>0</sup> (m.s <sup>-1</sup> )	0.092047	0.0696672	0.0528306	0.0396759	0.0296925	0.0221485	0.0145872		
57	Δ <sub>j</sub> <sup>0</sup> (kg.m <sup>-2</sup> .s)	9.442E-05	7.55E-05	0	0	0	0	0	0.0001699	
58	C <sub>bj</sub> <sup>0</sup> (g.l <sup>-1</sup> )	0.0010256	0.0010837	0	0	0	0	0	0.0021093	
59	χ <sub>j</sub> <sup>0</sup>	0.4862463	0.5137537	0	0	0	0	0		
60	χ <sub>j</sub> <sup>0</sup> .d <sub>j</sub> (mic)	267.43547	237.61108	0	0	0	0	0		
61	d <sub>50</sub> <sup>0</sup> (mic)								505.04655	
62	d <sub>50</sub> <sup>0</sup>								12.899011	
63	w <sub>s</sub> <sup>0</sup> (m.s <sup>-1</sup> )								0.0625076	
64	φ <sub>0</sub>								0.0088594	
65	w <sub>dj</sub> <sup>0</sup> (m.s <sup>-1</sup> )	0.0920466	0.0696669	0.0528303	0.0396757	0.0296923	0.0221483	0.0145871		
66	Δ <sub>j</sub> <sup>0</sup> (kg.m <sup>-2</sup> .s)	9.441E-05	7.55E-05	0	0	0	0	0	0.0001699	
67	C <sub>bj</sub> <sup>0</sup> (g.l <sup>-1</sup> )	0.0010256	0.0010837	0	0	0	0	0	0.0021093	

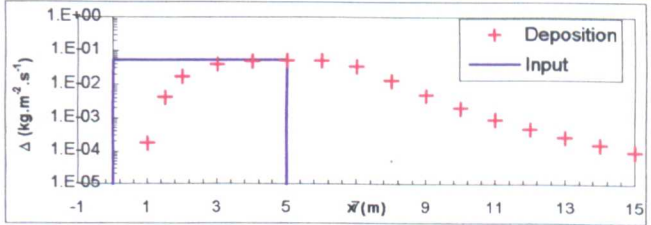


FIGURE 6.6: computation of the longitudinal distribution of the deposition rate  $\Delta$  in the case of a uniform continuous source (method described in §6.3.1.1). Series computations shown for  $x=1m$ , ranks  $n=0,1,2$  and 3.

In other cases where  $x$  is larger than  $x_1 + \ell_j$ , Equation [6.23] is automatically used for the calculations.

It can be seen in column J that the convergence of the series is rapid for  $x=1\text{m}$ , as only three terms of the series are required to get a value of the limit significant to the eighth order. This convergence is less rapid for larger coordinates: for  $x=5\text{m}$ , 6 terms are necessary to get the same accuracy, while  $x=15\text{m}$  necessitates 14. In practice, a fourth-order accuracy (i.e. to the tenth of gram per area per second) is sufficient for the range of parameters of this particular example (Appendix 4.3).

The graph indicates a distance of approximately 3m before the deposition rate reaches its maximum. As can be seen in row 27, this corresponds to the distance taken by the finer size fractions (i.e.  $181\mu\text{m}$ ) to reach the bed surface. Beyond that point, the graph forms a plateau, where  $\Delta$  increases only marginally (boxes F8 to F10) and converges towards  $i_0$ . It is interesting to notice that the maximum is reached at  $x=6\text{m}$ , beyond the fines input area. For coordinates larger than  $x=6\text{m}$ , the deposition rate starts to decrease towards 0. This last part of the curve exhibits a concave shape, indicating a gradual decrease in the decay rate. At  $x=15\text{m}$ , the residual deposition rate is only of  $9 \times 10^{-5} \text{kg.m}^{-2}.\text{s}^{-1}$ , which indicates that most fines have already deposited at this stage.

To summarise this section, a relatively simple method has been presented that allows computation of the deposition rates and near-bed concentrations resulting from the uniform release of sediment at the water surface between two points under uniform, 2D flow conditions. The range of application in terms of shear velocities and sediment sizes is limited to the conditions of application of [6.11]. In addition, a knowledge of the coefficients ( $r_i$ ) ( $=C_b/C_i$ ) is required. Lastly, this does not apply to suspendible particles because the particles are assumed to settle in the main flow at their terminal fall velocity before being eligible for deposition.

### 6.3.2 Non-uniform sources in uniform flow.

#### 6.3.2.1 Method

Most sources of fine sediment input in gravel-bed rivers are non-uniform and do not correspond to the ideal situations presented above. However, a given sediment input curve in one particular region of a river can be discretised with a mesh, i.e. approximated by a series of plateaux. The role played by each of these plateaux can then be analysed individually using the previous method. Considering a certain number of sections of uniform input rates  $i_j^k$  ( $j$ : size fraction index,  $k$ : section index) between the points of coordinates  $x_k$  and  $x_{k+1}$ , the corresponding concentration per unit length is:

$$c_{b0_j}^k = r_j \frac{i_{0_j}^k}{q} \quad [6.25]$$

To compute the total deposition rate at a given point with coordinate  $x$ : (1) the deposition rates due to each section  $\Delta_b^k(x)$  are computed for a given set of coordinates using the same method as described in §6.3.1.1; (2) for each coordinate, the components of the deposition rates due to each section are summed.

#### 6.3.2.2 Example of application

The previous method has been applied to the input function shown on Figure 6.8. This function was first discretised into a series of nine sections of various lengths (6m in average) (Figure 6.7). For each of these sections, the longitudinal deposition profile has been computed every two meters using the same spreadsheet as used in §6.3.1.2 (i.e. Figure 6.6). The different components were summed using another spreadsheet (Table 6.2), where all the deposition rates below  $10^{-6}\text{kg}\cdot\text{m}^{-2}\cdot\text{s}^{-1}$  have not been considered. The overall deposition profile is shown on Figure 6.7.

As in Figure 6.6, there is a shift between the input and the deposition due to the time required by the particles to settle through the flow. The difference varies between 0 and 4m, with an average of 2.25m. The peak of deposition reaches  $0.204\text{kg}\cdot\text{m}^{-2}\cdot\text{s}^{-1}$ , i.e.

2% above the maximum input rate. It can also be noticed that the deposition graph has a much more irregular shape than the input graph, particularly in its downward part. This is due to the presence of several discontinuities that can be observed towards the end of the longest section intervals (see sections 3, 4, 6, 7, 8, 9 on Figure 6.8). These breaks are caused by the fact that over a certain distance, the influence of the previous section(s) in the mesh becomes negligible (similar to Figure 6.6 after  $x=6$  to 7m), and only the section considered eventually counts in the overall deposition rate. As a result, the deposition curve converges towards the input curve.

x (m)	section 1	section 2	section 3	section 4	section 5	section 6	section 7	section 8	section 9	Total
2	1.66E-02									1.66E-02
4	4.68E-02									4.68E-02
6	3.29E-02	2.53E-02								5.82E-02
8	4.47E-03	7.02E-02	3.49E-04							7.50E-02
10	8.70E-04	1.77E-02	7.83E-02							9.69E-02
12	2.51E-04	2.52E-03	9.85E-02							1.01E-01
14	8.98E-05	5.93E-04	6.54E-02	6.09E-02						1.27E-01
16	3.59E-05	1.88E-04	8.37E-03	1.66E-01						1.74E-01
18	1.47E-05	7.05E-05	1.55E-03	1.74E-01						1.76E-01
20	5.64E-06	2.83E-05	4.33E-04	1.13E-01	7.00E-02					1.84E-01
22	1.84E-06	1.11E-05	1.50E-04	1.38E-02	1.90E-01					2.04E-01
24		3.87E-06	5.66E-05	2.45E-03	1.29E-01	5.19E-02				1.83E-01
26		1.08E-06	2.08E-05	6.63E-04	1.54E-02	1.42E-01				1.58E-01
28			6.62E-06	2.21E-04	2.67E-03	1.49E-01				1.52E-01
30			1.59E-06	7.88E-05	7.12E-04	9.75E-02	3.41E-02			1.32E-01
32				2.58E-05	2.36E-04	1.20E-02	9.43E-02			1.07E-01
34				6.65E-06	8.45E-05	2.17E-03	9.96E-02			1.02E-01
36				1.14E-06	2.86E-05	5.91E-04	1.00E-01			1.01E-01
38					7.92E-06	1.99E-04	6.55E-02	1.66E-02		8.23E-02
40					1.54E-06	7.21E-05	8.41E-03	4.68E-02		5.53E-02
42						2.44E-05	1.57E-03	4.97E-02		5.13E-02
44						6.59E-06	4.41E-04	5.00E-02		5.04E-02
46						1.22E-06	1.52E-04	3.32E-02	8.10E-03	4.14E-02
48							5.68E-05	4.55E-03	2.33E-02	2.79E-02
50							2.00E-05	8.99E-04	2.48E-02	2.58E-02
52							5.78E-06	2.62E-04	2.50E-02	2.52E-02
54							1.17E-06	9.43E-05	2.50E-02	2.51E-02
56								3.72E-05	1.68E-02	1.68E-02
58								1.45E-05	2.45E-03	2.47E-03
60								5.02E-06	5.13E-04	5.18E-04
62								1.35E-06	1.56E-04	1.57E-04
64									5.80E-05	5.80E-05
66									2.40E-05	2.40E-05
68									1.00E-05	1.00E-05
70									3.88E-06	3.88E-06
72									1.25E-06	1.25E-06

TABLE 6.2: non-uniform source, application of the method described in §6.3.2.1. Sum of all the deposition rates ( $\text{kg.m}^{-2}.\text{s}^{-1}$ ) obtained every 2m for each section of the discretisation function.

To solve this problem, the section lengths have to be reduced to a size comparable to those of sections 1, 2 or 5. A new mesh was set up with twice as many sections as the previous one, i.e. with an average section length of 3m (Figure 6.8). The graph of the deposition rates is this time very similar to the input diagram. It is still shifted downstream by an average distance of 2.3m. It can be seen that the rising limbs of the curves are closer to each other than the falling limbs (1.9m / 2.6m). This time, the peak reached by the deposition rate curve exceeds that of the input rate by 3% ( $0.206\text{kg}\cdot\text{m}^{-2}\cdot\text{s}^{-1}$ ).

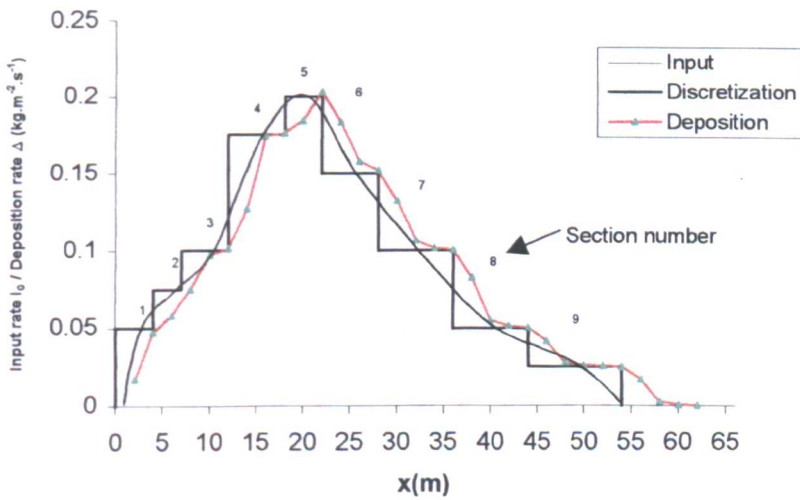


FIGURE 6.7: (non-uniform) input function, 9-section mesh and result from the model described in §6.3.2.1

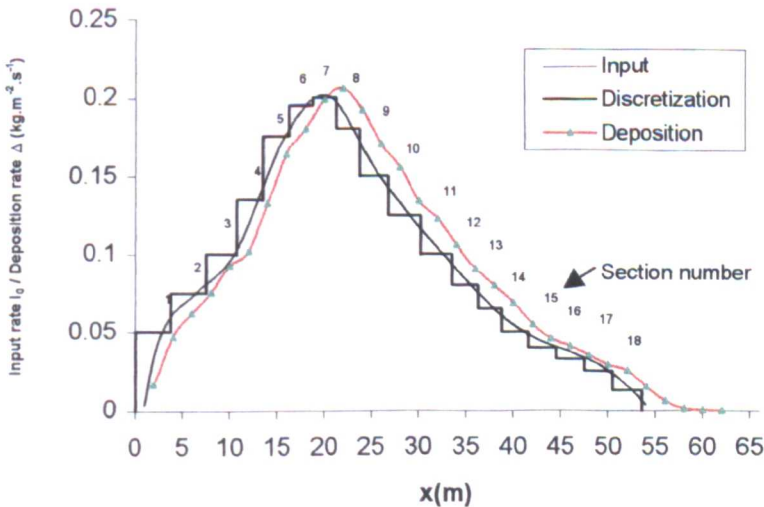


FIGURE 6.8: (non-uniform) input function, 18-section mesh and result from the model described in §6.3.2.1

### 6.3.3 Real-life applications and model sensitivity

The previous models are applied to two examples. In the absence of any other expression for the deposition velocity, Equation [5.27] is used to compute  $w_d$  in the context of these two examples, i.e. that of natural rivers.

#### 6.3.3.1 Example 1

Road construction works are carried out along a 1m-deep, 5m-wide, 0.2%-steep gravel-bed river over a section of approximately 100m. Research has indicated that intense rainfall events are likely to produce average sand inputs of  $10^{-2}\text{kg}\cdot\text{m}^{-2}\cdot\text{s}^{-1}$  into the river during several hours. The fine sediment composition is similar to that of LA-260 sand. What is the impact of such inputs likely to be on the gravel-bed environment?

The shear velocity  $u^*$  in this case is close to  $0.12\text{m}\cdot\text{s}^{-1}$ . Assuming a value of Manning's  $n$  of 0.04, bankfull flow is equal to  $3.60\text{m}^3\cdot\text{s}^{-1}$ . Studies indicate that increases in volumes of infiltrated sediment finer than 1mm of 5 to 10% can have deleterious consequences on the river fauna (§1.2.2). These correspond in this case to accumulations of fines of the order of  $10^1\text{kg}\cdot\text{m}^{-2}$  over periods of time of the order of  $10^4\text{s}$  ( $10^0$  to  $10^1$  hours), i.e.  $\Delta \approx 10^{-3}\text{kg}\cdot\text{m}^{-2}\cdot\text{s}^{-1}$ . Application of the model described in §6.3.1 (Figure 6.9) indicates that such a level is reached or exceeded approximately between  $x_{\min}=30\text{m}$  and  $x_{\max}=180\text{m}$  downstream of the initial input ( $x_0$ ).

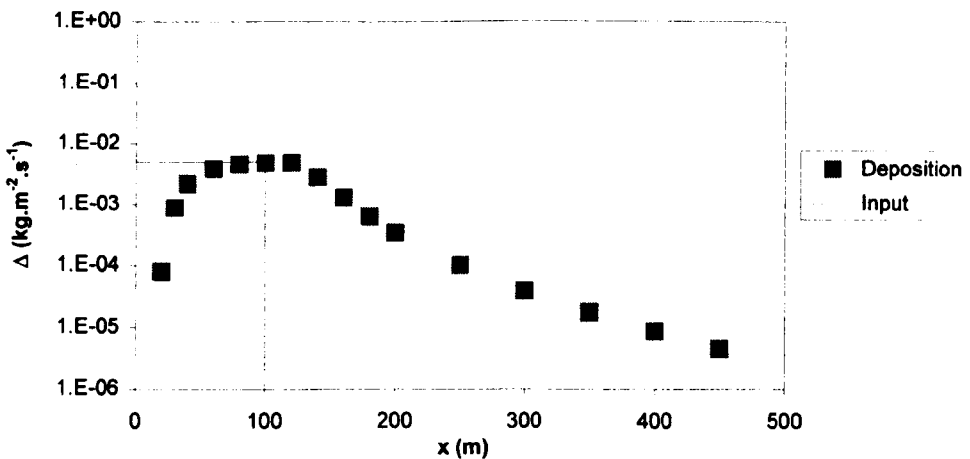


FIGURE 6.9: application of the model described in §6.3.1 to Example 1

Parameter	$u^*=0.07\text{m}\cdot\text{s}^{-1}$	$u^*=0.10\text{m}\cdot\text{s}^{-1}$	$Q=2\text{m}^3\cdot\text{s}^{-1}$	$Q=5\text{m}^3\cdot\text{s}^{-1}$
$x_{\text{max}}$	165	175	135	205
Parameter	$i_0=0.005\text{kg}\cdot\text{m}^{-2}\cdot\text{s}^{-1}$	$i_0=0.015\text{kg}\cdot\text{m}^{-2}\cdot\text{s}^{-1}$	$d\sim 200\mu\text{m}$	$d\sim 400\mu\text{m}$
$x_{\text{max}}$	165	195	155	225

TABLE 6.3: model sensitivity assessment on the value of the coordinate  $x_{\text{max}}$ , i.e. the maximum coordinate at which  $\Delta \geq 10^{-3}\text{kg}\cdot\text{m}^{-2}\cdot\text{s}^{-1}$ . The reference values of the parameters are  $u^*=0.12\text{m}\cdot\text{s}^{-1}$ ,  $Q=3.60\text{m}^3\cdot\text{s}^{-1}$ ,  $i_0=0.01\text{kg}\cdot\text{m}^{-2}\cdot\text{s}^{-1}$  and  $d=260\mu\text{m}$ .

Some of the initial parameters were varied to test the sensitivity of the model. Results of the coordinate  $x_{\text{max}}$  were computed in each case. These results are indicated in Table 6.3. Changes in the values of the shear velocity do not bring important variations in  $x_{\text{max}}$ , whereas the model is more sensitive to changes in flow rate and fine sediment size.

### 6.3.3.2 Example 2

A 20m-wide, 3m-deep, 0.05%-steep gravel-bed river erodes its banks over a 1000m-long reach. This produces an additional input of sand of median size  $d_{50}=200\mu\text{m}$  into the river. The input rate is approximately  $2 \times 10^{-3}\text{kg}\cdot\text{m}^{-2}\cdot\text{s}^{-1}$  for the average flow over the first and last 400m and  $5 \times 10^{-3}\text{kg}\cdot\text{m}^{-2}\cdot\text{s}^{-1}$  over the central 200m. Flood flows capable of flushing fines out of the gravel-bed occur one to four times a year. To what extent does this eroding reach affect the bed?

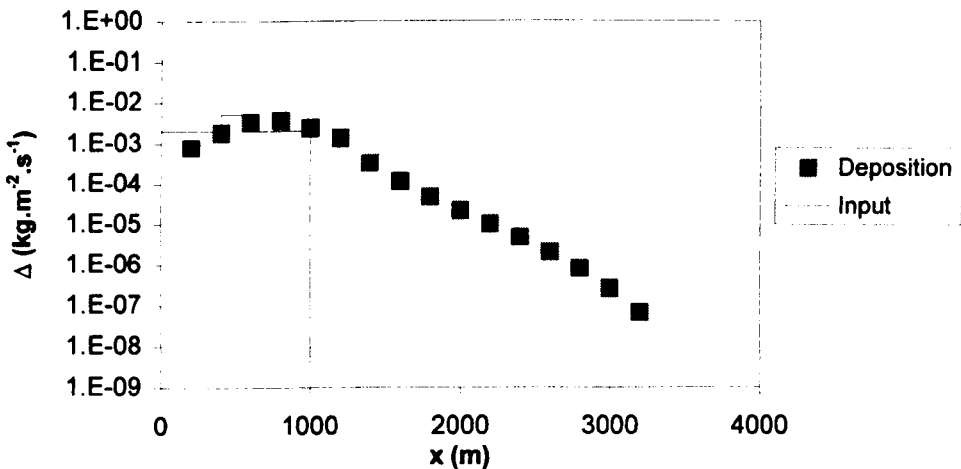


FIGURE 6.10: application of the model described in §6.3.2 to Example 2

Shear velocity and discharge at bankfull conditions are respectively  $0.10\text{m}\cdot\text{s}^{-1}$  and  $Q=58\text{m}^3\cdot\text{s}^{-1}$  ( $n=0.04$ ). Given the frequency of occurrence of flushing flows, fines accumulation takes place over several months per year in general, i.e. over periods of the order of  $10^7\text{s}$ . Critical accumulations of  $10^1\text{kg}\cdot\text{m}^{-2}$  can thus be reached with deposition rates of sediment of the order of  $10^{-6}\text{kg}\cdot\text{m}^{-2}\cdot\text{s}^{-1}$ . Application of the method described in §6.3.2 (Figure 6.10) indicates that this is likely to occur up to  $x_{\text{max}}\sim 2600\text{m}$ .

## 6.4 Conclusion

The results obtained in Chapters IV and V, and in particular the concept of deposition velocity, have been applied to model downstream sorting of fine sediments in gravel-bed rivers. In the context of uniform, 2-D flow conditions, several cases have been analysed where a source of sediment is released at the water surface, settles in the water column at its terminal fall velocity and deposits into the bed. Particles likely to be suspended have not been included in order to simplify the procedure of computation of the near-bed concentration resulting from an input at the water surface. However, these particles could be taken into account by evaluating their longitudinal and vertical distributions against distance, using for example Jobson and Sayre's (1970) method.

For a point source, a method based on the sediment concentration decay equation and [5.27] was derived, using a mathematical series. The model results match the experimental results closely and confirm the role played by the turbulence damping coefficient of deposition. The concentration coefficients ( $r_j$ ) ( $= C_{b_j} / C_b$ ) were computed by comparing model and experimental data, indicating a peak of  $\sim 2.6$  for particles close to  $300\mu\text{m}$  in diameter. By integration, it was possible to extend the analysis to uniform, continuous sediment sources, and by discretisation, to non-uniform sources. It was found that continuous sources cause, after a certain distance, deposition at the same rate as the input. The interest of the model is that this particular distance can be determined, as well as the distance over which significant deposition occurs further downstream. For non-uniform sources, it is possible to obtain good results by discretisation if a proper mesh is constructed (with relatively short section lengths  $\Delta x$ ). The example presented indicates

that the longitudinal shift between input and deposition is lower in parts of the curve where the input rate increases, compared to parts where it decreases.

# Chapter VII

## Conclusion

### 7.1 Summary of the main points

Increased land erosion and drainage combined with larger impoundments for water consumption can result in increased levels of sediments infiltrating into gravel river beds. This can cause a threat to the ecology of rivers and to fish populations. It also has implications for sediment transport and groundwater recharge. However, the infiltration process is poorly researched, particularly the passage of the fine particles from the open-channel medium to the porous medium through the bed surface layer, i.e. the deposition process.

Two preliminary series of experiments were carried out. The first one was concerned with the observation of sediment deposition and infiltration within a perspex-walled flume. Fine sediment infiltration in gravel-bed rivers is characterised by two main patterns i.e. siltation, where deposited particles pass directly to the bottom of the bed, and clogging, which consists in the accumulation of relatively large matrix particles near the top of the sub-surface. These two patterns were observed for median size ratios  $D/d$  that were consistent with the literature. In addition, it was found that:

- 1) there exists an intermediate pattern, specific to poorly-graded gravel beds, where particles infiltrate through isolated gaps by forming a series of piled-up cones of infiltration. This infiltration pattern occurs for sediment size ratios close to  $D/d \sim 40$ .
- 2) pools tend to act as sediment traps because they induce re-circulation currents and lower flow velocities. Fine particles deposit preferentially at the head of pools.

- 3) interstitial flows can facilitate the deeper infiltration of fines, particularly in between two consecutive pools.

Previous studies indicated that deposition is proportional to the concentration of fines and to the fall velocity. Connections between deposition rates and bed shear stress, structure of near-bed turbulence, and transport mode were also reported. The aim of the second preliminary series of experiments was to check some of these links and to prepare the main series of experiments. Fine sediment was released into an 8m-long flume, and deposited through a single layer of gravel into a funnel-shaped sediment trap, where instantaneous deposition rates were measured. The results of the experiments indicated that:

- 1) deposition rates are proportional to the initial sediment concentration  $C_0$ , and to the corresponding near-bed concentration  $C_b$ . The ratio of the deposition rate  $\Delta$  to the near-bed concentration of fines  $C_b$  has the dimension of a velocity, and represents an average settling velocity of the particles through the bed surface layer or deposition velocity  $w_d$ .
- 2) mathematical expressions of the spatial distribution of the deposition rate  $\Delta$  and the near-bed concentration  $C_b$  in the case of a point release were derived, based on the concept of deposition velocity. These two variables follow an exponential decay, with a decay rate equal to  $r w_d / q$  ( $r$  is the coefficient such that  $C_b = r C$  and  $q$  is the unit discharge).

The main series of experiments investigated the physical mechanisms and the main parameters controlling deposition. Deposition velocities were measured in different gravel-size and flow conditions. The ratio between the deposition velocity  $w_d$  and the fall velocity  $w_s$ , which gives an indication of the effects of near-bed turbulence and the bed surface on fine sediment, was also computed. It was referred to as the dimensionless deposition velocity  $w_d^*$ . Results indicated that:

- 1) the deposition velocity generally increases with grain size, but tends to stabilise in the upper range (bedload particles).
- 2) the median size of near-bed and deposited sediment decreases with longitudinal distance. The sediment deposited is coarser than the corresponding near-bed sediment. The gap between deposited and near-bed sediment's  $d_{50}$  tends to decrease with increasing shear velocity.
- 3) for the experiments with LA-260 (medium-size) sand, it was found that the dimensionless deposition velocity  $w_d^*$  ( $= w_d / w_s$ ) generally decreased with grain size from a value larger than 1 below  $200\mu\text{m}$  to a value lower than 1 above  $350\mu\text{m}$ . Deposition was thus enhanced for the finest particles and hindered for the largest ones. For B3-100 (very fine) sand experiments, values of  $w_d^*$  were significantly lower than with LA-260 (no enhanced deposition), but similar variations were observed.
- 4) the deposition velocity of fine particles decreases with increasing shear velocity, particularly so for medium-size sand particles ( $\sim 300\text{-}350\mu\text{m}$ ).
- 5) gravel size does not have a significant influence on  $w_d^*$  for particles larger than  $200\mu\text{m}$ . Some observations suggest that deposition of particles finer than  $200\mu\text{m}$  may increase through larger gravel beds, but this contradicts the results of Einstein (1968) on silt particles.
- 6) suspended particles are directly influenced by the structure of near-bed turbulence, which causes phenomena like enhanced deposition. The depositional behaviour of these particles can be described by a relationship between the so-called deposition parameter  $w_d^+$  ( $= w_d u^* / (g d)$ ) and the dimensionless grain size  $d^*$  ( $d^* = d (g \rho_s^* / \nu^2)^{1/3}$ ).
- 7) particles transported by saltation have a relatively low dimensionless deposition velocity because of their tendency to be re-entrained in the flow by the bed surface.

A model based on a simple representation of the bed surface supports the validity of a mechanical interpretation of the phenomenon, but requires some knowledge on the landing angles of the particles.

- 8) turbulence damping, which depends on the size of the fines transported and on their concentration, also influences the deposition of both suspended and saltating particles. This phenomenon can be described using van Rijn's  $\phi$  coefficient. The deposition rates tend to increase with increasing damping.

These results have been applied to model downstream sorting of fine particles in gravel-bed rivers in 2-D uniform flow conditions. To simplify the procedure of computation of the near-bed velocity, particles likely to be transported by suspension were not considered. It was found that:

- 1) experimental data indicate that, in the case of a point-source, the decay rate of the deposition rate and the near-bed concentration decreases with increasing longitudinal distance and with increasing shear velocity. It is possible to model this phenomenon using a mathematical series. This method takes into account the fact that the damping coefficient decreases with distance downstream, as a result of the reduction of sediment concentration and near-bed sediment size.
- 2) by integration, it is possible to extend the point-source analysis to uniform, continuous sediment sources, and by discretisation, to non-uniform sources. The models show that continuous sources cause, after a certain distance, deposition at the same rate as the input.

## 7.2 Discussion

The process of fine sediment deposition/infiltration into porous media has been studied experimentally. The preliminary series of tests on infiltration has provided useful information concerning various aspects of the infiltration process. It has shown that the spatial distribution of fine sediment within gravel bed rivers depends on a complex

interaction between grain size, hydraulic and hydrological conditions. It was found in particular that the formation of sand seals depends not only on the relative size of the gravel and the fine particles, but also on the intensity of the interstitial flow and of the surface flow (which can generate vibrations within the gravel framework) and on the presence of bedforms. This suggests that infiltration patterns can rapidly shift from siltation to clogging and vice versa in rivers where the relative sediment size  $D/d$  is close to critical ( $D/d \sim 40$  to  $50$ ). Mobile-bed conditions (which represent the key aspect of the matrix sediment distribution problem) could unfortunately not be tested due to the restricted size of the C4 flume.

The two following series of experiments were concerned with the deposition process. Both were similar in terms of experimental set-up and background. Only the methods were changed as the main series of experiments benefited from the results obtained in the previous series.

In terms of flow and friction parameters, two methods were used to measure the shear velocity  $u^*$ . The Reynolds stress profile method proved to be less reliable than the law of the wall method due to the large proportion of non-linear profiles obtained. It is possible that in experiments with deeper flows and more uniform beds, the Reynolds stress method would have been more successful. However, the manufacturers of the ADV probes have recently reported some problems in the operation of the ADV. Certain users have reported the presence of cross-pulse interference, due to reflected pulses from the boundary. Because the probe was not originally designed to be used over porous beds, some investigations are under way to measure the possible effects of cross pulses on the results in this case. In the present study, the use of the side-looking version of the probe, which does not require a minimum flow depth, would have probably been more appropriate to carry out the flow measurements.

In terms of deposition, all the experimental results have shown that deposition rates are primarily related to near-bed sediment concentrations. The main areas of deposition in rivers are thus associated with the zones receiving the largest fine sediment transport rates, e.g. near the thalweg. The main series of experiments has also indicated that the dimensionless deposition velocity  $w_d^*$  generally tends to decrease as grain size increases (§4.4.5). This is an unexpected result for two reasons. Firstly, logic would suggest that the finest particles should be infrequently deposited because of near-bed

turbulence, and therefore have a  $w_d^*$  close to 0. Secondly, it seems logical to consider that the coarser fines, which are less affected by turbulence, should deposit into the bed at or near their still water fall velocity and thus exhibit a  $w_d^*$  close to 1. The experimental results indicate almost the opposite trend. This is largely due the major role played by the mode of transport (suspended load, bed load) on the deposition process, as the finest particles are “hydraulically deposited” (little influence of gravity), and the coarsest ones tend to be mechanically kept in transport by reflecting off the bed surface. The results of the experiments suggest in fact a distinction between three ranges of fine particles: a lower range, an intermediate range and an upper range.

Concerning the lower range or Stokes’ range, the finest particles of LA-260 sand have in general been found to deposit through the bed surface at velocities faster than their natural fall velocity  $w_s$ . This phenomenon, previously observed above the bed (Jobson and Sayre, 1970), illustrates the fact that Stokes’ range particles are exclusively influenced by flow motions, and not by gravity. The reason for this phenomenon may lie in the ‘turbulent frictional mechanisms and lateral momentum exchanges, which result in significant transport of turbulent motion into the porous medium’ (Richardson and Parr, 1991). Lee eddies taking place within bed surface pores can trap very fine particles and act as agents of particle size selectivity (§2.1.1). These eddies can form reservoirs of fines which can be either ejected, or entrained into the subsurface bed-pores by sweep events. Equation [5.15] gives an expression of the deposition parameter  $w_d^+$  ( $= w_d u^* / (g d)$ ) against turbulence and friction parameters, based on the present knowledge of the structure of sweep events over coarse beds. Progress in this field may lead to progress on the deposition process of very fine particles as well.

The intermediate range includes particles influenced by both gravity and turbulence. The depositional behaviour of this range can be represented by the rising parts of the best-fit curves on Figure 4.13 (e.g. between  $\sim 220$  and  $\sim 320\mu\text{m}$  for LA-260 sand), or by Equation [5.6]. This equation is similar to that obtained for the lower range of particles ([5.15]) and confirms the significant role played by the deposition parameter  $w_d^+$  on the deposition process. However, in this case,  $w_d^+$  depends on the dimensionless grain size. It also depends on, at least, another parameter, which might be related to turbulence damping.

Lastly, the upper range of particles refers to particles mainly influenced by gravity, and transported by saltation. This mode of transport brings a totally different process of deposition than the Stokes' range and the intermediate range. It is characterised by a gradual reduction of the dimensionless deposition velocity with grain size (Figure 4.14), which can lead to a decline in the deposition velocity (Figure 4.12). Equation [5.20] indicates that deposition is mainly influenced in this case by the characteristics of the bed (particularly its porosity) and by the near-bed flow velocity (the landing angle depends also to a large extent on these two). The characteristics of near-bed turbulence play a relatively minor role in this case.

The shear velocity, and thus the level of turbulence, has generally been found to influence the deposition velocity negatively in the present experimental conditions with medium-size sand (Figure 4.15). However, the analysis of this influence size class by size class indicates that the negative relationship is systematically observed only two times, i.e. for the 231 $\mu$  and the 275 $\mu$  classes (Figures 4.16a, b and c). For the other size classes (either finer or coarser), there are some contradictions in the experimental results, particularly so for the experiments with finer gravel (Figures 4.16a and 4.16b). The fact that the best agreement is obtained for the two main size classes present in the LA-260 compound suggest that the lower percentages of sediment of the other classes have led to inaccuracies in the results, via lower transport and deposition rates. More experiments with the B3-100 sand would have been helpful to confirm this observation. Other possible causes for reduced accuracy include the non-uniformity of the bed sediment, and the relatively small water depth. As a matter of fact, a deeper and longer flume would probably have been more adequate for 1 to 1 scale experiments, but would also probably have required more time and much more sediment.

The damping of turbulence by fine sediment has been described as influencing the depositional behaviour of all ranges of fine particles. Van Rijn's  $\phi$  coefficient was used to represent this phenomenon, which depends on the overall sediment concentration and fall velocity of the transported mixture. This influence has to be viewed in a non-uniform sediment context. For example, assume that the deposition velocity of the size fraction  $i_1 = [150\mu\text{m}, 212\mu\text{m}]$  (represented by 181 $\mu\text{m}$ ) through a constant type of gravel is measured using LA-260 and B3-100 (both sand include a substantial proportion of the size fraction  $i_1$ ). LA-260 sand is coarser than B3-100, thus it carries more momentum

when it is transported, which results in a lower turbulent activity near the bed by damping and thus by larger deposition velocities. Thus, in the same conditions of bed surface and flow,  $i_1$  deposits quicker with LA-260 particles than with B3-100. Similarly, for a constant sediment mixture, larger concentrations tend to increase turbulence damping. This effect is negligible for relatively low near-bed concentrations (e.g.  $<0.50 \text{ g}\cdot\ell^{-1}$ , Appendix 3.4), but Figure 4.17 indicates that it begins to affect deposition at near-bed concentrations well below  $8.60 \text{ g}\cdot\ell^{-1}$ , maybe of the order of  $1.00 \text{ g}\cdot\ell^{-1}$  as suggested by Teisson *et al.* (1992). The proposed expression of the deposition velocity  $w_d$  (Equation [5.27]), which is based on the results of only three experiments for the turbulence damping term, applies only over a very restricted range of parameters and conditions. Its aim is not for practical application, but to provide a basis for future research. The detailed study of the influence of turbulence damping on deposition represents indeed a logical extension of the present study.

The results of the experimental work were applied to model the downstream deposition rates resulting from point sources and extended sources in 2D. Three cases (point-source, continuous source and non-uniform source of fine sediment in 2D uniform flow) were analysed, and expressions based on mathematical series were derived. The main limitations of these models are the conditions of application of Equation [5.27] and the restriction to non-suspendible size fractions. Another limitation concerns the requirement of the coefficients ( $r_i$ ), which can be measured experimentally, or using existing formulae (e.g. van Rijn, 1984).

The application of these models to very fine particles represents one of their most interesting potential developments, notably in terms of equilibrium sediment transport rates and boundary conditions of suspended sediment transport equations. In most existing models, the deposition rate of fine sediment has been assumed to equal the product of the near-bed concentration and the fall velocity in still water (e.g. Celik and Rodi, 1988; Holly and Rahuel, 1989; Ouillon and Le Guennec, 1996). This study has shown that this assumption is inaccurate in the case of coarse bed surfaces. Improvements of the models could be obtained using the concept of deposition velocity, which would result in a more accurate sink term in the sediment mass balance equation.

Sink terms of bedload transport equations could also be improved using a method similar to that developed in §5.4.

Other potential areas of interest include the study of: (1) the extension of the present study to wider ranges of shear velocities, fine sediment size and sediment concentrations; (2) the influence of gravel bed characteristics like porosity and bedforms, and the effect of vegetation on deposition; (3) the re-suspension process, particularly the mechanisms of fine sediment flushing in mobile bed conditions.

# References

- Abbott, J.E. and J.R.D. Francis, 1977. Saltating and suspended trajectories of solid grains in a water stream. *Philosophical Transactions*, Royal Society of London, Series A, 284, 225-254.
- Abt, S.R., W.P. Clary and C.I. Thornton, 1994. Sediment deposition and entrapment in vegetated streambeds. *Journal of Irrigation and Drainage Engineering*, A.S.C.E., 120(6), 1098-1111.
- Ackers, P and W. White, 1973. Sediment transport: new approaches and analysis. *Journal of the Hydraulics Division*, A.S.C.E., 99(11), 2041-2060.
- Adams, F. N. and R. L. Beschta, 1980. Gravel-bed composition in Oregon coastal streams. *Canadian Journal of Fisheries and Aquatic Sciences*, 37(10), 1514-1521.
- Allan, A. and L. Frostick, 1997. Winnowing, entrainment, and matrix particle size: the behaviour of sand-gravel mixtures in a laboratory flume. Abstracts, 6<sup>th</sup> International Conference on Fluvial Sedimentology, Cape Town.
- Alonso, C.V., F.D. Theurer and D.W. Zachmann, 1994. Tucannon River Offsite Study: sediment intrusion and dissolved-oxygen transport model. U.S. Department of Agriculture, Agricultural Research Service, National Sedimentation Laboratory, Oxford, Mississippi.
- A.S.C.E. Task Committee on Sediment Transport and Aquatic Habitats, Sedimentation Committee, 1992. Sediment and aquatic habitat in river systems. *Journal of Hydraulic Engineering*, 118(5), 669-687.
- Ashworth, P.J., J.L. Best, J.O. Leddy and G.W. Geehan, 1994. The physical modelling of braided rivers and deposition of fine-grained sediment. In M.J. Kirkby (ed.) *Process Models and Theoretical Morphology*. John Wiley.
- Bailey, J.E., S.P. Rice, J.J. Pella and S.G. Taylor, 1980. Effects of seeding density of pink salmon, *Oncorhynchus Gorbuscha*, eggs on water chemistry, fry characteristics, and fry survival in gravel incubators. *Fisheries Bulletin*, 78, 649-658.

- Bagnold, R.A., 1966. An approach to the sediment transport problem from general physics. *U.S. Geological Survey Professional Papers*, 422-I.
- Bayazit, M., 1976. Free surface flow in a channel of large relative roughness. *Journal of Hydraulic Research*, 14(2), 115-126.
- Beschta, R. L. & W. L. Jackson, 1979. The intrusion of fine sediment into a stable gravel-bed. *Journal of the Fisheries Research Board of Canada*, 36, 204-210.
- Bluck, B.J., 1971. Sedimentation in the meandering River Endrick. *Scottish Journal of Geology*, 7(2), 93-138.
- Boussinesq, J., 1896. Théorie de l'écoulement tourbillonnant et tumultueux des liquides dans les lits rectilignes à grande section (tuyaux de conduite et canaux découverts), quand cet écoulement s'est régularisé en un régime uniforme, c'est-à-dire, moyennement pareil à travers toutes les sections normales du lit. *Comptes Rendus de l'Académie des Sciences*, 72, 1290-1295 (in french).
- Bray, D.I., and K.S. Davar, 1987. Resistance of flow in gravel-bed rivers. *Canadian Journal of Civil Engineering*, Canadian Society of Civil Engineers, 14, 77-86.
- Bridge, J.S. and S.J. Bennett, 1992. A model for the entrainment and transport of sediment grains of mixed sizes, shapes and densities. *Water Resources Research*, 28(2), 337-363.
- Brookes, A., 1988. Channelized rivers: perspectives for environmental management. John Wiley, Chichester.
- Camp, T.R., 1943. The effect of turbulence on retarding settling. Proceedings of the 2nd Hydraulics Conference, University of Iowa Studies in Engineering, Bulletin 27, 307-317.
- Cao, Z., 1995. Turbulent bursting-based sediment entrainment function. *Journal of Hydraulic Engineering*, A.S.C.E., 123(3), 233-236.
- Carling, P.A., 1984. Deposition of fine and coarse sand in an open-work gravel bed. *Canadian Journal of Fisheries and Aquatic Sciences/Journal Canadien des Sciences Halieutiques et Aquatiques*, 41, 263-270.
- Carling, P.A., 1987. Bed stability in gravel streams with reference to stream regulation and ecology. In K. Richards (ed.) *River Channels: Environment and Process*, Basil Blackwell, Oxford, 321-348.

- Carling, P.A. and C.P. McCahon, 1987. Natural siltation of brown trout (*Salmo trutta* L.) spawning gravels during low-flow conditions. In J.F. Craig and B.J. Kemper (eds.), *Regulated Streams: Advances in Ecology*, Plenum Press, New York, 229-244.
- Carling, P.A. and M.S. Glaister, 1987. Rapid deposition of sand and gravel mixtures downstream of a negative step: the role of matrix-infilling and particle-overpassing in the process of bar-front accretion. *Journal of the Geological Society of London*, 144, 543-551.
- Carling, P.A. and N.A. Reader, 1982. Structure, composition and bulk properties of upland stream gravels. *Earth, Surface Processes and Landforms*, 7, 349-365.
- Celik, I and W. Rodi, 1988. Modeling suspended sediment transport in nonequilibrium situations. *Journal of Hydraulic Engineering, A.S.C.E.*, 114(10), 1157-1191.
- Chang, H.H., 1988. *Fluvial Processes in River Engineering*. John Wiley & Sons.
- Cheng, N.S., 1997. Simplified settling velocity formula for sediment particle. *Journal of Hydraulic Engineering, A.S.C.E.*, 123(2), 149-152.
- Church, M.A., D.G. McLean and J.F. Wolcott, 1987. River bed gravels: sampling and analysis. In Thorne, C.R., J.C. Bathurst and R.D. Hey (eds.) *Sediment Transport in Gravel-Bed Rivers*. Wiley, Chichester, 43-87.
- Coleman, N.L., 1981. Velocity profiles with suspended sediment. *Journal of Hydraulic Research*, 19(3), 211-229.
- Cordone, A.J. and Kelley, D.W., 1961. The influences of inorganic sediment on the aquatic life of streams. *California Fish and Game*, 47, 189-228.
- Dhamotharan, S., A. Wood, G. Parker and H. Stefan, 1980. Bedload transport in gravel streams. St Anthony Fall Hydraulic Laboratory Project Report 190, University of Minnesota, Minneapolis.
- Diplas, P., 1995. Modelling of fine and coarse sediment interaction over alternate bars. *Journal of Hydrology*, 159, 335-351.
- Diplas, P. and G. Parker, 1985. Pollution of gravel spawning grounds due to fine sediment. St. Anthony Falls Hydraulic Laboratory Project Report 240, University of Minnesota, Minneapolis.

- Diplas, P. and G. Parker, 1992. Deposition of fines in gravel-bed streams. In P. Billi, R.D. Hey, C.R. Thorne and P. Tacconi (eds), *Dynamics of Gravel-Bed Rivers*, Wiley, Chichester, 313-329.
- Dobbins, W.E., 1943. Effect of turbulence on sedimentation. *Transactions*, A.S.C.E., 109, Paper No. 2218, 629-678.
- Einstein, H. A., 1968. Deposition of suspended particles in a gravel-bed. *Journal of the Hydraulics Division*, A.S.C.E., 94(5), 1197-1205.
- Einstein, H.A., 1970. Closure of 'Deposition of suspended particles in a gravel bed'. *Journal of the Hydraulics Division*, A.S.C.E., 96(2), 581-582.
- Einstein, H.A. and N. Chien, 1955. Effects of heavy sediment concentration near the bed on velocity and sediment distribution, University of California, Berkeley, and U.S. Army Corps of Engineers, Missouri River Division, Report No. 8, 96 pages.
- Einstein, H.A. and R.B. Krone, 1962. Experiments to determine modes of cohesive sediment transport in salt water. *Journal of Geophysical Research*, 67(4), 1451-1461.
- Fernandez de la Mora, J. and S.K. Friedlander, 1982. Aerosol and gas deposition to fully rough surfaces: filtration model for blade shaped elements. *International Journal of Heat and Mass Transfer*, 25, 1725-1735.
- Fernandez Luque, R., and R. van Beek, 1976. Erosion and transport of bed-load sediment. *Journal of Hydraulic Research*, 14(2), 127-144.
- Fletcher, W.K., W.E. McLean and T. Sweeten, 1995. An instrument to monitor infiltration of fine sediment into stable gravel stream beds. *Aquacultural Engineering*, 14(4), 289-296.
- Frostick, L. E., 1997. Proceedings of the International Conference on Fluvial Sedimentology, Cape Town.
- Frostick, L. E., P. M. Lucas and I. Reid, 1984. The infiltration of fine matrices into coarse-grained alluvial sediments and its implications for stratigraphical interpretation. *Journal of the Geological Society of London*, 141(6), 955-965.
- García, M.H., Y. Niño and F. López, 1996. Laboratory observations of particle entrainment into suspension by turbulent bursting. In P.J. Ashworth, S.J. Bennett, J.L. Best and S.J. McLelland (eds.), *Coherent Flow Structures in Open Channels*, John Wiley, 63-86.

- Graf, W.H. and Song, T., 1995. Bed-shear stress in non-uniform and unsteady open-channel flows. *Journal of Hydraulic Research*, 33(5), 699-704.
- Grass, A.J., 1971. Structural features of turbulent flow over smooth and rough boundaries. *Journal of Fluid Mechanics*, 50, 233-255.
- Grass, A.J., R.J. Stuart and M. Mansour-Tehrani, 1991. Vortical structures and coherent motion in turbulent flow over smooth and rough boundaries. *Philosophical Transactions*, Royal Society of London, A336, 35-65.
- Happ, S.C., 1950. Stream channel control. In P.D. Trask (ed.), *Applied Sedimentation*. John Wiley, New York., 319-335.
- Happ, S.C., Rittenhouse G. and G.C. Dobson, 1940. Some principles of accelerated stream and valley sedimentation. In S.A. Schumm (ed.), *River Morphology*. Dowden, Hutchinson and Ross. Stroudsburg, Pennsylvania.
- Hazen, A., 1904. On sedimentation. *Transactions*, A.S.C.E., 53, 45-71.
- Hey, R.D., 1979. Flow resistance in gravel-bed rivers. *Journal of the Hydraulics Division*, A.S.C.E., 105(4), 365-379.
- Holly Jr., F.M. and J.L. Rahuel, 1990. New numerical/physical framework for mobile-bed modelling, Part I: Numerical and physical principles. *Journal of Hydraulic Research*, 28(4), 401-416.
- Hoyal, D.C.J.D., J.V. DePinto, J.F. Atkinson and S.W. Taylor, 1995. The effect of turbulence on sediment deposition. *Journal of Hydraulic Research*, 33(3), 349-360.
- Jain, S.C., 1990. Armor or pavement. *Journal of Hydraulic Engineering*, 116(3), 436-440.
- Jobson, H.E. and W.W. Sayre, 1970. Vertical transfer in open-channel flow. *Journal of the Hydraulics Division*, A.S.C.E., 96(3), 703-724.
- Julien, P.Y., 1995. *Erosion and Sedimentation*. Cambridge University Press.
- Jullien, R. and P. Meakin, 1988. Ballistic deposition and segregation of polydisperse spheres. *Europhysics Letters*, 6(7), 629-634.
- Kamphuis, J.W., 1974. Determination of sand roughness for fixed beds. *Journal of Hydraulic Research*, 12(2), 193-203.
- Kirkbride, A., 1993. Observations of the influence of bed roughness on turbulence structure in depth limited flows over gravel beds. In N.J. Clifford, J.R. French and

- J. Hardisty (eds.). *Turbulence: Perspectives on Flow and Sediment Transport*, John Wiley, 185-196.
- Klein, R.D., 1993. Sediment flux, fine sediment intrusion, and gravel permeability in a coastal stream, Northwestern California. In S.S.Y. Yang (ed.), *Advances in Hydro-Science and -Engineering*, 1, 273-280.
- Kline, S.J., W.C. Reynolds, F.A. Schraub and P.W. Runstadler, 1967. The structure of turbulent boundary layers. *Journal of Fluid Mechanics*, 95, 741-773.
- Kondolf, G.M. and P.R. Wilcock, 1996. The flushing flow problem: defining and evaluating objectives. *Water Resources Research*, 32(8), 2589-2599.
- Krone, R.B., 1962. Flume studies of the transport of sediment in estuarial shoaling processes. Hydraulic Engineering Laboratory and Sanitary Engineering Research Laboratory, University of California, Berkeley.
- Lau, Y.L., 1983. Suspended sediment effect on flow residence. *Journal of the Hydraulics Division, A.S.C.E.*, 109(5), 757-763.
- Lauck, T., R. Lamberson and T.E. Lisle, 1993. A simulation model for the infiltration of heterogeneous sediment into a stream bed. In S.S.Y. Yang (ed.), *Advances in Hydro-Science and -Engineering*, 1, 229-236.
- Lee, A., 1981. Atlantic salmon: the 'leaper' struggles to survive. *National Geographic*, 160(5), 600-615.
- Leopold, L.B., M.G. Wolman and J.P. Miller, 1964. *Fluvial processes in geomorphology*. W.H. Freeman & Co., San Francisco.
- Lisle, T. E., 1989. Sediment transport and resulting deposition in spawning gravels, North Coastal California. *Water Resources Research*, 25(6), 1303-1319.
- Maitland, P.S. and R.N. Campbell, 1992. *Freshwater Fishes of the British Isles*. Harper and Collins, London.
- McCave, I.N. and S.A. Swift, 1976. A physical model for the rate of deposition of fine-grained sediments in the deep sea. *Geological Society of America Bulletin*, 87, 541-546.
- Meland, N. and J.O. Normann, 1969. Transport velocities of individual size fractions in heterogeneous bed load. *Geogr. Am. Ser.*, A51, 127-144
- Milhous, R.T., 1973. Sediment transport in a gravel bottomed stream. Ph.D. thesis, Oregon State University, Corvallis, Oregon.

- Milhous, R.T., 1982. Effect of sediment transport and flow regulation on the ecology of gravel-bed rivers. In R.D. Hey, J.C. Bathurst and C.R. Thorne (eds.), *Gravel-bed rivers*. Wiley, Chichester, 819-841.
- Milner, N.J., J. Scullion, P.A. Carling, D.T. Crisp, 1981. The effect of discharge on sediment dynamics and consequent effects on invertebrates and salmonids in upland rivers, *Advances in Applied Biology*, 6, 153-220.
- Nakagawa, H. and I. Nezu, 1981. Structure of space-time correlations of bursting phenomena in an open-channel flow. *Journal of Fluid Mechanics*, 104, 1-43.
- Niño, Y. and M.H. García, 1996. Experiments on particle-turbulence interactions in the near-wall region of an open-channel flow: implications for sediment transport. *Journal of Fluid Mechanics*, 326, 285-319.
- Niño, Y., M.H. García and L. Ayala, 1994. Gravel saltation: 1 Experiments. *Water Resources Research*, 30(6), 1907-1914.
- Nowell, A.R.M. and M. Church, 1978. Turbulent flow in a depth-limited boundary layer. *Journal of Geophysical Research*, 84, 4816-4824.
- Oron, A. and C. Gutfinger, 1986. On turbulent deposition of particles to rough surfaces. *Journal of Aerosol Science*, 17(6), 903-920.
- Ouillon, S. and B. Le Guennec, 1996. Modelling non-cohesive suspended sediment transport in 2D vertical free surface flows. *Journal of Hydraulic Research*, 34(2), 219-236 (in french).
- Owen, M.W., 1969. Discussion on 'Deposition of suspended particles in a gravel-bed' by H.A. Einstein. *Journal of the Hydraulics Division A.S.C.E.*, 95(3), 1085-1087.
- Parker, G., P.C. Klingeman and D.G. McLean, 1982. Bedload and size distribution in paved gravel-bed streams. *Journal of the Hydraulics Division, A.S.C.E.*, 108(4), 544-571.
- Parker, G., 1995. Routing of sand through a gravel-bed river: one-dimensional model. 4<sup>th</sup> Conference on Gravel-Bed Rivers, Gold Bar, Washington, U.S.A.
- Partheniades, E., 1977. Unified view of wash load and bed material load. *Journal of the Hydraulics Division, A.S.C.E.*, 103(9), 1037-1057.
- Pettijohn, E.J., 1975. *Sedimentary rocks*, 3rd edn., Harper International, New York.
- Petts, G.E., 1988a. Accumulation of fine sediment within substrate gravels along two regulated rivers, U.K.. *Regulated Rivers: Research and Management*, 2, 141-153.

- Petts, G.E., 1988b. Regulated rivers in the U.K.. *Regulated Rivers: Research and Management*, 2, 369-387.
- Phillips, R.W., R.L. Lantz, E.W. Claire and J.R. Moring, 1975. Some effects of gravel mixtures on emergence of coho salmon and steelhead trout fry. *Transactions, American Fisheries Society*, 3, 461-466.
- Raudkivi, A.J., 1990. Loose-boundary hydraulics. 3rd edition. Pergamon Press, Oxford.
- Raupach, M.R., 1981. Conditional statistics of Reynolds stress in rough-wall and smooth-wall turbulent boundary layers. *Journal of Fluid Mechanics*, 108, 363-382.
- Richardson, C.P. and A.D. Parr, 1991. Friction and free-surface flow over porous media. *Journal of Hydraulic Engineering, A.S.C.E.*, 117(11), 1496-1512.
- Robinson, S.K., 1991. Coherent motions in the turbulent boundary layer. *Annual Review of Fluid Mechanics*, 23, 601-639.
- Sakthivadivel, R. and H.A. Einstein, 1970. Clogging of porous column of spheres of sediment. *Journal of the Hydraulics Division, A.S.C.E.*, 96(2), 461-472.
- Sambrook-Smith, G.H., 1996. Bimodal fluvial bed sediments: origin, spatial extent and processes. *Progress in Physical Geography*, 20(4), 402-417.
- Sayre, W.W., 1968. Dispersion of mass in open channel flow. *Hydraulic papers*, 3, Colorado State University, Fort Collins.
- Schack, C.J., Pratsinis, S.E. and S.K. Friedlander, 1985. A general correlation for deposition of suspended particles from turbulent gases to completely rough surfaces. *Atmospheric Environment*, 19(6), 953-960.
- Schälchi, U., 1992. The clogging of coarse gravel river beds by fine sediment. *Hydrologia*, 235/236, 189-197.
- Schälchli, U., 1995. Basic equations for siltation of riverbeds. *Journal of Hydraulic Engineering, A.S.C.E.*, 121(3), 274-287.
- Shen, H. and N.L. Ackermann, 1982. Constitutive relationships for fluid-solid mixtures. *Journal of the Engineering Mechanics Division A.S.C.E.*, 108(5), 748-763.
- Schmidt, J.C., D.M. Rubin and H. Ikeda, 1993. Flume simulation of recirculating flow and sedimentation. *Water Resources Research*, 29(8), 2925-2939.

- Sear, D.A., 1992. Impact of hydroelectric power releases on sediment transport processes in pool-riffle sequences. In P. Billi, R.D. Hey, C.R. Thorne and P. Tacconi (eds.), *Dynamics of Gravel-Bed Rivers*. Wiley, Chichester, 629-650.
- Sear, D.A., 1993. Fine sediment infiltration into gravel spawning beds within a regulated river experiencing floods: ecological implications for salmonids, *Regulated Rivers: Research and Management*, 8, 373-390.
- Smith, C.R., 1996. Coherent flow structures in smooth-wall turbulent boundary layers: facts, mechanisms and speculation. In P.J. Ashworth, S.J. Bennett, J.L. Best and S.J. McLelland (eds.), *Coherent Flow Structures in Open Channels*, John Wiley, 1-39.
- Stokes, G.G., 1851. On the effect of internal friction of fluids on the motion of pendulums. *Transactions*, Cambridge Philosophical Society, 9(2), 8-106.
- Stow, D.A.V. and A.J. Bowen, 1980. A physical model for the transport and sorting of fine-grained sediment by turbidity currents. *Sedimentology*, 27, 31-46.
- Stuart, T.A., 1953. Water currents through permeable gravels and their significance to spawning salmonids, etc. *Nature*, 172, 407-408.
- Teisson, C., 1997. A review of cohesive sediment transport models. In N. Burt, R. Parker and J. Watts (eds.), *Cohesive Sediment*, John Wiley, Chichester, 367-381.
- Teisson, C., O. Simonin, J.C Galland and D. Laurence, 1992. Turbulence and mud sedimentation: a Reynolds stress model and a two-phase flow model. *Proceedings of the Coastal Engineering 1992 Conference*, 2853-2866.
- Thibodeaux, L. J. and J. D. Boyle, 1987. Bedform-generated convective transport in bottom sediment. *Nature*, 325, 341-343.
- Thoms, M.C., 1987. Channel sedimentation within the urbanised River Tame, U.K., *Regulated Rivers: Research and Management*, 1, 229-246.
- Tien, C., 1989. Granular filtration of aerosols and hydrosols. *Butterworths Series in Chemical Engineering*, Boston.
- Tipping, E., C. Woof and K. Clarke, 1993. Deposition and resuspension of fine particles in a riverine 'dead-zone'. *Hydrological processes*, 7, 263-277
- Toro-Escobar, C.M., G. Parker and C. Paola, 1996. Transfer function for the deposition of poorly sorted gravel in response to streambed aggradation. *Journal of Hydraulic Research*, 34(1), 35-53.

- Trask, P.D., 1950. Dynamics of sedimentation. In P.D. Trask (ed.), *Applied Sedimentation*. John Wiley, New York., 3-40.
- Turnpenny, A.W.H. and R. Williams, 1980. Effects of sedimentation on the gravels of an industrial river system. *Journal of Fish Biology*, 17, 681-693.
- Uncles, R.J., R.C.A. Elliott and S.A. Weston, 1985. Observed fluxes of water, silt and suspended sediment in a partly mixed estuary. *Estuarine and Coastal Shelf Science*, 20, 147-167.
- Vanoni, V.A., 1946. Transportation of suspended sediment by water. *Transactions*, A.S.C.E., 111, 67-133.
- Vanoni, V.A., 1984. Fifty years of sedimentation. *Journal of Hydraulic Engineering*, A.S.C.E., 110(8), 1022-1057.
- van Rijn, L.C., 1982. Equivalent roughness of alluvial bed. *Journal of the Hydraulics Division*, A.S.C.E., 108(10), 1215-1218.
- van't Woudt, B.D. and K. Nicolle, 1978. Flow processes below a gravelly riverbed. *Journal of Hydrology (N.Z.)*, 17(2), 103-120.
- Wesche, T.A., 1985. Stream channel modifications and reclamation structures to enhance fish habitat. In J.A. Gore (ed.), *The restoration of rivers and streams: theories and experience*. Butterworth, London, 103-163.
- Wiberg, P.L., and J.G. Smith, 1985. A theoretical model for saltating grains in water. *Journal of Geophysical Research*, 90(C4), 7341-7354.
- Wilcock, P.R., G.M. Kondolf, W.V.G. Matthews and A.F. Barta, 1996. Specification of sediment maintenance flows for a large gravel-bed river. *Water Resources Research*, 32(9), 2911-2921.
- Wu, F. and H.W. Shen, 1993. An application of nonhomogeneous poisson process in sediment infiltration into gravel bed. *Proceedings, Hydraulic Engineering '93*, 1511-1516.
- Yalin, S., 1992. *River mechanics*. Pergamon Press, Oxford.
- Zagni, A.F.E. and K.V.H. Smith, 1976. Channel flow over permeable beds of graded spheres. *Journal of the Hydraulics Division*, A.S.C.E., 102(2), 207-222.

# Appendices

Appendix 1.1: sediment size classes specifications.....	166
Appendix 3.1: spatial distribution equation for the near-bed concentration $C_b$ and the deposition rate and derivation of the expression of the deposition velocity $w_d$ .....	167
Appendix 3.2: example of computation of $w_d$ (Experiment A5).....	171
Appendix 3.3: average deposition rate $\Delta_0$ against initial sediment concentration $C_0$ .....	173
Appendix 3.4: deposition rate $\Delta$ against estimated near-bed concentration.....	176
Appendix 4.1: velocity profiles.....	179
Appendix 4.2: Reynolds stress profiles.....	184
Appendix 4.3: measured deposition rates and near-bed sediment concentrations - main series of experiments.....	190
Appendix 4.4: median grain sizes of deposited and near-bed fine sediment samples.....	192
Appendix 4.5: ratio between deposited and transported median sample sizes ( $=d_{50dep}/d_{50tpd}$ ) expressed as a percentage of the transported sediment's median size.....	194
Appendix 4.6: average deposition velocities $w_d$ .....	195
Appendix 4.7: main series experimental data and details on the calculation of the deposition velocities.....	197
Appendix 5.1: deposition of particles transported by saltation: computation of the landing angles $\beta$ .....	219
Appendix 5.2: percentage of error between the experimental results and equation [5.27] for experiments with LA-260 and B3-100 sand.....	220
Appendix 6: longitudinal distribution of $\Delta$ for a line source: evaluation of $(r_i)$ for Experiment D3.....	222

Appendix 1.1: sediment size classes specifications

Limiting particle diameter		Size class			
mm	$\phi$ units				
2048	-11	very large	boulders	gravel	
1024	-10	large			
512	-9	medium			
256	-8	small			
128	-7	large	cobbles		
64	-6	small	pebbles		
32	-5	very coarse			
16	-4	coarse			
8	-3	medium			
4	-2	fine			
2	-1	very fine	granules		
1	0	( $\mu\text{m}$ ) very coarse	sand		
1/2	1	500 coarse			
1/4	2	250 medium			
1/8	3	125 fine			
1/16	4	63 very fine			
1/32	5	31 coarse	silt		
1/64	6	16 medium			
1/128	7	8 fine			
1/256	8	4 very fine	clay		
1/512	9	2 coarse			
1/1024	10	1 medium			
1/2048	11	0.5 fine			
1/4096	12	0.25 very fine			

British standards BS1377

Method of test for soils for civil engineering purposes (1977)

Appendix 3.1: spatial distribution equation for the near-bed concentration  $C_b$  and the deposition rate  $\Delta$ , and derivation of the expression of the deposition velocity  $w_d$  including the shift due to the vertical gap between the near-bed concentration and deposition rates measurement points.

Following a similar approach to that of Einstein (1968), the mass balance of fine sediment within a control volume of width  $dx$  (Fig. A31.1) can be expressed as:

$$Cqdt = (C + dC)qdt + C_b w_d dxdt \quad [A31.1]$$

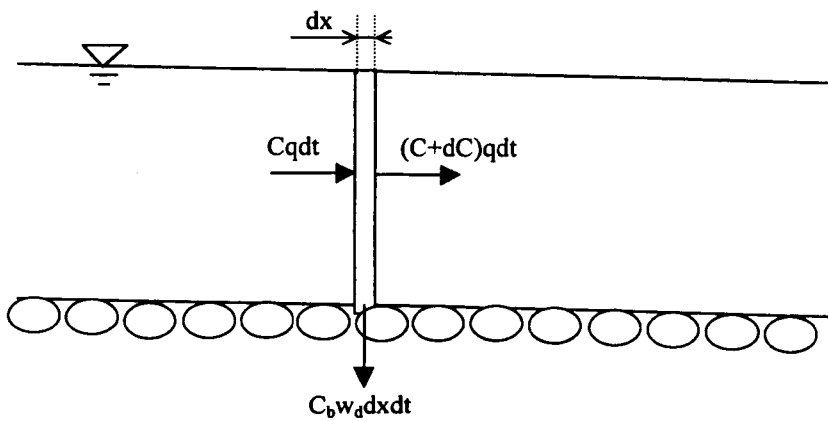


FIGURE A31.1: fine sediment mass balance within a control volume of length  $dx$ , over the whole water column depth.

where  $C$  is the depth-averaged concentration ( $\text{kg.m}^{-3}$ ),  $q$  the discharge per unit width ( $\text{m}^2.\text{s}^{-1}$ ). To solve this equation, it is assumed that depth averaged and near-bed concentrations are related through a constant coefficient  $r$  according to:

$$C_b = rC \quad [A31.2]$$

As a result, [A31.2] yields the equation describing the longitudinal variations of sediment concentration resulting from a deposition velocity  $w_d$ :

$$C_{b(x)} = C_{b_0} e^{-\frac{r w_d x}{q}} \quad [A31.3]$$

Combining Equations [3.1] and [A31.3], the longitudinal variations of the deposition rate read:

$$\Delta_{b(x)} = C_{b_0} w_d e^{-r \frac{w_d}{q} x} \quad [A31.4]$$

Let us consider a short longitudinal section of bed of length  $\partial x$  centred at the abscissa  $x$  (Figure A31.2) over which the average near-bed fine sediment concentration  $C_b$  is assumed to be constant and equal to  $C_{b(x)}$ .

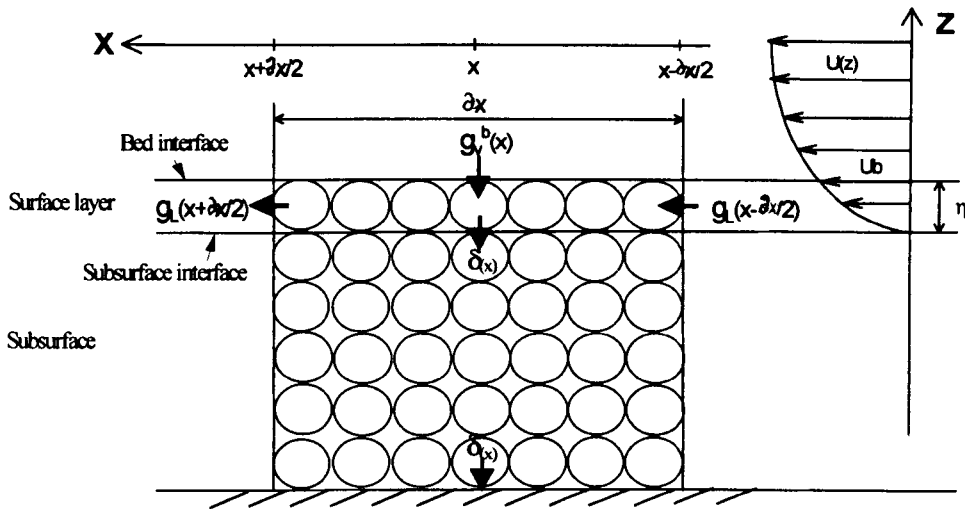


FIGURE A31.2: simplified representation of the bed framework over a small distance  $\partial x$  and definition of the flux variables

Based on [A31.4], this assumption is fulfilled if  $r w_d \partial x / 2q$  is sufficiently small to apply a Taylor series expansion to the exponential function. Assuming that there is no lateral water circulation below the bed surface layer, and that the settling fines infiltrate freely through the bed pores, the vertical mass transport rate of fines  $g_v$  is constant within the subsurface and equal to the deposition rate per unit length at the bottom of the permeable bed  $\delta$ . Subsequently, the continuity equation applied to the bed surface layer over the length  $\partial x$  (Figure A31.2) reads:

$$g_{v(x)}^b - \delta_{(x)} + g_{L(x-\partial x/2)} - g_{L(x+\partial x/2)} = 0 \quad [\text{A31.5}]$$

where  $g_v^b$  is the vertical mass transport rate of fines at the bed surface and  $g_L$  the longitudinal mass transport rate within the bed surface layer. The latter is given by:

$$g_{L(x)} = C_{s(x)} u_s \eta \quad [\text{A31.6}]$$

where  $C_s$  and  $u_s$  are respectively the mean sediment mass concentration ( $\text{kg.m}^{-3}$ ) and the mean longitudinal velocity of the fine particles within the bed surface layer ( $\text{m.s}^{-1}$ ), and  $\eta$  is the thickness of that layer (m) (Figure A31.2). Assuming that  $C_s$  is proportional to the near-bed sediment concentration  $C_b$ , it follows the same decay law, i.e.:

$$C_{s(x)} = C_{s(0)} e^{\frac{-r_s w_d x}{q}} \quad [\text{A31.7}]$$

where  $r_s$  is the coefficient such that  $C_s = r_s C$ .

The variation in sediment concentration  $C_s$  between  $x - \partial x / 2$  and  $x + \partial x / 2$  can be estimated with the first-order Taylor series expansion of [A31.7], as:

$$C_{s(x-\partial x/2)} - C_{s(x+\partial x/2)} = C_{s(x)} r_s \frac{w_d \partial x}{q} \quad [\text{A31.8}]$$

From [A31.6] and [A31.8], the expression for the net mass longitudinal transport rate over  $\partial x$  is thus:

$$g_{L(x-\partial x/2)} - g_{L(x+\partial x/2)} = C_{s(x)} r_s \frac{w_d \partial x u_s \eta}{q} \quad [\text{A31.9}]$$

In the vertical direction, the mass transport rate at the bed surface is derived from Equation [3.1] as:

$$g_{v(x)}^b = C_{b(x)} w_d \partial x \quad [\text{A31.10}]$$

Combining [A31.5], [A31.9] and [A31.10], the deposition rate,  $\delta$ , is given by:

$$\delta_{(x)} = \partial x w_d \left( C_{b(x)} + C_{s(x)} r_s \frac{u_s \eta}{q} \right) \quad [\text{A31.11}]$$

which yields the following expression for the effective settling velocity at the bed interface as a function of the deposition rate at the bottom of the permeable bed  $\Delta (= \delta / \partial x)$ :

$$w_d = \frac{\Delta_{(x)}}{C_{b(x)} + C_{s(x)} r_s \frac{u_s \eta}{U h}} \quad [\text{A31.12}]$$

where  $U$  is the mean flow velocity and  $h$  the water depth. The difficulty in [A31.12] lies in the calculation of the parameters  $C_s$  and  $u_s$ , respectively mean concentration and velocity of the fine particles within the bed surface, which can require the use of sophisticated sampling and particle tracking techniques. The longitudinal flow velocity within the bed surface is limited by the size of the pores and by the turbulent currents and eddies occurring there, whilst the movement of the fine particles entrained in this direction is hindered by contacts with the coarse grains. Thus the order of magnitude of  $u_s$  is  $\sim 10^{-2} \text{m.s}^{-1}$ , compared to a value of  $\sim 10^0 \text{m.s}^{-1}$  for the mean flow velocity  $U$ . Similarly, the bed surface thickness  $\eta$  has typically an order of magnitude of  $\sim 10^{-2} \text{m}$  to  $\sim 10^{-1} \text{m}$ , while the water depth  $h$  is normally close to  $\sim 10^0 \text{m}$ . The concentration  $C_s$  being of the same order as the near-bed concentration  $C_b$ , and  $r_s$  close to  $10^0$ , the second term of the denominator in [A31.12] is thus typically 3 to 4 orders of magnitude less than the first term, and can be neglected. Thus, the deposition velocity  $w_d$  is simply given by:

$$w_d \cong \frac{\Delta_{(x)}}{C_{b(x)}} \quad [\text{A31.13}]$$

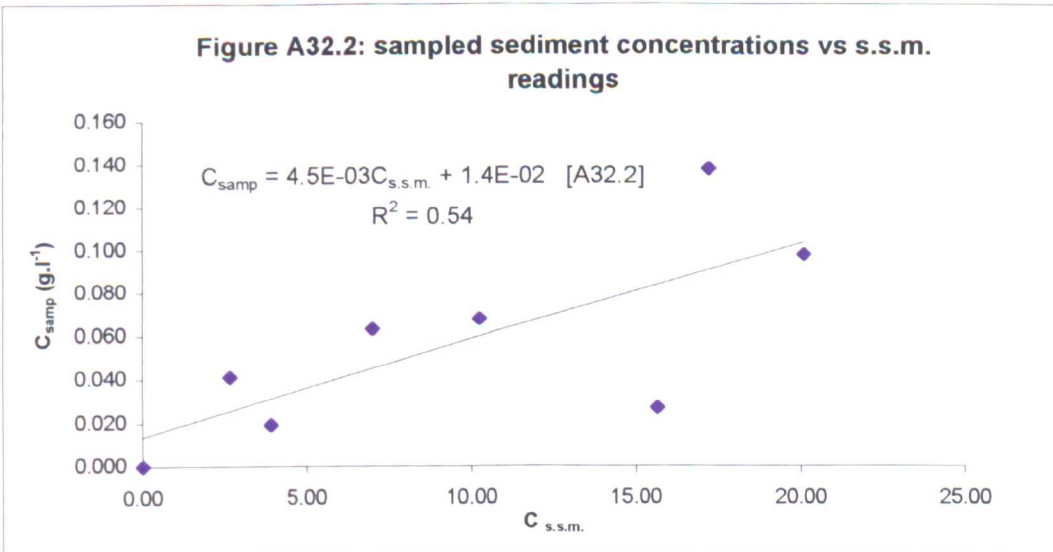
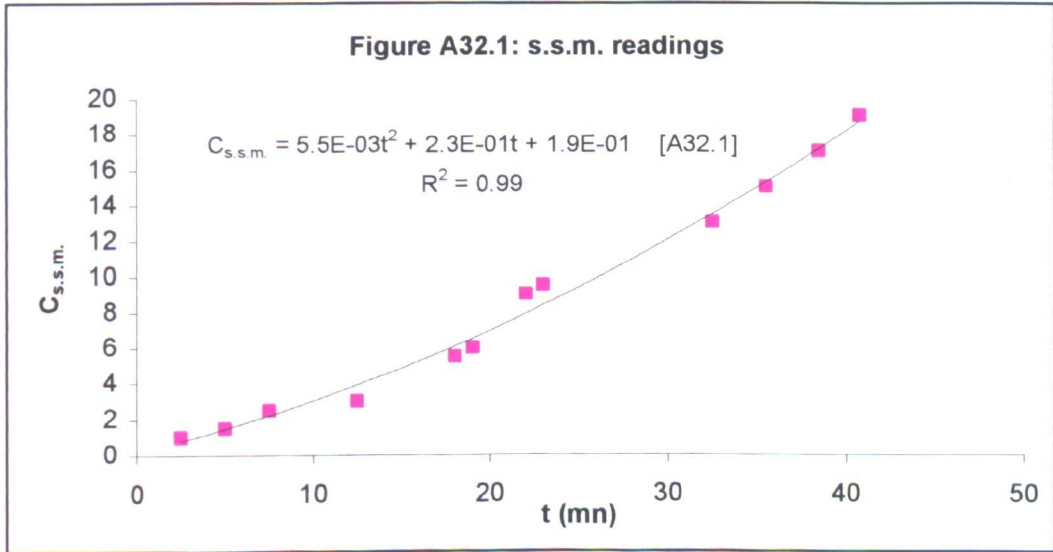
Appendix 3.2: example of computation of  $w_d$  (exp. A5)

The estimated suspended solids monitor (s.s.m.) index (4<sup>th</sup> column) is computed from the 2nd order best-fit equation ([A32.1]) obtained from all the readings (Figure A32.1). The estimated near-bed concentration (5<sup>th</sup> column) is computed from the calibration equation ([A32.2]) obtained from the plot of the concentrations measured from the samples against the s.s.m. readings (Figure A32.2). The mass of sediment deposited in the funnel-shaped trap (7th column) is computed by multiplying the volume of sediment deposited by 1.51 (value obtained from calibration tests). The deposition rate  $\Delta$  (6<sup>th</sup> column) is computed by dividing the difference between two consecutive mass readings (7<sup>th</sup> column) by the time elapsed between the two readings (3rd column).

input (g.s)	$C_0$ (g.l <sup>-1</sup> )	time (mn)	$C_{s.s.m.}$	$C_b$ (g.l <sup>-1</sup> )	$\Delta$ (g.s.m <sup>-2</sup> )	deposit (g)	depos.(m)	$\Delta_0$ (g.l <sup>-1</sup> )
10.97	0.23	2	0.67	0.017		13.59	9	
10.97	0.23	3	0.93	0.018	0.74	21.14	14	
10.97	0.23	4	1.20	0.019	0.44	25.67	17	
10.97	0.23	5	1.48	0.020	0.59	31.71	21	
10.97	0.23	6	1.77	0.022	0.44	36.24	24	
10.97	0.23	7	2.07	0.023	0.89	45.3	30	
10.97	0.23	8	2.38	0.024	0.74	52.85	35	
10.97	0.23	9	2.71	0.026	0.59	58.89	39	
10.97	0.23	10.5	3.21	0.028	0.89	72.48	48	
10.97	0.23	11.5	3.56	0.030	1.19	84.56	56	
10.97	0.23	13	4.11	0.032	0.49	92.11	61	
10.97	0.23	14	4.49	0.034	0.74	99.66	66	
10.97	0.23	15	4.88	0.036	0.89	108.72	72	0.72
17.74	0.37	17.5	5.90	0.040		123.82	82	
17.74	0.37	18.5	6.33	0.042	1.78	141.94	94	
17.74	0.37	19.5	6.77	0.044	1.04	152.51	101	
17.74	0.37	20.5	7.21	0.046	1.04	163.08	108	
17.74	0.37	21.5	7.68	0.048	1.19	175.16	116	
17.74	0.37	22.5	8.15	0.050	1.78	193.28	128	
17.74	0.37	23.5	8.63	0.052	0.89	202.34	134	
17.74	0.37	24.5	9.12	0.055	1.63	218.95	145	
17.74	0.37	25.5	9.63	0.057	1.93	238.58	158	
17.74	0.37	27.5	10.67	0.061	0.89	256.7	170	
17.74	0.37	28.5	11.21	0.064	2.37	280.86	186	
17.74	0.37	29.5	11.76	0.066	1.19	292.94	194	1.43
23.34	0.49	31.5	12.89	0.071		327.67	217	
23.34	0.49	32.5	13.47	0.074	2.67	354.85	235	
23.34	0.49	33.5	14.06	0.077	1.78	372.97	247	
23.34	0.49	36	15.59	0.084		27.18	18	
23.34	0.49	37	16.22	0.086	2.67	54.36	36	
23.34	0.49	38	16.86	0.089	2.37	78.52	52	
23.34	0.49	39	17.51	0.092	2.67	105.7	70	
23.34	0.49	40	18.18	0.095	1.48	120.8	80	
23.34	0.49	41	18.85	0.098	3.11	152.51	101	
23.34	0.49	42	19.54	0.101	3.11	184.22	122	
23.34	0.49	43	20.24	0.104	2.08	205.36	136	
23.34	0.49	44	20.94	0.108	2.22	228.01	151	
23.34	0.49	45	21.66	0.111	2.52	253.68	168	
23.34	0.49	46	22.39	0.114	3.26	286.9	190	
23.34	0.49	47	23.13	0.117	2.67	314.08	208	2.51

X=4.58m input (g.s <sup>-1</sup> )	time (mn)	C <sub>s.s.m.</sub>	X=4.58m input (g.s <sup>-1</sup> )	time (mn)	Sampler C <sub>b</sub> (g.l <sup>-1</sup> )	Interpolate C <sub>s.s.m.</sub>
10.97	2.5	1			0.000	0.00
10.97	5	1.5				
10.97	7.5	2.5	10.97	9	0.041	2.65
10.97	12.5	3	10.97	14.5	0.019	3.91
17.74	18	5.5				
17.74	19	6	17.74	20	0.063	7.00
17.74	22	9				
17.74	23	9.5	17.74	25	0.068	10.24
23.34	32.5	13				
23.34	35.5	15	23.34	36.5	0.027	15.67
23.34	38.5	17	23.34	38.75	0.138	17.22
23.34	40.75	19	23.34	42	0.098	20.11

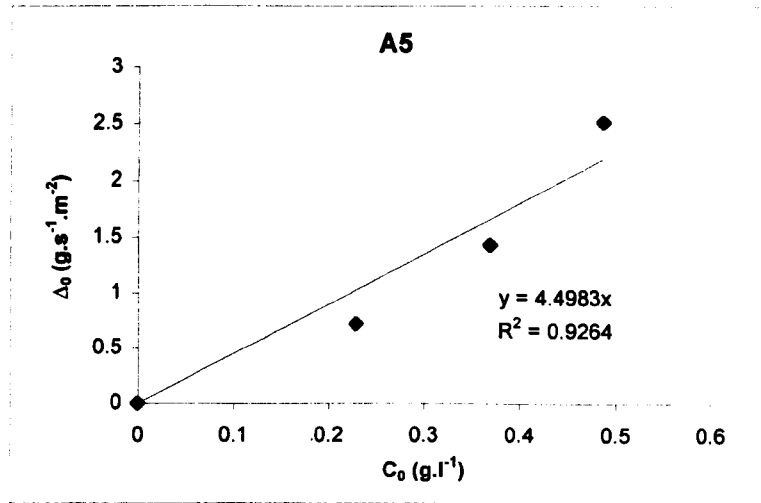
The value of the s.s.m. reading corresponding to the time when the near-bed sediment sample has been taken (7<sup>th</sup> column) is obtained by interpolation between the previous and the following readings (from the 3<sup>rd</sup> column)



Appendix 3.3: average deposition rate  $\Delta_0$  against initial sediment concentration  $C_0$

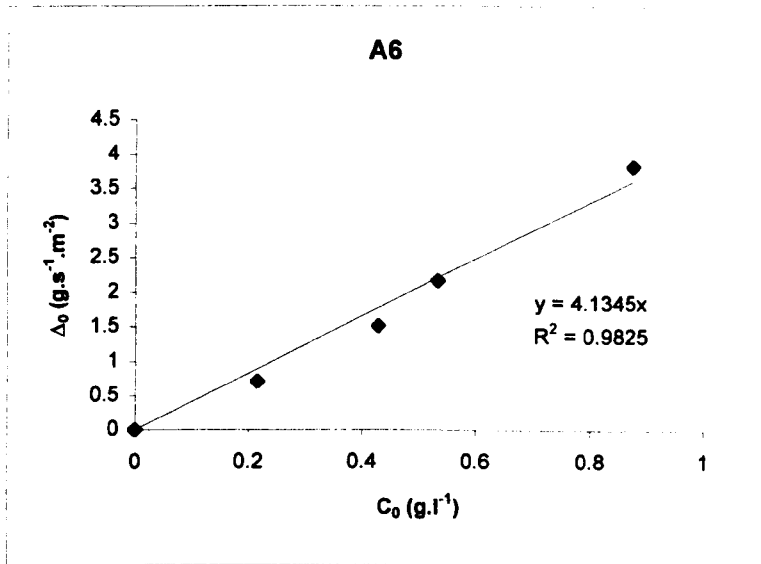
A5

$C_0$ (g.l <sup>-1</sup> )	$\Delta_0$ (g.s <sup>-1</sup> .m <sup>-2</sup> )
0	0
0.228538	0.72075
0.36955	1.428806
0.48625	2.509194



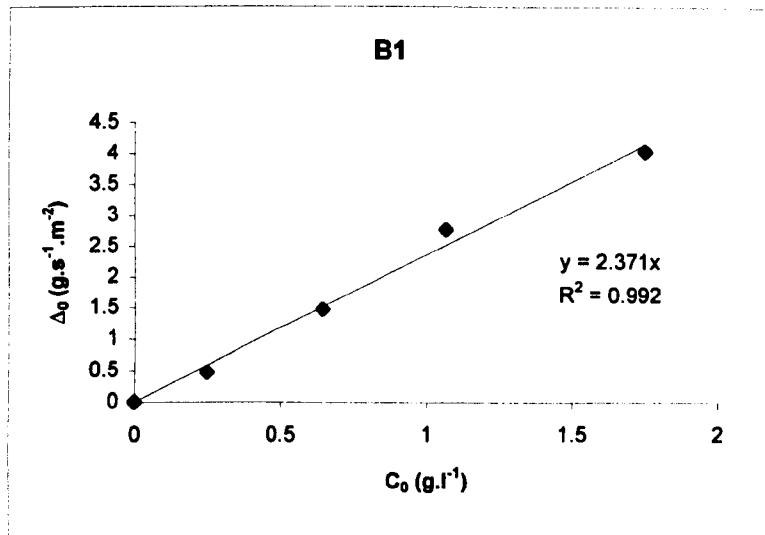
A6

$C_0$ (g.l <sup>-1</sup> )	$\Delta_0$ (g.s <sup>-1</sup> .m <sup>-2</sup> )
0	0
0.215417	0.708549
0.429792	1.507726
0.534792	2.160956
0.875208	3.826164



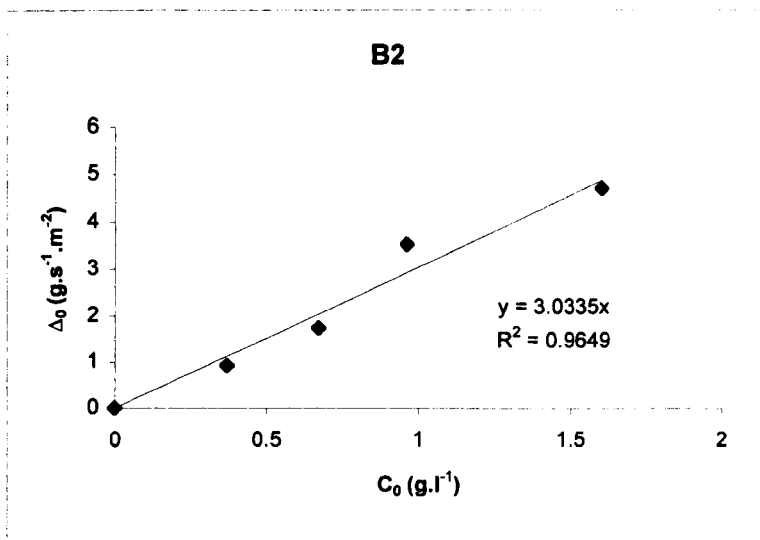
B1

$C_0$ (g.l <sup>-1</sup> )	$\Delta_0$ (g.s <sup>-1</sup> .m <sup>-2</sup> )
0	0
0.248958	0.476682
0.644375	1.483009
1.069792	2.780642
1.750417	4.033785



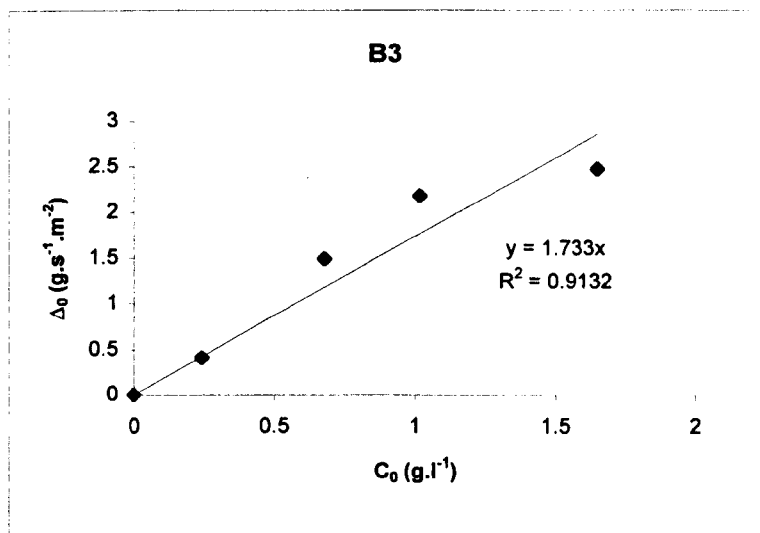
B2

$C_0$ (g.l <sup>-1</sup> )	$\Delta_0$ (g.s <sup>-1</sup> .m <sup>-2</sup> )
0	0
0.372083	0.922761
0.671042	1.737239
0.962708	3.509789
1.604583	4.686309



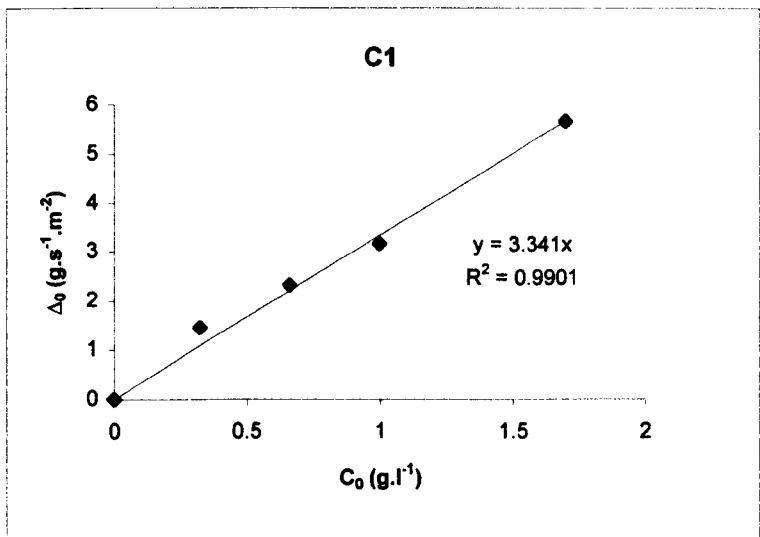
B3

$C_0$ (g.l <sup>-1</sup> )	$\Delta_0$ (g.s <sup>-1</sup> .m <sup>-2</sup> )
0	0
0.243542	0.407828
0.67875	1.483009
1.018125	2.17508
1.648333	2.478744



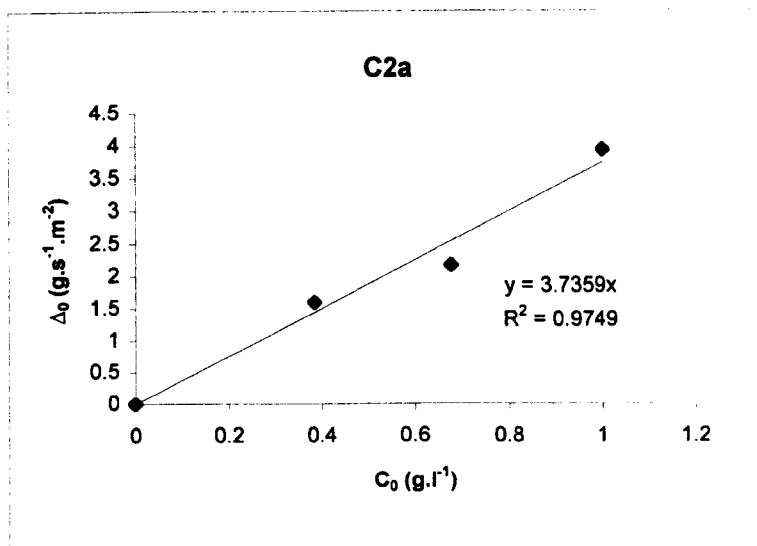
C1

$C_0$ (g.l <sup>-1</sup> )	$\Delta_0$ (g.s <sup>-1</sup> .m <sup>-2</sup> )
0	0
0.324792	1.450053
0.66125	2.323381
0.99875	3.163753
1.699375	5.665095



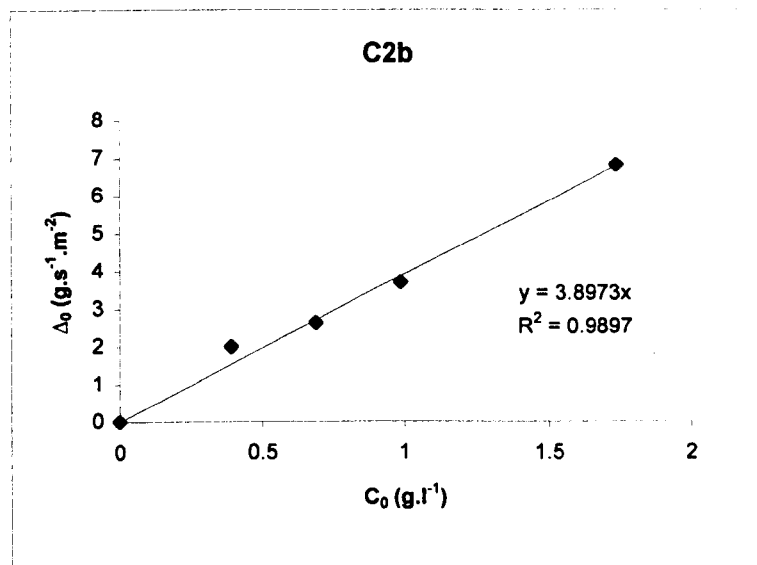
C2a

$C_0$ (g.l <sup>-1</sup> )	$\Delta_0$ (g.s <sup>-1</sup> .m <sup>-2</sup> )
0	0
0.384624	1.588938
0.677833	2.160956
1.000216	3.929974



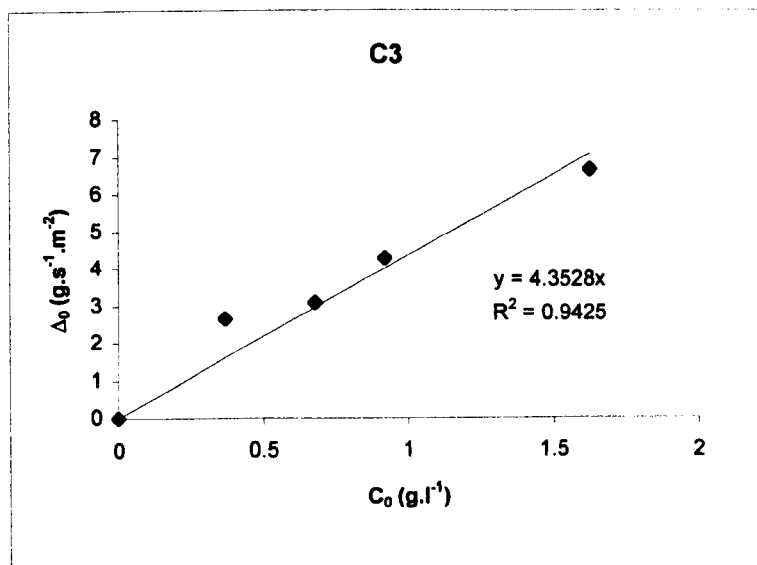
C2b

$C_0$ (g.l <sup>-1</sup> )	$\Delta_0$ (g.s <sup>-1</sup> .m <sup>-2</sup> )
0	0
0.390459	1.99147
0.689989	2.610096
0.987574	3.677863
1.736885	6.792182

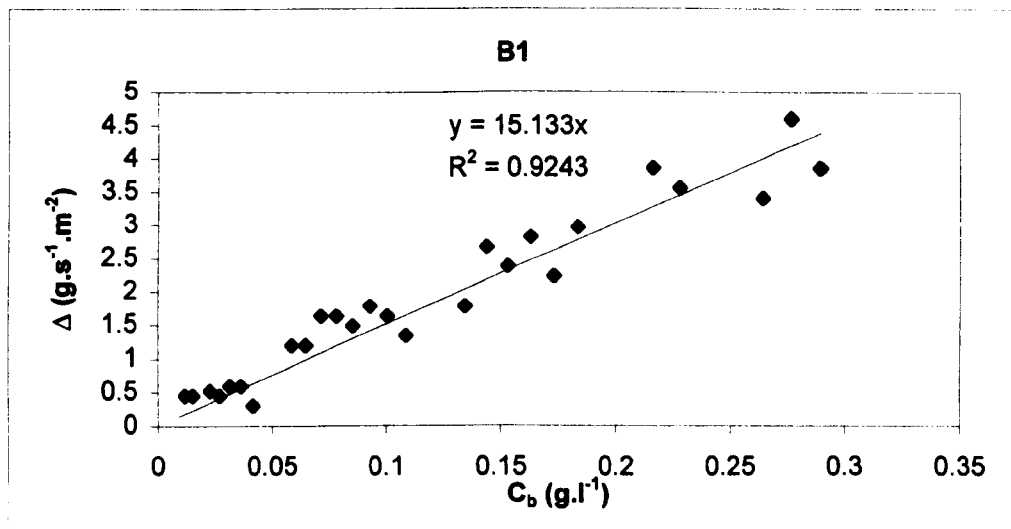
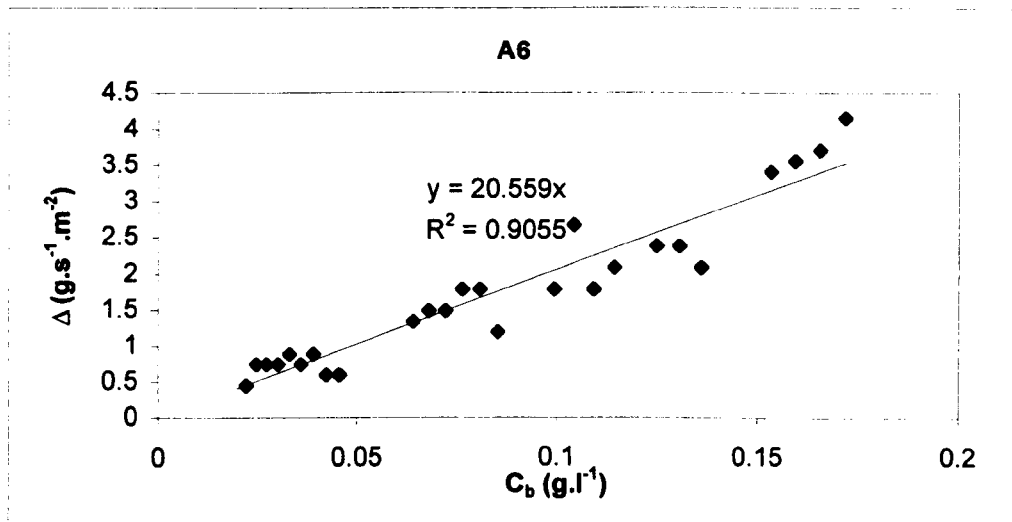
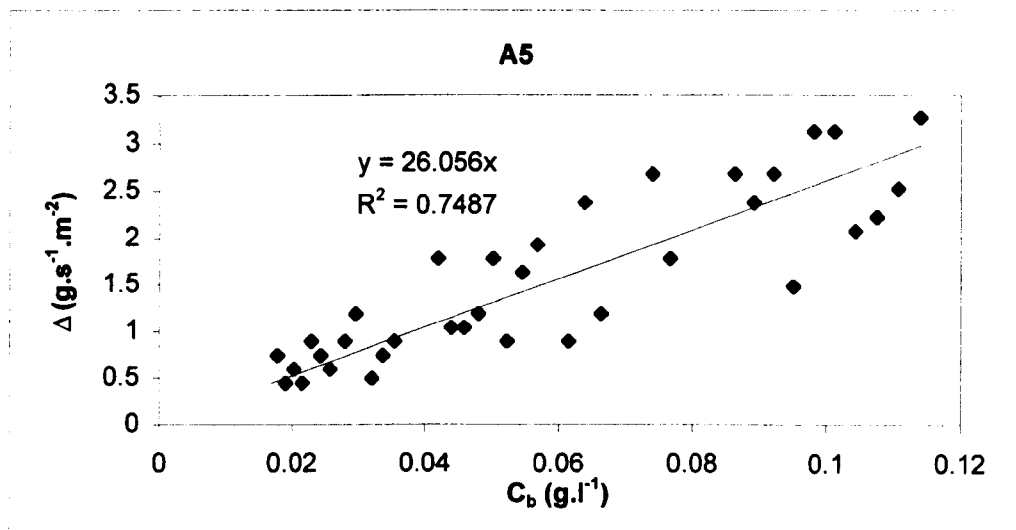


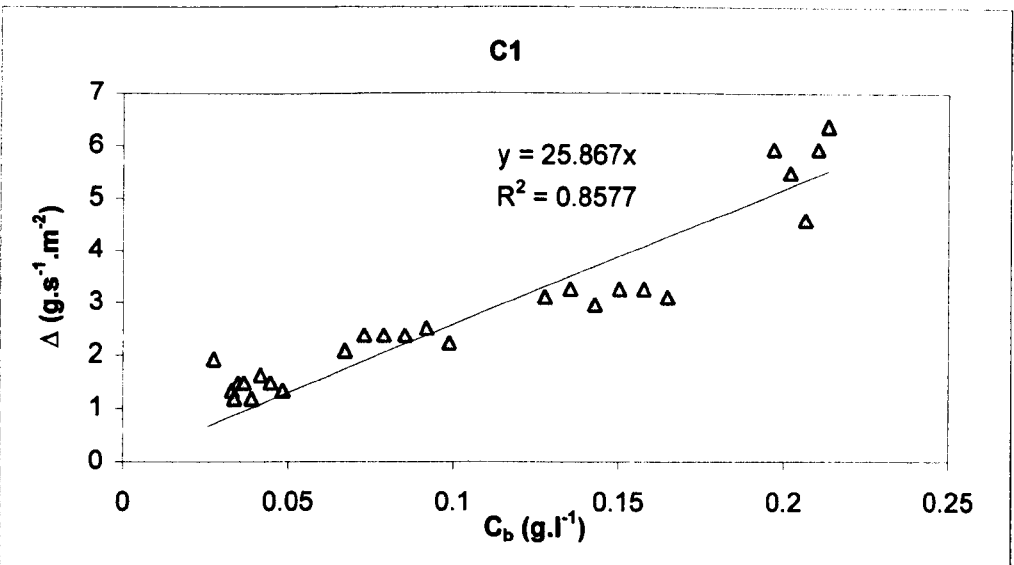
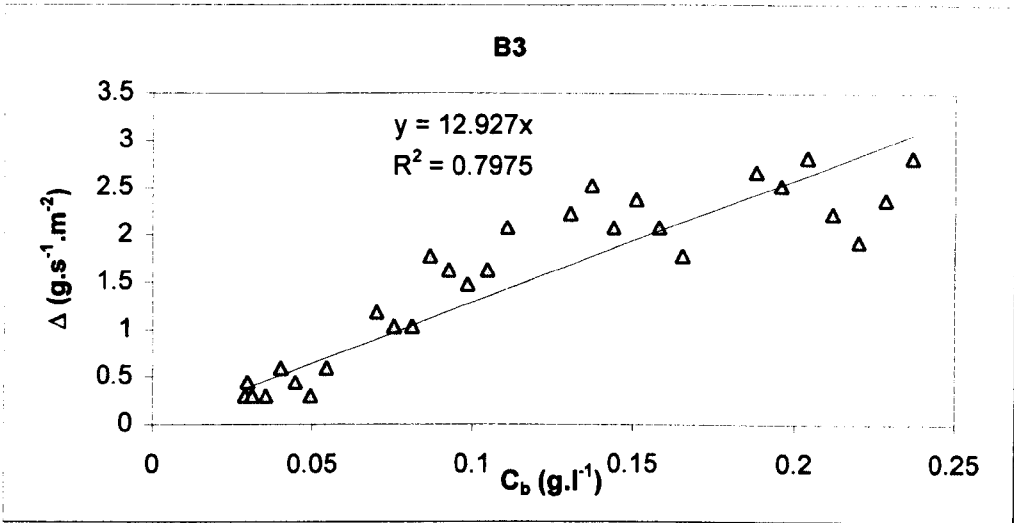
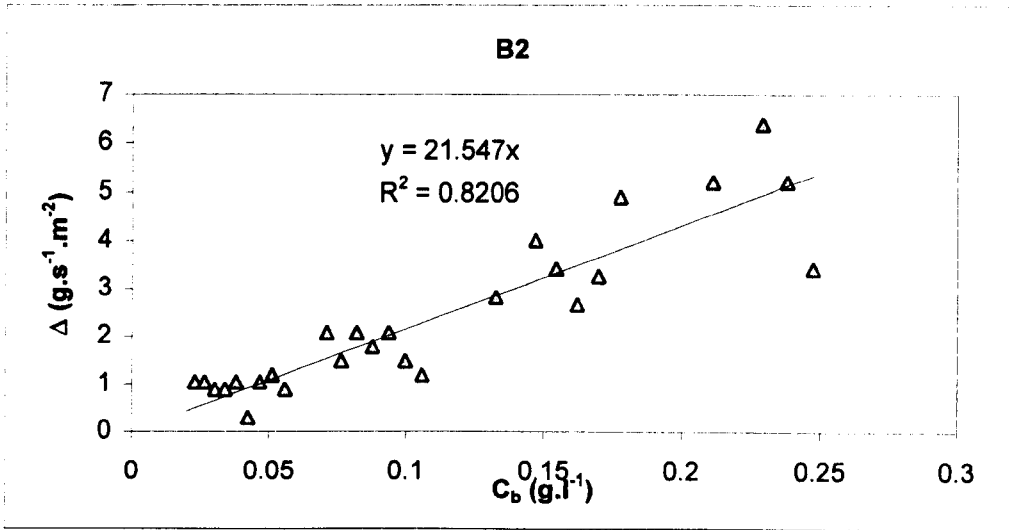
C3

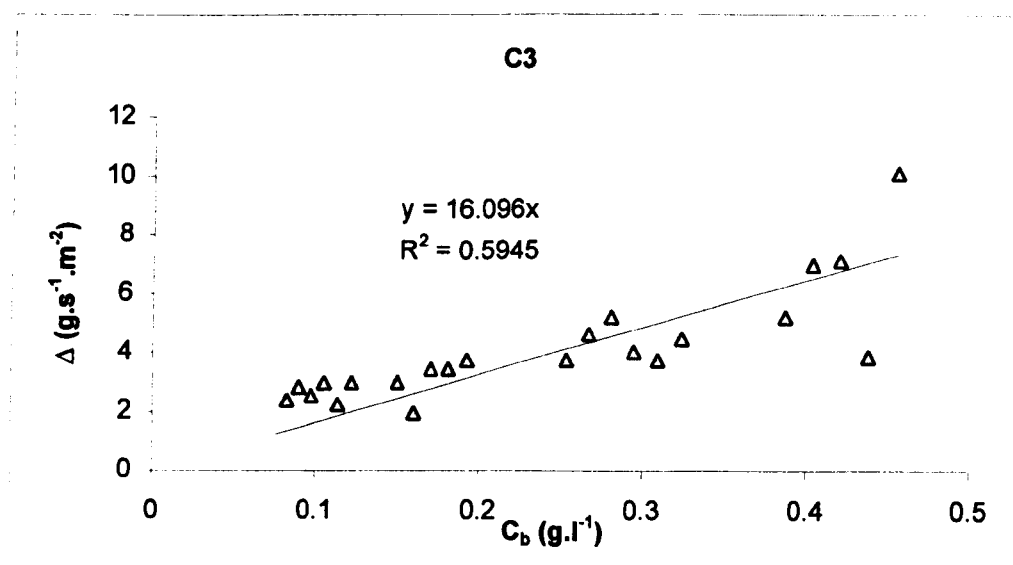
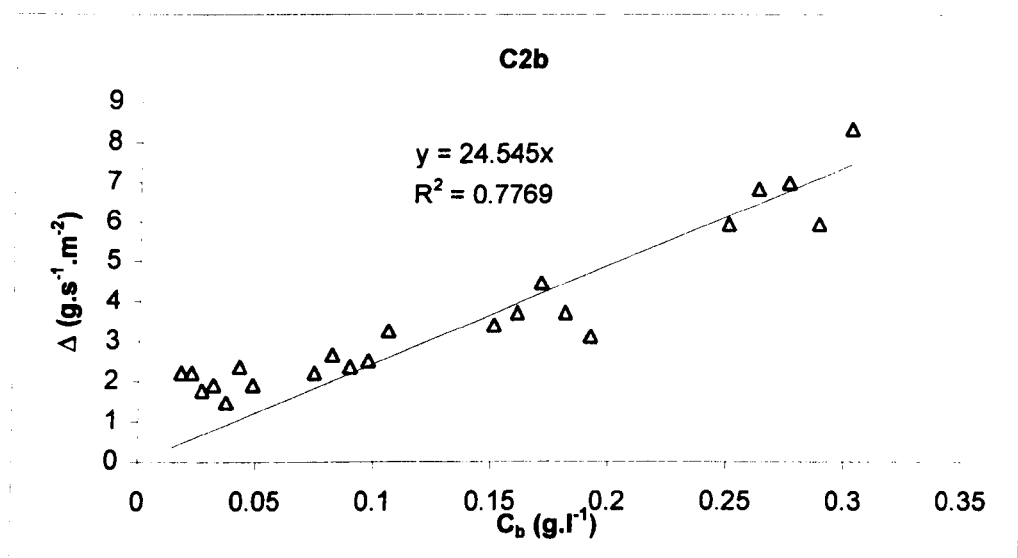
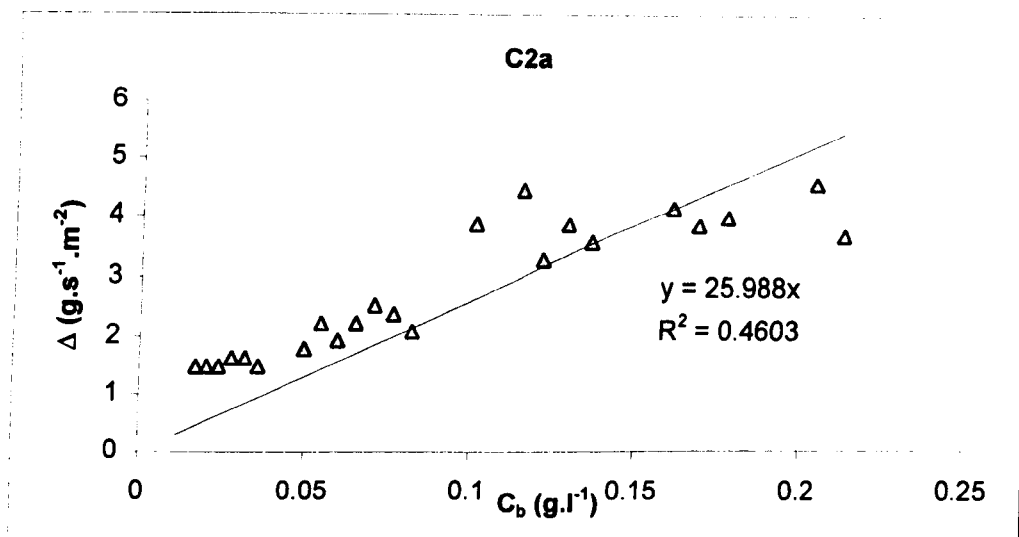
$C_0$ (g.l <sup>-1</sup> )	$\Delta_0$ (g.s <sup>-1</sup> .m <sup>-2</sup> )
0	0
0.369064	2.6447
0.679778	3.084659
0.922416	4.27601
1.626506	6.643881



Appendix 3.4: deposition rate  $\Delta$  against estimated near-bed concentration







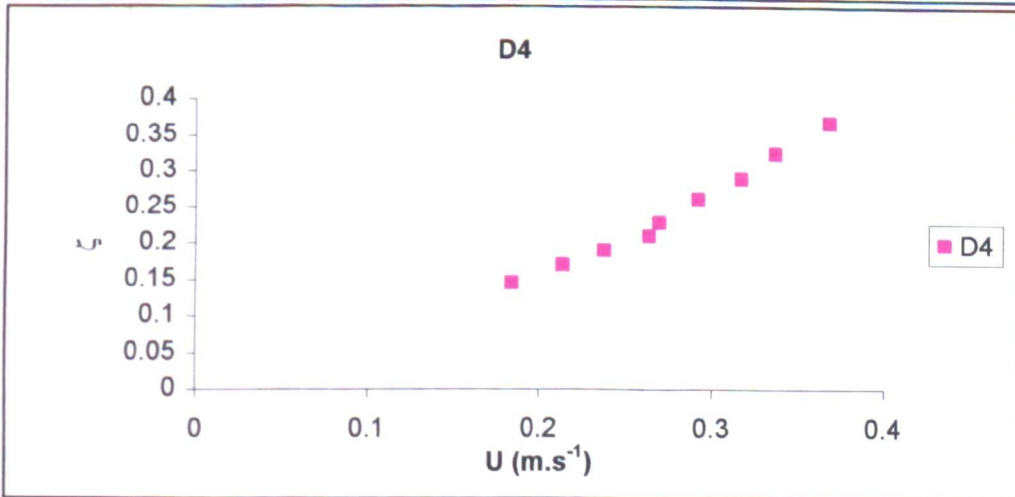
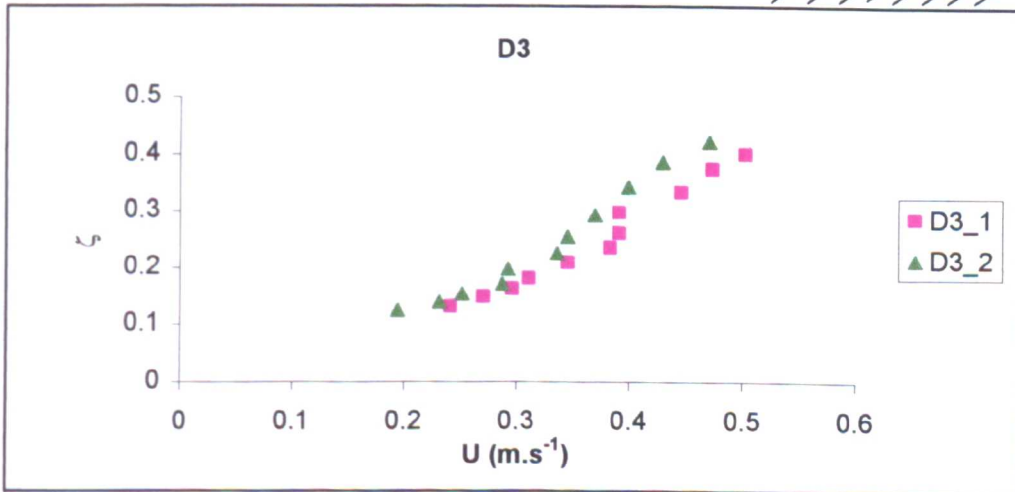
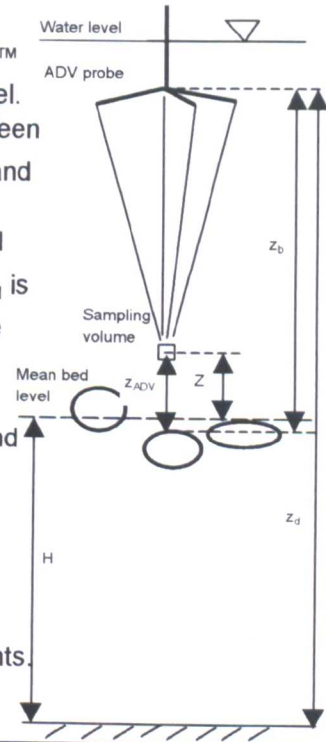
Appendix 4.1: velocity profiles

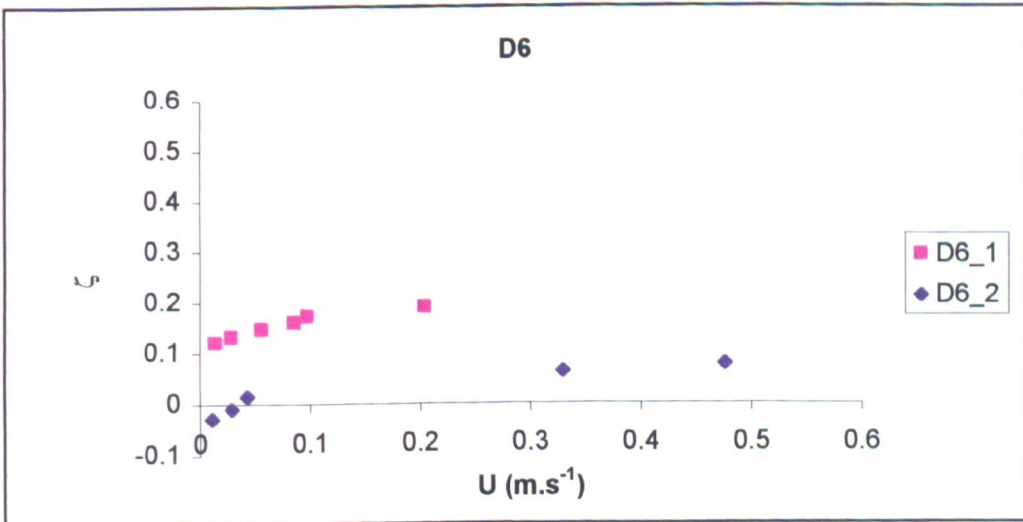
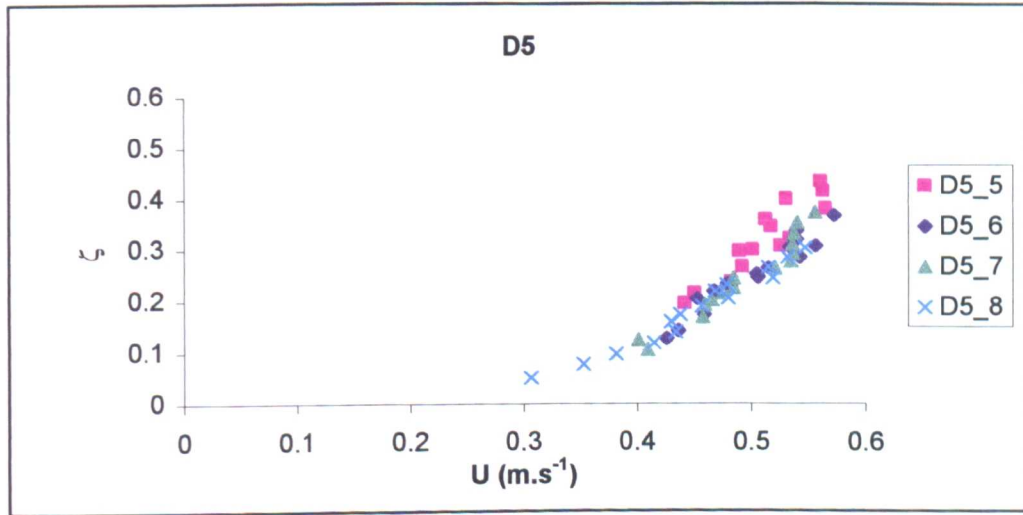
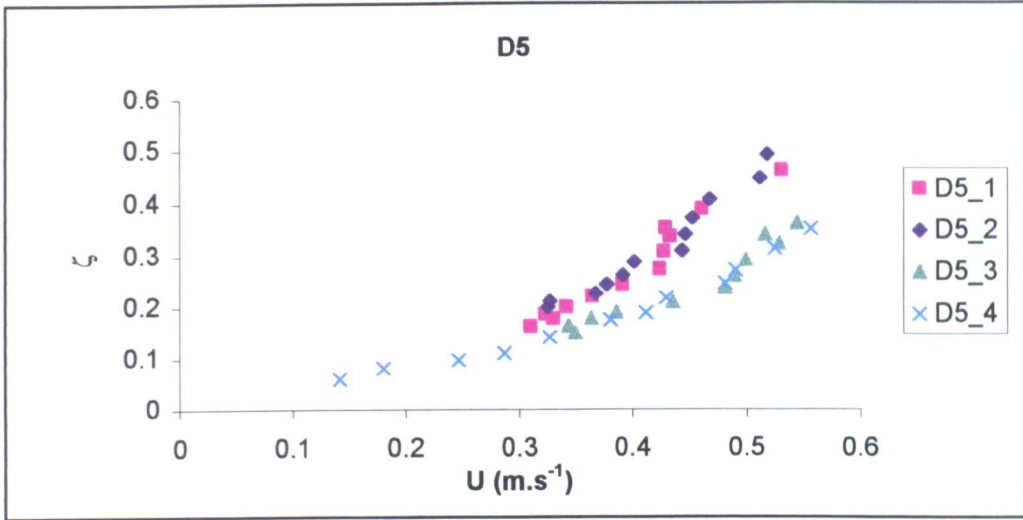
Velocity measurements were carried out using an ADV Sontek™ probe.  $Z$  is the elevation relatively to the mean bed surface level. The ADV software provides readings of the distance  $z_{ADV}$  between the bed surface level (which changes for each measurement) and the sampling volume (i.e. where velocities are measured). To compute  $Z$  from  $z_{ADV}$ , the distance between the mean bed level and the bed surface is required. It is equal to  $z_b - z_d + H$ , where  $z_d$  is the distance between the transmitting transducer and the flume bed level (measured with a gauge),  $z_b$  is the distance between the transmitting transducer and the bed (indicated by the ADV software) and  $\eta$  is the elevation between the mean bed level and the flume bed (125mm).

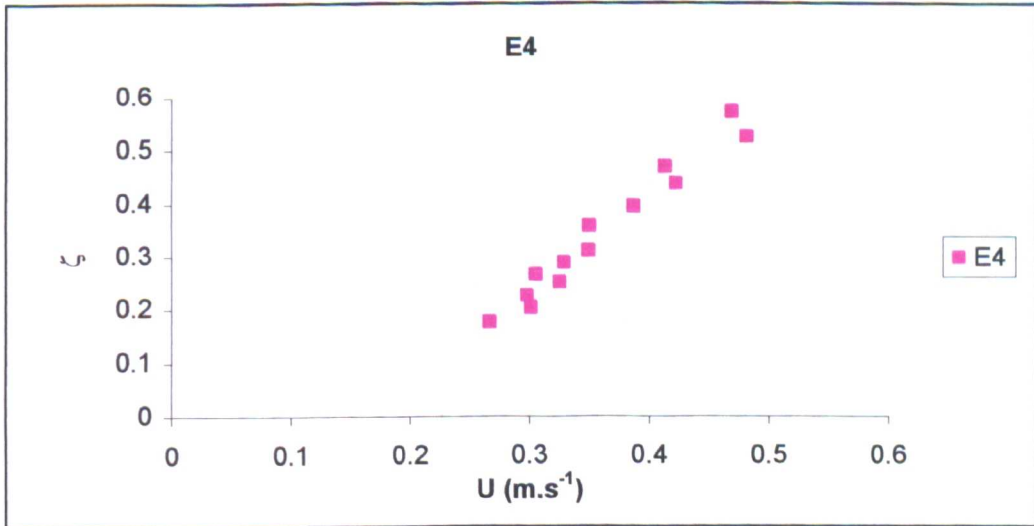
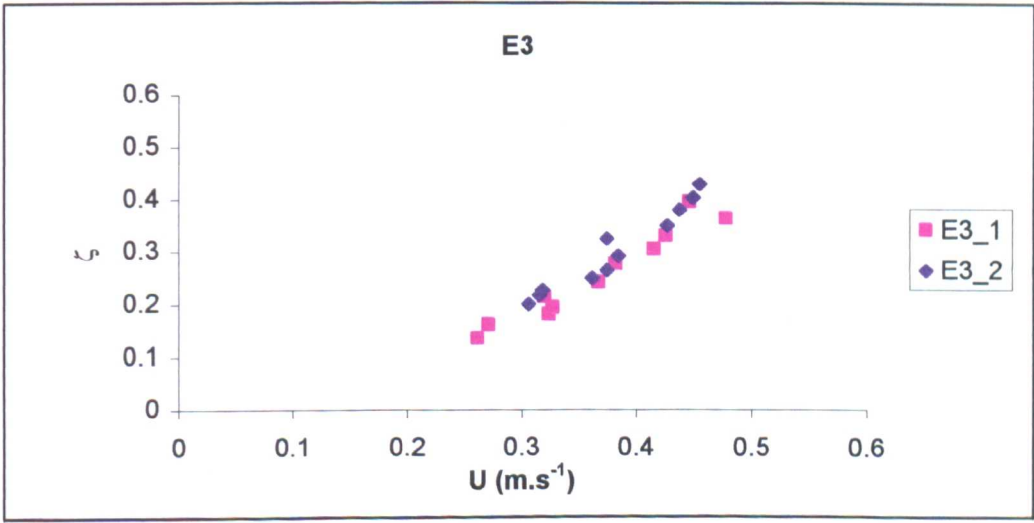
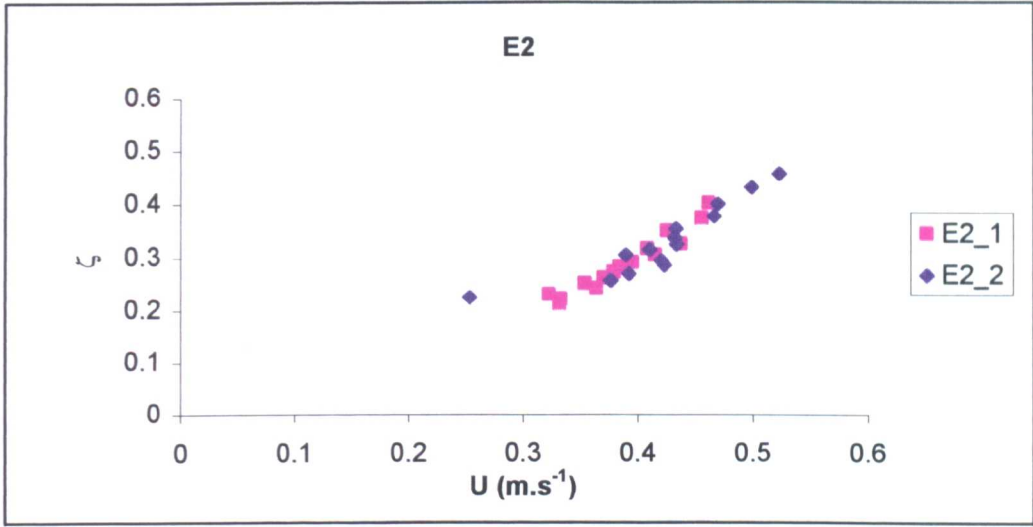
$Z$  is thus obtained as:  $Z = z_{ADV} + z_d - H - z_b$

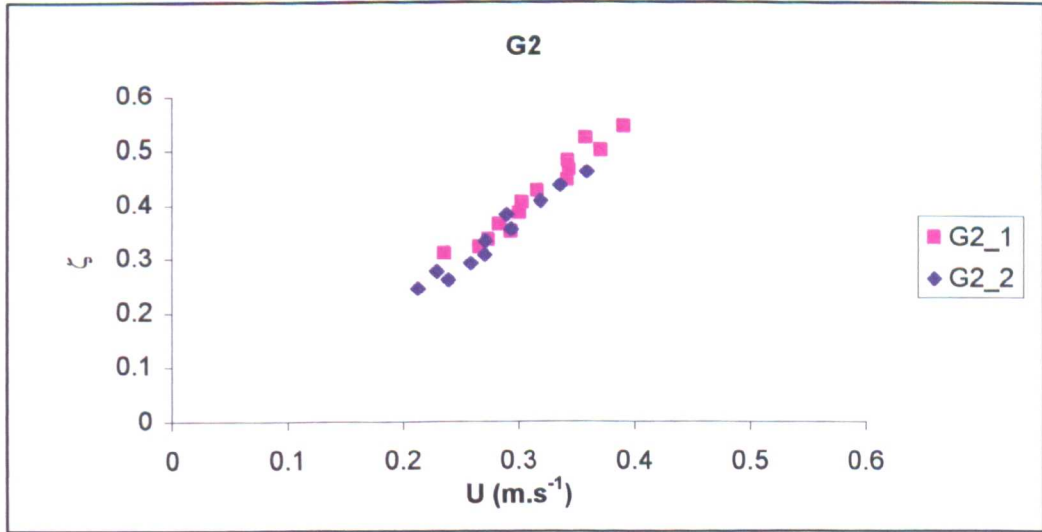
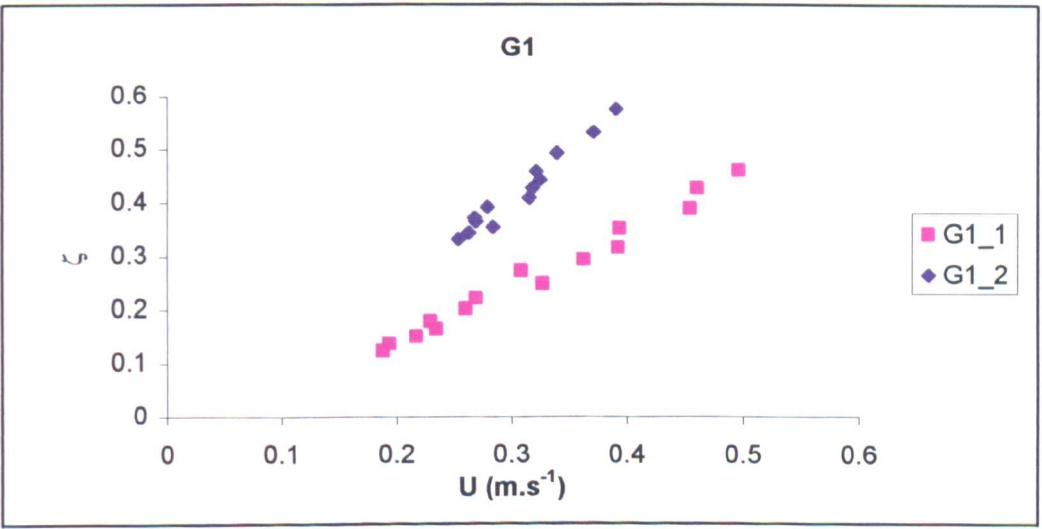
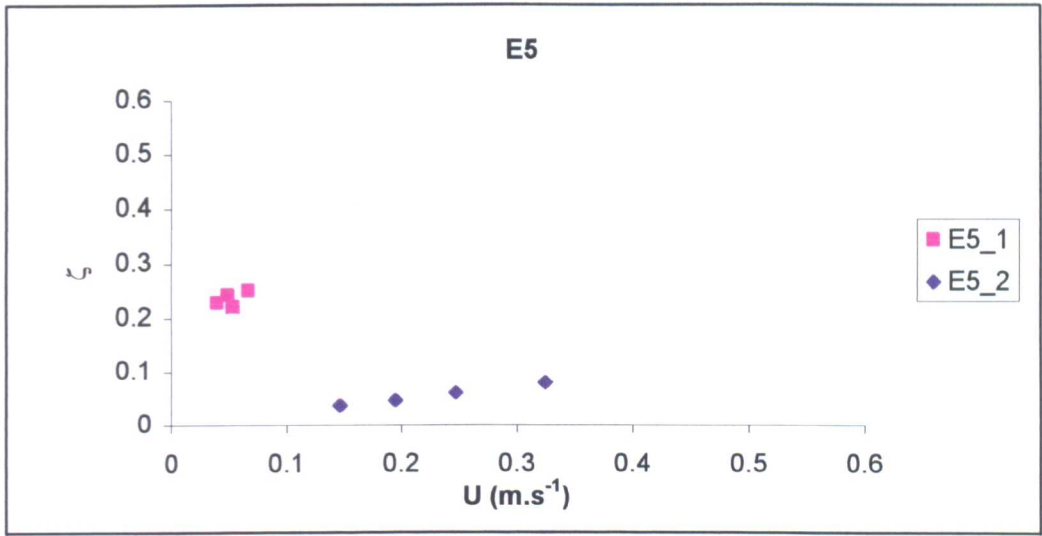
and  $z$  as:  $z = Z + \Delta z = z_{ADV} + z_d - H - z_b + \Delta z$

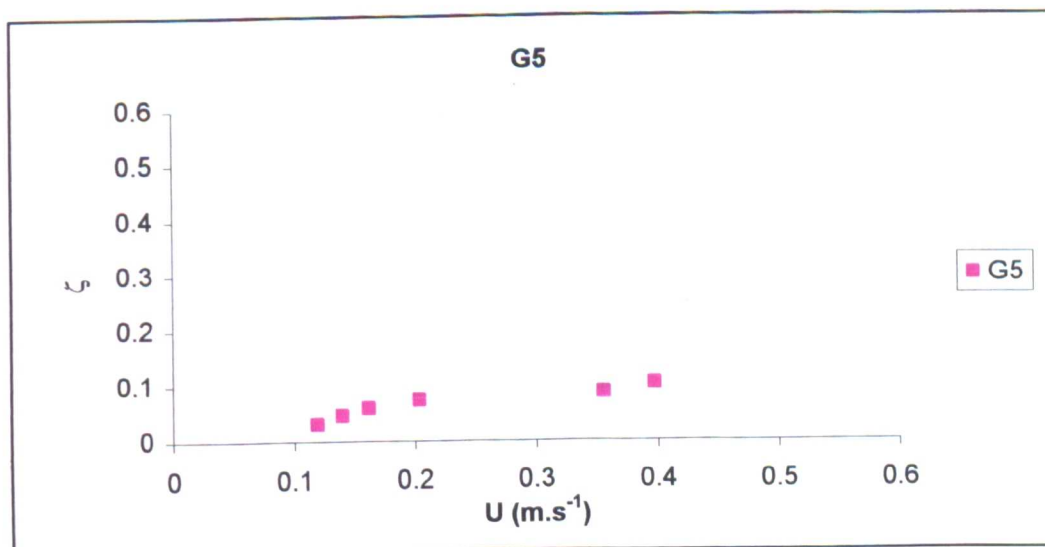
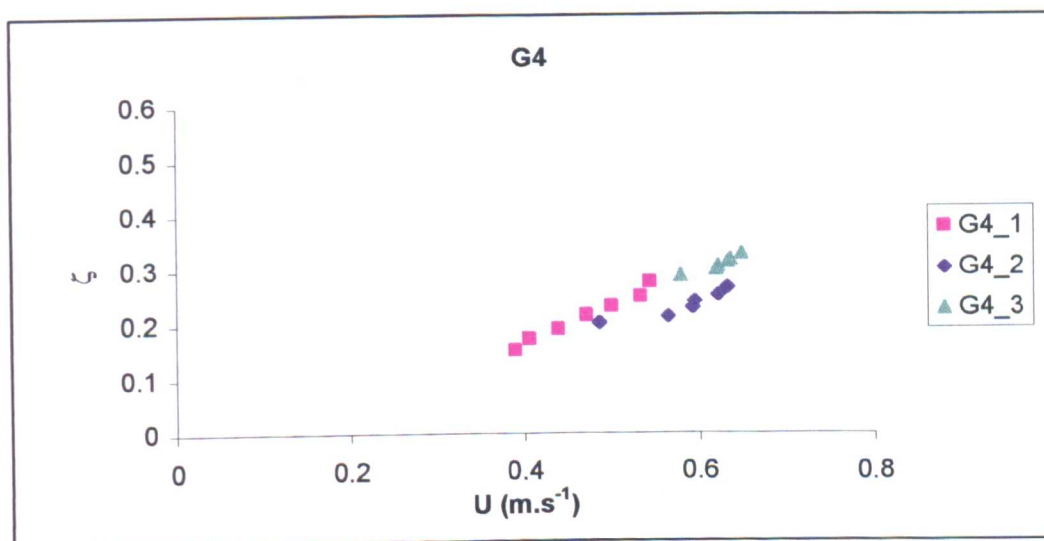
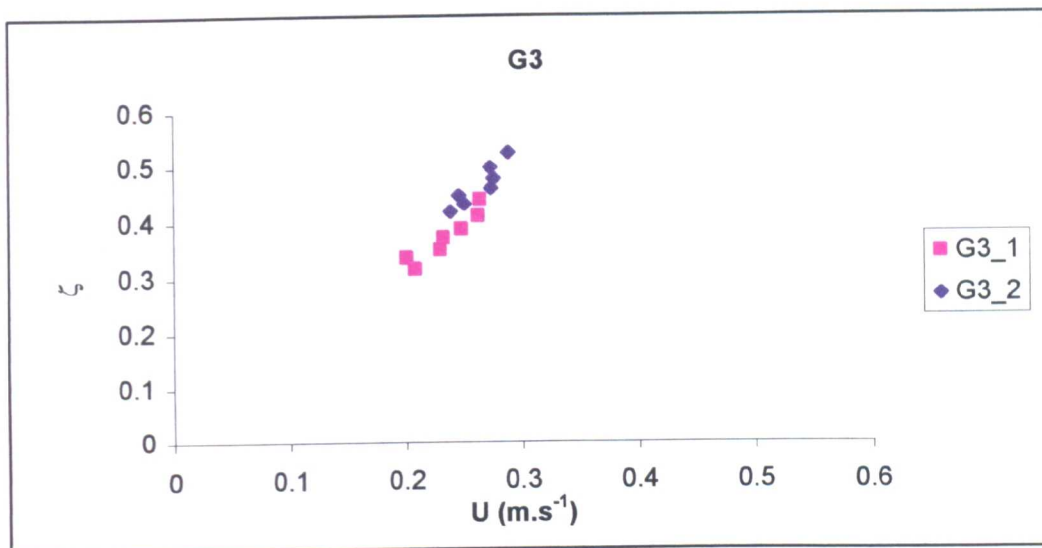
Velocity measurements are the results of 30s to 1mn-samples carried out at 25Hz, i.e. average over 600 to 1200 measurements.



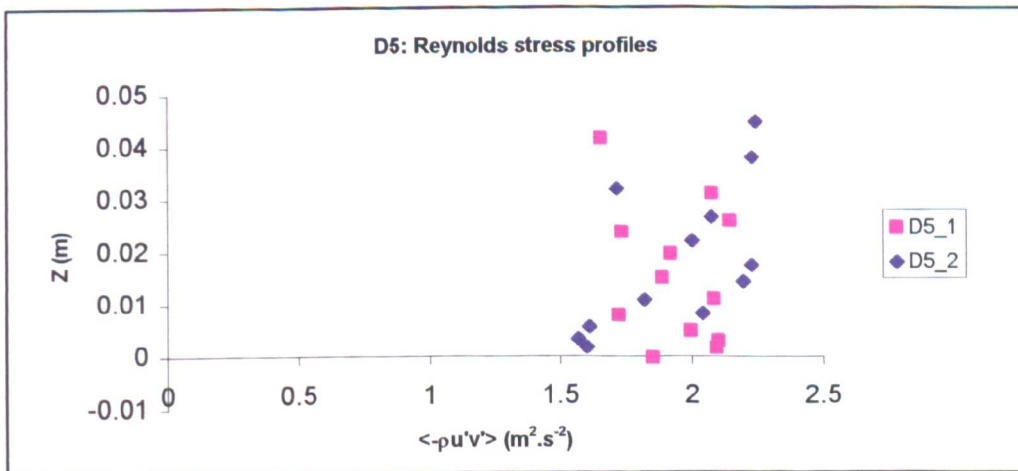
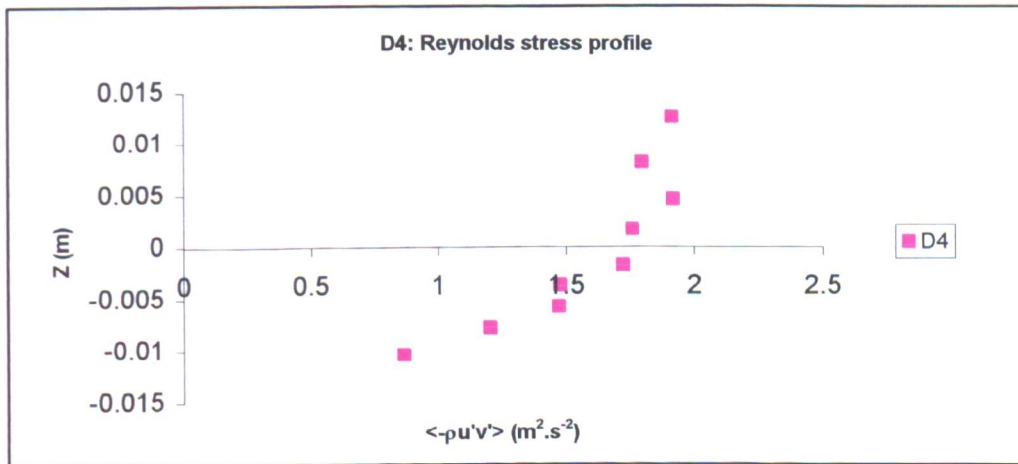
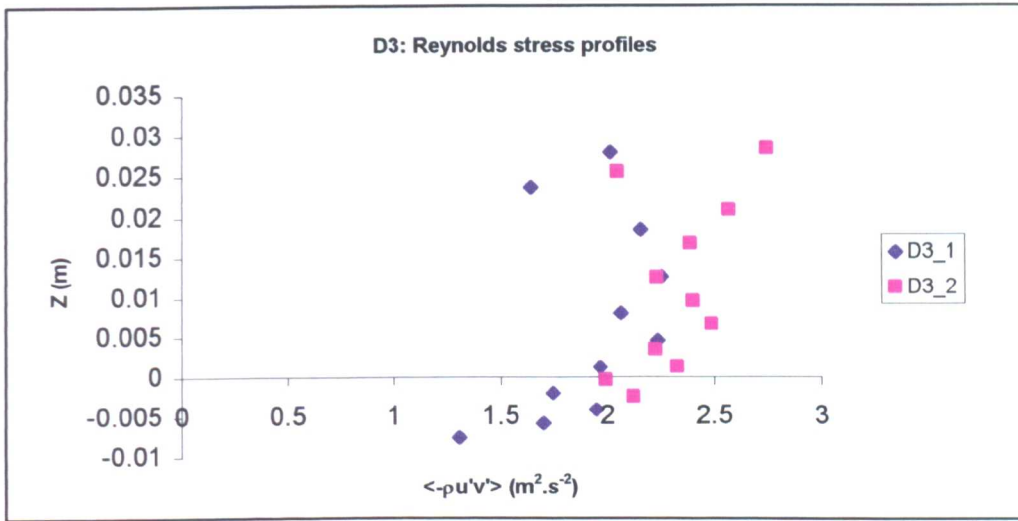


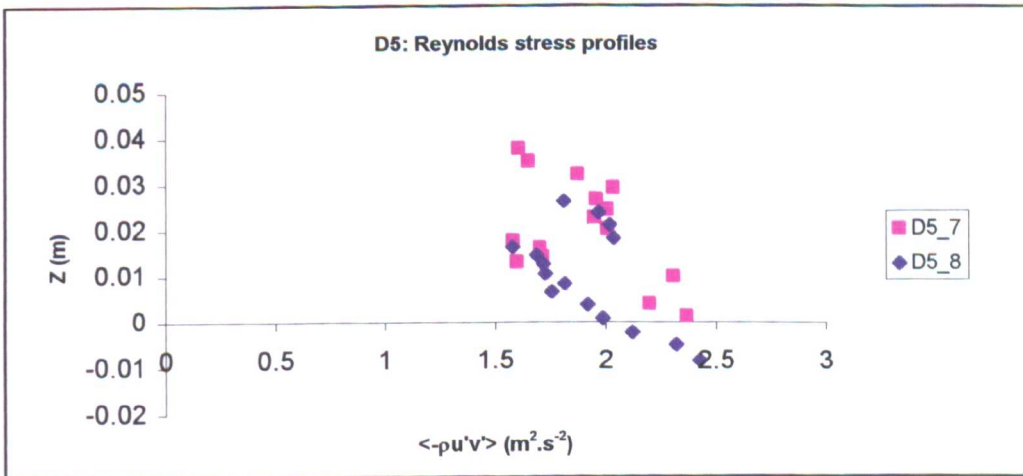
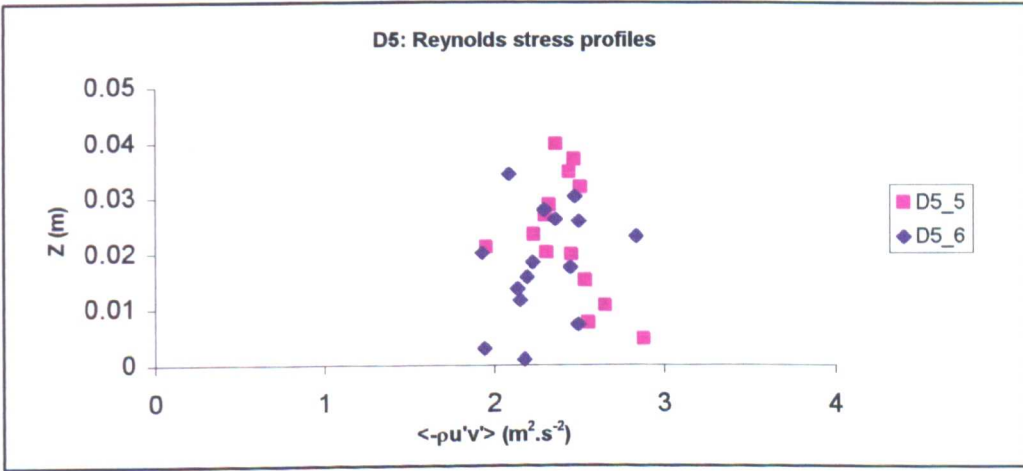
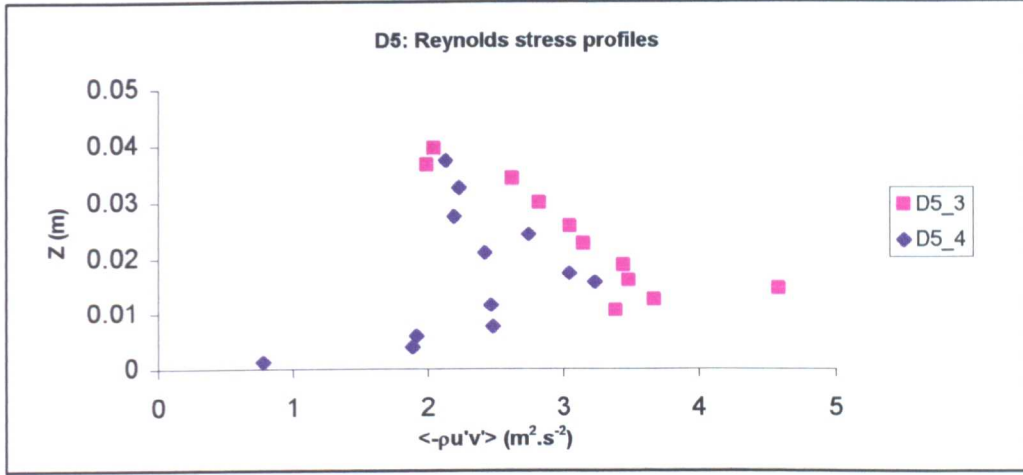


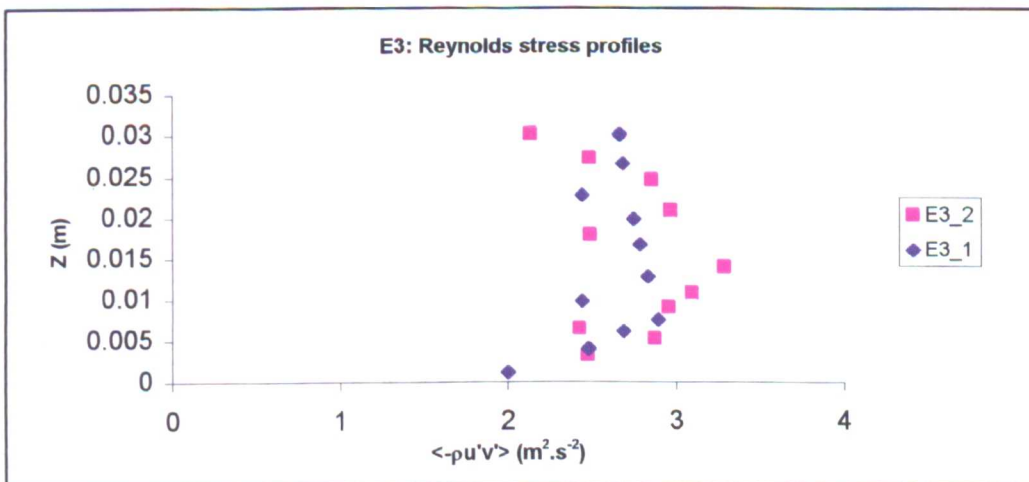
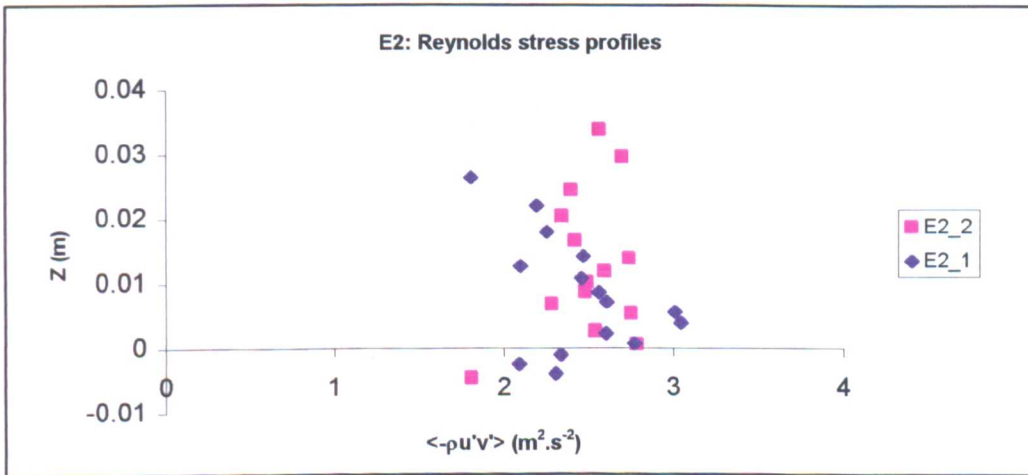
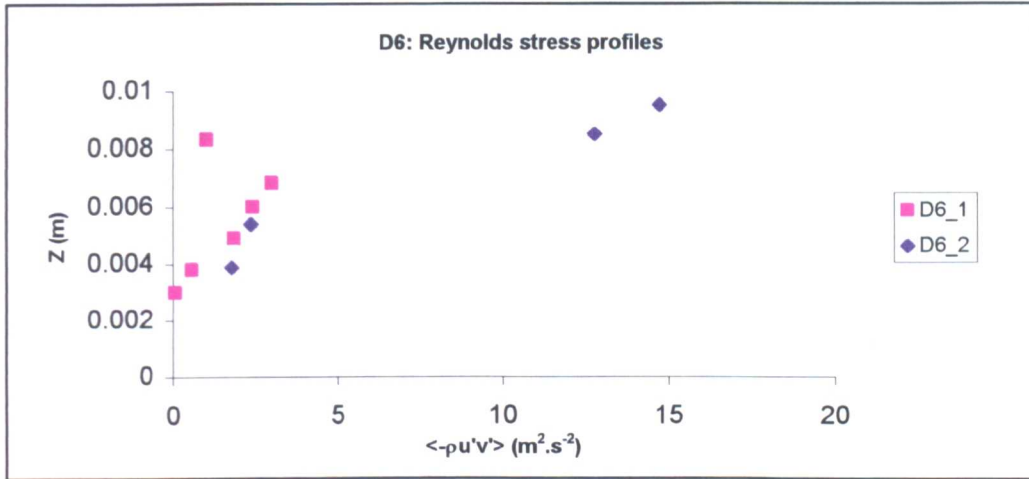


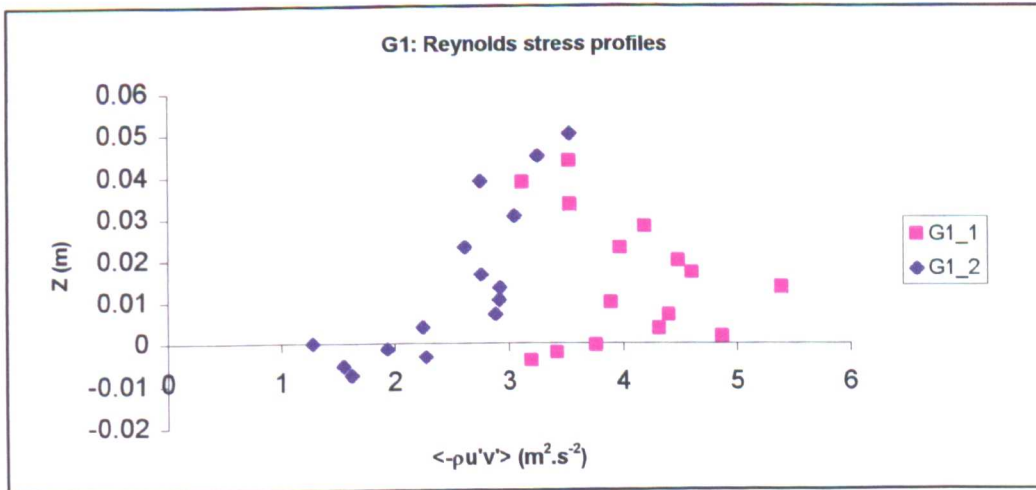
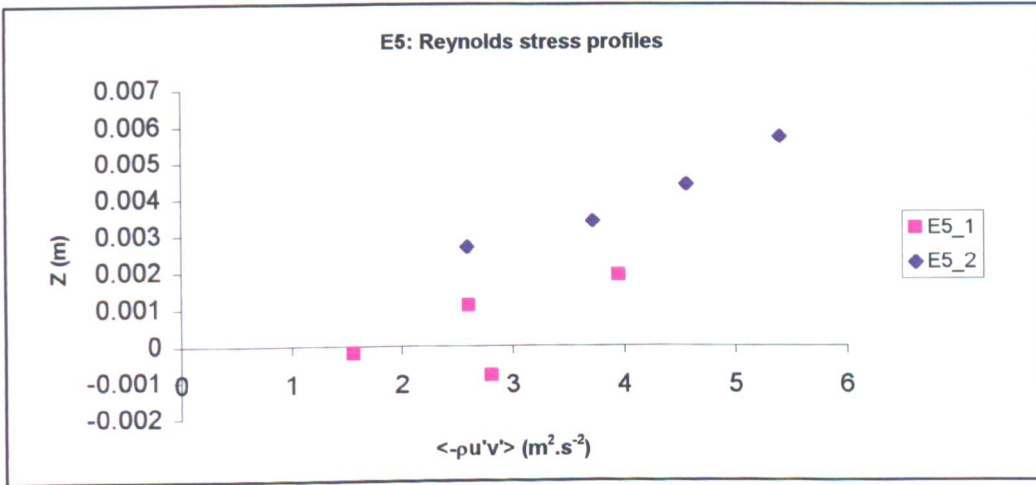
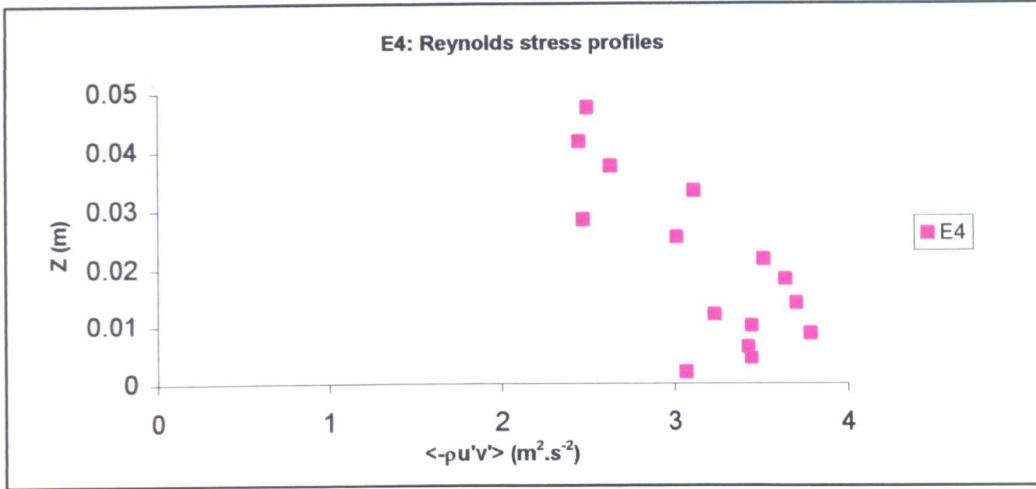


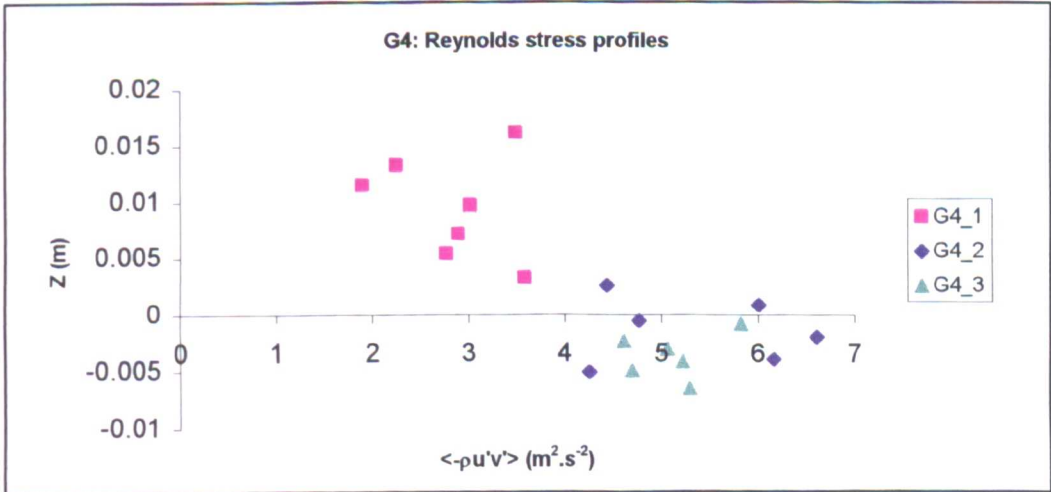
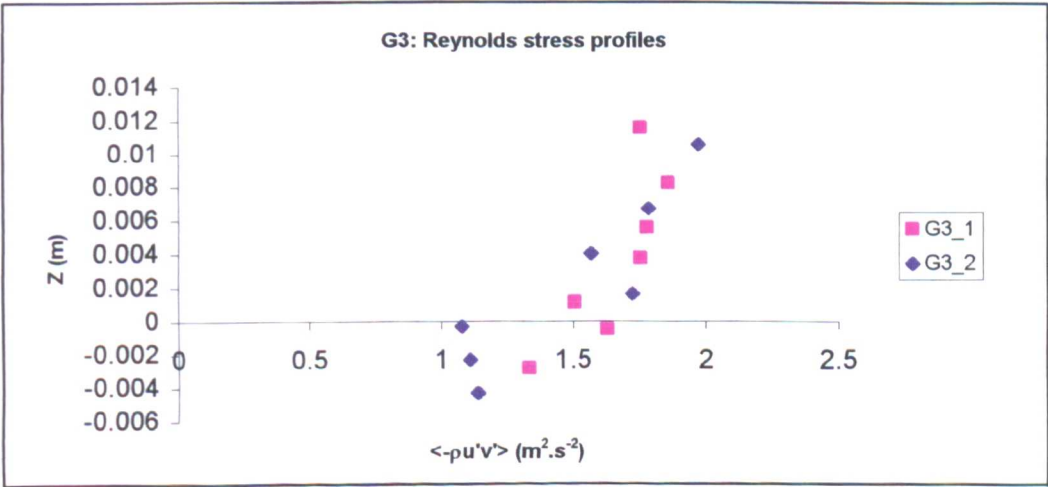
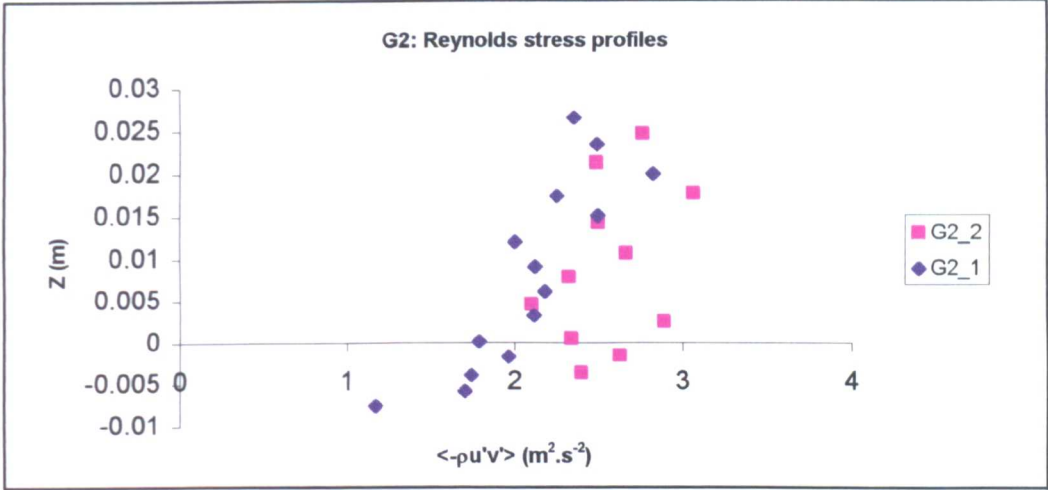
Appendix 4.2: Reynolds stress profiles

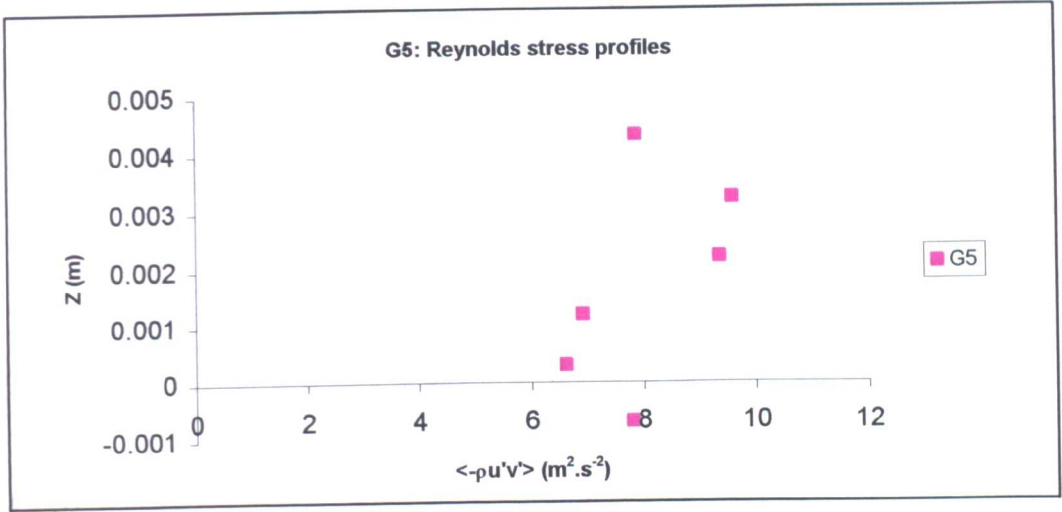












Appendix 4.3: measured deposition rates and near-bed sediment concentrations - main series of experiments

Deposition rates  $\Delta$  ( $\text{kg}\cdot\text{m}^{-1}\cdot\text{s}^{-2}$ )

LA-260	trap #	3.1	3.2	4.1	4.2	5	7	$l_0$	$d_{50}$
run	X (m)	0.9	1.1	1.3	1.5	1.74	2.62	( $\text{g}\cdot\text{s}^{-1}$ )	( $\mu\text{m}$ )
D3		0.0118	0.0087	0.0051	0.0051	0.0037	0.0014	43	260
D4		0.0122	0.0085	0.0051	0.0039	0.0027	0.0011	43	260
D5		0.0145	0.0153	0.0105	0.0080	0.0073	0.0035	43	260
D6		0.0203	0.0158	0.0135	0.0096	0.0087	0.0038	40	260
E2		0.0141	0.0128	0.0094	0.0072	0.0067	0.0023	43	260
E3b		0.0154	0.0096	0.0069	0.0063	0.0046	0.0016	44	260
E4		0.0139	0.0079	0.0055	0.0036	0.0021	0.0007	43	260
E5		0.0220	0.0160	0.0159	0.0118	0.0082	0.0045	47	260
G1		0.0132	0.0124	0.0105	0.0066	0.0059	0.0025	42	260
G2b		0.0123	0.0090	0.0080	0.0050	0.0039	0.0012	44	260
G3		0.0110	0.0065	0.0048	0.0032	0.0023	0.0006	43	260
G4		0.0178	0.0130	0.0126	0.0138	0.0092	0.0060	43	260
G5		0.0176	0.0151	0.0123	0.0133	0.0071	0.0032	42	260
E6		0.2483	0.1949	0.1303	0.1170	0.0717	0.0301	438	260
< $\Delta$ > (exclud. E6)		0.0151	0.0116	0.0092	0.0075	0.0056	0.0025		

B3-100	trap #	3.1	3.2	4.1	4.2	5	7	$l_0$	$d_{50}$
run	X (m)	0.9	1.1	1.3	1.5	1.74	2.62	( $\text{g}\cdot\text{s}^{-1}$ )	( $\mu\text{m}$ )
D7		0.0043	0.0049	0.0046	0.0055	0.0041	0.0047	35	100
E7		0.0043	0.0049	0.0046	0.0055	0.0041	0.0047	35	100
G6		0.0082	0.0070	0.0046	0.0068	0.0061	0.0056	36	100
G7		0.0052	0.0052	0.0045	0.0053	0.0042	0.0040	35	100
< $\Delta$ >		0.0055	0.0055	0.0046	0.0058	0.0046	0.0047		

Near-bed concentrations  $C_b$  ( $\text{kg}\cdot\text{m}^{-3}$ )

	trap #	3.1	3.2	4.1	4.2	5	7	$l_0$	$d_{50}$
run	X (m)	0.9	1.1	1.3	1.5	1.74	2.62	( $\text{g}\cdot\text{s}^{-1}$ )	( $\mu\text{m}$ )
D3		0.415	0.365	0.403	0.237	0.159	0.083	43	260
D4		0.472	0.314	0.243	0.180	0.133	0.074	43	260
D5		0.597	0.823	0.527	0.282	0.419	0.197	43	260
D6		0.771	0.586	0.786	0.556	0.299	0.230	40	260
E2		0.467	0.435	0.440	0.330	0.312	0.155	43	260
E3b		0.451	0.469	0.377	0.204	0.232	0.083	44	260
E4		0.591	0.273	0.190	0.158	0.123	0.043	43	260
E5		0.974	0.847	0.780	0.660	0.545	0.183	47	260
G1		0.536	0.403	0.342	0.402	0.227	0.152	42	260
G2b		0.658	0.320	0.313	0.219	0.153	0.058	44	260
G3		0.280	0.225	0.234	0.132	0.100	0.044	43	260
G4		0.663	0.884	0.936	0.540	0.541	0.261	43	260
G5		0.894	0.515	0.622	0.379	0.311	0.194	42	260
E6		8.588	7.154	5.151	4.828	2.973	1.634	438	260
< $C_b$ > (exclud. E6)		0.5976	0.4970	0.4764	0.3291	0.2734	0.1352		

B3-100	trap #	3.1	3.2	4.1	4.2	5	7	$l_0$	$d_{50}$
run	X (m)	0.9	1.1	1.3	1.5	1.74	2.62	( $\text{g}\cdot\text{s}^{-1}$ )	( $\mu\text{m}$ )
D7		1.686	1.752	1.895	1.704	1.712	1.631	35	100
E7		1.608	1.692	1.807	1.694	1.617	1.516	35	100
G6		2.473	2.427	2.483	2.470	2.434	2.161	36	100
G7		1.582	1.646	1.667	1.509	1.473	1.401	35	100
< $C_b$ >		1.8372	1.8794	1.9633	1.8441	1.8088	1.6776		

Appendix 4.4

Median grain sizes ( $d_{50}$ ) of deposited fine sediment samples classified by type of sand, run label and trap label.

Deposited fine sediment		(microns)					
LA-260							
run	X (m)	0.9	1.1	1.3	1.5	1.74	2.62
	trap #	3.1	3.2	4.1	4.2	5	7
D3		242.3	236.6	235.0	233.1	230.2	221.8
D4		238.5	234.5	227.7	223.7	221.0	208.2
D5		241.8	242.1	236.9	230.9	231.2	209.3
D6		250.9	247.3	243.4	243.2	240.5	231.0
E2		243.1	243.4	238.8	239.2	237.9	230.3
E3b		235.7	236.0	232.6	230.9	227.7	217.3
E4		236.2	230.1	225.4	222.7	220.2	200.0
E5		248.3	248.5	246.7	243.2	241.4	230.7
E6		261.0	260.3	249.8	248.8	245.8	238.1
G1		247.2	244.1	245.4	242.3	237.8	231.8
G2b		242.1	239.6	234.3	231.9	229.6	222.2
G3		234.4	228.3	226.1	220.3	220.9	200.1
G4		253.2	255.8	255.4	252.1	249.4	241.9
G5		252.1	244.8	245.9	241.5	238.9	232.0
average		244.77	242.24	238.82	235.98	233.74	222.48
B3-100							
run	X (m)	0.9	1.1	1.3	1.5	1.74	2.62
	trap #	3.1	3.2	4.1	4.2	5	7
D7		95.7	97.8	96.4	95.5	98.4	93.8
E7		97.6	99.2	98.6	94.8	94.2	92.1
G6		91.0	87.8	91.2	88.2	89.9	86.2
G7		99.7	98.6	94.4	95.6	94.1	90.9
average		96.00	95.86	95.14	93.53	94.14	90.78

Median grain sizes ( $d_{50}$ ) of near-bed fine sediment samples classified by type of sand, run label and trap label.

Near-bed transported fine sediment		(microns)					
LA-260							
run	X (m)	0.9	1.1	1.3	1.5	1.74	2.62
	trap #	3.1	3.2	4.1	4.2	5	7
D3		229.6	228.3	225.4	220.9	217.7	201.2
D4		227.7	216.3	209.0	206.1	196.7	177.5
D5		228.4	228.2	226.1	213.9	215.9	196.5
D6		241.8	237.1	237.5	236.5	231.4	224.4
E2		236.1	232.9	230.5	230.6	227.3	218.0
E3b		229.4	228.0	225.5	219.9	219.5	204.3
E4		230.0	220.4	211.3	212.7	202.5	172.9
E5		242.7	240.4	239.2	234.8	233.8	222.5
E6		251.1	244.9	243.4	241.0	237.1	228.7
G1		241.2	237.1	234.0	235.1	230.2	222.9
G2b		235.9	228.2	225.4	225.2	219.7	205.5
G3		222.9	221.8	221.0	206.8	202.5	181.8
G4		245.7	250.4	249.2	242.2	242.1	236.0
G5		245.6	239.5	241.8	234.6	232.9	226.7
average		236.30	232.39	229.95	225.74	222.09	208.50
B3-100							
run	X (m)	0.9	1.1	1.3	1.5	1.74	2.62
	trap #	3.1	3.2	4.1	4.2	5	7
D7		73.6	74.3	75.8	73.6	73.8	72.7
E7		73.3	75.8	77.9	76.2	74.7	72.7
G6		71.3	72.0	71.6	71.0	70.6	67.9
G7		72.1	74.7	76.0	72.5	72.0	71.8
average		72.57	74.19	75.30	73.33	72.80	71.27

Appendix 4.5

Ratio between deposited and transported median sample sizes ( $=d_{50dep}/d_{50tp}$ )  
 expressed in percentage of the transported median size

LA-260									
run	X (m)	0.9	1.1	1.3	1.5	1.74	2.62		
	trap #	3.1	3.2	4.1	4.2	5	7	average	$u^*$ (m.s <sup>-1</sup> )
D3		5.50	3.61	4.25	5.51	5.75	10.23	5.81	0.076
D4		4.76	8.39	8.96	8.55	12.35	17.32	10.05	0.072
D5		5.86	6.10	4.81	7.95	7.06	6.48	6.38	0.084
D6		3.75	4.32	2.52	2.85	3.92	2.92	3.38	0.097
E2		2.97	4.50	3.59	3.74	4.66	5.61	4.18	0.086
E3b		2.73	3.51	3.14	4.99	3.73	6.38	4.08	0.076
E4		2.67	4.42	6.65	4.72	8.71	15.67	7.14	0.068
E5		2.32	3.38	3.16	3.56	3.27	3.68	3.23	0.102
E6		3.94	6.28	2.61	3.21	3.66	4.12	3.97	0.102
G1		2.50	2.93	4.86	3.07	3.28	3.99	3.44	0.086
G2b		2.63	5.02	3.96	2.98	4.51	8.11	4.53	0.08
G3		5.14	2.91	2.30	6.52	9.11	10.07	6.01	0.078
G4		3.04	2.17	2.48	4.07	3.01	2.52	2.88	0.121
G5		2.65	2.20	1.72	2.94	2.59	2.34	2.41	0.096
average		3.61	4.27	3.93	4.62	5.40	7.10	4.82	
B3-100									
run	X (m)	0.9	1.1	1.3	1.5	1.74	2.62		
	trap #	3.1	3.2	4.1	4.2	5	7	average	$u^*$ (m.s <sup>-1</sup> )
D7		30.00	31.56	27.31	29.68	33.23	29.08	30.15	0.1
E7		33.04	30.93	26.66	24.35	26.10	26.69	27.96	0.1
G6		27.71	22.06	27.30	24.36	27.23	26.93	25.93	0.121
G7		38.37	31.96	24.21	31.87	30.73	26.74	30.65	0.1
average		32.28	29.13	26.37	27.57	29.32	27.36	28.67	

Appendix 4.6

Average deposition velocities  $w_d$  ( $m.s^{-1}$ )

LA-260										
$d_m$ ( $\mu m$ )	run	D3	D4	D5	D6	E2	E3b	E4	averag	$w_s$ ( $20^\circ$ )
550		0.024	0.040	0.039	0.048	0.058	0.032	0.043	0.0405	0.068
462.5		0.047	0.049	0.061	0.046	0.048	0.057	0.039	0.0494	0.0571
390		0.054	0.046	0.043	0.039	0.051	0.049	0.043	0.0463	0.0475
327.5		0.049	0.048	0.039	0.035	0.041	0.045	0.045	0.0432	0.0387
275		0.034	0.040	0.029	0.027	0.030	0.034	0.036	0.0329	0.031
231		0.025	0.028	0.024	0.021	0.023	0.025	0.027	0.0247	0.0244
181		0.017	0.017	0.017	0.016	0.017	0.019	0.020	0.0174	0.017
106.5		0.005	0.006	0.008	0.009	0.010	0.010	0.010	0.0083	0.007
average		0.0319	0.0341	0.0323	0.0301	0.0347	0.0338	0.0329	0.0328	
$u^*$ ( $m.s^{-1}$ )		0.08	0.077	0.088	0.097	0.091	0.08	0.073		

LA-260										
$d_m$ ( $\mu m$ )	run	E5	E6	G1	G2b	G3	G4	G5	averag	$w_s$ ( $20^\circ$ )
550		0.032	0.057	0.050	0.032	0.049	0.032	0.034	0.0435	0.0680
462.5		0.038	0.050	0.044	0.046	0.052	0.036	0.041	0.0503	0.0571
390		0.034	0.045	0.054	0.043	0.047	0.032	0.036	0.0465	0.0475
327.5		0.031	0.037	0.040	0.042	0.051	0.027	0.032	0.0427	0.0387
275		0.024	0.028	0.029	0.032	0.038	0.022	0.027	0.0327	0.0310
231		0.019	0.023	0.023	0.026	0.028	0.019	0.023	0.0247	0.0244
181		0.015	0.017	0.019	0.018	0.021	0.019	0.020	0.0173	0.0170
106.5		0.007	0.009	0.010	0.008	0.011	0.007	0.009	0.0082	0.0070
average		0.0249	0.0334	0.0337	0.0307	0.0371	0.0242	0.0278	0.0332	
$u^*$ ( $m.s^{-1}$ )		0.102	0.102	0.092	0.086	0.083	0.121	0.097		

B3-100							
$d_m$ (mm)	run	D7	E7	G6	G7	averag	$w_s$ ( $20^\circ C$ )
275		0.025	0.018		0.019	0.0204	0.0310
231		0.020	0.016	0.017	0.018	0.0178	0.0244
196		0.014	0.012	0.012	0.015	0.0132	0.0192
165		0.009	0.009	0.009	0.011	0.0093	0.0147
137.5		0.006	0.007	0.006	0.008	0.0068	0.0109
115.5		0.005	0.005	0.005	0.006	0.0053	0.0081
98		0.004	0.004	0.004	0.004	0.0038	0.0060
82.5		0.003	0.003	0.003	0.003	0.0029	0.0044
69		0.002	0.002	0.002	0.002	0.0023	0.0031
58		0.001	0.001		0.002	0.0016	0.0022
49		0.001	0.001		0.001	0.0013	0.0016
41.5		0.001	0.001		0.001	0.0008	0.0012
average		0.0076	0.0065		0.0075	0.0071	
$u^*$ ( $m.s^{-1}$ )		0.097	0.102	0.121	0.097		

Average dimensionless deposition velocities  $w_d^*$  ( $=w_d/w_s$ ). Reference settling velocities ( $w_s$ ) are computed from Cheng (1997)

LA-260										
$d_m$ ( $\mu\text{m}$ )	run	D3	D4	D5	D6	E2	E3b	E4	$d_m$ ( $\mu\text{m}$ )	average
550		0.36	0.59	0.58	0.71	0.86	0.48	0.64	550	0.068
462.5		0.83	0.86	1.09	0.82	0.86	1.00	0.68	462.5	0.0571
390		1.17	0.97	0.94	0.83	1.10	1.03	0.91	390	0.0475
327.5		1.30	1.26	1.04	0.92	1.08	1.17	1.18	327.5	0.0387
275		1.14	1.31	0.96	0.87	1.01	1.10	1.18	275	0.031
231		1.05	1.14	1.01	0.89	0.97	1.04	1.13	231	0.0244
181		1.01	0.99	1.05	0.97	1.03	1.11	1.19	181	0.017
106.5		0.82	0.91	1.15	1.36	1.52	1.47	1.38	106.5	0.007
average		0.960	1.004	0.979	0.920	1.054	1.050	1.036	averag	0.036
$u^*$ ( $\text{m}\cdot\text{s}^{-1}$ )		0.08	0.077	0.088	0.097	0.091	0.08	0.073		

LA-260										
$d_m$ ( $\mu\text{m}$ )	run	E5	E6	G1	G2b	G3	G4	G5	$d_m$ ( $\mu\text{m}$ )	average
550		0.47	0.85	0.75	0.47	0.73	0.48	0.50	550	0.068
462.5		0.66	0.89	0.80	0.81	0.92	0.64	0.72	462.5	0.0571
390		0.71	0.95	1.19	0.91	1.02	0.68	0.77	390	0.0475
327.5		0.81	0.97	1.08	1.08	1.34	0.72	0.82	327.5	0.0387
275		0.78	0.92	1.00	1.05	1.25	0.73	0.88	275	0.031
231		0.80	0.95	1.01	1.06	1.19	0.80	0.95	231	0.0244
181		0.88	1.04	1.18	1.04	1.27	1.14	1.16	181	0.017
106.5		1.03	1.37	1.48	1.19	1.67	1.03	1.28	106.5	0.007
average		0.768	0.991	1.062	0.951	1.174	0.777	0.887	averag	0.036
$u^*$ ( $\text{m}\cdot\text{s}^{-1}$ )		0.102	0.102	0.092	0.086	0.083	0.121	0.097		

B3-100						
$d_m$ ( $\mu\text{m}$ )	run	D7	E7	G6	G7	average
275		0.81	0.58		0.60	0.661
231		0.84	0.65	0.71	0.73	0.733
196		0.73	0.62	0.64	0.77	0.691
165		0.64	0.60	0.58	0.73	0.637
137.5		0.59	0.61	0.58	0.74	0.632
115.5		0.64	0.64	0.62	0.71	0.654
98		0.62	0.61	0.62	0.71	0.640
82.5		0.63	0.66	0.66	0.69	0.659
69		0.67	0.72	0.75	0.77	0.725
58		0.66	0.67		0.79	0.706
49		0.76	0.88		0.82	0.821
41.5		0.62	0.75		0.72	0.698
average		0.684	0.665		0.731	0.688
$u^*$ ( $\text{m}\cdot\text{s}^{-1}$ )		0.097	0.102	0.121	0.097	

Appendix 4.7: main series experimental data and details on the calculation of the deposition velocities

D3	Location	Deposited $\Delta_i$		Sample	Volume of $C_{bi}$		time (mn)	39
	x (m)	(kg)	(kg.m.s <sup>-2</sup> )	mass (g)	water (l)	(g.l <sup>-1</sup> )		
trap#3.1	0.9	1.44	0.0118	31.76	76.5	0.415	$t^{\circ}$ (°C)	18
trap#3.2	1.1	1.066	0.0087	27.6	75.6	0.365	$v$ (m <sup>2</sup> .s <sup>-1</sup> )	1.05E-06
trap#4.1	1.3	0.626	0.0051	30.46	75.6	0.403	$\rho_w$ (kg.m <sup>-3</sup> )	1000
trap#4.2	1.5	0.618	0.0051	18.14	76.6	0.237	$\rho_s$ (kg.m <sup>-3</sup> )	2700
trap#5	1.74	0.674	0.0037	12.05	76.0	0.159	$g$ (m.s <sup>-2</sup> )	9.8
trap#7	2.62	0.225	0.0014	6.3	75.6	0.083	$\rho_s^*$	1.7

Size ( $\mu$ m)	$w_a$ (m.s <sup>-1</sup> )	Near-bed $\chi_{3,1}$ (g.l <sup>-1</sup> )	$C_{b3,1}$ (g.l <sup>-1</sup> )	Deposited $\delta_{3,1}$ exp	$\Delta_{3,1}$ exp	$w_{d3,1}^*$	$w_{d3,1}$ (m.s <sup>-1</sup> )
		sample (g)		sample (g) (kg.m <sup>-2</sup> .s <sup>-1</sup> )			
550	0.067	0.014	0.0004	1.84E-04	0.045	0.0004	5.28E-06
462.5	0.056	0.012	0.0004	1.58E-04	0.1	0.0010	1.17E-05
390	0.046	0.15	0.0048	1.97E-03	1.28	0.0127	1.50E-04
327.5	0.038	1.04	0.0329	1.37E-02	6.23	0.0620	7.31E-04
275	0.030	7.26	0.2300	9.55E-02	34.29	0.3411	4.02E-03
231	0.024	13.7	0.4340	1.80E-01	40.94	0.4073	4.80E-03
181	0.016	8.27	0.2620	1.09E-01	16.98	0.1689	1.99E-03
106.5	0.007	1.12	0.0355	1.47E-02	0.66	0.0066	7.74E-05
		31.566		4.15E-01	100.525		1.18E-02

Average	
$w_d^*$	$w_d$ (m.s <sup>-1</sup> )
0.492	0.033
0.741	0.042
1.077	0.050
1.175	0.044
1.041	0.031
0.963	0.023
0.930	0.015
0.761	0.005

Size ( $\mu$ m)	$w_a$ (m.s <sup>-1</sup> )	Near-bed $\chi_{3,2}$ (g.l <sup>-1</sup> )	$C_{b3,2}$ (g.l <sup>-1</sup> )	Deposited $\delta_{3,2}$ exp	$\Delta_{3,2}$ exp	$w_{d3,2}^*$	$w_{d3,2}$ (m.s <sup>-1</sup> )
		sample (g)		sample (g) (kg.m <sup>-2</sup> .s <sup>-1</sup> )			
550	0.067	0.005	0.0002	6.67E-05	0.07	0.0007	6.08E-06
462.5	0.056	0.009	0.0003	1.20E-04	0.065	0.0006	5.65E-06
390	0.046	0.09	0.0033	1.20E-03	0.75	0.0075	6.52E-05
327.5	0.038	0.73	0.0267	9.74E-03	4.26	0.0424	3.70E-04
275	0.030	6.32	0.2310	8.43E-02	29.53	0.2940	2.57E-03
231	0.024	11.53	0.4215	1.54E-01	44.01	0.4382	3.82E-03
181	0.016	7.52	0.2749	1.00E-01	20.74	0.2065	1.80E-03
106.5	0.007	1.15	0.0420	1.53E-02	1.02	0.0102	8.86E-05
		27.354		3.65E-01	100.445		8.73E-03

Size ( $\mu$ m)	$w_a$ (m.s <sup>-1</sup> )	Near-bed $\chi_{4,1}$ (g.l <sup>-1</sup> )	$C_{b4,1}$ (g.l <sup>-1</sup> )	Deposited $\delta_{4,1}$ exp	$\Delta_{4,1}$ exp	$w_{d4,1}^*$	$w_{d4,1}$ (m.s <sup>-1</sup> )
		sample (g)		sample (g) (kg.m <sup>-2</sup> .s <sup>-1</sup> )			
550	0.067	0.011	0.0004	1.47E-04	0.03	0.0003	1.55E-06
462.5	0.056	0.007	0.0002	9.32E-05	0.03	0.0003	1.55E-06
390	0.046	0.08	0.0026	1.07E-03	0.625	0.0063	3.22E-05
327.5	0.038	0.66	0.0218	8.79E-03	3.62	0.0364	1.87E-04
275	0.030	6.06	0.2004	8.07E-02	27.85	0.2801	1.44E-03
231	0.024	12.95	0.4283	1.73E-01	44.59	0.4485	2.30E-03
181	0.016	9.18	0.3036	1.22E-01	21.58	0.2170	1.11E-03
106.5	0.007	1.29	0.0427	1.72E-02	1.1	0.0111	5.67E-05
		30.238		4.03E-01	99.425		5.12E-03

Size ( $\mu$ m)	$w_a$ (m.s <sup>-1</sup> )	Near-bed $\chi_{4,2}$ (g.l <sup>-1</sup> )	$C_{b4,2}$ (g.l <sup>-1</sup> )	Deposited $\delta_{4,2}$ exp	$\Delta_{4,2}$ exp	$w_{d4,2}^*$	$w_{d4,2}$ (m.s <sup>-1</sup> )
		sample (g)		sample (g) (kg.m <sup>-2</sup> .s <sup>-1</sup> )			
550	0.067	0.006	0.0003	7.90E-05	0.07	0.0007	3.50E-06
462.5	0.056	0.006	0.0003	7.90E-05	0.05	0.0005	2.50E-06
390	0.046	0.03	0.0017	3.95E-04	0.5	0.0049	2.50E-05
327.5	0.038	0.26	0.0145	3.42E-03	3.295	0.0326	1.65E-04
275	0.030	2.99	0.1663	3.94E-02	26.41	0.2609	1.32E-03
231	0.024	7.49	0.4165	9.86E-02	45.55	0.4500	2.28E-03
181	0.016	6.15	0.3420	8.10E-02	24.1	0.2381	1.20E-03
106.5	0.007	1.05	0.0584	1.38E-02	1.24	0.0123	6.20E-05
		17.982		2.37E-01	101.215		5.06E-03

Size ( $\mu$ m)	$w_a$ (m.s <sup>-1</sup> )	Near-bed $\chi_{5,1}$ (g.l <sup>-1</sup> )	$C_{b5,1}$ (g.l <sup>-1</sup> )	Deposited $\delta_{5,1}$ exp	$\Delta_{5,1}$ exp	$w_{d5,1}^*$	$w_{d5,1}$ (m.s <sup>-1</sup> )
		sample (g)		sample (g) (kg.m <sup>-2</sup> .s <sup>-1</sup> )			
550	0.067	0.008	0.0007	1.06E-04	0.05	0.0005	1.84E-06
462.5	0.056	0.003	0.0003	3.98E-05	0.06	0.0006	2.20E-06
390	0.046	0.02	0.0017	2.65E-04	0.34	0.0034	1.25E-05
327.5	0.038	0.14	0.0117	1.86E-03	2.67	0.0267	9.80E-05
275	0.030	1.89	0.1581	2.51E-02	23.57	0.2353	8.65E-04
231	0.024	4.64	0.3883	6.16E-02	44.98	0.4490	1.65E-03
181	0.016	4.28	0.3581	5.68E-02	26.4	0.2635	9.69E-04
106.5	0.007	0.97	0.0812	1.29E-02	2.11	0.0211	7.75E-05
		11.951		1.59E-01	100.18		3.68E-03

Size ( $\mu$ m)	$w_a$ (m.s <sup>-1</sup> )	Near-bed $\chi_{7,1}$ (g.l <sup>-1</sup> )	$C_{b7,1}$ (g.l <sup>-1</sup> )	Deposited $\delta_{7,1}$ exp	$\Delta_{7,1}$ exp	$w_{d7,1}^*$	$w_{d7,1}$ (m.s <sup>-1</sup> )
		sample (g)		sample (g) (kg.m <sup>-2</sup> .s <sup>-1</sup> )			
550	0.067	0.006	0.0010	8.03E-05	0.03	0.0003	4.34E-07
462.5	0.056	0.002	0.0003	2.68E-05	0.045	0.0005	6.50E-07
390	0.046	0.011	0.0018	1.47E-04	0.3	0.0030	4.34E-06
327.5	0.038	0.04	0.0064	5.35E-04	1.95	0.0196	2.82E-05
275	0.030	0.615	0.0988	8.23E-03	17.08	0.1713	2.47E-04
231	0.024	2.02	0.3246	2.70E-02	41.22	0.4133	5.96E-04
181	0.016	2.63	0.4226	3.52E-02	34.42	0.3451	4.98E-04
106.5	0.007	0.9	0.1446	1.20E-02	4.69	0.0470	6.78E-05
		6.224		8.33E-02	99.735		1.44E-03

D4

	Location	Deposited $\Delta_i$		Sample mass (g)	Volume of $C_{bi}$					
	x (m)	(kg)	( $\text{kg}\cdot\text{m}\cdot\text{s}^{-2}$ )		water (l)	( $\text{g}\cdot\text{l}^{-1}$ )				
trap#3.1	0.9	1.527	0.0122	37.22	78.8	0.472	time (mn)	40		
trap#3.2	1.1	1.07	0.0085	24.91	79.3	0.314	$t^{\circ}$ ( $^{\circ}\text{C}$ )	19.3		
trap#4.1	1.3	0.641	0.0051	19.09	78.5	0.243	$v$ ( $\text{m}^2\cdot\text{s}^{-1}$ )	1.02E-06		
trap#4.2	1.5	0.493	0.0039	14.05	78.0	0.180	$\rho_w$ ( $\text{kg}\cdot\text{m}^{-3}$ )	1000		
trap#5	1.74	0.503	0.0027	10.34	78.0	0.133	$\rho_s$ ( $\text{kg}\cdot\text{m}^{-3}$ )	2700		
trap#7	2.62	0.182	0.0011	5.71	77.1	0.074	$g$ ( $\text{m}\cdot\text{s}^{-2}$ )	9.8		
							$\rho_s^*$	1.7		

Size ( $\mu\text{m}$ )	$w_s$ ( $\text{m}\cdot\text{s}^{-1}$ )	Near-bed		Deposited $\delta_{3.1}^i$ exp		$\Delta_{3.1}^i$ exp		$w_{d3.1}^*$		Average	
		$\chi_{3.1}^i$ ( $\text{g}\cdot\text{l}^{-1}$ )	$C_{b3.1}^i$ ( $\text{g}\cdot\text{l}^{-1}$ )	sample (g)	sample (g)	( $\text{kg}\cdot\text{m}^{-2}\cdot\text{s}^{-1}$ )	$w_{d3.1}^*$	$w_{d3.1}$ ( $\text{m}\cdot\text{s}^{-1}$ )	$w_d^*$	$w_d$ ( $\text{m}\cdot\text{s}^{-1}$ )	
550	0.068	0.006	0.0002	7.66E-05	0.032	0.0003	3.90E-06	0.754	0.051	0.581	0.039
462.5	0.057	0.016	0.0004	2.04E-04	0.075	0.0007	9.14E-06	0.789	0.045	0.853	0.048
390	0.047	0.17	0.0046	2.17E-03	0.88	0.0088	1.07E-04	1.048	0.049	1.239	0.058
327.5	0.038	1.16	0.0314	1.48E-02	5.07	0.0507	6.18E-04	1.088	0.042	1.347	0.052
275	0.031	8.76	0.2369	1.12E-01	31.38	0.3137	3.82E-03	1.114	0.034	1.294	0.040
231	0.024	14.39	0.3891	1.84E-01	41.69	0.4168	5.08E-03	1.145	0.028	1.129	0.027
181	0.017	10.57	0.2858	1.35E-01	19.67	0.1966	2.40E-03	1.059	0.018	0.978	0.016
106.5	0.007	1.91	0.0516	2.44E-02	1.23	0.0123	1.50E-04	0.896	0.006	0.904	0.006
		36.982		4.72E-01	100.027		1.22E-02				

Size ( $\mu\text{m}$ )	$w_s$ ( $\text{m}\cdot\text{s}^{-1}$ )	Near-bed		Deposited $\delta_{3.2}^i$ exp		$\Delta_{3.2}^i$ exp		$w_{d3.2}^*$		Average	
		$\chi_{3.2}^i$ ( $\text{g}\cdot\text{l}^{-1}$ )	$C_{b3.2}^i$ ( $\text{g}\cdot\text{l}^{-1}$ )	sample (g)	sample (g)	( $\text{kg}\cdot\text{m}^{-2}\cdot\text{s}^{-1}$ )	$w_{d3.2}^*$	$w_{d3.2}$ ( $\text{m}\cdot\text{s}^{-1}$ )	$w_d^*$	$w_d$ ( $\text{m}\cdot\text{s}^{-1}$ )	
550	0.068	0.006	0.0002	7.66E-05	0.012	0.0001	1.02E-06	0.198	0.013	0.581	0.039
462.5	0.057	0.007	0.0003	8.94E-05	0.051	0.0005	4.35E-06	0.858	0.049	0.853	0.048
390	0.047	0.03	0.0012	3.83E-04	0.56	0.0056	4.78E-05	2.647	0.125	1.239	0.058
327.5	0.038	0.36	0.0146	4.60E-03	3.8	0.0380	3.24E-04	1.839	0.071	1.347	0.052
275	0.031	3.86	0.1570	4.93E-02	29.09	0.2906	2.48E-03	1.641	0.050	1.294	0.040
231	0.024	9.16	0.3725	1.17E-01	40.61	0.4057	3.46E-03	1.227	0.030	1.129	0.027
181	0.017	9.09	0.3696	1.16E-01	23.78	0.2376	2.03E-03	1.042	0.017	0.978	0.016
106.5	0.007	2.08	0.0846	2.66E-02	2.2	0.0220	1.88E-04	1.030	0.007	0.904	0.006
		24.593		3.14E-01	100.103		8.54E-03				

Size ( $\mu\text{m}$ )	$w_s$ ( $\text{m}\cdot\text{s}^{-1}$ )	Near-bed		Deposited $\delta_{4.1}^i$ exp		$\Delta_{4.1}^i$ exp		$w_{d4.1}^*$		Average	
		$\chi_{4.1}^i$ ( $\text{g}\cdot\text{l}^{-1}$ )	$C_{b4.1}^i$ ( $\text{g}\cdot\text{l}^{-1}$ )	sample (g)	sample (g)	( $\text{kg}\cdot\text{m}^{-2}\cdot\text{s}^{-1}$ )	$w_{d4.1}^*$	$w_{d4.1}$ ( $\text{m}\cdot\text{s}^{-1}$ )	$w_d^*$	$w_d$ ( $\text{m}\cdot\text{s}^{-1}$ )	
550	0.068	0.0045	0.0002	5.77E-05	0.017	0.0002	8.72E-07	0.224	0.015	0.581	0.039
462.5	0.057	0.003	0.0002	3.84E-05	0.04	0.0004	2.05E-06	0.941	0.053	0.853	0.048
390	0.047	0.02	0.0011	2.56E-04	0.35	0.0035	1.79E-05	1.487	0.070	1.239	0.058
327.5	0.038	0.18	0.0095	2.31E-03	2.36	0.0237	1.21E-04	1.368	0.052	1.347	0.052
275	0.031	2.38	0.1253	3.05E-02	21.89	0.2194	1.12E-03	1.199	0.037	1.294	0.040
231	0.024	6.63	0.3492	8.49E-02	43.03	0.4312	2.21E-03	1.076	0.026	1.129	0.027
181	0.017	7.61	0.4008	9.75E-02	29.06	0.2912	1.49E-03	0.911	0.015	0.978	0.016
106.5	0.007	2.16	0.1138	2.77E-02	3.04	0.0305	1.56E-04	0.821	0.006	0.904	0.006
		18.9875		2.43E-01	99.787		5.12E-03				

Size ( $\mu\text{m}$ )	$w_s$ ( $\text{m}\cdot\text{s}^{-1}$ )	Near-bed		Deposited $\delta_{4.2}^i$ exp		$\Delta_{4.2}^i$ exp		$w_{d4.2}^*$		Average	
		$\chi_{4.2}^i$ ( $\text{g}\cdot\text{l}^{-1}$ )	$C_{b4.2}^i$ ( $\text{g}\cdot\text{l}^{-1}$ )	sample (g)	sample (g)	( $\text{kg}\cdot\text{m}^{-2}\cdot\text{s}^{-1}$ )	$w_{d4.2}^*$	$w_{d4.2}$ ( $\text{m}\cdot\text{s}^{-1}$ )	$w_d^*$	$w_d$ ( $\text{m}\cdot\text{s}^{-1}$ )	
550	0.068	0.003	0.0002	3.90E-05	0.034	0.0003	1.34E-06	0.508	0.034	0.581	0.039
462.5	0.057	0.002	0.0001	2.60E-05	0.034	0.0003	1.34E-06	0.907	0.051	0.853	0.048
390	0.047	0.021	0.0015	2.73E-04	0.24	0.0024	9.46E-06	0.734	0.035	1.239	0.058
327.5	0.038	0.13	0.0094	1.69E-03	1.92	0.0192	7.56E-05	1.166	0.045	1.347	0.052
275	0.031	1.68	0.1213	2.19E-02	19.04	0.1906	7.50E-04	1.118	0.034	1.294	0.040
231	0.024	4.6	0.3322	5.99E-02	41.45	0.4150	1.63E-03	1.130	0.027	1.129	0.027
181	0.017	5.66	0.4088	7.37E-02	33.01	0.3305	1.30E-03	1.053	0.018	0.978	0.016
106.5	0.007	1.75	0.1264	2.28E-02	4.16	0.0416	1.64E-04	1.049	0.007	0.904	0.006
		13.846		1.80E-01	99.888		3.94E-03				

Size ( $\mu\text{m}$ )	$w_s$ ( $\text{m}\cdot\text{s}^{-1}$ )	Near-bed		Deposited $\delta_5^i$ exp		$\Delta_5^i$ exp		$w_{d5}^*$		Average	
		$\chi_5^i$ ( $\text{g}\cdot\text{l}^{-1}$ )	$C_{b5}^i$ ( $\text{g}\cdot\text{l}^{-1}$ )	sample (g)	sample (g)	( $\text{kg}\cdot\text{m}^{-2}\cdot\text{s}^{-1}$ )	$w_{d5}^*$	$w_{d5}$ ( $\text{m}\cdot\text{s}^{-1}$ )	$w_d^*$	$w_d$ ( $\text{m}\cdot\text{s}^{-1}$ )	
550	0.068	0.001	0.0001	1.31E-05	0.039	0.0004	1.05E-06	1.181	0.080	0.581	0.039
462.5	0.057	0.002	0.0002	2.62E-05	0.049	0.0005	1.31E-06	0.883	0.050	0.853	0.048
390	0.047	0.01	0.0010	1.31E-04	0.24	0.0024	6.44E-06	1.042	0.049	1.239	0.058
327.5	0.038	0.07	0.0069	9.18E-04	1.73	0.0173	4.64E-05	1.318	0.051	1.347	0.052
275	0.031	0.94	0.0929	1.23E-02	16.72	0.1675	4.48E-04	1.185	0.036	1.294	0.040
231	0.024	3.03	0.2996	3.97E-02	40.88	0.4095	1.10E-03	1.143	0.028	1.129	0.027
181	0.017	4.43	0.4381	5.81E-02	35.47	0.3553	9.51E-04	0.976	0.016	0.978	0.016
106.5	0.007	1.63	0.1612	2.14E-02	4.7	0.0471	1.26E-04	0.860	0.006	0.904	0.006
		10.113		1.33E-01	99.828		2.68E-03				

Size ( $\mu\text{m}$ )	$w_s$ ( $\text{m}\cdot\text{s}^{-1}$ )	Near-bed		Deposited $\delta_7^i$ exp		$\Delta_7^i$ exp		$w_{d7}^*$		Average	
		$\chi_7^i$ ( $\text{g}\cdot\text{l}^{-1}$ )	$C_{b7}^i$ ( $\text{g}\cdot\text{l}^{-1}$ )	sample (g)	sample (g)	( $\text{kg}\cdot\text{m}^{-2}\cdot\text{s}^{-1}$ )	$w_{d7}^*$	$w_{d7}$ ( $\text{m}\cdot\text{s}^{-1}$ )	$w_d^*$	$w_d$ ( $\text{m}\cdot\text{s}^{-1}$ )	
550	0.068	0.001	0.0002	1.36E-05	0.05	0.0005	5.72E-07	0.623	0.042	0.581	0.039
462.5	0.057	0.001	0.0002	1.36E-05	0.05	0.0005	5.72E-07	0.741	0.042	0.853	0.048
390	0.047	0.0075	0.0014	1.02E-04	0.2	0.0020	2.29E-06	0.476	0.022	1.239	0.058
327.5	0.038	0.018	0.0033	2.45E-04	1.07	0.0108	1.22E-05	1.304	0.050	1.347	0.052
275	0.031	0.23	0.0422	3.13E-03	12.64	0.1271	1.44E-04	1.506	0.046	1.294	0.040
231	0.024	1.1	0.2019	1.49E-02	33.37	0.3355	3.81E-04	1.057	0.026	1.129	0.027
181	0.017	2.58	0.4736	3.51E-02	42.64	0.4287	4.87E-04	0.829	0.014	0.978	0.016
106.5	0.007	1.51	0.2772	2.05E-02	9.44	0.0949	1.08E-04	0.767	0.005	0.904	0.006
		5.4475		7.40E-02	99.46		1.14E-03				

D5

	Location	Deposited $\Delta_i$		Sample Volume of $C_{bi}$		
	x (m)	(kg)	(kg.m.s <sup>-2</sup> )	mass (g)	water (l)	(g.l <sup>-1</sup> )
trap#3.1	0.9	1.819	0.0145	48.06	80.5	0.597
trap#3.2	1.1	1.917	0.0153	65.58	79.7	0.823
trap#4.1	1.3	1.32	0.0105	41.52	78.8	0.527
trap#4.2	1.5	1.002	0.0080	22.29	79.0	0.282
trap#5	1.74	1.379	0.0073	33.05	78.8	0.419
trap#7	2.62	0.562	0.0035	15.24	77.3	0.197

time (mn)	40
t° (°C)	17.1
v (m <sup>2</sup> .s <sup>-1</sup> )	1.08E-06
ρw (kg.m <sup>-3</sup> )	1000
ρs (kg.m <sup>-3</sup> )	2700
g (m.s <sup>-2</sup> )	9.8
ρs*	1.7

Average

$w_{d3.1}^*$	$w_{d3.1}$ (m.s <sup>-1</sup> )
0.575	0.038
1.077	0.060
0.935	0.043
1.030	0.038
0.954	0.028
1.001	0.023
1.041	0.017
1.138	0.007

Size (μm)	$w_s$ (m.s <sup>-1</sup> )	Near-bed $\chi_{3.1}$ (g.l <sup>-1</sup> )		$C_{b3.1}$ (g.l <sup>-1</sup> )		Deposited $\delta_{3.1}$ exp		$\Delta_{3.1}$ exp		$w_{d3.1}^*$	$w_{d3.1}$ (m.s <sup>-1</sup> )
		sample (g)		sample (g)		sample (g)		(kg.m <sup>-2</sup> .s <sup>-1</sup> )			
550	0.066	0.003	0.0001	3.77E-05		0.013	0.0001	1.88E-06		0.754	0.050
462.5	0.056	0.024	0.0005	3.01E-04		0.18	0.0018	2.61E-05		1.558	0.087
390	0.046	0.31	0.0065	3.89E-03		1.68	0.0168	2.44E-04		1.360	0.063
327.5	0.037	1.85	0.0389	2.32E-02		7.43	0.0742	1.08E-03		1.243	0.046
275	0.030	11.76	0.2473	1.48E-01		32.78	0.3273	4.75E-03		1.082	0.032
231	0.023	17.54	0.3688	2.20E-01		37.27	0.3721	5.40E-03		1.052	0.025
181	0.016	12.19	0.2563	1.53E-01		18.15	0.1812	2.63E-03		1.067	0.017
106.5	0.007	3.88	0.0816	4.87E-02		2.65	0.0265	3.84E-04		1.206	0.008
		47.557		5.97E-01		100.153		1.45E-02			

Size (μm)	$w_s$ (m.s <sup>-1</sup> )	Near-bed $\chi_{3.2}$ (g.l <sup>-1</sup> )		$C_{b3.2}$ (g.l <sup>-1</sup> )		Deposited $\delta_{3.2}$ exp		$\Delta_{3.2}$ exp		$w_{d3.2}^*$	$w_{d3.2}$ (m.s <sup>-1</sup> )
		sample (g)		sample (g)		sample (g)		(kg.m <sup>-2</sup> .s <sup>-1</sup> )			
550	0.066	0.01	0.0002	1.27E-04		0.026	0.0003	3.98E-06		0.473	0.031
462.5	0.056	0.041	0.0006	5.20E-04		0.1	0.0010	1.53E-05		0.530	0.029
390	0.046	0.42	0.0065	5.33E-03		1.33	0.0133	2.04E-04		0.831	0.038
327.5	0.037	2.51	0.0387	3.19E-02		7.39	0.0740	1.13E-03		0.952	0.036
275	0.030	15	0.2313	1.90E-01		33.37	0.3341	5.11E-03		0.902	0.027
231	0.023	25.52	0.3935	3.24E-01		37.22	0.3726	5.70E-03		0.755	0.018
181	0.016	16.74	0.2581	2.12E-01		18.42	0.1844	2.82E-03		0.824	0.013
106.5	0.007	4.62	0.0712	5.86E-02		2.03	0.0203	3.11E-04		0.811	0.005
		64.861		8.23E-01		99.886		1.53E-02			

Size (μm)	$w_s$ (m.s <sup>-1</sup> )	Near-bed $\chi_{4.1}$ (g.l <sup>-1</sup> )		$C_{b4.1}$ (g.l <sup>-1</sup> )		Deposited $\delta_{4.1}$ exp		$\Delta_{4.1}$ exp		$w_{d4.1}^*$	$w_{d4.1}$ (m.s <sup>-1</sup> )
		sample (g)		sample (g)		sample (g)		(kg.m <sup>-2</sup> .s <sup>-1</sup> )			
550	0.066	0.005	0.0001	6.44E-05		0.005	0.0001	5.28E-07		0.124	0.008
462.5	0.056	0.015	0.0004	1.93E-04		0.07	0.0007	7.40E-06		0.689	0.038
390	0.046	0.2	0.0049	2.58E-03		0.93	0.0093	9.83E-05		0.829	0.038
327.5	0.037	1.38	0.0337	1.78E-02		5.42	0.0544	5.73E-04		0.864	0.032
275	0.030	9.55	0.2335	1.23E-01		29.83	0.2992	3.15E-03		0.861	0.026
231	0.023	15.04	0.3677	1.94E-01		39.72	0.3984	4.20E-03		0.929	0.022
181	0.016	10.84	0.2650	1.40E-01		20.74	0.2080	2.19E-03		0.974	0.016
106.5	0.007	3.87	0.0946	4.98E-02		2.98	0.0299	3.15E-04		0.967	0.006
		40.9		5.27E-01		99.695		1.05E-02			

Size (μm)	$w_s$ (m.s <sup>-1</sup> )	Near-bed $\chi_{4.2}$ (g.l <sup>-1</sup> )		$C_{b4.2}$ (g.l <sup>-1</sup> )		Deposited $\delta_{4.2}$ exp		$\Delta_{4.2}$ exp		$w_{d4.2}^*$	$w_{d4.2}$ (m.s <sup>-1</sup> )
		sample (g)		sample (g)		sample (g)		(kg.m <sup>-2</sup> .s <sup>-1</sup> )			
550	0.066	0.003	0.0001	3.87E-05		0.01	0.0001	8.02E-07		0.312	0.021
462.5	0.056	0.004	0.0002	5.16E-05		0.05	0.0005	4.01E-06		1.399	0.078
390	0.046	0.07	0.0032	9.03E-04		0.66	0.0066	5.30E-05		1.275	0.059
327.5	0.037	0.45	0.0206	5.81E-03		4.34	0.0435	3.48E-04		1.608	0.060
275	0.030	3.65	0.1668	4.71E-02		24.43	0.2451	1.96E-03		1.399	0.042
231	0.023	7.31	0.3341	9.43E-02		40.7	0.4083	3.27E-03		1.485	0.035
181	0.016	7.05	0.3223	9.09E-02		24.52	0.2460	1.97E-03		1.342	0.022
106.5	0.007	3.34	0.1527	4.31E-02		4.96	0.0498	3.98E-04		1.413	0.009
		21.877		2.82E-01		99.67		8.00E-03			

Size (μm)	$w_s$ (m.s <sup>-1</sup> )	Near-bed $\chi_5$ (g.l <sup>-1</sup> )		$C_{b5}$ (g.l <sup>-1</sup> )		Deposited $\delta_5$ exp		$\Delta_5$ exp		$w_{d5}^*$	$w_{d5}$ (m.s <sup>-1</sup> )
		sample (g)		sample (g)		sample (g)		(kg.m <sup>-2</sup> .s <sup>-1</sup> )			
550	0.066	0.001	0.0000	1.28E-05		0.012	0.0001	8.83E-07		1.036	0.069
462.5	0.056	0.005	0.0002	6.42E-05		0.041	0.0004	3.02E-06		0.845	0.047
390	0.046	0.11	0.0034	1.41E-03		0.575	0.0058	4.23E-05		0.651	0.030
327.5	0.037	0.68	0.0208	8.74E-03		3.95	0.0396	2.91E-04		0.892	0.033
275	0.030	5.51	0.1688	7.08E-02		25.62	0.2570	1.89E-03		0.895	0.027
231	0.023	11.42	0.3499	1.47E-01		39.95	0.4007	2.94E-03		0.859	0.020
181	0.016	10.73	0.3288	1.38E-01		24.76	0.2483	1.82E-03		0.820	0.013
106.5	0.007	4.18	0.1281	5.37E-02		4.8	0.0481	3.53E-04		1.006	0.007
		32.636		4.19E-01		99.708		7.34E-03			

Size (μm)	$w_s$ (m.s <sup>-1</sup> )	Near-bed $\chi_7$ (g.l <sup>-1</sup> )		$C_{b7}$ (g.l <sup>-1</sup> )		Deposited $\delta_7$ exp		$\Delta_7$ exp		$w_{d7}^*$	$w_{d7}$ (m.s <sup>-1</sup> )
		sample (g)		sample (g)		sample (g)		(kg.m <sup>-2</sup> .s <sup>-1</sup> )			
550	0.066	0.003	0.0002	4.04E-05		0.057	0.0006	2.02E-06		0.752	0.050
462.5	0.056	0.002	0.0001	2.89E-05		0.061	0.0006	2.16E-06		1.442	0.080
390	0.046	0.018	0.0012	2.42E-04		0.21	0.0021	7.43E-06		0.666	0.031
327.5	0.037	0.13	0.0089	1.75E-03		1.15	0.0116	4.07E-05		0.623	0.023
275	0.030	1.72	0.1175	2.32E-02		11.44	0.1153	4.05E-04		0.587	0.017
231	0.023	4.29	0.2930	5.78E-02		35.23	0.3549	1.25E-03		0.925	0.022
181	0.016	5.37	0.3667	7.23E-02		40.1	0.4040	1.42E-03		1.217	0.020
106.5	0.007	3.11	0.2124	4.19E-02		11.01	0.1109	3.89E-04		1.423	0.009
		14.643		1.97E-01		99.258		3.51E-03			

D6	Location	Deposited $\Delta_1$		Sample Volume of $C_{b1}$			time (mn) 43 $t^{\circ}$ ( $^{\circ}\text{C}$ ) 18.9 $v$ ( $\text{m}^2\cdot\text{s}^{-1}$ ) $1.03\text{E-}06$ $\rho_w$ ( $\text{kg}\cdot\text{m}^{-3}$ ) 1000 $\rho_s$ ( $\text{kg}\cdot\text{m}^{-3}$ ) 2700 $g$ ( $\text{m}\cdot\text{s}^{-2}$ ) 9.8 $\rho_s^*$ 1.7			
	x (m)	(kg)	( $\text{kg}\cdot\text{m}\cdot\text{s}^{-2}$ )	mass (g)	water (l)	( $\text{g}\cdot\text{l}^{-1}$ )				
trap#3.1	0.9	2.822	0.0203	65.17	84.5	0.771				
trap#3.2	1.1	2.066	0.0158	48.85	83.3	0.586				
trap#4.1	1.3	1.885	0.0135	65.79	83.7	0.786				
trap#4.2	1.5	1.258	0.0096	46.6	83.8	0.556				
trap#5	1.74	1.771	0.0087	24.55	82.2	0.299				
trap#7	2.62	0.623	0.0038	18.42	80.2	0.230				

Average	
$w_d^*$	$w_d$ ( $\text{m}\cdot\text{s}^{-1}$ )
0.707	0.048
0.818	0.046
0.828	0.039
0.914	0.035
0.869	0.027
0.890	0.021
0.967	0.016
1.355	0.009

Size ( $\mu\text{m}$ )	$w_s$ ( $\text{m}\cdot\text{s}^{-1}$ )	Near-bed $\chi_{3,1}$ ( $\text{g}\cdot\text{l}^{-1}$ )		$C_{b3,1}$ ( $\text{g}\cdot\text{l}^{-1}$ )		Deposited $\delta_{3,1}$ exp		$\Delta_{3,1}$ exp		$w_{d3,1}^*$	$w_{d3,1}$ ( $\text{m}\cdot\text{s}^{-1}$ )
		sample (g)		sample (g)		sample (g)		(kg.m <sup>-2</sup> .s <sup>-1</sup> )			
550	0.067	0.0325	0.0005	3.86E-04	0.039	0.0008	1.58E-05	0.608	0.041		
462.5	0.057	0.16	0.0025	1.90E-03	0.22	0.0044	8.92E-05	0.831	0.047		
390	0.047	1.15	0.0177	1.37E-02	1.48	0.0296	6.00E-04	0.937	0.044		
327.5	0.038	4.86	0.0748	5.77E-02	5.45	0.1090	2.21E-03	1.003	0.038		
275	0.031	20.94	0.3224	2.49E-01	18.14	0.3627	7.35E-03	0.969	0.030		
231	0.024	24.98	0.3846	2.97E-01	18.11	0.3621	7.34E-03	1.031	0.025		
181	0.017	12	0.1848	1.42E-01	6.3	0.1260	2.55E-03	1.076	0.018		
106.5	0.007	0.83	0.0128	9.86E-03	0.28	0.0056	1.14E-04	1.694	0.012		
		64.9525		7.71E-01		50.019		2.03E-02			

Size ( $\mu\text{m}$ )	$w_s$ ( $\text{m}\cdot\text{s}^{-1}$ )	Near-bed $\chi_{3,2}$ ( $\text{g}\cdot\text{l}^{-1}$ )		$C_{b3,2}$ ( $\text{g}\cdot\text{l}^{-1}$ )		Deposited $\delta_{3,2}$ exp		$\Delta_{3,2}$ exp		$w_{d3,2}^*$	$w_{d3,2}$ ( $\text{m}\cdot\text{s}^{-1}$ )
		sample (g)		sample (g)		sample (g)		(kg.m <sup>-2</sup> .s <sup>-1</sup> )			
550	0.067	0.01	0.0002	1.20E-04	0.026	0.0005	8.18E-06	1.009	0.068		
462.5	0.057	0.07	0.0014	8.43E-04	0.15	0.0030	4.72E-05	0.990	0.056		
390	0.047	0.56	0.0115	6.75E-03	1.09	0.0217	3.43E-04	1.084	0.051		
327.5	0.038	2.8	0.0575	3.37E-02	4.56	0.0909	1.43E-03	1.115	0.043		
275	0.031	14.21	0.2920	1.71E-01	17.92	0.3574	5.64E-03	1.079	0.033		
231	0.024	19.77	0.4062	2.38E-01	19.04	0.3797	5.99E-03	1.048	0.025		
181	0.017	10.45	0.2147	1.26E-01	7.08	0.1412	2.23E-03	1.063	0.018		
106.5	0.007	0.8	0.0164	9.64E-03	0.28	0.0056	8.81E-05	1.345	0.009		
		48.67		5.86E-01		50.146		1.58E-02			

Size ( $\mu\text{m}$ )	$w_s$ ( $\text{m}\cdot\text{s}^{-1}$ )	Near-bed $\chi_{4,1}$ ( $\text{g}\cdot\text{l}^{-1}$ )		$C_{b4,1}$ ( $\text{g}\cdot\text{l}^{-1}$ )		Deposited $\delta_{4,1}$ exp		$\Delta_{4,1}$ exp		$w_{d4,1}^*$	$w_{d4,1}$ ( $\text{m}\cdot\text{s}^{-1}$ )
		sample (g)		sample (g)		sample (g)		(kg.m <sup>-2</sup> .s <sup>-1</sup> )			
550	0.067	0.0105	0.0002	1.26E-04	0.0165	0.0003	4.48E-06	0.529	0.036		
462.5	0.057	0.08	0.0012	9.58E-04	0.09	0.0018	2.44E-05	0.451	0.025		
390	0.047	0.73	0.0111	8.74E-03	0.86	0.0172	2.33E-04	0.569	0.027		
327.5	0.038	3.79	0.0577	4.54E-02	3.99	0.0799	1.08E-03	0.625	0.024		
275	0.031	18.95	0.2886	2.27E-01	16.59	0.3324	4.50E-03	0.650	0.020		
231	0.024	28.2	0.4294	3.38E-01	19.78	0.3963	5.37E-03	0.662	0.016		
181	0.017	12.96	0.1973	1.55E-01	8.22	0.1647	2.23E-03	0.863	0.014		
106.5	0.007	0.95	0.0145	1.14E-02	0.36	0.0072	9.77E-05	1.263	0.009		
		65.6705		7.86E-01		49.9065		1.35E-02			

Size ( $\mu\text{m}$ )	$w_s$ ( $\text{m}\cdot\text{s}^{-1}$ )	Near-bed $\chi_{4,2}$ ( $\text{g}\cdot\text{l}^{-1}$ )		$C_{b4,2}$ ( $\text{g}\cdot\text{l}^{-1}$ )		Deposited $\delta_{4,2}$ exp		$\Delta_{4,2}$ exp		$w_{d4,2}^*$	$w_{d4,2}$ ( $\text{m}\cdot\text{s}^{-1}$ )
		sample (g)		sample (g)		sample (g)		(kg.m <sup>-2</sup> .s <sup>-1</sup> )			
550	0.067	0.004	0.0001	4.79E-05	0.0135	0.0003	2.61E-06	0.809	0.054		
462.5	0.057	0.0445	0.0010	5.33E-04	0.085	0.0017	1.64E-05	0.545	0.031		
390	0.047	0.44	0.0095	5.27E-03	0.74	0.0149	1.43E-04	0.579	0.027		
327.5	0.038	2.4	0.0517	2.87E-02	3.69	0.0742	7.13E-04	0.650	0.025		
275	0.031	13.57	0.2923	1.62E-01	16.82	0.3383	3.25E-03	0.655	0.020		
231	0.024	19.06	0.4105	2.28E-01	19.73	0.3968	3.81E-03	0.696	0.017		
181	0.017	10.1	0.2175	1.21E-01	8.24	0.1657	1.59E-03	0.791	0.013		
106.5	0.007	0.81	0.0174	9.70E-03	0.4	0.0080	7.73E-05	1.172	0.008		
		46.4285		5.56E-01		49.7185		9.61E-03			

Size ( $\mu\text{m}$ )	$w_s$ ( $\text{m}\cdot\text{s}^{-1}$ )	Near-bed $\chi_{5,1}$ ( $\text{g}\cdot\text{l}^{-1}$ )		$C_{b5,1}$ ( $\text{g}\cdot\text{l}^{-1}$ )		Deposited $\delta_{5,1}$ exp		$\Delta_{5,1}$ exp		$w_{d5,1}^*$	$w_{d5,1}$ ( $\text{m}\cdot\text{s}^{-1}$ )
		sample (g)		sample (g)		sample (g)		(kg.m <sup>-2</sup> .s <sup>-1</sup> )			
550	0.067	0.0025	0.0001	3.05E-05	0.011	0.0002	1.92E-06	0.932	0.063		
462.5	0.057	0.014	0.0006	1.71E-04	0.07	0.0014	1.22E-05	1.262	0.071		
390	0.047	0.16	0.0065	1.95E-03	0.6	0.0121	1.05E-04	1.140	0.054		
327.5	0.038	0.93	0.0380	1.14E-02	3.31	0.0665	5.77E-04	1.331	0.051		
275	0.031	6.12	0.2500	7.47E-02	15.69	0.3152	2.73E-03	1.198	0.037		
231	0.024	10.32	0.4216	1.26E-01	20.84	0.4186	3.63E-03	1.201	0.029		
181	0.017	6.25	0.2553	7.83E-02	8.79	0.1766	1.53E-03	1.205	0.020		
106.5	0.007	0.68	0.0278	8.30E-03	0.47	0.0094	8.19E-05	1.450	0.010		
		24.4765		2.99E-01		49.781		8.67E-03			

Size ( $\mu\text{m}$ )	$w_s$ ( $\text{m}\cdot\text{s}^{-1}$ )	Near-bed $\chi_{7,1}$ ( $\text{g}\cdot\text{l}^{-1}$ )		$C_{b7,1}$ ( $\text{g}\cdot\text{l}^{-1}$ )		Deposited $\delta_{7,1}$ exp		$\Delta_{7,1}$ exp		$w_{d7,1}^*$	$w_{d7,1}$ ( $\text{m}\cdot\text{s}^{-1}$ )
		sample (g)		sample (g)		sample (g)		(kg.m <sup>-2</sup> .s <sup>-1</sup> )			
550	0.067	0.00075	0.0000	9.43E-06	0.003	0.0001	2.26E-07	0.356	0.024		
462.5	0.057	0.003	0.0002	3.77E-05	0.0235	0.0005	1.77E-06	0.830	0.047		
390	0.047	0.0485	0.0027	6.10E-04	0.25	0.0050	1.88E-05	0.658	0.031		
327.5	0.038	0.34	0.0186	4.27E-03	1.65	0.0331	1.24E-04	0.762	0.029		
275	0.031	3.62	0.1980	4.55E-02	12.21	0.2451	9.19E-04	0.662	0.020		
231	0.024	7.68	0.4201	9.65E-02	21.56	0.4328	1.62E-03	0.701	0.017		
181	0.017	5.88	0.3216	7.39E-02	13.15	0.2640	9.90E-04	0.804	0.013		
106.5	0.007	0.71	0.0388	8.92E-03	0.97	0.0195	7.30E-05	1.203	0.008		
		18.28225		2.30E-01		49.8165		3.75E-03			

D7	Location	Deposited $\Delta_1$		Sample		Volume of $C_{N1}$		time (mn) 32 $t^0$ (°C) 20 $v$ (m <sup>2</sup> .s <sup>-1</sup> ) 1E-06 $\rho w$ (kg.m <sup>-3</sup> ) 1000 $\rho s$ (kg.m <sup>-3</sup> ) 2680 $g$ (m.s <sup>-2</sup> ) 9.8 $\rho s^*$ 1.68	
	x (m)	(kg)	(kg.m.s <sup>-2</sup> )	mass (g)	water (l)	(g.l <sup>-1</sup> )	(g.l <sup>-1</sup> )		
trap#3.1	0.9	0.445	0.0043	113.3	67.2	1.686			
trap#3.2	1.1	0.473	0.0049	116.2	66.3	1.752			
trap#4.1	1.3	0.474	0.0046	125.1	66.0	1.895			
trap#4.2	1.5	0.539	0.0055	113.9	66.8	1.704			
trap#5	1.74	0.629	0.0041	114.7	67.0	1.712			
trap#7	2.62	0.58	0.0047	108.5	66.5	1.631			

Size ( $\mu$ m)	$w_a$ (m.s <sup>-1</sup> )	Near-bed $\chi_{3,1}$ (g.l <sup>-1</sup> )		$C_{3,1}$ (g.l <sup>-1</sup> )		Deposited $\delta_{3,1}$ exp		$\Delta_{3,1}$ exp		$w_{d3,1}^*$	$w_{d3,1}$ (m.s <sup>-1</sup> )
		sample (g)	(g)	(g)	(g)	sample (g)	(kg.m <sup>2</sup> .s <sup>-1</sup> )	(kg.m <sup>2</sup> .s <sup>-1</sup> )	(kg.m <sup>2</sup> .s <sup>-1</sup> )		
275	0.0307	0.05	0.0010	1.74E-03	0.63	0.0129	5.56E-05	1.043	0.0320		
231	0.0242	0.11	0.0023	3.82E-03	0.93	0.0191	8.21E-05	0.889	0.0215		
196	0.0190	0.22	0.0045	7.64E-03	1.22	0.0251	1.08E-04	0.742	0.0141		
165	0.0145	0.96	0.0198	3.33E-02	3.22	0.0662	2.84E-04	0.587	0.0085		
137.5	0.0107	1.98	0.0408	6.88E-02	4.7	0.0966	4.15E-04	0.561	0.0060		
115.5	0.0080	4.21	0.0867	1.48E-01	7.02	0.1442	6.20E-04	0.533	0.0042		
98	0.0059	7.27	0.1497	2.53E-01	10.25	0.2106	9.05E-04	0.605	0.0036		
82.5	0.0043	8.58	0.1767	2.98E-01	8.05	0.1654	7.11E-04	0.553	0.0024		
69	0.0031	7.64	0.1574	2.65E-01	5.94	0.1220	5.24E-04	0.641	0.0020		
58	0.0022	5.08	0.1048	1.76E-01	2.97	0.0610	2.62E-04	0.672	0.0015		
49	0.0016	4.16	0.0857	1.45E-01	2.05	0.0421	1.81E-04	0.786	0.0013		
41.5	0.0012	3.34	0.0688	1.16E-01	1	0.0205	8.83E-05	0.660	0.0008		
19	0.0002	4.95	0.1020	1.72E-01	0.69	0.0142	6.09E-05	1.444	0.0004		
		48.55		1.69E+00	48.67		4.30E-03				

Average	
$w_d^*$	$w_d$ (m.s <sup>-1</sup> )
0.931	0.0286
0.836	0.0202
0.728	0.0138
0.641	0.0093
0.594	0.0064
0.643	0.0051
0.619	0.0037
0.632	0.0027
0.666	0.0021
0.664	0.0015
0.760	0.0012
0.625	0.0007
1.230	0.0003

Size ( $\mu$ m)	$w_a$ (m.s <sup>-1</sup> )	Near-bed $\chi_{3,2}$ (g.l <sup>-1</sup> )		$C_{3,2}$ (g.l <sup>-1</sup> )		Deposited $\delta_{3,2}$ exp		$\Delta_{3,2}$ exp		$w_{d3,2}^*$	$w_{d3,2}$ (m.s <sup>-1</sup> )
		sample (g)	(g)	(g)	(g)	sample (g)	(kg.m <sup>2</sup> .s <sup>-1</sup> )	(kg.m <sup>2</sup> .s <sup>-1</sup> )	(kg.m <sup>2</sup> .s <sup>-1</sup> )		
275	0.0307	0.08	0.0016	2.88E-03	0.6	0.0123	5.95E-05	0.673	0.0207		
231	0.0242	0.14	0.0029	5.04E-03	1.05	0.0214	1.04E-04	0.854	0.0207		
196	0.0190	0.27	0.0055	9.72E-03	1.33	0.0272	1.32E-04	0.714	0.0136		
165	0.0145	1.01	0.0208	3.64E-02	3.41	0.0696	3.38E-04	0.640	0.0093		
137.5	0.0107	2.18	0.0448	7.85E-02	5.19	0.1060	5.15E-04	0.610	0.0066		
115.5	0.0080	4.26	0.0876	1.53E-01	8.02	0.1638	7.95E-04	0.652	0.0052		
98	0.0059	7.47	0.1535	2.69E-01	9.51	0.1942	9.43E-04	0.592	0.0035		
82.5	0.0043	8.49	0.1745	3.06E-01	8.72	0.1781	8.65E-04	0.655	0.0028		
69	0.0031	7.6	0.1562	2.74E-01	5.58	0.1140	5.53E-04	0.656	0.0020		
58	0.0022	4.98	0.1024	1.79E-01	2.59	0.0529	2.57E-04	0.648	0.0014		
49	0.0016	4.19	0.0861	1.51E-01	1.76	0.0359	1.74E-04	0.725	0.0012		
41.5	0.0012	3.21	0.0660	1.16E-01	0.75	0.0153	7.44E-05	0.558	0.0006		
19	0.0002	4.77	0.0980	1.72E-01	0.45	0.0092	4.46E-05	1.059	0.0003		
		48.65		1.75E+00	48.96		4.85E-03				

Size ( $\mu$ m)	$w_a$ (m.s <sup>-1</sup> )	Near-bed $\chi_{4,1}$ (g.l <sup>-1</sup> )		$C_{4,1}$ (g.l <sup>-1</sup> )		Deposited $\delta_{4,1}$ exp		$\Delta_{4,1}$ exp		$w_{d4,1}^*$	$w_{d4,1}$ (m.s <sup>-1</sup> )
		sample (g)	(g)	(g)	(g)	sample (g)	(kg.m <sup>2</sup> .s <sup>-1</sup> )	(kg.m <sup>2</sup> .s <sup>-1</sup> )	(kg.m <sup>2</sup> .s <sup>-1</sup> )		
275	0.0307	0.065	0.0013	2.56E-03	0.41	0.0084	3.86E-05	0.492	0.0151		
231	0.0242	0.13	0.0027	5.11E-03	0.77	0.0158	7.25E-05	0.586	0.0142		
196	0.0190	0.27	0.0056	1.06E-02	1.12	0.0230	1.05E-04	0.523	0.0099		
165	0.0145	1.02	0.0212	4.01E-02	3.09	0.0635	2.91E-04	0.499	0.0072		
137.5	0.0107	2.42	0.0502	9.52E-02	5.2	0.1069	4.89E-04	0.478	0.0051		
115.5	0.0080	4.52	0.0938	1.78E-01	7.84	0.1612	7.38E-04	0.522	0.0042		
98	0.0059	7.76	0.1610	3.05E-01	9.85	0.2025	9.27E-04	0.513	0.0030		
82.5	0.0043	8.33	0.1728	3.28E-01	8.58	0.1764	8.08E-04	0.571	0.0025		
69	0.0031	7.48	0.1552	2.94E-01	5.56	0.1143	5.23E-04	0.577	0.0018		
58	0.0022	4.88	0.1013	1.92E-01	2.74	0.0563	2.58E-04	0.608	0.0013		
49	0.0016	4.04	0.0838	1.59E-01	1.97	0.0405	1.85E-04	0.732	0.0012		
41.5	0.0012	2.96	0.0614	1.16E-01	0.88	0.0181	8.28E-05	0.617	0.0007		
19	0.0002	4.32	0.0896	1.70E-01	0.62	0.0127	5.84E-05	1.400	0.0003		
		48.195		1.90E+00	48.63		4.58E-03				

Size ( $\mu$ m)	$w_a$ (m.s <sup>-1</sup> )	Near-bed $\chi_{4,2}$ (g.l <sup>-1</sup> )		$C_{4,2}$ (g.l <sup>-1</sup> )		Deposited $\delta_{4,2}$ exp		$\Delta_{4,2}$ exp		$w_{d4,2}^*$	$w_{d4,2}$ (m.s <sup>-1</sup> )
		sample (g)	(g)	(g)	(g)	sample (g)	(kg.m <sup>2</sup> .s <sup>-1</sup> )	(kg.m <sup>2</sup> .s <sup>-1</sup> )	(kg.m <sup>2</sup> .s <sup>-1</sup> )		
275	0.0307	0.035	0.0007	1.23E-03	0.37	0.0076	4.18E-05	1.105	0.0339		
231	0.0242	0.09	0.0019	3.17E-03	0.75	0.0153	8.48E-05	1.106	0.0267		
196	0.0190	0.19	0.0039	6.70E-03	1.02	0.0209	1.15E-04	0.907	0.0172		
165	0.0145	0.86	0.0178	3.03E-02	3.15	0.0644	3.56E-04	0.810	0.0118		
137.5	0.0107	2.03	0.0420	7.15E-02	4.81	0.0983	5.44E-04	0.707	0.0076		
115.5	0.0080	4.01	0.0829	1.41E-01	7.85	0.1605	8.88E-04	0.790	0.0063		
98	0.0059	7.54	0.1559	2.66E-01	9.91	0.2026	1.12E-03	0.712	0.0042		
82.5	0.0043	8.57	0.1772	3.02E-01	9.12	0.1864	1.03E-03	0.791	0.0034		
69	0.0031	7.48	0.1547	2.64E-01	5.97	0.1220	6.75E-04	0.831	0.0026		
58	0.0022	5.39	0.1115	1.90E-01	2.69	0.0550	3.04E-04	0.724	0.0016		
49	0.0016	4.25	0.0879	1.50E-01	1.93	0.0395	2.18E-04	0.914	0.0015		
41.5	0.0012	2.96	0.0612	1.04E-01	0.84	0.0172	9.50E-05	0.790	0.0009		
19	0.0002	4.95	0.1024	1.74E-01	0.51	0.0104	5.77E-05	1.348	0.0003		
		48.355		1.70E+00	48.92		5.53E-03				

Size ( $\mu$ m)	$w_a$ (m.s <sup>-1</sup> )	Near-bed $\chi_5$ (g.l <sup>-1</sup> )		$C_{5}$ (g.l <sup>-1</sup> )		Deposited $\delta_5$ exp		$\Delta_5$ exp		$w_{d5}^*$	$w_{d5}$ (m.s <sup>-1</sup> )
		sample (g)	(g)	(g)	(g)	sample (g)	(kg.m <sup>2</sup> .s <sup>-1</sup> )	(kg.m <sup>2</sup> .s <sup>-1</sup> )	(kg.m <sup>2</sup> .s <sup>-1</sup> )		
275	0.0307	0.04	0.0008	1.42E-03	0.37	0.0076	3.15E-05	0.721	0.0221		
231	0.0242	0.1	0.0021	3.56E-03	0.79	0.0163	6.73E-05	0.782	0.0189		
196	0.0190	0.2	0.0042	7.12E-03	1.14	0.0235	9.71E-05	0.718	0.0136		
165	0.0145	0.9	0.0187	3.21E-02	3.22	0.0663	2.74E-04	0.589	0.0086		
137.5	0.0107	2.09	0.0435	7.44E-02	5.7	0.1173	4.86E-04	0.607	0.0065		
115.5	0.0080	3.79	0.0789	1.35E-01	7.92	0.1630	6.75E-04	0.628	0.0050		
98	0.0059	7.47	0.1555	2.66E-01	10.79	0.2221	9.19E-04	0.583	0.0035		
82.5	0.0043	8.71	0.1813	3.10E-01	8.21	0.1690	6.99E-04	0.522	0.0023		
69	0.0031	7.43	0.1546	2.65E-01	5.31	0.1093	4.52E-04	0.554	0.0017		
58	0.0022	5.16	0.1074	1.84E-01	2.39	0.0492	2.04E-04	0.501	0.0011		
49	0.0016	4.09	0.0851	1.46E-01	1.62	0.0333	1.38E-04	0.594	0.0009		
41.5	0.0012	3.34	0.0695	1.19E-01	0.7	0.0144	5.96E-05	0.435	0.0005		
19	0.0002	4.73	0.0984	1.68E-01	0.42	0.0086	3.58E-05	0.866	0.0002		
		48.05		1.71E+00	48.58		4.14E-03				

Size ( $\mu\text{m}$ )	$w_s$ ( $\text{m}\cdot\text{s}^{-1}$ )	Near-bed			Deposited $\delta_T^+$ exp			$w_{d7}^{1*}$	$w_{d7}$ ( $\text{m}\cdot\text{s}^{-1}$ )
		$\chi_T^+$ ( $\text{g}\cdot\text{l}^{-1}$ )	$C_{b7}^+$ ( $\text{g}\cdot\text{l}^{-1}$ )	sample (g)	sample (g)	$\Delta_T^+$ exp	( $\text{kg}\cdot\text{m}^{-2}\cdot\text{s}^{-1}$ )		
275	0.0307	0.01	0.0002	3.42E-04	0.17	0.0035	1.63E-05	1.555	0.0477
231	0.0242	0.045	0.0009	1.54E-03	0.31	0.0063	2.97E-05	0.800	0.0193
196	0.0190	0.13	0.0027	4.44E-03	0.67	0.0137	6.42E-05	0.762	0.0145
165	0.0145	0.72	0.0151	2.46E-02	2.67	0.0546	2.56E-04	0.717	0.0104
137.5	0.0107	1.83	0.0383	6.25E-02	4.19	0.0856	4.02E-04	0.598	0.0064
115.5	0.0080	4.14	0.0867	1.41E-01	8.57	0.1751	8.22E-04	0.731	0.0058
98	0.0059	6.92	0.1449	2.36E-01	10.38	0.2121	9.95E-04	0.711	0.0042
82.5	0.0043	8.66	0.1813	2.96E-01	9.28	0.1896	8.90E-04	0.697	0.0030
69	0.0031	7.44	0.1558	2.54E-01	6.02	0.1230	5.77E-04	0.737	0.0023
58	0.0022	4.67	0.0978	1.60E-01	3.05	0.0623	2.92E-04	0.829	0.0018
49	0.0016	4.49	0.0940	1.53E-01	2.06	0.0421	1.98E-04	0.808	0.0013
41.5	0.0012	3.54	0.0741	1.21E-01	1	0.0204	9.59E-05	0.688	0.0008
19	0.0002	5.17	0.1082	1.77E-01	0.57	0.0116	5.46E-05	1.262	0.0003
		47.765		1.63E+00	48.94		4.69E-03		

E2	Location	Deposited $\Delta_i$		Sample	Volume of $C_{bi}$			
	x (m)	(kg)	(kg.m.s <sup>-2</sup> )	mass (g)	water (l)	(g.l <sup>-1</sup> )		
trap#3.1	0.9	1.81	0.0141	38.03	81.5	0.467	time (mn)	41
trap#3.2	1.1	1.65	0.0128	34.79	80.0	0.435	t° (°C)	18
trap#4.1	1.3	1.203	0.0094	36.19	82.2	0.440	v (m <sup>2</sup> .s <sup>-1</sup> )	1.05E-06
trap#4.2	1.5	0.928	0.0072	27.04	82.0	0.330	ρw (kg.m <sup>-3</sup> )	1000
trap#5	1.74	1.285	0.0067	25.24	80.8	0.312	ρs (kg.m <sup>-3</sup> )	2700
trap#7	2.62	0.382	0.0023	12.57	81.2	0.155	g (m.s <sup>-2</sup> )	9.8
							ρs*	1.7

Size (μm)	w <sub>s</sub> (m.s <sup>-1</sup> )	Near-bed	χ <sub>3,1</sub> <sup>i</sup> (g.l <sup>-1</sup> )	C <sub>b3,1</sub> <sup>i</sup> (g.l <sup>-1</sup> )	Deposited	δ <sub>3,1</sub> <sup>i</sup> exp	Δ <sub>3,1</sub> <sup>i</sup> exp	W <sub>d3,1</sub> <sup>i</sup> *	w <sub>d3,1</sub> <sup>i</sup> (m.s <sup>-1</sup> )
		sample (g)			sample (g)		(kg.m <sup>-2</sup> .s <sup>-1</sup> )		
550	0.067	0.006	0.0002	7.44E-05	0.019	0.0002	2.68E-06	0.540	0.036
462.5	0.056	0.04	0.0011	4.96E-04	0.15	0.0015	2.12E-05	0.762	0.043
390	0.046	0.34	0.0090	4.22E-03	1.55	0.0155	2.19E-04	1.118	0.052
327.5	0.038	1.98	0.0526	2.46E-02	7.46	0.0748	1.05E-03	1.137	0.043
275	0.030	10.88	0.2892	1.35E-01	33.53	0.3361	4.74E-03	1.165	0.035
231	0.024	15.47	0.4112	1.92E-01	39.58	0.3968	5.59E-03	1.232	0.029
181	0.016	7.96	0.2116	9.87E-02	16.16	0.1620	2.28E-03	1.411	0.023
106.5	0.007	0.95	0.0252	1.18E-02	1.3	0.0130	1.84E-04	2.338	0.016
		37.626		4.67E-01	99.749		1.41E-02		

Average	
W <sub>d</sub> <sup>i</sup> *	w <sub>d</sub> <sup>i</sup> (m.s <sup>-1</sup> )
0.860	0.057
0.853	0.048
1.088	0.051
1.075	0.041
1.004	0.030
0.959	0.023
1.028	0.017
1.508	0.010

Size (μm)	w <sub>s</sub> (m.s <sup>-1</sup> )	Near-bed	χ <sub>3,2</sub> <sup>i</sup> (g.l <sup>-1</sup> )	C <sub>b3,2</sub> <sup>i</sup> (g.l <sup>-1</sup> )	Deposited	δ <sub>3,2</sub> <sup>i</sup> exp	Δ <sub>3,2</sub> <sup>i</sup> exp	W <sub>d3,2</sub> <sup>i</sup> *	w <sub>d3,2</sub> <sup>i</sup> (m.s <sup>-1</sup> )
		sample (g)			sample (g)		(kg.m <sup>-2</sup> .s <sup>-1</sup> )		
550	0.067	0.002	0.0001	2.52E-05	0.019	0.0002	2.45E-06	1.451	0.097
462.5	0.056	0.017	0.0005	2.15E-04	0.13	0.0013	1.68E-05	1.393	0.078
390	0.046	0.22	0.0064	2.78E-03	1.55	0.0155	2.00E-04	1.548	0.072
327.5	0.038	1.38	0.0400	1.74E-02	7.68	0.0770	9.90E-04	1.506	0.057
275	0.030	9.16	0.2658	1.16E-01	33.58	0.3368	4.33E-03	1.242	0.037
231	0.024	14.56	0.4225	1.84E-01	39.78	0.3990	5.13E-03	1.179	0.028
181	0.016	8.14	0.2362	1.03E-01	15.9	0.1595	2.05E-03	1.217	0.020
106.5	0.007	0.98	0.0284	1.24E-02	1.05	0.0105	1.35E-04	1.641	0.011
		34.459		4.35E-01	99.689		1.28E-02		

Size (μm)	w <sub>s</sub> (m.s <sup>-1</sup> )	Near-bed	χ <sub>4,1</sub> <sup>i</sup> (g.l <sup>-1</sup> )	C <sub>b4,1</sub> <sup>i</sup> (g.l <sup>-1</sup> )	Deposited	δ <sub>4,1</sub> <sup>i</sup> exp	Δ <sub>4,1</sub> <sup>i</sup> exp	W <sub>d4,1</sub> <sup>i</sup> *	w <sub>d4,1</sub> <sup>i</sup> (m.s <sup>-1</sup> )
		sample (g)			sample (g)		(kg.m <sup>-2</sup> .s <sup>-1</sup> )		
550	0.067	0.003	0.0001	3.68E-05	0.015	0.0002	1.41E-06	0.573	0.038
462.5	0.056	0.016	0.0004	1.96E-04	0.09	0.0009	8.46E-06	0.768	0.043
390	0.046	0.17	0.0047	2.09E-03	1.08	0.0108	1.01E-04	1.047	0.049
327.5	0.038	1.27	0.0354	1.56E-02	5.79	0.0581	5.44E-04	0.925	0.035
275	0.030	8.6	0.2396	1.06E-01	30.48	0.3058	2.86E-03	0.900	0.027
231	0.024	15.58	0.4341	1.91E-01	42.14	0.4227	3.96E-03	0.875	0.021
181	0.016	9.2	0.2563	1.13E-01	18.6	0.1866	1.75E-03	0.945	0.015
106.5	0.007	1.05	0.0293	1.29E-02	1.49	0.0149	1.40E-04	1.630	0.011
		35.889		4.40E-01	99.685		9.37E-03		

Size (μm)	w <sub>s</sub> (m.s <sup>-1</sup> )	Near-bed	χ <sub>4,2</sub> <sup>i</sup> (g.l <sup>-1</sup> )	C <sub>b4,2</sub> <sup>i</sup> (g.l <sup>-1</sup> )	Deposited	δ <sub>4,2</sub> <sup>i</sup> exp	Δ <sub>4,2</sub> <sup>i</sup> exp	W <sub>d4,2</sub> <sup>i</sup> *	w <sub>d4,2</sub> <sup>i</sup> (m.s <sup>-1</sup> )
		sample (g)			sample (g)		(kg.m <sup>-2</sup> .s <sup>-1</sup> )		
550	0.067	0.001	0.0000	1.24E-05	0.01	0.0001	7.23E-07	0.876	0.059
462.5	0.056	0.009	0.0003	1.11E-04	0.067	0.0007	4.85E-06	0.778	0.044
390	0.046	0.12	0.0045	1.48E-03	0.97	0.0097	7.02E-05	1.019	0.047
327.5	0.038	0.92	0.0345	1.14E-02	5.64	0.0565	4.08E-04	0.951	0.036
275	0.030	6.63	0.2483	8.19E-02	31.92	0.3196	2.31E-03	0.936	0.028
231	0.024	11.34	0.4247	1.40E-01	40.17	0.4022	2.91E-03	0.877	0.021
181	0.016	6.78	0.2539	8.37E-02	19.62	0.1964	1.42E-03	1.034	0.017
106.5	0.007	0.9	0.0337	1.11E-02	1.49	0.0149	1.08E-04	1.454	0.010
		26.7		3.30E-01	99.887		7.23E-03		

Size (μm)	w <sub>s</sub> (m.s <sup>-1</sup> )	Near-bed	χ <sub>5</sub> <sup>i</sup> (g.l <sup>-1</sup> )	C <sub>b5</sub> <sup>i</sup> (g.l <sup>-1</sup> )	Deposited	δ <sub>5</sub> <sup>i</sup> exp	Δ <sub>5</sub> <sup>i</sup> exp	W <sub>d5</sub> <sup>i</sup> *	w <sub>d5</sub> <sup>i</sup> (m.s <sup>-1</sup> )
		sample (g)			sample (g)		(kg.m <sup>-2</sup> .s <sup>-1</sup> )		
550	0.067	0.006	0.0000	0.00E+00	0.01	0.0001	6.69E-07		
462.5	0.056	0.006	0.0002	7.57E-05	0.053	0.0005	3.55E-06	0.836	0.047
390	0.046	0.08	0.0032	1.01E-03	0.79	0.0079	5.29E-05	1.127	0.052
327.5	0.038	0.63	0.0255	7.95E-03	5.2	0.0522	3.48E-04	1.160	0.044
275	0.030	5.44	0.2199	6.87E-02	30.35	0.3046	2.03E-03	0.982	0.030
231	0.024	10.55	0.4265	1.33E-01	42.24	0.4239	2.83E-03	0.897	0.021
181	0.016	7.09	0.2866	8.95E-02	19.85	0.1992	1.33E-03	0.906	0.015
106.5	0.007	0.94	0.0380	1.19E-02	1.16	0.0116	7.77E-05	0.981	0.007
		24.736		3.12E-01	99.653		6.67E-03		

Size (μm)	w <sub>s</sub> (m.s <sup>-1</sup> )	Near-bed	χ <sub>7</sub> <sup>i</sup> (g.l <sup>-1</sup> )	C <sub>b7</sub> <sup>i</sup> (g.l <sup>-1</sup> )	Deposited	δ <sub>7</sub> <sup>i</sup> exp	Δ <sub>7</sub> <sup>i</sup> exp	W <sub>d7</sub> <sup>i</sup> *	w <sub>d7</sub> <sup>i</sup> (m.s <sup>-1</sup> )
		sample (g)			sample (g)		(kg.m <sup>-2</sup> .s <sup>-1</sup> )		
550	0.067	0.002	0.0000	0.00E+00	0.01	0.0001	2.34E-07		
462.5	0.056	0.002	0.0002	2.53E-05	0.035	0.0004	8.19E-07	0.577	0.032
390	0.046	0.019	0.0016	2.40E-04	0.32	0.0032	7.49E-06	0.670	0.031
327.5	0.038	0.15	0.0123	1.90E-03	2.37	0.0238	5.54E-05	0.774	0.029
275	0.030	1.86	0.1519	2.35E-02	24.28	0.2440	5.68E-04	0.801	0.024
231	0.024	4.97	0.4060	6.29E-02	44.07	0.4428	1.03E-03	0.693	0.016
181	0.016	4.38	0.3578	5.54E-02	25.31	0.2543	5.92E-04	0.652	0.011
106.5	0.007	0.86	0.0703	1.09E-02	3.12	0.0314	7.30E-05	1.006	0.007
		12.241		1.55E-01	99.515		2.33E-03		

E3b	Location	Deposited $\Delta_i$		Sample	Volume of $C_{ij}$		time (mn) 42 $t^{\circ}$ ( $^{\circ}$ C) 19.3 $v$ ( $m^2 \cdot s^{-1}$ ) 1.02E-06 $\rho_w$ ( $kg \cdot m^{-3}$ ) 1000 $\rho_s$ ( $kg \cdot m^{-3}$ ) 2700 $g$ ( $m \cdot s^{-2}$ ) 9.8 $\rho_s^*$ 1.7		
	x (m)	(kg)	( $kg \cdot m \cdot s^{-2}$ )	mass (g)	water (l)	( $g \cdot l^{-1}$ )			
	trap#3.1	0.9	2.03	0.0154	37.41	83.0			0.451
	trap#3.2	1.1	1.258	0.0096	38.22	81.5			0.469
	trap#4.1	1.3	0.907	0.0069	31.01	82.3			0.377
	trap#4.2	1.5	0.828	0.0063	16.89	82.8			0.204
	trap#5	1.74	0.916	0.0046	19.15	82.7			0.232
	trap#7	2.62	0.277	0.0016	6.56	79.0			0.083

Size ( $\mu m$ )	$w_s$ ( $m \cdot s^{-1}$ )	Near-bed $\chi_{3,1}^i$ ( $g \cdot l^{-1}$ )		$C_{b3,1}^i$ ( $g \cdot l^{-1}$ )	Deposited $\delta_{3,1}^i$ exp		$\Delta_{3,1}^i$ exp	$w_{d3,1}^*$	$w_{d3,1}$ ( $m \cdot s^{-1}$ )
		sample (g)	sample (g)		sample (g)	( $kg \cdot m^{-2} \cdot s^{-1}$ )			
550	0.068	0.0025	0.0001	3.04E-05	0.0055	0.0001	1.71E-06	0.831	0.056
462.5	0.057	0.014	0.0004	1.70E-04	0.0355	0.0007	1.10E-05	1.140	0.065
390	0.047	0.16	0.0043	1.95E-03	0.37	0.0074	1.15E-04	1.252	0.059
327.5	0.038	1.06	0.0286	1.29E-02	2.18	0.0439	6.77E-04	1.368	0.052
275	0.031	8.53	0.2304	1.04E-01	14.01	0.2820	4.35E-03	1.365	0.042
231	0.024	16.25	0.4390	1.98E-01	21.94	0.4416	6.82E-03	1.426	0.034
181	0.017	10.06	0.2718	1.23E-01	10.72	0.2158	3.33E-03	1.621	0.027
106.5	0.007	0.94	0.0254	1.14E-02	0.42	0.0085	1.30E-04	1.662	0.011
		37.0165		4.51E-01	49.681		1.54E-02		

Average	
$w_d^*$	$w_d$ ( $m \cdot s^{-1}$ )
0.477	0.032
1.228	0.070
1.028	0.048
1.165	0.045
1.097	0.034
1.040	0.025
1.102	0.018
1.463	0.010

Size ( $\mu m$ )	$w_s$ ( $m \cdot s^{-1}$ )	Near-bed $\chi_{3,2}^i$ ( $g \cdot l^{-1}$ )		$C_{b3,2}^i$ ( $g \cdot l^{-1}$ )	Deposited $\delta_{3,2}^i$ exp		$\Delta_{3,2}^i$ exp	$w_{d3,2}^*$	$w_{d3,2}$ ( $m \cdot s^{-1}$ )
		sample (g)	sample (g)		sample (g)	( $kg \cdot m^{-2} \cdot s^{-1}$ )			
550	0.068	0.002	0.0001	2.48E-05	0.0045	0.0001	8.65E-07	0.517	0.035
462.5	0.057	0.007	0.0002	8.67E-05	0.032	0.0006	6.15E-06	1.251	0.071
390	0.047	0.1	0.0026	1.24E-03	0.3	0.0060	5.77E-05	0.988	0.047
327.5	0.038	0.84	0.0222	1.04E-02	2.15	0.0432	4.13E-04	1.036	0.040
275	0.031	8.33	0.2201	1.03E-01	14.38	0.2892	2.77E-03	0.873	0.027
231	0.024	16.73	0.4420	2.07E-01	21.78	0.4380	4.19E-03	0.837	0.020
181	0.017	10.9	0.2880	1.35E-01	10.46	0.2104	2.01E-03	0.888	0.015
106.5	0.007	0.94	0.0248	1.16E-02	0.62	0.0125	1.19E-04	1.493	0.010
		37.849		4.69E-01	49.7265		9.56E-03		

Size ( $\mu m$ )	$w_s$ ( $m \cdot s^{-1}$ )	Near-bed $\chi_{4,1}^i$ ( $g \cdot l^{-1}$ )		$C_{b4,1}^i$ ( $g \cdot l^{-1}$ )	Deposited $\delta_{4,1}^i$ exp		$\Delta_{4,1}^i$ exp	$w_{d4,1}^*$	$w_{d4,1}$ ( $m \cdot s^{-1}$ )
		sample (g)	sample (g)		sample (g)	( $kg \cdot m^{-2} \cdot s^{-1}$ )			
550	0.068	0.001	0.0000	1.23E-05	0.0015	0.0000	2.09E-07	0.252	0.017
462.5	0.057	0.0045	0.0001	5.53E-05	0.0145	0.0003	2.02E-06	0.645	0.037
390	0.047	0.06	0.0020	7.37E-04	0.18	0.0036	2.51E-05	0.723	0.034
327.5	0.038	0.51	0.0166	6.26E-03	1.51	0.0305	2.11E-04	0.876	0.034
275	0.031	6.09	0.1986	7.48E-02	12.87	0.2602	1.79E-03	0.782	0.024
231	0.024	13.51	0.4406	1.66E-01	22.19	0.4487	3.09E-03	0.772	0.019
181	0.017	9.58	0.3124	1.18E-01	12.06	0.2439	1.68E-03	0.852	0.014
106.5	0.007	0.91	0.0297	1.12E-02	0.63	0.0127	8.78E-05	1.146	0.008
		30.6655		3.77E-01	49.456		6.90E-03		

Size ( $\mu m$ )	$w_s$ ( $m \cdot s^{-1}$ )	Near-bed $\chi_{4,2}^i$ ( $g \cdot l^{-1}$ )		$C_{b4,2}^i$ ( $g \cdot l^{-1}$ )	Deposited $\delta_{4,2}^i$ exp		$\Delta_{4,2}^i$ exp	$w_{d4,2}^*$	$w_{d4,2}$ ( $m \cdot s^{-1}$ )
		sample (g)	sample (g)		sample (g)	( $kg \cdot m^{-2} \cdot s^{-1}$ )			
550	0.068	0.001	0.0001	1.22E-05	0.002	0.0000	2.53E-07	0.306	0.021
462.5	0.057	0.0015	0.0001	1.83E-05	0.008	0.0002	1.01E-06	0.972	0.055
390	0.047	0.021	0.0013	2.57E-04	0.14	0.0028	1.77E-05	1.463	0.069
327.5	0.038	0.21	0.0126	2.57E-03	1.25	0.0251	1.58E-04	1.605	0.062
275	0.031	2.55	0.1528	3.11E-02	12.16	0.2440	1.54E-03	1.607	0.049
231	0.024	7.09	0.4247	8.66E-02	22.7	0.4555	2.87E-03	1.371	0.033
181	0.017	6.04	0.3618	7.38E-02	12.71	0.2551	1.61E-03	1.298	0.022
106.5	0.007	0.78	0.0467	9.53E-03	0.86	0.0173	1.09E-04	1.662	0.011
		16.6935		2.04E-01	49.83		6.29E-03		

Size ( $\mu m$ )	$w_s$ ( $m \cdot s^{-1}$ )	Near-bed $\chi_{5,1}^i$ ( $g \cdot l^{-1}$ )		$C_{b5,1}^i$ ( $g \cdot l^{-1}$ )	Deposited $\delta_{5,1}^i$ exp		$\Delta_{5,1}^i$ exp	$w_{d5,1}^*$	$w_{d5,1}$ ( $m \cdot s^{-1}$ )
		sample (g)	sample (g)		sample (g)	( $kg \cdot m^{-2} \cdot s^{-1}$ )			
550	0.068	0.0005	0.0000	0.00E+00	0.002	0.0000	1.86E-07		
462.5	0.057	0.0005	0.0000	6.16E-06	0.008	0.0002	7.46E-07	2.134	0.121
390	0.047	0.018	0.0010	2.22E-04	0.1	0.0020	9.32E-06	0.892	0.042
327.5	0.038	0.16	0.0085	1.97E-03	0.95	0.0191	8.86E-05	1.171	0.045
275	0.031	2.7	0.1436	3.33E-02	10.67	0.2143	9.95E-04	0.974	0.030
231	0.024	8.16	0.4341	1.01E-01	22.46	0.4511	2.09E-03	0.862	0.021
181	0.017	6.95	0.3697	8.57E-02	14.63	0.2938	1.36E-03	0.950	0.016
106.5	0.007	0.81	0.0431	9.98E-03	0.97	0.0195	9.04E-05	1.321	0.009
		18.7985		2.32E-01	49.79		4.64E-03		

Size ( $\mu m$ )	$w_s$ ( $m \cdot s^{-1}$ )	Near-bed $\chi_{7,1}^i$ ( $g \cdot l^{-1}$ )		$C_{b7,1}^i$ ( $g \cdot l^{-1}$ )	Deposited $\delta_{7,1}^i$ exp		$\Delta_{7,1}^i$ exp	$w_{d7,1}^*$	$w_{d7,1}$ ( $m \cdot s^{-1}$ )
		sample (g)	sample (g)		sample (g)	( $kg \cdot m^{-2} \cdot s^{-1}$ )			
550	0.068		0.0000	0.00E+00		0.0000	0.00E+00		
462.5	0.057		0.0000	0.00E+00		0.0000	0.00E+00		
390	0.047	0.003	0.0005	3.91E-05	0.047	0.0009	1.56E-06	0.848	0.040
327.5	0.038	0.03	0.0047	3.91E-04	0.42	0.0085	1.40E-05	0.931	0.036
275	0.031	0.54	0.0847	7.04E-03	6.36	0.1282	2.11E-04	0.978	0.030
231	0.024	2.28	0.3578	2.97E-02	20.99	0.4232	6.97E-04	0.972	0.023
181	0.017	2.96	0.4645	3.86E-02	19.53	0.3938	6.49E-04	1.003	0.017
106.5	0.007	0.56	0.0879	7.30E-03	2.25	0.0454	7.48E-05	1.494	0.010
		6.373		8.31E-02	49.597		1.65E-03		

E4	Location	Deposited $\Delta_i$		Sample		Volume of $C_{bi}$		time (mn) 43 $t^o$ ( $^oC$ ) 19.4 $\nu$ ( $m^2.s^{-1}$ ) 1.02E-06 $\rho_w$ ( $kg.m^{-3}$ ) 1000 $\rho_s$ ( $kg.m^{-3}$ ) 2700 $g$ ( $m.s^{-2}$ ) 9.8 $\rho_s^*$ 1.7		
	x (m)	(kg)	( $kg.m.s^{-2}$ )	mass (g)	water (l)	( $g.l^{-1}$ )	( $g.l^{-1}$ )			
trap#3.1	0.9	1.877	0.0139	49.72	84.2	0.591				
trap#3.2	1.1	1.069	0.0079	22.69	83.0	0.273				
trap#4.1	1.3	0.744	0.0055	16.01	84.3	0.190				
trap#4.2	1.5	0.487	0.0036	13.31	84.3	0.158				
trap#5	1.74	0.429	0.0021	10.34	83.8	0.123				
trap#7	2.62	0.118	0.0007	3.61	83.0	0.043				

Average

$W_d^{1*}$	$W_d$ ( $m.s^{-1}$ )
0.518	0.035
0.675	0.038
0.762	0.036
1.066	0.041
1.222	0.038
1.141	0.028
1.138	0.019
1.282	0.009

Size ( $\mu m$ )	$w_s$ ( $m.s^{-1}$ )	Near-bed $\chi_{3,1}$ ( $g.l^{-1}$ )	$C_{b3,1}$ ( $g.l^{-1}$ )	Deposited $\delta_{3,1}$ exp	$\Delta_{3,1}$ exp	$W_{d3,1}^*$	$W_{d3,1}$ ( $m.s^{-1}$ )
		sample (g)		sample (g)	( $kg.m^{-2}.s^{-1}$ )		
550	0.068	0.009	0.0002	1.08E-04	0.0065	0.0001	1.82E-06
462.5	0.057	0.032	0.0006	3.83E-04	0.046	0.0009	1.29E-05
390	0.047	0.3	0.0061	3.59E-03	0.39	0.0078	1.09E-04
327.5	0.038	1.71	0.0346	2.05E-02	2.35	0.0472	6.57E-04
275	0.031	11.88	0.2407	1.42E-01	14.64	0.2938	4.10E-03
231	0.024	20.57	0.4168	2.46E-01	20.54	0.4123	5.75E-03
181	0.017	13.18	0.2671	1.58E-01	11.04	0.2216	3.09E-03
106.5	0.007	1.67	0.0338	2.00E-02	0.81	0.0163	2.27E-04
		49.351		5.91E-01	49.8225		1.39E-02

Size ( $\mu m$ )	$w_s$ ( $m.s^{-1}$ )	Near-bed $\chi_{3,2}$ ( $g.l^{-1}$ )	$C_{b3,2}$ ( $g.l^{-1}$ )	Deposited $\delta_{3,2}$ exp	$\Delta_{3,2}$ exp	$W_{d3,2}^*$	$W_{d3,2}$ ( $m.s^{-1}$ )
		sample (g)		sample (g)	( $kg.m^{-2}.s^{-1}$ )		
550	0.068	0.0005	0.0000	6.04E-06	0.003	0.0001	4.77E-07
462.5	0.057	0.004	0.0002	4.83E-05	0.018	0.0004	2.86E-06
390	0.047	0.046	0.0020	5.56E-04	0.21	0.0042	3.34E-05
327.5	0.038	0.37	0.0164	4.47E-03	1.63	0.0327	2.59E-04
275	0.031	3.98	0.1759	4.81E-02	12.13	0.2431	1.93E-03
231	0.024	8.98	0.3970	1.09E-01	20.97	0.4202	3.34E-03
181	0.017	7.72	0.3413	9.33E-02	13.86	0.2777	2.20E-03
106.5	0.007	1.52	0.0672	1.84E-02	1.08	0.0216	1.72E-04
		22.6205		2.73E-01	49.901		7.94E-03

Size ( $\mu m$ )	$w_s$ ( $m.s^{-1}$ )	Near-bed $\chi_{4,1}$ ( $g.l^{-1}$ )	$C_{b4,1}$ ( $g.l^{-1}$ )	Deposited $\delta_{4,1}$ exp	$\Delta_{4,1}$ exp	$W_{d4,1}^*$	$W_{d4,1}$ ( $m.s^{-1}$ )
		sample (g)		sample (g)	( $kg.m^{-2}.s^{-1}$ )		
550	0.068	0.0005	0.0000	6.02E-06	0.004	0.0001	4.43E-07
462.5	0.057	0.002	0.0001	2.41E-05	0.006	0.0001	6.64E-07
390	0.047	0.015	0.0010	1.81E-04	0.1	0.0020	1.11E-05
327.5	0.038	0.14	0.0089	1.69E-03	0.9	0.0180	9.96E-05
275	0.031	1.88	0.1193	2.27E-02	9.72	0.1948	1.08E-03
231	0.024	5.81	0.3687	7.00E-02	22	0.4408	2.44E-03
181	0.017	6.4	0.4062	7.71E-02	15.28	0.3062	1.69E-03
106.5	0.007	1.51	0.0958	1.82E-02	1.9	0.0381	2.10E-04
		15.7575		1.90E-01	49.91		5.52E-03

Size ( $\mu m$ )	$w_s$ ( $m.s^{-1}$ )	Near-bed $\chi_{4,2}$ ( $g.l^{-1}$ )	$C_{b4,2}$ ( $g.l^{-1}$ )	Deposited $\delta_{4,2}$ exp	$\Delta_{4,2}$ exp	$W_{d4,2}^*$	$W_{d4,2}$ ( $m.s^{-1}$ )
		sample (g)		sample (g)	( $kg.m^{-2}.s^{-1}$ )		
550	0.068	0.004	0.0003	4.82E-05	0.002	0.0000	1.45E-07
462.5	0.057	0.001	0.0001	1.20E-05	0.006	0.0001	4.34E-07
390	0.047	0.025	0.0019	3.01E-04	0.0685	0.0014	4.96E-06
327.5	0.038	0.14	0.0107	1.69E-03	0.73	0.0146	5.29E-05
275	0.031	1.63	0.1243	1.96E-02	8.99	0.1800	6.51E-04
231	0.024	4.91	0.3745	5.91E-02	21.17	0.4239	1.53E-03
181	0.017	5.17	0.3944	6.22E-02	17.25	0.3454	1.25E-03
106.5	0.007	1.23	0.0938	1.48E-02	1.72	0.0344	1.25E-04
		13.11		1.58E-01	49.9365		3.62E-03

Size ( $\mu m$ )	$w_s$ ( $m.s^{-1}$ )	Near-bed $\chi_5^1$ ( $g.l^{-1}$ )	$C_{b5}^1$ ( $g.l^{-1}$ )	Deposited $\delta_5^1$ exp	$\Delta_5^1$ exp	$W_{d5}^1$	$W_{d5}^1$ ( $m.s^{-1}$ )
		sample (g)		sample (g)	( $kg.m^{-2}.s^{-1}$ )		
550	0.068	0.0005	0.0000	0.00E+00	0.006	0.0001	2.56E-07
462.5	0.057	0.0005	0.0000	6.10E-06	0.005	0.0001	2.14E-07
390	0.047	0.005	0.0005	6.10E-05	0.063	0.0013	2.69E-06
327.5	0.038	0.05	0.0049	6.10E-04	0.63	0.0127	2.69E-05
275	0.031	0.91	0.0900	1.11E-02	7.82	0.1573	3.34E-04
231	0.024	3.47	0.3430	4.23E-02	20.89	0.4202	8.92E-04
181	0.017	4.46	0.4409	5.44E-02	18.02	0.3625	7.70E-04
106.5	0.007	1.22	0.1206	1.49E-02	2.28	0.0459	9.74E-05
		10.1155		1.23E-01	49.714		2.12E-03

Size ( $\mu m$ )	$w_s$ ( $m.s^{-1}$ )	Near-bed $\chi_7^1$ ( $g.l^{-1}$ )	$C_{b7}^1$ ( $g.l^{-1}$ )	Deposited $\delta_7^1$ exp	$\Delta_7^1$ exp	$W_{d7}^1$	$W_{d7}^1$ ( $m.s^{-1}$ )
		sample (g)		sample (g)	( $kg.m^{-2}.s^{-1}$ )		
550	0.068	0.0025	0.0007	3.14E-05	0.006	0.0001	8.32E-08
462.5	0.057	0.01	0.0009	0.00E+00	0.007	0.0001	9.70E-08
390	0.047	0.01	0.0029	1.26E-04	0.029	0.0006	4.02E-07
327.5	0.038	0.01	0.0029	1.26E-04	0.19	0.0038	2.63E-06
275	0.031	0.09	0.0260	1.13E-03	3.72	0.0752	5.16E-05
231	0.024	0.61	0.1762	7.66E-03	16.37	0.3310	2.27E-04
181	0.017	1.72	0.4968	2.16E-02	23.89	0.4830	3.31E-04
106.5	0.007	1.02	0.2946	1.28E-02	5.25	0.1061	7.28E-05
		3.4625		4.35E-02	49.462		6.86E-04

E5

	Location	Deposited $\Delta_i$		Sample Volume of $C_{bi}$		
	x (m)	(kg)	(kg.m.s <sup>-2</sup> )	mass (g)	water (l)	(g.l <sup>-1</sup> )
trap#3.1	0.9	2.772	0.0220	74.15	76.1	0.974
trap#3.2	1.1	1.905	0.0160	64.21	75.8	0.847
trap#4.1	1.3	2.001	0.0159	59.26	76.0	0.780
trap#4.2	1.5	1.407	0.0118	49.79	75.5	0.660
trap#5	1.74	1.515	0.0082	41.23	75.6	0.545
trap#7	2.62	0.677	0.0045	13.74	74.9	0.183

time (mn)	39
t° (°C)	19.3
v (m <sup>2</sup> .s <sup>-1</sup> )	1.02E-06
ρw (kg.m <sup>-3</sup> )	1000
ρs (kg.m <sup>-3</sup> )	2700
g (m.s <sup>-2</sup> )	9.8
ρs*	1.7

Average

w <sub>d</sub> *	w <sub>d</sub> (m.s <sup>-1</sup> )
0.472	0.032
0.661	0.038
0.712	0.034
0.806	0.031
0.779	0.024
0.801	0.019
0.876	0.015
1.027	0.007

Size (μm)	w <sub>s</sub> (m.s <sup>-1</sup> )	Near-bed $\chi_{3,1}$ (g.l <sup>-1</sup> )		C <sub>b3,1</sub> (g.l <sup>-1</sup> )		Deposited $\delta_{3,1}$ exp		$\Delta_{3,1}$ exp		w <sub>d3,1</sub> *	w <sub>d3,1</sub> (m.s <sup>-1</sup> )
		sample (g)		sample (g)		sample (g)		(kg.m <sup>-2</sup> .s <sup>-1</sup> )			
550	0.068	0.0305	0.0004	4.02E-04	0.0265	0.0005	1.17E-05	0.429	0.029		
462.5	0.057	0.18	0.0024	2.37E-03	0.135	0.0027	5.94E-05	0.441	0.025		
390	0.047	1.35	0.0183	1.78E-02	1.18	0.0236	5.19E-04	0.619	0.029		
327.5	0.038	5.72	0.0775	7.55E-02	4.78	0.0958	2.10E-03	0.727	0.028		
275	0.031	24.14	0.3269	3.18E-01	18	0.3607	7.92E-03	0.811	0.025		
231	0.024	28.93	0.3918	3.82E-01	19.05	0.3818	8.38E-03	0.910	0.022		
181	0.017	12.78	0.1731	1.69E-01	6.62	0.1327	2.91E-03	1.030	0.017		
106.5	0.007	0.71	0.0096	9.37E-03	0.11	0.0022	4.84E-05	0.754	0.005		
		73.8405		9.74E-01		49.9015		2.20E-02			

Size (μm)	w <sub>s</sub> (m.s <sup>-1</sup> )	Near-bed $\chi_{3,2}$ (g.l <sup>-1</sup> )		C <sub>b3,2</sub> (g.l <sup>-1</sup> )		Deposited $\delta_{3,2}$ exp		$\Delta_{3,2}$ exp		w <sub>d3,2</sub> *	w <sub>d3,2</sub> (m.s <sup>-1</sup> )
		sample (g)		sample (g)		sample (g)		(kg.m <sup>-2</sup> .s <sup>-1</sup> )			
550	0.068	0.0155	0.0002	2.05E-04	0.021	0.0004	6.74E-06	0.486	0.033		
462.5	0.057	0.09	0.0014	1.19E-03	0.17	0.0034	5.46E-05	0.806	0.046		
390	0.047	0.84	0.0131	1.11E-02	1.17	0.0234	3.75E-04	0.716	0.034		
327.5	0.038	4.23	0.0662	5.61E-02	4.76	0.0952	1.53E-03	0.710	0.027		
275	0.031	20.29	0.3175	2.69E-01	18.15	0.3631	5.82E-03	0.706	0.022		
231	0.024	25.84	0.4043	3.43E-01	18.76	0.3753	6.02E-03	0.728	0.018		
181	0.017	11.91	0.1863	1.58E-01	6.79	0.1358	2.18E-03	0.823	0.014		
106.5	0.007	0.7	0.0110	9.28E-03	0.17	0.0034	5.46E-05	0.857	0.006		
		63.9155		8.47E-01		49.991		1.60E-02			

Size (μm)	w <sub>s</sub> (m.s <sup>-1</sup> )	Near-bed $\chi_{4,1}$ (g.l <sup>-1</sup> )		C <sub>b4,1</sub> (g.l <sup>-1</sup> )		Deposited $\delta_{4,1}$ exp		$\Delta_{4,1}$ exp		w <sub>d4,1</sub> *	w <sub>d4,1</sub> (m.s <sup>-1</sup> )
		sample (g)		sample (g)		sample (g)		(kg.m <sup>-2</sup> .s <sup>-1</sup> )			
550	0.068	0.009	0.0002	1.19E-04	0.016	0.0003	5.09E-06	0.635	0.043		
462.5	0.057	0.06	0.0010	7.92E-04	0.115	0.0023	3.66E-05	0.815	0.046		
390	0.047	0.62	0.0105	8.18E-03	0.98	0.0197	3.12E-04	0.809	0.038		
327.5	0.038	3.31	0.0560	4.37E-02	4.53	0.0909	1.44E-03	0.861	0.033		
275	0.031	18.78	0.3176	2.48E-01	17.6	0.3533	5.60E-03	0.736	0.023		
231	0.024	23.94	0.4049	3.16E-01	19.43	0.3900	6.18E-03	0.811	0.020		
181	0.017	11.71	0.1980	1.55E-01	6.94	0.1393	2.21E-03	0.852	0.014		
106.5	0.007	0.7	0.0118	9.24E-03	0.21	0.0042	6.68E-05	1.055	0.007		
		59.129		7.80E-01		49.821		1.59E-02			

Size (μm)	w <sub>s</sub> (m.s <sup>-1</sup> )	Near-bed $\chi_{4,2}$ (g.l <sup>-1</sup> )		C <sub>b4,2</sub> (g.l <sup>-1</sup> )		Deposited $\delta_{4,2}$ exp		$\Delta_{4,2}$ exp		w <sub>d4,2</sub> *	w <sub>d4,2</sub> (m.s <sup>-1</sup> )
		sample (g)		sample (g)		sample (g)		(kg.m <sup>-2</sup> .s <sup>-1</sup> )			
550	0.068	0.0065	0.0001	8.66E-05	0.011	0.0002	2.61E-06	0.446	0.030		
462.5	0.057	0.0385	0.0008	5.13E-04	0.06	0.0012	1.42E-05	0.489	0.028		
390	0.047	0.405	0.0082	5.39E-03	0.72	0.0144	1.71E-04	0.671	0.032		
327.5	0.038	2.37	0.0478	3.16E-02	3.75	0.0750	8.89E-04	0.734	0.028		
275	0.031	13.05	0.2634	1.74E-01	16.77	0.3354	3.97E-03	0.745	0.023		
231	0.024	22.4	0.4521	2.98E-01	20.62	0.4124	4.89E-03	0.678	0.016		
181	0.017	10.5	0.2119	1.40E-01	7.72	0.1544	1.83E-03	0.780	0.013		
106.5	0.007	0.775	0.0156	1.03E-02	0.35	0.0070	8.29E-05	1.171	0.008		
		49.545		6.60E-01		50.001		1.18E-02			

Size (μm)	w <sub>s</sub> (m.s <sup>-1</sup> )	Near-bed $\chi_{5}$ (g.l <sup>-1</sup> )		C <sub>b5</sub> (g.l <sup>-1</sup> )		Deposited $\delta_{5}$ exp		$\Delta_{5}$ exp		w <sub>d5</sub> *	w <sub>d5</sub> (m.s <sup>-1</sup> )
		sample (g)		sample (g)		sample (g)		(kg.m <sup>-2</sup> .s <sup>-1</sup> )			
550	0.068	0.0025	0.0001	3.32E-05	0.005	0.0001	8.21E-07	0.366	0.025		
462.5	0.057	0.0175	0.0004	2.32E-04	0.0535	0.0011	8.78E-06	0.667	0.038		
390	0.047	0.24	0.0058	3.19E-03	0.55	0.0110	9.03E-05	0.602	0.028		
327.5	0.038	1.54	0.0375	2.04E-02	3.29	0.0661	5.40E-04	0.689	0.026		
275	0.031	11.4	0.2776	1.51E-01	16.35	0.3283	2.68E-03	0.578	0.018		
231	0.024	17.29	0.4210	2.30E-01	20.56	0.4128	3.38E-03	0.609	0.015		
181	0.017	9.9	0.2411	1.31E-01	8.68	0.1743	1.43E-03	0.647	0.011		
106.5	0.007	0.68	0.0166	9.03E-03	0.32	0.0064	5.25E-05	0.849	0.006		
		41.07		5.45E-01		49.8085		8.18E-03			

Size (μm)	w <sub>s</sub> (m.s <sup>-1</sup> )	Near-bed $\chi_{7}$ (g.l <sup>-1</sup> )		C <sub>b7</sub> (g.l <sup>-1</sup> )		Deposited $\delta_{7}$ exp		$\Delta_{7}$ exp		w <sub>d7</sub> *	w <sub>d7</sub> (m.s <sup>-1</sup> )
		sample (g)		sample (g)		sample (g)		(kg.m <sup>-2</sup> .s <sup>-1</sup> )			
550	0.068	0.0000	0.0000	0.00E+00	0.0035	0.0001	3.15E-07				
462.5	0.057	0.0025	0.0002	3.38E-05	0.016	0.0003	1.44E-06	0.751	0.043		
390	0.047	0.024	0.0018	3.25E-04	0.145	0.0029	1.31E-05	0.854	0.040		
327.5	0.038	0.21	0.0155	2.84E-03	1.35	0.0270	1.22E-04	1.116	0.043		
275	0.031	2.4	0.1770	3.25E-02	12.13	0.2430	1.09E-03	1.096	0.034		
231	0.024	5.77	0.4256	7.80E-02	22.36	0.4480	2.01E-03	1.068	0.026		
181	0.017	4.65	0.3430	6.29E-02	13.15	0.2635	1.18E-03	1.123	0.019		
106.5	0.007	0.5	0.0369	6.76E-03	0.76	0.0152	6.84E-05	1.475	0.010		
		13.5565		1.83E-01		49.9145		4.49E-03			

E6	Location	Deposited $\Delta_i$		Sample	Volume of $C_{bi}$		time (mn) 6 $t^{\circ}$ ( $^{\circ}$ C) 19.2 $v$ ( $m^2 \cdot s^{-1}$ ) 1.02E-06 $\rho_w$ ( $kg \cdot m^{-3}$ ) 1000 $\rho_s$ ( $kg \cdot m^{-3}$ ) 2700 $g$ ( $m \cdot s^{-2}$ ) 9.8 $\rho_s^*$ 1.7	
	x (m)	(kg)	( $kg \cdot m \cdot s^{-2}$ )	mass (g)	water (l)	( $g \cdot l^{-1}$ )		
trap#3.1	0.9	4.822	0.2483	109.32	12.7	8.588		
trap#3.2	1.1	3.56	0.1949	91.07	12.7	7.154		
trap#4.1	1.3	2.531	0.1303	65.57	12.7	5.151		
trap#4.2	1.5	2.138	0.1170	60.76	12.6	4.828		
trap#5	1.74	2.044	0.0717	37.42	12.6	2.973		
trap#7	2.62	0.698	0.0301	20.8	12.7	1.634		

Size ( $\mu m$ )	$w_s$ ( $m \cdot s^{-1}$ )	Near-bed $\chi_{3,1}$ ( $g \cdot l^{-1}$ ) $C_{b3,1}$ ( $g \cdot l^{-1}$ )			Deposited $\delta_{3,1}$ exp $\Delta_{3,1}$ exp			$w_{d3,1}^*$	$w_{d3,1}$ ( $m \cdot s^{-1}$ )
		sample (g)			sample (g)		( $kg \cdot m^{-2} \cdot s^{-1}$ )		
550	0.067	0.075	0.0015	1.29E-02	0.18	0.0036	8.96E-04	1.030	0.070
462.5	0.057	0.335	0.0067	5.76E-02	0.65	0.0130	3.24E-03	0.992	0.056
390	0.047	1.51	0.0302	2.60E-01	2.58	0.0517	1.28E-02	1.051	0.049
327.5	0.038	4.98	0.0997	8.56E-01	6.96	0.1395	3.46E-02	1.057	0.040
275	0.031	18.51	0.3705	3.18E+00	18.7	0.3748	9.31E-02	0.955	0.029
231	0.024	17.28	0.3458	2.97E+00	15.91	0.3189	7.92E-02	1.106	0.027
181	0.017	6.85	0.1371	1.18E+00	4.81	0.0964	2.39E-02	1.215	0.020
106.5	0.007	0.425	0.0085	7.30E-02	0.1	0.0020	4.98E-04	0.996	0.007
		49.965		8.59E+00	49.89		2.48E-01		

Average	
$w_d^*$	$w_d$ ( $m \cdot s^{-1}$ )
0.775	0.052
0.885	0.050
0.947	0.045
0.971	0.037
0.917	0.028
0.948	0.023
1.037	0.017
1.364	0.009

Size ( $\mu m$ )	$w_s$ ( $m \cdot s^{-1}$ )	Near-bed $\chi_{3,2}$ ( $g \cdot l^{-1}$ ) $C_{b3,2}$ ( $g \cdot l^{-1}$ )			Deposited $\delta_{3,2}$ exp $\Delta_{3,2}$ exp			$w_{d3,2}^*$	$w_{d3,2}$ ( $m \cdot s^{-1}$ )
		sample (g)			sample (g)		( $kg \cdot m^{-2} \cdot s^{-1}$ )		
550	0.067	0.053	0.0011	7.60E-03	0.12	0.0024	4.68E-04	0.912	0.062
462.5	0.057	0.21	0.0042	3.01E-02	0.62	0.0124	2.42E-03	1.416	0.080
390	0.047	1.16	0.0233	1.66E-01	2.54	0.0508	9.91E-03	1.265	0.060
327.5	0.038	4.25	0.0852	6.10E-01	7.05	0.1411	2.75E-02	1.178	0.045
275	0.031	16.76	0.3361	2.40E+00	18.44	0.3691	7.19E-02	0.976	0.030
231	0.024	18.79	0.3768	2.70E+00	16.36	0.3275	6.38E-02	0.982	0.024
181	0.017	8.13	0.1630	1.17E+00	4.72	0.0945	1.84E-02	0.943	0.016
106.5	0.007	0.52	0.0104	7.46E-02	0.11	0.0022	4.29E-04	0.840	0.006
		49.873		7.15E+00	49.96		1.95E-01		

Size ( $\mu m$ )	$w_s$ ( $m \cdot s^{-1}$ )	Near-bed $\chi_{4,1}$ ( $g \cdot l^{-1}$ ) $C_{b4,1}$ ( $g \cdot l^{-1}$ )			Deposited $\delta_{4,1}$ exp $\Delta_{4,1}$ exp			$w_{d4,1}^*$	$w_{d4,1}$ ( $m \cdot s^{-1}$ )
		sample (g)			sample (g)		( $kg \cdot m^{-2} \cdot s^{-1}$ )		
550	0.067	0.021	0.0003	1.66E-03	0.046	0.0009	1.20E-04	1.073	0.072
462.5	0.057	0.16	0.0025	1.26E-02	0.22	0.0044	5.74E-04	0.802	0.045
390	0.047	0.94	0.0144	7.42E-02	1.34	0.0268	3.50E-03	1.001	0.047
327.5	0.038	4.36	0.0668	3.44E-01	5.18	0.1037	1.35E-02	1.025	0.039
275	0.031	22.98	0.3520	1.81E+00	18.09	0.3620	4.72E-02	0.849	0.026
231	0.024	24.51	0.3755	1.93E+00	18.15	0.3632	4.73E-02	1.015	0.024
181	0.017	11.62	0.1780	9.17E-01	6.67	0.1335	1.74E-02	1.134	0.019
106.5	0.007	0.69	0.0106	5.44E-02	0.27	0.0054	7.04E-04	1.890	0.013
		65.281		5.15E+00	49.966		1.30E-01		

Size ( $\mu m$ )	$w_s$ ( $m \cdot s^{-1}$ )	Near-bed $\chi_{4,2}$ ( $g \cdot l^{-1}$ ) $C_{b4,2}$ ( $g \cdot l^{-1}$ )			Deposited $\delta_{4,2}$ exp $\Delta_{4,2}$ exp			$w_{d4,2}^*$	$w_{d4,2}$ ( $m \cdot s^{-1}$ )
		sample (g)			sample (g)		( $kg \cdot m^{-2} \cdot s^{-1}$ )		
550	0.067	0.013	0.0002	1.04E-03	0.03	0.0006	7.02E-05	1.003	0.068
462.5	0.057	0.12	0.0020	9.58E-03	0.16	0.0032	3.75E-04	0.690	0.039
390	0.047	0.9	0.0149	7.18E-02	1.12	0.0224	2.62E-03	0.776	0.037
327.5	0.038	4.11	0.0679	3.28E-01	4.44	0.0888	1.04E-02	0.828	0.032
275	0.031	19.29	0.3188	1.54E+00	18.63	0.3727	4.36E-02	0.925	0.028
231	0.024	24.73	0.4087	1.97E+00	18.65	0.3731	4.37E-02	0.918	0.022
181	0.017	10.69	0.1767	8.53E-01	6.69	0.1339	1.57E-02	1.097	0.018
106.5	0.007	0.65	0.0107	5.19E-02	0.26	0.0052	6.09E-04	1.715	0.012
		60.503		4.83E+00	49.98		1.17E-01		

Size ( $\mu m$ )	$w_s$ ( $m \cdot s^{-1}$ )	Near-bed $\chi_{5,1}$ ( $g \cdot l^{-1}$ ) $C_{b5,1}$ ( $g \cdot l^{-1}$ )			Deposited $\delta_{5,1}$ exp $\Delta_{5,1}$ exp			$w_{d5,1}^*$	$w_{d5,1}$ ( $m \cdot s^{-1}$ )
		sample (g)			sample (g)		( $kg \cdot m^{-2} \cdot s^{-1}$ )		
550	0.067	0.008	0.0002	6.40E-04	0.019	0.0004	2.73E-05	0.631	0.043
462.5	0.057	0.041	0.0011	3.28E-03	0.11	0.0022	1.58E-04	0.849	0.048
390	0.047	0.35	0.0094	2.80E-02	0.84	0.0168	1.21E-03	0.915	0.043
327.5	0.038	1.88	0.0506	1.51E-01	3.81	0.0763	5.47E-03	0.949	0.036
275	0.031	11.21	0.3018	8.97E-01	18.08	0.3620	2.60E-02	0.944	0.029
231	0.024	15.07	0.4058	1.21E+00	19.12	0.3829	2.75E-02	0.944	0.023
181	0.017	7.96	0.2143	6.37E-01	7.56	0.1514	1.09E-02	1.018	0.017
106.5	0.007	0.62	0.0167	4.96E-02	0.4	0.0080	5.74E-04	1.691	0.012
		37.139		2.97E+00	49.939		7.17E-02		

Size ( $\mu m$ )	$w_s$ ( $m \cdot s^{-1}$ )	Near-bed $\chi_{7,1}$ ( $g \cdot l^{-1}$ ) $C_{b7,1}$ ( $g \cdot l^{-1}$ )			Deposited $\delta_{7,1}$ exp $\Delta_{7,1}$ exp			$w_{d7,1}^*$	$w_{d7,1}$ ( $m \cdot s^{-1}$ )
		sample (g)			sample (g)		( $kg \cdot m^{-2} \cdot s^{-1}$ )		
550	0.067	0.0015	0.0001	1.18E-04	0.006	0.0001	3.62E-06		
462.5	0.057	0.006	0.0003	4.74E-04	0.025	0.0005	1.51E-05	0.562	0.032
390	0.047	0.07	0.0034	5.52E-03	0.29	0.0058	1.75E-04	0.673	0.032
327.5	0.038	0.51	0.0246	4.03E-02	2.02	0.0405	1.22E-03	0.791	0.030
275	0.031	4.73	0.2285	3.73E-01	16.18	0.3244	9.77E-03	0.854	0.026
231	0.024	9.025	0.4359	7.12E-01	20.58	0.4126	1.24E-02	0.724	0.017
181	0.017	5.71	0.2758	4.51E-01	10.17	0.2039	6.14E-03	0.814	0.014
106.5	0.007	0.65	0.0314	5.13E-02	0.61	0.0122	3.68E-04	1.049	0.007
		20.7025		1.63E+00	49.881		3.01E-02		

E7	Location	Deposited $\Delta_1$		Sample	Volume of $C_{b1}$		time (mn) 32 $t^0$ (°C) 20.1 $v$ (m <sup>2</sup> .s <sup>-1</sup> ) 1E-06 $\rho_w$ (kg.m <sup>-3</sup> ) 1000 $\rho_s$ (kg.m <sup>-3</sup> ) 2680 $g$ (m.s <sup>-2</sup> ) 9.8 $\rho_s^*$ 1.68	
	x (m)	(kg)	(kg.m.s <sup>-2</sup> )	mass (g)	water (l)	(g.l <sup>-1</sup> )		
trap#3.1	0.9	0.445	0.0043	102.3	63.6	1.607		
trap#3.2	1.1	0.473	0.0049	107.7	63.6	1.692		
trap#4.1	1.3	0.474	0.0046	115	63.6	1.807		
trap#4.2	1.5	0.539	0.0055	107.8	63.6	1.694		
trap#5	1.74	0.629	0.0041	102.9	63.6	1.617		
trap#7	2.62	0.58	0.0047	96.5	63.6	1.516		

Size ( $\mu\text{m}$ )	$w_a$ (m.s <sup>-1</sup> )	Near-bed $\chi_{3,1}$ (g.l <sup>-1</sup> )		$C_{b3,1}$ (g.l <sup>-1</sup> )		Deposited $\delta_{3,1}$ exp		$\Delta_{3,1}$ exp		$w_{d3,1}^*$	$w_{d3,1}$ (m.s <sup>-1</sup> )
		sample (g)		sample (g)		sample (g)		(kg.m <sup>-2</sup> .s <sup>-1</sup> )			
275	0.0307	0.055	0.0011	1.81E-03	0.61	0.0124	5.32E-05	0.959	0.0295		
231	0.0242	0.11	0.0022	3.61E-03	1.03	0.0209	8.99E-05	1.028	0.0249		
196	0.0190	0.215	0.0044	7.06E-03	1.28	0.0260	1.12E-04	0.832	0.0158		
165	0.0145	0.88	0.0180	2.89E-02	3.24	0.0658	2.83E-04	0.673	0.0098		
137.5	0.0108	1.91	0.0390	6.27E-02	5.33	0.1083	4.65E-04	0.689	0.0074		
115.5	0.0080	4.13	0.0844	1.36E-01	7.85	0.1595	6.85E-04	0.634	0.0051		
98	0.0059	7.25	0.1481	2.38E-01	10.02	0.2035	8.75E-04	0.619	0.0037		
82.5	0.0043	8.87	0.1812	2.91E-01	8.37	0.1700	7.31E-04	0.580	0.0025		
69	0.0031	7.69	0.1571	2.52E-01	5.61	0.1140	4.90E-04	0.628	0.0019		
58	0.0022	5.31	0.1085	1.74E-01	2.76	0.0561	2.41E-04	0.624	0.0014		
49	0.0016	4.1	0.0837	1.35E-01	1.83	0.0372	1.60E-04	0.742	0.0012		
41.5	0.0012	3.48	0.0711	1.14E-01	0.8	0.0163	6.98E-05	0.529	0.0006		
19	0.0002	4.96	0.1013	1.63E-01	0.5	0.0102	4.36E-05	1.090	0.0003		
		48.96		1.61E+00		49.23		4.30E-03			

Average	
$w_d^*$	$w_d$ (m.s <sup>-1</sup> )
0.577	0.0177
0.646	0.0156
0.620	0.0118
0.599	0.0087
0.610	0.0066
0.642	0.0051
0.612	0.0036
0.657	0.0028
0.719	0.0022
0.669	0.0015
0.881	0.0014
0.751	0.0009
1.405	0.0003

Size ( $\mu\text{m}$ )	$w_a$ (m.s <sup>-1</sup> )	Near-bed $\chi_{3,2}$ (g.l <sup>-1</sup> )		$C_{b3,2}$ (g.l <sup>-1</sup> )		Deposited $\delta_{3,2}$ exp		$\Delta_{3,2}$ exp		$w_{d3,2}^*$	$w_{d3,2}$ (m.s <sup>-1</sup> )
		sample (g)		sample (g)		sample (g)		(kg.m <sup>-2</sup> .s <sup>-1</sup> )			
275	0.0307	0.09	0.0019	3.13E-03	0.58	0.0118	5.73E-05	0.595	0.0183		
231	0.0242	0.165	0.0034	5.74E-03	0.9	0.0183	8.89E-05	0.640	0.0155		
196	0.0190	0.3	0.0062	1.04E-02	1.2	0.0244	1.19E-04	0.597	0.0114		
165	0.0145	1.11	0.0228	3.86E-02	3.48	0.0708	3.44E-04	0.612	0.0089		
137.5	0.0108	2.37	0.0488	8.25E-02	6.29	0.1281	6.22E-04	0.700	0.0075		
115.5	0.0080	4.38	0.0901	1.53E-01	8.12	0.1653	8.02E-04	0.660	0.0053		
98	0.0059	8.02	0.1650	2.79E-01	9.45	0.1924	9.34E-04	0.563	0.0033		
82.5	0.0043	8.31	0.1710	2.89E-01	8.04	0.1637	7.95E-04	0.635	0.0027		
69	0.0031	7.41	0.1525	2.58E-01	5.43	0.1105	5.37E-04	0.673	0.0021		
58	0.0022	5.31	0.1092	1.85E-01	2.62	0.0533	2.59E-04	0.632	0.0014		
49	0.0016	3.52	0.0724	1.23E-01	1.73	0.0352	1.71E-04	0.873	0.0014		
41.5	0.0012	3.14	0.0646	1.09E-01	0.84	0.0171	8.30E-05	0.657	0.0008		
19	0.0002	4.48	0.0922	1.56E-01	0.44	0.0090	4.35E-05	1.134	0.0003		
		48.605		1.69E+00		49.12		4.85E-03			

Size ( $\mu\text{m}$ )	$w_a$ (m.s <sup>-1</sup> )	Near-bed $\chi_{4,1}$ (g.l <sup>-1</sup> )		$C_{b4,1}$ (g.l <sup>-1</sup> )		Deposited $\delta_{4,1}$ exp		$\Delta_{4,1}$ exp		$w_{d4,1}^*$	$w_{d4,1}$ (m.s <sup>-1</sup> )
		sample (g)		sample (g)		sample (g)		(kg.m <sup>-2</sup> .s <sup>-1</sup> )			
275	0.0307	0.11	0.0023	4.10E-03	0.44	0.0090	4.11E-05	0.326	0.0100		
231	0.0242	0.21	0.0043	7.82E-03	0.81	0.0165	7.57E-05	0.399	0.0097		
196	0.0190	0.37	0.0076	1.38E-02	1.15	0.0235	1.07E-04	0.410	0.0078		
165	0.0145	1.36	0.0280	5.07E-02	3.49	0.0712	3.26E-04	0.442	0.0064		
137.5	0.0108	2.61	0.0538	9.72E-02	5.39	0.1100	5.03E-04	0.481	0.0052		
115.5	0.0080	4.82	0.0994	1.80E-01	8.85	0.1806	8.27E-04	0.578	0.0046		
98	0.0059	8.29	0.1709	3.09E-01	9.45	0.1929	8.83E-04	0.481	0.0029		
82.5	0.0043	8	0.1649	2.98E-01	8.33	0.1700	7.78E-04	0.604	0.0026		
69	0.0031	7	0.1443	2.61E-01	5.62	0.1147	5.25E-04	0.651	0.0020		
58	0.0022	4.98	0.1027	1.86E-01	2.56	0.0522	2.39E-04	0.582	0.0013		
49	0.0016	3.58	0.0738	1.33E-01	1.7	0.0347	1.59E-04	0.745	0.0012		
41.5	0.0012	2.93	0.0604	1.09E-01	0.78	0.0159	7.29E-05	0.578	0.0007		
19	0.0002	4.24	0.0874	1.58E-01	0.43	0.0088	4.02E-05	1.034	0.0003		
		48.5		1.81E+00		49		4.58E-03			

Size ( $\mu\text{m}$ )	$w_a$ (m.s <sup>-1</sup> )	Near-bed $\chi_{4,2}$ (g.l <sup>-1</sup> )		$C_{b4,2}$ (g.l <sup>-1</sup> )		Deposited $\delta_{4,2}$ exp		$\Delta_{4,2}$ exp		$w_{d4,2}^*$	$w_{d4,2}$ (m.s <sup>-1</sup> )
		sample (g)		sample (g)		sample (g)		(kg.m <sup>-2</sup> .s <sup>-1</sup> )			
275	0.0307	0.06	0.0012	2.11E-03	0.215	0.0045	2.47E-05	0.381	0.0117		
231	0.0242	0.14	0.0029	4.93E-03	0.5	0.0104	5.75E-05	0.482	0.0117		
196	0.0190	0.24	0.0050	8.45E-03	0.8	0.0166	9.20E-05	0.572	0.0109		
165	0.0145	1.02	0.0212	3.59E-02	2.62	0.0545	3.01E-04	0.577	0.0084		
137.5	0.0108	2.2	0.0457	7.74E-02	4.96	0.1031	5.70E-04	0.684	0.0074		
115.5	0.0080	4.32	0.0898	1.52E-01	7.9	0.1642	9.08E-04	0.750	0.0060		
98	0.0059	8.1	0.1683	2.85E-01	10.09	0.2097	1.16E-03	0.685	0.0041		
82.5	0.0043	8.7	0.1808	3.06E-01	9.06	0.1883	1.04E-03	0.786	0.0034		
69	0.0031	7.36	0.1530	2.59E-01	5.95	0.1237	6.84E-04	0.855	0.0026		
58	0.0022	5.47	0.1137	1.93E-01	2.82	0.0586	3.24E-04	0.760	0.0017		
49	0.0016	3.76	0.0781	1.32E-01	1.84	0.0382	2.12E-04	1.000	0.0016		
41.5	0.0012	3.02	0.0628	1.06E-01	0.86	0.0179	9.89E-05	0.805	0.0009		
19	0.0002	3.73	0.0775	1.31E-01	0.49	0.0102	5.63E-05	1.745	0.0004		
		48.12		1.69E+00		48.105		5.53E-03			

Size ( $\mu\text{m}$ )	$w_s$ ( $\text{m}\cdot\text{s}^{-1}$ )	Near-bed			Deposited			$w_{d5}^*$	$w_{d5}$ ( $\text{m}\cdot\text{s}^{-1}$ )
		$\chi_5^1$ ( $\text{g}\cdot\Gamma^{-1}$ )	$C_{b5}^1$ ( $\text{g}\cdot\Gamma^{-1}$ )	sample (g)	$\delta_5^1$ exp	$\Delta_5^1$ exp	sample (g)		
275	0.0307	0.05	0.0010	1.68E-03	0.34	0.0069	2.87E-05	0.558	0.0171
231	0.0242	0.11	0.0023	3.69E-03	0.7	0.0143	5.92E-05	0.663	0.0160
196	0.0190	0.205	0.0043	6.87E-03	0.96	0.0196	8.12E-05	0.621	0.0118
165	0.0145	0.89	0.0185	2.98E-02	2.86	0.0584	2.42E-04	0.557	0.0081
137.5	0.0108	2.02	0.0419	6.77E-02	4.51	0.0921	3.81E-04	0.523	0.0056
115.5	0.0080	4.62	0.0958	1.55E-01	7.58	0.1549	6.41E-04	0.519	0.0041
98	0.0059	7.42	0.1538	2.49E-01	10.2	0.2084	8.62E-04	0.584	0.0035
82.5	0.0043	8.62	0.1787	2.89E-01	8.72	0.1781	7.37E-04	0.590	0.0026
69	0.0031	7.29	0.1511	2.44E-01	6.07	0.1240	5.13E-04	0.680	0.0021
58	0.0022	6.2	0.1285	2.08E-01	3.19	0.0652	2.70E-04	0.586	0.0013
49	0.0016	3.64	0.0755	1.22E-01	2.18	0.0445	1.84E-04	0.945	0.0015
41.5	0.0012	2.99	0.0620	1.00E-01	1.14	0.0233	9.64E-05	0.832	0.0010
19	0.0002	4.18	0.0867	1.40E-01	0.5	0.0102	4.23E-05	1.227	0.0003
		48.235		1.62E+00	48.95		4.14E-03		

Size ( $\mu\text{m}$ )	$w_s$ ( $\text{m}\cdot\text{s}^{-1}$ )	Near-bed			Deposited			$w_{d7}^*$	$w_{d7}$ ( $\text{m}\cdot\text{s}^{-1}$ )
		$\chi_7^1$ ( $\text{g}\cdot\Gamma^{-1}$ )	$C_{b7}^1$ ( $\text{g}\cdot\Gamma^{-1}$ )	sample (g)	$\delta_7^1$ exp	$\Delta_7^1$ exp	sample (g)		
275	0.0307	0.02	0.0004	6.26E-04	0.13	0.0026	1.24E-05	0.644	0.0198
231	0.0242	0.07	0.0014	2.19E-03	0.37	0.0075	3.53E-05	0.666	0.0161
196	0.0190	0.16	0.0033	5.01E-03	0.69	0.0140	6.59E-05	0.691	0.0131
165	0.0145	0.81	0.0167	2.54E-02	2.83	0.0576	2.70E-04	0.732	0.0106
137.5	0.0108	2.01	0.0415	6.30E-02	4.15	0.0844	3.96E-04	0.584	0.0063
115.5	0.0080	4.01	0.0828	1.26E-01	7.44	0.1514	7.10E-04	0.710	0.0057
98	0.0059	7.15	0.1477	2.24E-01	10.32	0.2100	9.85E-04	0.741	0.0044
82.5	0.0043	8.52	0.1760	2.67E-01	9.03	0.1837	8.62E-04	0.747	0.0032
69	0.0031	7.59	0.1568	2.38E-01	6.36	0.1294	6.07E-04	0.827	0.0026
58	0.0022	5.87	0.1213	1.84E-01	3.54	0.0720	3.38E-04	0.829	0.0018
49	0.0016	4.1	0.0847	1.28E-01	2.11	0.0429	2.01E-04	0.981	0.0016
41.5	0.0012	3.09	0.0638	9.68E-02	1.29	0.0262	1.23E-04	1.102	0.0013
19	0.0002	5.01	0.1035	1.57E-01	0.89	0.0181	8.50E-05	2.202	0.0005
		48.41		1.52E+00	49.15		4.69E-03		

G1	Location	Deposited $\Delta_j$		Sample	Volume of $C_{bj}$		time (mn)	42
	x (m)	(kg)	(kg.m.s <sup>-2</sup> )	mass (g)	water (l)	(g.l <sup>-1</sup> )		
trap#3.1	0.9	1.742	0.0132	44.3	82.7	0.536	$t^{\circ}$ (°C)	16.4
trap#3.2	1.1	1.633	0.0124	32.54	80.8	0.403	$v$ (m <sup>2</sup> .s <sup>-1</sup> )	1.1E-06
trap#4.1	1.3	1.385	0.0105	28.08	82.0	0.342	$\rho_w$ (kg.m <sup>-3</sup> )	1000
trap#4.2	1.5	0.874	0.0066	32.98	82.0	0.402	$\rho_s$ (kg.m <sup>-3</sup> )	2700
trap#5	1.74	1.173	0.0059	18.52	81.7	0.227	$g$ (m.s <sup>-2</sup> )	9.8
trap#7	2.62	0.422	0.0025	12.12	79.8	0.152	$\rho_s^*$	1.7

Size ( $\mu$ m)	$w_s$ (m.s <sup>-1</sup> )	Near-bed	$\chi_{3,1}$ (g.l <sup>-1</sup> )	$C_{b3,1}$ (g.l <sup>-1</sup> )	Deposited $\delta_{3,1}$ exp	$\Delta_{3,1}$ exp	$w_{d3,1}^*$	$w_{d3,1}$ (m.s <sup>-1</sup> )	
		sample (g)			sample (g)	(kg.m <sup>-2</sup> .s <sup>-1</sup> )			
550	0.066	0.012	0.0003	1.47E-04	0.008	0.0003	3.55E-06	0.366	0.024
462.5	0.055	0.078	0.0018	9.55E-04	0.079	0.0026	3.50E-05	0.665	0.037
390	0.046	0.56	0.0128	6.86E-03	0.545	0.0183	2.42E-04	0.772	0.035
327.5	0.037	2.93	0.0669	3.59E-02	2.76	0.0924	1.22E-03	0.923	0.034
275	0.029	14.52	0.3317	1.78E-01	10.73	0.3593	4.76E-03	0.909	0.027
231	0.023	16.6	0.3792	2.03E-01	11.12	0.3724	4.93E-03	1.052	0.024
181	0.016	8.26	0.1887	1.01E-01	4.4	0.1473	1.95E-03	1.213	0.019
106.5	0.006	0.82	0.0187	1.00E-02	0.22	0.0074	9.76E-05	1.510	0.010
		43.78		5.36E-01	29.862		1.32E-02		

Average

$w_{d3,1}^*$	$w_{d3,1}$ (m.s <sup>-1</sup> )
1.620	0.107
0.798	0.044
1.188	0.054
1.074	0.040
0.992	0.029
1.009	0.023
1.177	0.019
1.473	0.009

Size ( $\mu$ m)	$w_s$ (m.s <sup>-1</sup> )	Near-bed	$\chi_{3,2}$ (g.l <sup>-1</sup> )	$C_{b3,2}$ (g.l <sup>-1</sup> )	Deposited $\delta_{3,2}$ exp	$\Delta_{3,2}$ exp	$w_{d3,2}^*$	$w_{d3,2}$ (m.s <sup>-1</sup> )	
		sample (g)			sample (g)	(kg.m <sup>-2</sup> .s <sup>-1</sup> )			
550	0.066	0.004	0.0001	5.01E-05	0.006	0.0002	2.50E-06	0.756	0.050
462.5	0.055	0.037	0.0012	4.63E-04	0.033	0.0011	1.37E-05	0.537	0.030
390	0.046	0.27	0.0084	3.38E-03	0.49	0.0164	2.04E-04	1.321	0.060
327.5	0.037	1.71	0.0532	2.14E-02	2.46	0.0825	1.02E-03	1.293	0.048
275	0.029	9.73	0.3026	1.22E-01	10.14	0.3399	4.22E-03	1.176	0.035
231	0.023	12.91	0.4015	1.62E-01	11.43	0.3832	4.76E-03	1.276	0.029
181	0.016	6.71	0.2087	8.40E-02	5	0.1676	2.08E-03	1.556	0.025
106.5	0.006	0.78	0.0243	9.77E-03	0.27	0.0091	1.12E-04	1.788	0.012
		32.151		4.03E-01	29.829		1.24E-02		

Size ( $\mu$ m)	$w_s$ (m.s <sup>-1</sup> )	Near-bed	$\chi_{4,1}$ (g.l <sup>-1</sup> )	$C_{b4,1}$ (g.l <sup>-1</sup> )	Deposited $\delta_{4,1}$ exp	$\Delta_{4,1}$ exp	$w_{d4,1}^*$	$w_{d4,1}$ (m.s <sup>-1</sup> )	
		sample (g)			sample (g)	(kg.m <sup>-2</sup> .s <sup>-1</sup> )			
550	0.066	0.001	0.0000	1.24E-05	0.008	0.0003	2.82E-06	3.445	0.227
462.5	0.055	0.021	0.0008	2.60E-04	0.053	0.0018	1.87E-05	1.299	0.072
390	0.046	0.15	0.0054	1.86E-03	0.49	0.0164	1.72E-04	2.033	0.093
327.5	0.037	1.2	0.0434	1.49E-02	2.48	0.0829	8.73E-04	1.588	0.059
275	0.029	7.64	0.2764	9.47E-02	10.57	0.3534	3.72E-03	1.335	0.039
231	0.023	11.56	0.4182	1.43E-01	11.29	0.3775	3.97E-03	1.203	0.028
181	0.016	6.28	0.2272	7.78E-02	4.73	0.1581	1.66E-03	1.345	0.021
106.5	0.006	0.79	0.0286	9.79E-03	0.29	0.0097	1.02E-04	1.621	0.010
		27.642		3.42E-01	29.911		1.05E-02		

Size ( $\mu$ m)	$w_s$ (m.s <sup>-1</sup> )	Near-bed	$\chi_{4,2}$ (g.l <sup>-1</sup> )	$C_{b4,2}$ (g.l <sup>-1</sup> )	Deposited $\delta_{4,2}$ exp	$\Delta_{4,2}$ exp	$w_{d4,2}^*$	$w_{d4,2}$ (m.s <sup>-1</sup> )	
		sample (g)			sample (g)	(kg.m <sup>-2</sup> .s <sup>-1</sup> )			
550	0.066	0.001	0.0000	1.24E-05	0.012	0.0004	2.67E-06	3.271	0.216
462.5	0.055	0.018	0.0006	2.23E-04	0.07	0.0023	1.56E-05	1.267	0.070
390	0.046	0.165	0.0051	2.04E-03	0.48	0.0161	1.07E-04	1.146	0.052
327.5	0.037	1.41	0.0434	1.75E-02	2.21	0.0741	4.92E-04	0.762	0.028
275	0.029	9.33	0.2872	1.16E-01	9.77	0.3274	2.18E-03	0.639	0.019
231	0.023	13.71	0.4221	1.70E-01	11.94	0.4001	2.66E-03	0.679	0.016
181	0.016	7.05	0.2170	8.73E-02	5.08	0.1702	1.13E-03	0.814	0.013
106.5	0.006	0.8	0.0246	9.91E-03	0.28	0.0094	6.23E-05	0.978	0.006
		32.484		4.02E-01	29.842		6.64E-03		

Size ( $\mu$ m)	$w_s$ (m.s <sup>-1</sup> )	Near-bed	$\chi_5$ (g.l <sup>-1</sup> )	$C_{b5}$ (g.l <sup>-1</sup> )	Deposited $\delta_5$ exp	$\Delta_5$ exp	$w_{d5}^*$	$w_{d5}$ (m.s <sup>-1</sup> )	
		sample (g)			sample (g)	(kg.m <sup>-2</sup> .s <sup>-1</sup> )			
550	0.066	0.001	0.0001	1.25E-05	0.007	0.0002	1.39E-06	1.688	0.111
462.5	0.055	0.007	0.0004	8.76E-05	0.019	0.0006	3.78E-06	0.782	0.043
390	0.046	0.07	0.0039	8.76E-04	0.26	0.0087	5.18E-05	1.294	0.059
327.5	0.037	0.6	0.0331	7.51E-03	1.53	0.0512	3.05E-04	1.097	0.041
275	0.029	4.44	0.2451	5.56E-02	9.22	0.3088	1.84E-03	1.121	0.033
231	0.023	7.67	0.4233	9.60E-02	12.13	0.4063	2.42E-03	1.091	0.025
181	0.016	4.65	0.2567	5.82E-02	6.2	0.2077	1.23E-03	1.333	0.021
106.5	0.006	0.68	0.0375	8.51E-03	0.49	0.0164	9.76E-05	1.781	0.011
		18.118		2.27E-01	29.856		5.94E-03		

Size ( $\mu$ m)	$w_s$ (m.s <sup>-1</sup> )	Near-bed	$\chi_7$ (g.l <sup>-1</sup> )	$C_{b7}$ (g.l <sup>-1</sup> )	Deposited $\delta_7$ exp	$\Delta_7$ exp	$w_{d7}^*$	$w_{d7}$ (m.s <sup>-1</sup> )	
		sample (g)			sample (g)	(kg.m <sup>-2</sup> .s <sup>-1</sup> )			
550	0.066	0.001	0.0001	1.30E-05	0.002	0.0001	1.68E-07	0.197	0.013
462.5	0.055	0.0045	0.0004	5.84E-05	0.009	0.0003	7.58E-07	0.235	0.013
390	0.046	0.028	0.0024	3.63E-04	0.11	0.0037	9.26E-06	0.559	0.025
327.5	0.037	0.19	0.0162	2.47E-03	0.845	0.0283	7.12E-05	0.780	0.029
275	0.029	2.18	0.1863	2.83E-02	7.66	0.2569	6.45E-04	0.774	0.023
231	0.023	4.91	0.4195	6.37E-02	13.12	0.4400	1.10E-03	0.752	0.017
181	0.016	3.73	0.3187	4.84E-02	7.31	0.2452	6.16E-04	0.799	0.013
106.5	0.006	0.66	0.0564	8.56E-03	0.76	0.0255	6.40E-05	1.161	0.007
		11.7035		1.52E-01	29.816		2.51E-03		

G2b

	Location	Deposited $\Delta_i$		Sample		Volume of $C_{bi}$			
	x (m)	(kg)	(kg.m.s <sup>-2</sup> )	mass (g)	water (l)	(g.l <sup>-1</sup> )	(g.l <sup>-1</sup> )		
trap#3.1	0.9	1.666	0.0123	52.83	80.3	0.658		time (mn)	42
trap#3.2	1.1	1.151	0.0090	25.77	80.5	0.320		t <sup>o</sup> (°C)	19.4
trap#4.1	1.3	1.093	0.0080	25.07	80.2	0.313		v (m <sup>2</sup> .s <sup>-1</sup> )	1.02E-06
trap#4.2	1.5	0.645	0.0050	17.79	81.3	0.219		pw (kg.m <sup>-3</sup> )	1000
trap#5	1.74	0.782	0.0039	12.35	80.8	0.153		ps (kg.m <sup>-3</sup> )	2700
trap#7	2.62	0.193	0.0012	4.56	78.8	0.058		g (m.s <sup>-2</sup> )	9.8
								ps*	1.7

Average

$w_d^*$	$w_d$ (m.s <sup>-1</sup> )
0.472	0.032
0.804	0.046
0.902	0.043
1.078	0.041
1.045	0.032
1.054	0.025
1.037	0.017
1.180	0.008

Size (μm)	$w_s$ (m.s <sup>-1</sup> )	Near-bed $\chi_{3.1}$ (g.l <sup>-1</sup> )		$C_{b3.1}$ (g.l <sup>-1</sup> )		Deposited $\delta_{3.1}$ exp		$\Delta_{3.1}$ exp		$w_{d3.1}^*$	$w_{d3.1}$ (m.s <sup>-1</sup> )
		sample (g)		sample (g)		sample (g)		(kg.m <sup>-2</sup> .s <sup>-1</sup> )			
550	0.068	0.012	0.0002	1.50E-04	0.0115	0.0002	2.84E-06	0.280	0.019		
462.5	0.057	0.07	0.0013	8.76E-04	0.09	0.0018	2.22E-05	0.447	0.025		
390	0.047	0.63	0.0120	7.89E-03	0.72	0.0145	1.78E-04	0.478	0.023		
327.5	0.038	2.92	0.0556	3.66E-02	3.36	0.0677	8.30E-04	0.591	0.023		
275	0.031	14.17	0.2697	1.77E-01	16.44	0.3313	4.06E-03	0.745	0.023		
231	0.024	22.95	0.4368	2.87E-01	20.21	0.4073	4.99E-03	0.719	0.017		
181	0.017	11.03	0.2099	1.38E-01	8.48	0.1709	2.09E-03	0.903	0.015		
106.5	0.007	0.76	0.0145	9.51E-03	0.31	0.0062	7.66E-05	1.171	0.008		
		52.542		6.58E-01	49.6215		1.23E-02				

Size (μm)	$w_s$ (m.s <sup>-1</sup> )	Near-bed $\chi_{3.2}$ (g.l <sup>-1</sup> )		$C_{b3.2}$ (g.l <sup>-1</sup> )		Deposited $\delta_{3.2}$ exp		$\Delta_{3.2}$ exp		$w_{d3.2}^*$	$w_{d3.2}$ (m.s <sup>-1</sup> )
		sample (g)		sample (g)		sample (g)		(kg.m <sup>-2</sup> .s <sup>-1</sup> )			
550	0.068	0.002	0.0001	2.51E-05	0.0085	0.0002	1.55E-06	0.916	0.062		
462.5	0.057	0.013	0.0005	1.63E-04	0.0615	0.0012	1.12E-05	1.214	0.069		
390	0.047	0.11	0.0043	1.38E-03	0.48	0.0097	8.77E-05	1.348	0.064		
327.5	0.038	0.75	0.0294	9.41E-03	2.96	0.0601	5.41E-04	1.498	0.058		
275	0.031	5.81	0.2276	7.29E-02	15.3	0.3107	2.80E-03	1.249	0.038		
231	0.024	10.67	0.4180	1.34E-01	21.29	0.4324	3.89E-03	1.202	0.029		
181	0.017	7.51	0.2942	9.42E-02	8.81	0.1789	1.61E-03	1.018	0.017		
106.5	0.007	0.66	0.0259	8.28E-03	0.33	0.0067	6.03E-05	1.060	0.007		
		25.525		3.20E-01	49.24		9.00E-03				

Size (μm)	$w_s$ (m.s <sup>-1</sup> )	Near-bed $\chi_{4.1}$ (g.l <sup>-1</sup> )		$C_{b4.1}$ (g.l <sup>-1</sup> )		Deposited $\delta_{4.1}$ exp		$\Delta_{4.1}$ exp		$w_{d4.1}^*$	$w_{d4.1}$ (m.s <sup>-1</sup> )
		sample (g)		sample (g)		sample (g)		(kg.m <sup>-2</sup> .s <sup>-1</sup> )			
550	0.068	0.001	0.0000	1.26E-05	0.0025	0.0001	4.07E-07	0.479	0.032		
462.5	0.057	0.0045	0.0002	5.66E-05	0.032	0.0006	5.21E-06	1.621	0.092		
390	0.047	0.0535	0.0022	6.73E-04	0.3	0.0061	4.89E-05	1.539	0.073		
327.5	0.038	0.5	0.0201	6.29E-03	1.84	0.0373	3.00E-04	1.241	0.048		
275	0.031	5.06	0.2036	6.37E-02	13.37	0.2709	2.18E-03	1.113	0.034		
231	0.024	10.56	0.4250	1.33E-01	22.16	0.4490	3.61E-03	1.123	0.027		
181	0.017	7.96	0.3203	1.00E-01	11.12	0.2253	1.81E-03	1.076	0.018		
106.5	0.007	0.71	0.0286	8.94E-03	0.53	0.0107	8.63E-05	1.406	0.010		
		24.849		3.13E-01	49.3545		8.04E-03				

Size (μm)	$w_s$ (m.s <sup>-1</sup> )	Near-bed $\chi_{4.2}$ (g.l <sup>-1</sup> )		$C_{b4.2}$ (g.l <sup>-1</sup> )		Deposited $\delta_{4.2}$ exp		$\Delta_{4.2}$ exp		$w_{d4.2}^*$	$w_{d4.2}$ (m.s <sup>-1</sup> )
		sample (g)		sample (g)		sample (g)		(kg.m <sup>-2</sup> .s <sup>-1</sup> )			
550	0.068	0.0015	0.0001	1.87E-05	0.0045	0.0001	4.58E-07	0.362	0.024		
462.5	0.057	0.005	0.0003	6.23E-05	0.0195	0.0004	1.98E-06	0.561	0.032		
390	0.047	0.0525	0.0030	6.54E-04	0.21	0.0042	2.14E-05	0.692	0.033		
327.5	0.038	0.39	0.0222	4.86E-03	1.58	0.0319	1.61E-04	0.861	0.033		
275	0.031	3.58	0.2040	4.46E-02	12.09	0.2439	1.23E-03	0.897	0.028		
231	0.024	7.35	0.4188	9.16E-02	22.85	0.4609	2.32E-03	1.049	0.025		
181	0.017	5.63	0.3208	7.02E-02	12.13	0.2447	1.23E-03	1.047	0.018		
106.5	0.007	0.54	0.0308	6.73E-03	0.69	0.0139	7.02E-05	1.517	0.010		
		17.549		2.19E-01	49.574		5.04E-03				

Size (μm)	$w_s$ (m.s <sup>-1</sup> )	Near-bed $\chi_{5}$ (g.l <sup>-1</sup> )		$C_{b5}$ (g.l <sup>-1</sup> )		Deposited $\delta_5$ exp		$\Delta_5$ exp		$w_{d5}^*$	$w_{d5}$ (m.s <sup>-1</sup> )
		sample (g)		sample (g)		sample (g)		(kg.m <sup>-2</sup> .s <sup>-1</sup> )			
550	0.068	0.001	0.0001	1.26E-05	0.0035	0.0001	2.77E-07	0.324	0.022		
462.5	0.057	0.002	0.0002	2.53E-05	0.0145	0.0003	1.15E-06	0.799	0.045		
390	0.047	0.0245	0.0020	3.10E-04	0.17	0.0034	1.34E-05	0.921	0.043		
327.5	0.038	0.16	0.0132	2.02E-03	1.28	0.0258	1.01E-04	1.304	0.050		
275	0.031	2	0.1655	2.53E-02	11.58	0.2337	9.16E-04	1.179	0.036		
231	0.024	4.87	0.4029	6.16E-02	21.95	0.4429	1.74E-03	1.166	0.028		
181	0.017	4.34	0.3590	5.49E-02	13.73	0.2770	1.09E-03	1.178	0.020		
106.5	0.007	0.69	0.0571	8.72E-03	0.83	0.0167	6.56E-05	1.095	0.008		
		12.0875		1.53E-01	49.558		3.92E-03				

Size (μm)	$w_s$ (m.s <sup>-1</sup> )	Near-bed $\chi_{7}$ (g.l <sup>-1</sup> )		$C_{b7}$ (g.l <sup>-1</sup> )		Deposited $\delta_7$ exp		$\Delta_7$ exp		$w_{d7}^*$	$w_{d7}$ (m.s <sup>-1</sup> )
		sample (g)		sample (g)		sample (g)		(kg.m <sup>-2</sup> .s <sup>-1</sup> )			
550	0.068	0.00125	0.0000	0.00E+00	0.0045	0.0001	1.09E-07	0.184	0.010		
462.5	0.057	0.0055	0.0003	1.62E-05	0.007	0.0001	1.69E-07	0.432	0.020		
390	0.047	0.03	0.0012	7.11E-05	0.06	0.0012	1.45E-05	0.973	0.037		
327.5	0.038	0.03	0.0067	3.88E-04	0.6	0.0122	1.45E-05	1.088	0.033		
275	0.031	0.44	0.0983	5.69E-03	7.88	0.1598	1.90E-04	1.063	0.026		
231	0.024	1.6	0.3574	2.07E-02	22.03	0.4468	5.32E-04	0.998	0.017		
181	0.017	1.92	0.4289	2.48E-02	17.25	0.3499	4.16E-04	0.832	0.006		
106.5	0.007	0.48	0.1072	6.20E-03	1.47	0.0298	3.55E-05				
		4.47675		5.79E-02	49.3015		1.19E-03				

G3	Location	Deposited $\Delta_i$		Sample	Volume of $C_{b_i}$		time (mn) 43 $t^0$ (°C) 18.1 $v$ (m <sup>2</sup> .s <sup>-1</sup> ) 1.05E-06 $\rho_w$ (kg.m <sup>-3</sup> ) 1000 $\rho_s$ (kg.m <sup>-3</sup> ) 2700 $g$ (m.s <sup>-2</sup> ) 9.8 $\rho_s^*$ 1.7	
	x (m)	(kg)	(kg.m.s <sup>-2</sup> )	mass (g)	water (l)	(g.l <sup>-1</sup> )		
trap#3.1	0.9	1.482	0.0110	23.69	84.5	0.280		
trap#3.2	1.1	0.876	0.0065	18.81	83.5	0.225		
trap#4.1	1.3	0.641	0.0048	19.68	84.2	0.234		
trap#4.2	1.5	0.437	0.0032	11.11	84.0	0.132		
trap#5	1.74	0.463	0.0023	8.47	84.3	0.100		
trap#7	2.62	0.105	0.0006	3.61	82.8	0.044		

Size ( $\mu\text{m}$ )	$w_s$ (m.s <sup>-1</sup> )	Near-bed $\chi_{3,1}$ (g.l <sup>-1</sup> )		$C_{b3,1}$ (g.l <sup>-1</sup> )	Deposited $\delta_{3,1}$ exp		$\Delta_{3,1}$ exp	$w_{d3,1}^*$	$w_{d3,1}$ (m.s <sup>-1</sup> )
		sample (g)	sample (g)	sample (g)	sample (g)	(kg.m <sup>-2</sup> .s <sup>-1</sup> )			
550	0.067	0.0035	0.0001	4.20E-05	0.016	0.0003	3.52E-06	1.253	0.084
462.5	0.056	0.012	0.0005	1.44E-04	0.075	0.0015	1.65E-05	2.042	0.115
390	0.047	0.1	0.0043	1.20E-03	0.55	0.0110	1.21E-04	2.168	0.101
327.5	0.038	0.54	0.0231	6.49E-03	2.42	0.0484	5.33E-04	2.174	0.082
275	0.030	4.37	0.1872	5.25E-02	13.37	0.2675	2.94E-03	1.858	0.056
231	0.024	9.38	0.4018	1.13E-01	20.8	0.4162	4.58E-03	1.715	0.041
181	0.016	7.63	0.3268	9.16E-02	11.91	0.2383	2.62E-03	1.743	0.029
106.5	0.007	1.31	0.0561	1.57E-02	0.84	0.0168	1.85E-04	1.759	0.012
		23.3455		2.80E-01	49.981		1.10E-02		

Average	
$w_{d3,1}^*$	$w_{d3,1}$ (m.s <sup>-1</sup> )
1.128	0.075
0.917	0.051
1.013	0.047
1.332	0.050
1.245	0.038
1.178	0.028
1.260	0.021
1.662	0.011

Size ( $\mu\text{m}$ )	$w_s$ (m.s <sup>-1</sup> )	Near-bed $\chi_{3,2}$ (g.l <sup>-1</sup> )		$C_{b3,2}$ (g.l <sup>-1</sup> )	Deposited $\delta_{3,2}$ exp		$\Delta_{3,2}$ exp	$w_{d3,2}^*$	$w_{d3,2}$ (m.s <sup>-1</sup> )
		sample (g)	sample (g)	sample (g)	sample (g)	(kg.m <sup>-2</sup> .s <sup>-1</sup> )			
550	0.067	0.001	0.0001	1.22E-05	0.017	0.0003	2.23E-06	2.735	0.183
462.5	0.056	0.01	0.0005	1.22E-04	0.037	0.0007	4.85E-06	0.710	0.040
390	0.047	0.07	0.0038	8.52E-04	0.35	0.0070	4.58E-05	1.157	0.054
327.5	0.038	0.39	0.0211	4.75E-03	1.81	0.0364	2.37E-04	1.322	0.050
275	0.030	3.35	0.1810	4.08E-02	10.64	0.2142	1.39E-03	1.132	0.034
231	0.024	7.38	0.3987	8.98E-02	20.99	0.4226	2.75E-03	1.292	0.031
181	0.016	6.17	0.3333	7.51E-02	14.31	0.2881	1.87E-03	1.520	0.025
106.5	0.007	1.14	0.0616	1.39E-02	1.51	0.0304	1.98E-04	2.133	0.014
		18.511		2.25E-01	49.664		6.50E-03		

Size ( $\mu\text{m}$ )	$w_s$ (m.s <sup>-1</sup> )	Near-bed $\chi_{4,1}$ (g.l <sup>-1</sup> )		$C_{b4,1}$ (g.l <sup>-1</sup> )	Deposited $\delta_{4,1}$ exp		$\Delta_{4,1}$ exp	$w_{d4,1}^*$	$w_{d4,1}$ (m.s <sup>-1</sup> )
		sample (g)	sample (g)	sample (g)	sample (g)	(kg.m <sup>-2</sup> .s <sup>-1</sup> )			
550	0.067	0.001	0.0001	1.21E-05	0.008	0.0002	7.66E-07	0.945	0.063
462.5	0.056	0.0055	0.0003	6.66E-05	0.021	0.0004	2.01E-06	0.538	0.030
390	0.047	0.052	0.0027	6.30E-04	0.17	0.0034	1.63E-05	0.555	0.026
327.5	0.038	0.31	0.0161	3.76E-03	1.49	0.0300	1.43E-04	1.005	0.038
275	0.030	3.25	0.1684	3.94E-02	10.37	0.2086	9.93E-04	0.835	0.025
231	0.024	7.96	0.4125	9.65E-02	20.37	0.4097	1.95E-03	0.853	0.020
181	0.016	6.55	0.3394	7.94E-02	15.5	0.3118	1.48E-03	1.139	0.019
106.5	0.007	1.17	0.0606	1.42E-02	1.79	0.0360	1.71E-04	1.809	0.012
		19.2985		2.34E-01	49.719		4.76E-03		

Size ( $\mu\text{m}$ )	$w_s$ (m.s <sup>-1</sup> )	Near-bed $\chi_{4,2}$ (g.l <sup>-1</sup> )		$C_{b4,2}$ (g.l <sup>-1</sup> )	Deposited $\delta_{4,2}$ exp		$\Delta_{4,2}$ exp	$w_{d4,2}^*$	$w_{d4,2}$ (m.s <sup>-1</sup> )
		sample (g)	sample (g)	sample (g)	sample (g)	(kg.m <sup>-2</sup> .s <sup>-1</sup> )			
550	0.067	0.001	0.0001	1.22E-05	0.005	0.0001	3.26E-07	0.399	0.027
462.5	0.056	0.001	0.0001	1.22E-05	0.009	0.0002	5.87E-07	0.857	0.048
390	0.047	0.012	0.0011	1.47E-04	0.12	0.0024	7.83E-06	1.149	0.053
327.5	0.038	0.08	0.0074	9.77E-04	0.86	0.0173	5.61E-05	1.520	0.057
275	0.030	1.15	0.1061	1.40E-02	8.3	0.1669	5.42E-04	1.278	0.039
231	0.024	3.82	0.3526	4.66E-02	20	0.4021	1.30E-03	1.181	0.028
181	0.016	4.68	0.4320	5.71E-02	17.82	0.3583	1.16E-03	1.240	0.020
106.5	0.007	1.09	0.1006	1.33E-02	2.62	0.0527	1.71E-04	1.922	0.013
		10.834		1.32E-01	49.734		3.24E-03		

Size ( $\mu\text{m}$ )	$w_s$ (m.s <sup>-1</sup> )	Near-bed $\chi_{5,1}$ (g.l <sup>-1</sup> )		$C_{b5,1}$ (g.l <sup>-1</sup> )	Deposited $\delta_{5,1}$ exp		$\Delta_{5,1}$ exp	$w_{d5,1}^*$	$w_{d5,1}$ (m.s <sup>-1</sup> )
		sample (g)	sample (g)	sample (g)	sample (g)	(kg.m <sup>-2</sup> .s <sup>-1</sup> )			
550	0.067	0.001	0.0001	1.22E-05	0.0055	0.0001	2.53E-07	0.310	0.021
462.5	0.056	0.001	0.0001	1.22E-05	0.0065	0.0001	2.99E-07	0.437	0.025
390	0.047	0.012	0.0015	1.46E-04	0.09	0.0018	4.13E-06	0.609	0.028
327.5	0.038	0.06	0.0073	7.30E-04	0.67	0.0134	3.08E-05	1.115	0.042
275	0.030	0.77	0.0933	9.37E-03	8.38	0.1679	3.85E-04	1.361	0.041
231	0.024	2.77	0.3356	3.37E-02	20.69	0.4146	9.50E-04	1.190	0.028
181	0.016	3.66	0.4434	4.45E-02	17.86	0.3579	8.20E-04	1.122	0.018
106.5	0.007	0.98	0.1187	1.19E-02	2.2	0.0441	1.01E-04	1.268	0.008
		8.254		1.00E-01	49.902		2.29E-03		

Size ( $\mu\text{m}$ )	$w_s$ (m.s <sup>-1</sup> )	Near-bed $\chi_{7,1}$ (g.l <sup>-1</sup> )		$C_{b7,1}$ (g.l <sup>-1</sup> )	Deposited $\delta_{7,1}$ exp		$\Delta_{7,1}$ exp	$w_{d7,1}^*$	$w_{d7,1}$ (m.s <sup>-1</sup> )
		sample (g)	sample (g)	sample (g)	sample (g)	(kg.m <sup>-2</sup> .s <sup>-1</sup> )			
550	0.067		0.0000	0.00E+00	0.0085	0.0002	1.04E-07		
462.5	0.056		0.0000	0.00E+00	0.018	0.0004	2.21E-07		
390	0.047	0.0025	0.0008	3.57E-05	0.06	0.0012	7.36E-07	0.443	0.021
327.5	0.038	0.009	0.0029	1.29E-04	0.34	0.0068	4.17E-06	0.859	0.032
275	0.030	0.12	0.0393	1.71E-03	4.23	0.0850	5.19E-05	1.003	0.030
231	0.024	0.68	0.2228	9.71E-03	15.75	0.3167	1.93E-04	0.839	0.020
181	0.016	1.55	0.5079	2.21E-02	23.52	0.4729	2.89E-04	0.794	0.013
106.5	0.007	0.69	0.2261	9.86E-03	5.81	0.1168	7.13E-05	1.082	0.007
		3.0515		4.36E-02	49.7365		6.10E-04		

G4	Location	Deposited $\Delta_i$		Sample	Volume of $C_{bi}$		time (mn)	43
	x (m)	(kg)	(kg.m.s <sup>-2</sup> )	mass (g)	water (l)	(g.l <sup>-1</sup> )		
trap#3.1	0.9	2.471	0.0178	54.88	82.8	0.663	$t^o$ (°C)	18.2
trap#3.2	1.1	1.707	0.0130	72.17	81.7	0.884	$v$ (m <sup>2</sup> .s <sup>-1</sup> )	1.05E-06
trap#4.1	1.3	1.752	0.0126	76.76	82.0	0.936	$\rho_w$ (kg.m <sup>-3</sup> )	1000
trap#4.2	1.5	1.807	0.0138	44.6	82.7	0.540	$\rho_s$ (kg.m <sup>-3</sup> )	2700
trap#5	1.74	1.881	0.0092	44.53	82.3	0.541	$g$ (m.s <sup>-2</sup> )	9.8
trap#7	2.62	0.993	0.0060	20.98	80.5	0.261	$\rho_s^*$	1.7

Size ( $\mu$ m)	$w_s$ (m.s <sup>-1</sup> )	Near-bed $\chi_{3,1}$ (g.l <sup>-1</sup> )		$C_{b3,1}$ (g.l <sup>-1</sup> )		Deposited $\delta_{3,1}$ exp		$\Delta_{3,1}$ exp		$w_{d3,1}^*$	$w_{d3,1}$ (m.s <sup>-1</sup> )
		sample (g)				sample (g)		(kg.m <sup>-2</sup> .s <sup>-1</sup> )			
550	0.067	0.044	0.0008	5.35E-04	0.065	0.0013	2.32E-05	0.648	0.043		
462.5	0.056	0.23	0.0042	2.80E-03	0.36	0.0072	1.29E-04	0.819	0.046		
390	0.047	1.41	0.0259	1.71E-02	1.92	0.0386	6.86E-04	0.859	0.040		
327.5	0.038	5.14	0.0943	6.25E-02	5.64	0.1135	2.02E-03	0.852	0.032		
275	0.030	18.12	0.3326	2.20E-01	18.01	0.3624	6.43E-03	0.966	0.029		
231	0.024	20.71	0.3801	2.52E-01	17.22	0.3465	6.15E-03	1.029	0.024		
181	0.016	5.61	0.1030	6.82E-02	5.95	0.1197	2.13E-03	1.895	0.031		
106.5	0.007	3.22	0.0591	3.92E-02	0.53	0.0107	1.89E-04	0.722	0.005		
		54.484		6.63E-01	49.695		1.78E-02				

Average	
$w_d^*$	$w_d$ (m.s <sup>-1</sup> )
0.476	0.032
0.639	0.036
0.684	0.032
0.714	0.027
0.726	0.022
0.794	0.019
1.139	0.019
1.033	0.007

Size ( $\mu$ m)	$w_s$ (m.s <sup>-1</sup> )	Near-bed $\chi_{3,2}$ (g.l <sup>-1</sup> )		$C_{b3,2}$ (g.l <sup>-1</sup> )		Deposited $\delta_{3,2}$ exp		$\Delta_{3,2}$ exp		$w_{d3,2}^*$	$w_{d3,2}$ (m.s <sup>-1</sup> )
		sample (g)				sample (g)		(kg.m <sup>-2</sup> .s <sup>-1</sup> )			
550	0.067	0.0765	0.0011	9.41E-04	0.09	0.0018	2.35E-05	0.373	0.025		
462.5	0.056	0.39	0.0054	4.80E-03	0.42	0.0084	1.10E-04	0.407	0.023		
390	0.047	2.27	0.0316	2.79E-02	2.09	0.0419	5.46E-04	0.420	0.020		
327.5	0.038	7.7	0.1072	9.47E-02	6.05	0.1212	1.58E-03	0.441	0.017		
275	0.030	25.72	0.3579	3.16E-01	18.44	0.3695	4.82E-03	0.504	0.015		
231	0.024	25.59	0.3561	3.15E-01	16.87	0.3381	4.41E-03	0.590	0.014		
181	0.016	8.17	0.1137	1.00E-01	5.42	0.1086	1.42E-03	0.857	0.014		
106.5	0.007	1.94	0.0270	2.39E-02	0.52	0.0104	1.36E-04	0.850	0.006		
		71.8565		8.84E-01	49.9		1.30E-02				

Size ( $\mu$ m)	$w_s$ (m.s <sup>-1</sup> )	Near-bed $\chi_{4,1}$ (g.l <sup>-1</sup> )		$C_{b4,1}$ (g.l <sup>-1</sup> )		Deposited $\delta_{4,1}$ exp		$\Delta_{4,1}$ exp		$w_{d4,1}^*$	$w_{d4,1}$ (m.s <sup>-1</sup> )
		sample (g)				sample (g)		(kg.m <sup>-2</sup> .s <sup>-1</sup> )			
550	0.067	0.073	0.0010	8.99E-04	0.06	0.0012	1.52E-05	0.252	0.017		
462.5	0.056	0.42	0.0055	5.17E-03	0.36	0.0072	9.11E-05	0.314	0.018		
390	0.047	2.52	0.0331	3.10E-02	2.05	0.0412	5.19E-04	0.359	0.017		
327.5	0.038	8.12	0.1068	1.00E-01	6.08	0.1223	1.54E-03	0.407	0.015		
275	0.030	26.39	0.3470	3.25E-01	18.3	0.3680	4.63E-03	0.472	0.014		
231	0.024	28.01	0.3683	3.45E-01	17.06	0.3431	4.32E-03	0.528	0.013		
181	0.016	9.6	0.1262	1.18E-01	5.67	0.1140	1.44E-03	0.739	0.012		
106.5	0.007	0.92	0.0121	1.13E-02	0.15	0.0030	3.80E-05	0.501	0.003		
		76.053		9.36E-01	49.73		1.26E-02				

Size ( $\mu$ m)	$w_s$ (m.s <sup>-1</sup> )	Near-bed $\chi_{4,2}$ (g.l <sup>-1</sup> )		$C_{b4,2}$ (g.l <sup>-1</sup> )		Deposited $\delta_{4,2}$ exp		$\Delta_{4,2}$ exp		$w_{d4,2}^*$	$w_{d4,2}$ (m.s <sup>-1</sup> )
		sample (g)				sample (g)		(kg.m <sup>-2</sup> .s <sup>-1</sup> )			
550	0.067	0.0185	0.0004	2.25E-04	0.039	0.0008	1.08E-05	0.714	0.048		
462.5	0.056	0.1	0.0023	1.22E-03	0.24	0.0048	6.63E-05	0.970	0.054		
390	0.047	0.77	0.0174	9.38E-03	1.61	0.0322	4.45E-04	1.019	0.047		
327.5	0.038	3.25	0.0734	3.96E-02	5.61	0.1124	1.55E-03	1.035	0.039		
275	0.030	14.56	0.3288	1.77E-01	18.26	0.3657	5.05E-03	0.941	0.028		
231	0.024	17.09	0.3859	2.08E-01	17.8	0.3565	4.92E-03	0.996	0.024		
181	0.016	8.04	0.1815	9.79E-02	6.11	0.1224	1.69E-03	1.048	0.017		
106.5	0.007	0.46	0.0104	5.60E-03	0.26	0.0052	7.19E-05	1.915	0.013		
		44.2885		5.40E-01	49.929		1.38E-02				

Size ( $\mu$ m)	$w_s$ (m.s <sup>-1</sup> )	Near-bed $\chi_{5,1}$ (g.l <sup>-1</sup> )		$C_{b5,1}$ (g.l <sup>-1</sup> )		Deposited $\delta_{5,1}$ exp		$\Delta_{5,1}$ exp		$w_{d5,1}^*$	$w_{d5,1}$ (m.s <sup>-1</sup> )
		sample (g)				sample (g)		(kg.m <sup>-2</sup> .s <sup>-1</sup> )			
550	0.067	0.016	0.0004	1.96E-04	0.028	0.0006	5.16E-06	0.393	0.026		
462.5	0.056	0.09	0.0020	1.10E-03	0.19	0.0038	3.50E-05	0.565	0.032		
390	0.047	0.76	0.0172	9.32E-03	1.37	0.0274	2.53E-04	0.582	0.027		
327.5	0.038	3.06	0.0693	3.75E-02	5.01	0.1003	9.24E-04	0.651	0.025		
275	0.030	14.6	0.3309	1.79E-01	18.09	0.3621	3.33E-03	0.616	0.019		
231	0.024	17.17	0.3891	2.10E-01	18.51	0.3705	3.41E-03	0.683	0.016		
181	0.016	7.98	0.1808	9.78E-02	6.52	0.1305	1.20E-03	0.747	0.012		
106.5	0.007	0.45	0.0102	5.52E-03	0.24	0.0048	4.42E-05	1.198	0.008		
		44.126		5.41E-01	49.958		9.21E-03				

Size ( $\mu$ m)	$w_s$ (m.s <sup>-1</sup> )	Near-bed $\chi_{7,1}$ (g.l <sup>-1</sup> )		$C_{b7,1}$ (g.l <sup>-1</sup> )		Deposited $\delta_{7,1}$ exp		$\Delta_{7,1}$ exp		$w_{d7,1}^*$	$w_{d7,1}$ (m.s <sup>-1</sup> )
		sample (g)				sample (g)		(kg.m <sup>-2</sup> .s <sup>-1</sup> )			
550	0.067	0.002	0.0001	2.50E-05	0.0000	0.0000	0.00E+00				
462.5	0.056	0.017	0.0008	2.12E-04	0.075	0.0015	9.02E-06	0.757	0.042		
390	0.047	0.18	0.0086	2.25E-03	0.75	0.0151	9.02E-05	0.862	0.040		
327.5	0.038	1.05	0.0503	1.31E-02	3.71	0.0747	4.46E-04	0.899	0.034		
275	0.030	5.97	0.2862	7.46E-02	16	0.3220	1.93E-03	0.854	0.026		
231	0.024	8.82	0.4228	1.10E-01	20.39	0.4104	2.45E-03	0.938	0.022		
181	0.016	2.77	0.1328	3.46E-02	7.32	0.1473	8.81E-04	1.547	0.025		
106.5	0.007	2.05	0.0983	2.56E-02	1.44	0.0290	1.73E-04	1.010	0.007		
		20.859		2.61E-01	49.685		5.98E-03				

G5	Location	Deposited $\Delta_i$		Sample mass (g)	Volume of $C_{bi}$		time (mn)	43
	x (m)	(kg)	(kg.m.s <sup>-3</sup> )		water (l)	(g.l <sup>-1</sup> )		
trap#3.1	0.9	2.444	0.0176	73.9	82.7	0.894	$t^{\circ}$ (°C)	19.6
trap#3.2	1.1	1.972	0.0151	42.61	82.7	0.515	$v$ (m <sup>2</sup> .s <sup>-1</sup> )	1.01E-06
trap#4.1	1.3	1.711	0.0123	50.87	81.8	0.622	$\rho_w$ (kg.m <sup>-3</sup> )	1000
trap#4.2	1.5	1.737	0.0133	31.42	83.0	0.379	$\rho_s$ (kg.m <sup>-3</sup> )	2700
trap#5	1.74	1.445	0.0071	25.99	83.5	0.311	$g$ (m.s <sup>-2</sup> )	9.8
trap#7	2.62	0.526	0.0032	15.91	82.0	0.194	$\rho_s^*$	1.7

Size ( $\mu$ m)	$w_s$ (m.s <sup>-1</sup> )	Near-bed $\chi_{3,1}$ (g.l <sup>-1</sup> )		$C_{b3,1}$ (g.l <sup>-1</sup> )	Deposited $\delta_{3,1}$ exp		$\Delta_{3,1}$ exp	$w_{d3,1}^*$	$w_{d3,1}$ (m.s <sup>-1</sup> )
		sample (g)			sample (g)	(kg.m <sup>-2</sup> .s <sup>-1</sup> )			
550	0.068	0.0515	0.0007	6.26E-04	0.07	0.0014	2.46E-05	0.581	0.039
462.5	0.057	0.27	0.0037	3.28E-03	0.31	0.0062	1.09E-04	0.584	0.033
390	0.047	1.71	0.0232	2.08E-02	1.68	0.0337	5.91E-04	0.602	0.028
327.5	0.038	6.37	0.0866	7.74E-02	5.51	0.1104	1.94E-03	0.651	0.025
275	0.031	25.14	0.3417	3.05E-01	18.15	0.3635	6.38E-03	0.678	0.021
231	0.024	28.2	0.3833	3.43E-01	17.97	0.3599	6.32E-03	0.761	0.018
181	0.017	11.13	0.1513	1.35E-01	6.11	0.1224	2.15E-03	0.943	0.016
106.5	0.007	0.7	0.0095	8.51E-03	0.125	0.0025	4.40E-05	0.749	0.005
		73.5715		8.94E-01	49.925		1.76E-02		

Average	
$w_d^*$	$w_d$ (m.s <sup>-1</sup> )
0.503	0.034
0.722	0.041
0.770	0.036
0.820	0.032
0.881	0.027
0.949	0.023
1.161	0.020
1.275	0.009

Size ( $\mu$ m)	$w_s$ (m.s <sup>-1</sup> )	Near-bed $\chi_{3,2}$ (g.l <sup>-1</sup> )		$C_{b3,2}$ (g.l <sup>-1</sup> )	Deposited $\delta_{3,2}$ exp		$\Delta_{3,2}$ exp	$w_{d3,2}^*$	$w_{d3,2}$ (m.s <sup>-1</sup> )
		sample (g)			sample (g)	(kg.m <sup>-2</sup> .s <sup>-1</sup> )			
550	0.068	0.022	0.0005	2.68E-04	0.0205	0.0004	6.18E-06	0.341	0.023
462.5	0.057	0.082	0.0019	9.98E-04	0.15	0.0030	4.52E-05	0.797	0.045
390	0.047	0.63	0.0149	7.67E-03	1.02	0.0204	3.07E-04	0.849	0.040
327.5	0.038	2.84	0.0671	3.46E-02	4.06	0.0813	1.22E-03	0.920	0.035
275	0.031	13.02	0.3074	1.58E-01	17.11	0.3425	5.16E-03	1.056	0.033
231	0.024	16.8	0.3967	2.04E-01	19.16	0.3835	5.78E-03	1.165	0.028
181	0.017	8.35	0.1971	1.02E-01	8.15	0.1631	2.46E-03	1.434	0.024
106.5	0.007	0.61	0.0144	7.42E-03	0.29	0.0058	8.74E-05	1.706	0.012
		42.354		5.15E-01	49.9605		1.51E-02		

Size ( $\mu$ m)	$w_s$ (m.s <sup>-1</sup> )	Near-bed $\chi_{4,1}$ (g.l <sup>-1</sup> )		$C_{b4,1}$ (g.l <sup>-1</sup> )	Deposited $\delta_{4,1}$ exp		$\Delta_{4,1}$ exp	$w_{d4,1}^*$	$w_{d4,1}$ (m.s <sup>-1</sup> )
		sample (g)			sample (g)	(kg.m <sup>-2</sup> .s <sup>-1</sup> )			
550	0.068	0.016	0.0003	1.97E-04	0.02	0.0004	4.93E-06	0.370	0.025
462.5	0.057	0.1	0.0020	1.23E-03	0.135	0.0027	3.32E-05	0.476	0.027
390	0.047	0.78	0.0154	9.58E-03	1	0.0200	2.46E-04	0.544	0.026
327.5	0.038	3.53	0.0698	4.34E-02	4.15	0.0831	1.02E-03	0.612	0.024
275	0.031	16.5	0.3260	2.03E-01	17.55	0.3516	4.32E-03	0.692	0.021
231	0.024	20.31	0.4013	2.50E-01	19.57	0.3920	4.82E-03	0.796	0.019
181	0.017	8.75	0.1729	1.07E-01	7.31	0.1464	1.80E-03	0.994	0.017
106.5	0.007	0.62	0.0123	7.62E-03	0.185	0.0037	4.56E-05	0.867	0.006
		50.606		6.22E-01	49.92		1.23E-02		

Size ( $\mu$ m)	$w_s$ (m.s <sup>-1</sup> )	Near-bed $\chi_{4,2}$ (g.l <sup>-1</sup> )		$C_{b4,2}$ (g.l <sup>-1</sup> )	Deposited $\delta_{4,2}$ exp		$\Delta_{4,2}$ exp	$w_{d4,2}^*$	$w_{d4,2}$ (m.s <sup>-1</sup> )
		sample (g)			sample (g)	(kg.m <sup>-2</sup> .s <sup>-1</sup> )			
550	0.068	0.005	0.0002	6.06E-05	0.0085	0.0002	2.26E-06	0.551	0.037
462.5	0.057	0.0285	0.0009	3.45E-04	0.085	0.0017	2.26E-05	1.151	0.065
390	0.047	0.28	0.0090	3.39E-03	0.69	0.0138	1.84E-04	1.145	0.054
327.5	0.038	1.57	0.0502	1.90E-02	3.31	0.0664	8.80E-04	1.203	0.046
275	0.031	8.36	0.2675	1.01E-01	16.44	0.3296	4.37E-03	1.401	0.043
231	0.024	13.36	0.4275	1.62E-01	19.71	0.3951	5.24E-03	1.335	0.032
181	0.017	7.09	0.2269	8.59E-02	9.32	0.1868	2.48E-03	1.712	0.029
106.5	0.007	0.56	0.0179	6.78E-03	0.32	0.0064	8.51E-05	1.818	0.013
		31.2535		3.79E-01	49.8835		1.33E-02		

Size ( $\mu$ m)	$w_s$ (m.s <sup>-1</sup> )	Near-bed $\chi_{5,1}$ (g.l <sup>-1</sup> )		$C_{b5,1}$ (g.l <sup>-1</sup> )	Deposited $\delta_{5,1}$ exp		$\Delta_{5,1}$ exp	$w_{d5,1}^*$	$w_{d5,1}$ (m.s <sup>-1</sup> )
		sample (g)			sample (g)	(kg.m <sup>-2</sup> .s <sup>-1</sup> )			
550	0.068	0.0015	0.0001	1.80E-05	0.0075	0.0002	1.06E-06	0.871	0.059
462.5	0.057	0.0135	0.0005	1.62E-04	0.0535	0.0011	7.58E-06	0.821	0.047
390	0.047	0.2	0.0077	2.41E-03	0.57	0.0114	8.08E-05	0.711	0.034
327.5	0.038	1.09	0.0421	1.31E-02	2.99	0.0599	4.24E-04	0.840	0.032
275	0.031	6.72	0.2596	8.08E-02	15.32	0.3070	2.17E-03	0.872	0.027
231	0.024	11	0.4250	1.32E-01	20.63	0.4134	2.92E-03	0.912	0.022
181	0.017	6.28	0.2426	7.55E-02	9.85	0.1974	1.40E-03	1.097	0.018
106.5	0.007	0.58	0.0224	6.97E-03	0.48	0.0096	6.80E-05	1.414	0.010
		25.885		3.11E-01	49.901		7.07E-03		

Size ( $\mu$ m)	$w_s$ (m.s <sup>-1</sup> )	Near-bed $\chi_{7,1}$ (g.l <sup>-1</sup> )		$C_{b7,1}$ (g.l <sup>-1</sup> )	Deposited $\delta_{7,1}$ exp		$\Delta_{7,1}$ exp	$w_{d7,1}^*$	$w_{d7,1}$ (m.s <sup>-1</sup> )
		sample (g)			sample (g)	(kg.m <sup>-2</sup> .s <sup>-1</sup> )			
550	0.068	0.001	0.0001	1.22E-05	0.004	0.0001	2.54E-07	0.306	0.021
462.5	0.057	0.004	0.0003	4.90E-05	0.022	0.0004	1.40E-06	0.501	0.029
390	0.047	0.037	0.0023	4.53E-04	0.26	0.0052	1.65E-05	0.771	0.036
327.5	0.038	0.36	0.0227	4.41E-03	1.85	0.0371	1.18E-04	0.692	0.027
275	0.031	3.48	0.2197	4.26E-02	12.11	0.2429	7.69E-04	0.586	0.018
231	0.024	6.63	0.4185	8.12E-02	22.56	0.4525	1.43E-03	0.727	0.018
181	0.017	4.83	0.3049	5.92E-02	12.32	0.2471	7.83E-04	0.785	0.013
106.5	0.007	0.5	0.0316	6.12E-03	0.73	0.0146	4.64E-05	1.097	0.008
		15.842		1.94E-01	49.856		3.17E-03		

G6

	Location	Deposited $\Delta_i$		Sample Volume of $C_{ij}$		
	x (m)	(kg)	(kg.m.s <sup>-3</sup> )	mass (g)	water (l)	(g.l <sup>-1</sup> )
trap#3.1	0.9	1.108	0.0082	196.98	79.7	2.473
trap#3.2	1.1	0.897	0.0070	197.78	81.5	2.427
trap#4.1	1.3	0.627	0.0046	197.81	79.7	2.483
trap#4.2	1.5	0.875	0.0068	196.71	79.7	2.470
trap#5	1.74	1.223	0.0061	195.06	80.2	2.434
trap#7	2.62	0.915	0.0056	168.52	78.0	2.161

time (mn)	42
t° (°C)	20.8
v (m <sup>2</sup> .s <sup>-1</sup> )	9.84E-07
$\rho_w$ (kg.m <sup>-3</sup> )	1000
$\rho_s$ (kg.m <sup>-3</sup> )	2680
g (m.s <sup>-2</sup> )	9.8
$\rho_s^*$	1.68

Average

$w_d^{i*}$	$w_d^i$ (m.s <sup>-1</sup> )
0.715	0.017
0.644	0.012
0.584	0.009
0.579	0.006
0.622	0.005
0.620	0.004
0.660	0.003
0.749	0.002
1.754	0.001

Size ( $\mu$ m)	$w_s$ (m.s <sup>-1</sup> )	Near-bed $\chi_{3,1}$ (g.l <sup>-1</sup> )		$C_{33,1}$ (g.l <sup>-1</sup> )	Deposited $\delta_{3,1}$ exp		$\Delta_{3,1}$ exp	$w_{d3,1}^*$	$w_{d3,1}$ (m.s <sup>-1</sup> )
		sample (g)			sample (g)	(kg.m <sup>-2</sup> .s <sup>-1</sup> )			
231	0.024	0.13	0.0017	4.25E-03	0.45	0.0092	7.48E-05	0.720	0.018
196	0.019	0.28	0.0037	9.15E-03	0.94	0.0192	1.56E-04	0.888	0.017
165	0.015	1.06	0.0140	3.46E-02	2.43	0.0496	4.04E-04	0.792	0.012
137.5	0.011	2.68	0.0354	8.76E-02	4.4	0.0897	7.32E-04	0.766	0.008
115.5	0.008	6.19	0.0818	2.02E-01	7.49	0.1528	1.25E-03	0.762	0.006
98	0.006	10.55	0.1394	3.45E-01	9.42	0.1921	1.57E-03	0.754	0.005
82.5	0.004	13.21	0.1745	4.32E-01	9.18	0.1872	1.53E-03	0.805	0.004
69	0.003	12.13	0.1602	3.96E-01	6.69	0.1364	1.11E-03	0.894	0.003
31.5	0.001	29.47	0.3893	9.63E-01	8.03	0.1638	1.34E-03	2.032	0.001
		75.7		2.47E+00	49.03		8.15E-03		

Size ( $\mu$ m)	$w_s$ (m.s <sup>-1</sup> )	Near-bed $\chi_{3,2}$ (g.l <sup>-1</sup> )		$C_{33,2}$ (g.l <sup>-1</sup> )	Deposited $\delta_{3,2}$ exp		$\Delta_{3,2}$ exp	$w_{d3,2}^*$	$w_{d3,2}$ (m.s <sup>-1</sup> )
		sample (g)			sample (g)	(kg.m <sup>-2</sup> .s <sup>-1</sup> )			
231	0.024	0.135	0.0027	6.61E-03	0.39	0.0079	5.54E-05	0.343	0.008
196	0.019	0.25	0.0050	1.22E-02	0.795	0.0161	1.13E-04	0.480	0.009
165	0.015	0.81	0.0163	3.96E-02	2.06	0.0417	2.92E-04	0.501	0.007
137.5	0.011	1.95	0.0393	9.54E-02	3.85	0.0779	5.47E-04	0.525	0.006
115.5	0.008	3.98	0.0802	1.95E-01	6.75	0.1366	9.58E-04	0.609	0.005
98	0.006	6.85	0.1381	3.35E-01	9.45	0.1913	1.34E-03	0.664	0.004
82.5	0.004	8.84	0.1782	4.33E-01	9.77	0.1978	1.39E-03	0.730	0.003
69	0.003	7.85	0.1583	3.84E-01	7.29	0.1476	1.03E-03	0.858	0.003
31.5	0.001	18.94	0.3818	9.27E-01	9.05	0.1832	1.28E-03	2.032	0.001
		49.605		2.43E+00	49.405		7.01E-03		

Size ( $\mu$ m)	$w_s$ (m.s <sup>-1</sup> )	Near-bed $\chi_{4,1}$ (g.l <sup>-1</sup> )		$C_{34,1}$ (g.l <sup>-1</sup> )	Deposited $\delta_{4,1}$ exp		$\Delta_{4,1}$ exp	$w_{d4,1}^*$	$w_{d4,1}$ (m.s <sup>-1</sup> )
		sample (g)			sample (g)	(kg.m <sup>-2</sup> .s <sup>-1</sup> )			
231	0.024	0.07	0.0014	3.52E-03	0.39	0.0079	3.65E-05	0.424	0.010
196	0.019	0.21	0.0043	1.06E-02	0.94	0.0191	8.81E-05	0.433	0.008
165	0.015	0.74	0.0150	3.72E-02	2.35	0.0477	2.20E-04	0.402	0.006
137.5	0.011	1.9	0.0385	9.56E-02	4.56	0.0926	4.27E-04	0.410	0.004
115.5	0.008	3.97	0.0804	2.00E-01	7.56	0.1536	7.08E-04	0.439	0.004
98	0.006	6.69	0.1355	3.36E-01	9.51	0.1932	8.91E-04	0.439	0.003
82.5	0.004	8.93	0.1808	4.49E-01	9.14	0.1857	8.56E-04	0.434	0.002
69	0.003	7.74	0.1567	3.89E-01	6.55	0.1330	6.14E-04	0.502	0.002
31.5	0.001	19.13	0.3874	9.62E-01	8.23	0.1672	7.71E-04	1.175	0.001
		49.38		2.48E+00	49.23		4.61E-03		

Size ( $\mu$ m)	$w_s$ (m.s <sup>-1</sup> )	Near-bed $\chi_{4,2}$ (g.l <sup>-1</sup> )		$C_{34,2}$ (g.l <sup>-1</sup> )	Deposited $\delta_{4,2}$ exp		$\Delta_{4,2}$ exp	$w_{d4,2}^*$	$w_{d4,2}$ (m.s <sup>-1</sup> )
		sample (g)			sample (g)	(kg.m <sup>-2</sup> .s <sup>-1</sup> )			
231	0.024	0.07	0.0014	3.49E-03	0.605	0.0124	8.45E-05	0.989	0.024
196	0.019	0.18	0.0036	8.98E-03	0.99	0.0202	1.38E-04	0.800	0.015
165	0.015	0.67	0.0135	3.34E-02	2.12	0.0433	2.96E-04	0.602	0.009
137.5	0.011	1.8	0.0364	8.98E-02	3.87	0.0790	5.41E-04	0.551	0.006
115.5	0.008	3.71	0.0750	1.85E-01	6.99	0.1428	9.77E-04	0.653	0.005
98	0.006	6.75	0.1364	3.37E-01	8.76	0.1789	1.22E-03	0.603	0.004
82.5	0.004	8.86	0.1791	4.42E-01	9.75	0.1991	1.36E-03	0.701	0.003
69	0.003	8	0.1617	3.99E-01	6.92	0.1413	9.67E-04	0.771	0.002
31.5	0.001	19.44	0.3929	9.70E-01	8.96	0.1830	1.25E-03	1.891	0.001
		49.48		2.47E+00	48.965		6.84E-03		

Size ( $\mu$ m)	$w_s$ (m.s <sup>-1</sup> )	Near-bed $\chi_5$ (g.l <sup>-1</sup> )		$C_{35}$ (g.l <sup>-1</sup> )	Deposited $\delta_5$ exp		$\Delta_5$ exp	$w_{d5}^*$	$w_{d5}$ (m.s <sup>-1</sup> )
		sample (g)			sample (g)	(kg.m <sup>-2</sup> .s <sup>-1</sup> )			
231	0.024	0.065	0.0013	3.20E-03	0.33	0.0067	4.11E-05	0.526	0.013
196	0.019	0.18	0.0036	8.86E-03	0.8	0.0163	9.98E-05	0.585	0.011
165	0.015	0.7	0.0142	3.45E-02	2.25	0.0458	2.81E-04	0.553	0.008
137.5	0.011	1.72	0.0348	8.47E-02	4.28	0.0871	5.34E-04	0.577	0.006
115.5	0.008	3.8	0.0769	1.87E-01	7.3	0.1485	9.10E-04	0.602	0.005
98	0.006	6.7	0.1356	3.30E-01	9.55	0.1943	1.19E-03	0.599	0.004
82.5	0.004	8.7	0.1761	4.28E-01	9.42	0.1916	1.17E-03	0.624	0.003
69	0.003	7.84	0.1587	3.86E-01	6.79	0.1381	8.47E-04	0.699	0.002
31.5	0.001	19.71	0.3989	9.71E-01	8.44	0.1717	1.05E-03	1.589	0.001
		49.415		2.43E+00	49.16		6.13E-03		

Size ( $\mu$ m)	$w_s$ (m.s <sup>-1</sup> )	Near-bed $\chi_7$ (g.l <sup>-1</sup> )		$C_{37}$ (g.l <sup>-1</sup> )	Deposited $\delta_7$ exp		$\Delta_7$ exp	$w_{d7}^*$	$w_{d7}$ (m.s <sup>-1</sup> )
		sample (g)			sample (g)	(kg.m <sup>-2</sup> .s <sup>-1</sup> )			
231	0.024	0.02	0.0004	8.73E-04	0.24	0.0049	2.75E-05	1.286	0.031
196	0.019	0.11	0.0022	4.80E-03	0.55	0.0112	6.29E-05	0.681	0.013
165	0.015	0.47	0.0095	2.05E-02	1.73	0.0351	1.98E-04	0.655	0.010
137.5	0.011	1.39	0.0281	6.07E-02	3.72	0.0755	4.26E-04	0.643	0.007
115.5	0.008	3.21	0.0649	1.40E-01	6.61	0.1341	7.56E-04	0.668	0.005
98	0.006	6.17	0.1247	2.69E-01	9.34	0.1895	1.07E-03	0.658	0.004
82.5	0.004	8.75	0.1768	3.82E-01	9.73	0.1974	1.11E-03	0.663	0.003
69	0.003	7.85	0.1586	3.43E-01	7.23	0.1467	8.27E-04	0.769	0.002
31.5	0.001	21.52	0.4348	9.40E-01	10.13	0.2056	1.16E-03	1.808	0.001
		49.49		2.16E+00	49.28		5.64E-03		

G7	Location	Deposited $\Delta_1$		Sample		Volume of $C_{59}$		time (mn) 32 t° (°C) 20.8 v (m <sup>2</sup> .s <sup>-1</sup> ) 9.84E-07 pw (kg.m <sup>-3</sup> ) 1000 ps (kg.m <sup>-3</sup> ) 2680 g (m.s <sup>-2</sup> ) 9.8 ps* 1.68	
	x (m)	(kg)	(kg.m.s <sup>-2</sup> )	mass (g)	water (l)	(g.l <sup>-1</sup> )	(g.l <sup>-1</sup> )		
trap#3.1	0.9	0.539	0.0052	98	62.0	1.582			
trap#3.2	1.1	0.51	0.0052	102	62.0	1.646			
trap#4.1	1.3	0.467	0.0045	101.6	60.9	1.667			
trap#4.2	1.5	0.52	0.0053	94.5	62.6	1.509			
trap#5	1.74	0.633	0.0042	93	63.1	1.473			
trap#7	2.62	0.491	0.0040	86.1	61.4	1.401			

Size (μm)	$w_a$ (m.s <sup>-1</sup> )	Near-bed $\chi_{3,1}$ (g.l <sup>-1</sup> )			Deposited $\delta_{3,1}$ exp			$\Delta_{3,1}$ exp		$w_{d3,1}^*$	$w_{d3,1}$ (m.s <sup>-1</sup> )
		$C_{3,1}$ (g.l <sup>-1</sup> )	sample (g)	sample (g)	sample (g)	(kg.m <sup>-2</sup> .s <sup>-1</sup> )	(kg.m <sup>-2</sup> .s <sup>-1</sup> )				
275	0.0310	0.05	0.0010	1.64E-03	0.46	0.0094	4.87E-05	0.960	0.0298		
231	0.0245	0.11	0.0023	3.60E-03	0.86	0.0175	9.11E-05	1.035	0.0253		
196	0.0192	0.2	0.0041	6.54E-03	1.25	0.0254	1.32E-04	1.052	0.0202		
165	0.0147	0.86	0.0178	2.81E-02	3.76	0.0765	3.98E-04	0.961	0.0142		
137.5	0.0109	2.06	0.0426	6.74E-02	5.87	0.1195	6.22E-04	0.845	0.0092		
115.5	0.0081	3.97	0.0821	1.30E-01	8.49	0.1728	8.99E-04	0.857	0.0069		
98	0.0060	6.41	0.1325	2.10E-01	9.89	0.2013	1.05E-03	0.829	0.0050		
82.5	0.0044	8.72	0.1803	2.85E-01	7.71	0.1569	8.17E-04	0.652	0.0029		
69	0.0031	7.37	0.1524	2.41E-01	5.43	0.1105	5.75E-04	0.760	0.0024		
58	0.0023	5.68	0.1175	1.86E-01	3.04	0.0619	3.22E-04	0.769	0.0017		
49	0.0016	4.4	0.0910	1.44E-01	1.36	0.0277	1.44E-04	0.616	0.0010		
41.5	0.0012	3.62	0.0749	1.18E-01	0.71	0.0144	7.52E-05	0.541	0.0006		
19	0.0003	4.91	0.1015	1.61E-01	0.31	0.0063	3.28E-05	0.817	0.0002		
		48.36		1.58E+00	49.14		5.20E-03				

Average	
$w_a^*$	$w_d$ (m.s <sup>-1</sup> )
0.599	0.0186
0.734	0.0180
0.769	0.0148
0.726	0.0107
0.745	0.0081
0.711	0.0058
0.709	0.0043
0.687	0.0030
0.765	0.0024
0.785	0.0018
0.823	0.0013
0.718	0.0008
1.389	0.0003

Size (μm)	$w_a$ (m.s <sup>-1</sup> )	Near-bed $\chi_{3,2}$ (g.l <sup>-1</sup> )			Deposited $\delta_{3,2}$ exp			$\Delta_{3,2}$ exp		$w_{d3,2}^*$	$w_{d3,2}$ (m.s <sup>-1</sup> )
		$C_{3,2}$ (g.l <sup>-1</sup> )	sample (g)	sample (g)	sample (g)	(kg.m <sup>-2</sup> .s <sup>-1</sup> )	(kg.m <sup>-2</sup> .s <sup>-1</sup> )				
275	0.0310	0.08	0.0017	2.73E-03	0.48	0.0098	5.15E-05	0.609	0.0189		
231	0.0245	0.16	0.0033	5.46E-03	0.86	0.0176	9.24E-05	0.692	0.0169		
196	0.0192	0.32	0.0066	1.09E-02	1.26	0.0259	1.35E-04	0.645	0.0124		
165	0.0147	1.12	0.0232	3.82E-02	3.53	0.0724	3.79E-04	0.674	0.0099		
137.5	0.0109	2.05	0.0425	6.99E-02	5.65	0.1159	6.07E-04	0.795	0.0087		
115.5	0.0081	4.42	0.0915	1.51E-01	7.85	0.1611	8.43E-04	0.692	0.0056		
98	0.0060	7.6	0.1574	2.59E-01	10.18	0.2089	1.09E-03	0.700	0.0042		
82.5	0.0044	8.2	0.1698	2.80E-01	7.81	0.1602	8.39E-04	0.683	0.0030		
69	0.0031	7.32	0.1516	2.50E-01	5.35	0.1098	5.75E-04	0.733	0.0023		
58	0.0023	4.72	0.0977	1.61E-01	2.91	0.0597	3.12E-04	0.862	0.0019		
49	0.0016	4.2	0.0870	1.43E-01	1.59	0.0326	1.71E-04	0.734	0.0012		
41.5	0.0012	3.27	0.0677	1.11E-01	0.8	0.0164	8.59E-05	0.656	0.0008		
19	0.0003	4.83	0.1000	1.65E-01	0.47	0.0096	5.05E-05	1.225	0.0003		
		48.29		1.65E+00	48.74		5.23E-03				

Size (μm)	$w_a$ (m.s <sup>-1</sup> )	Near-bed $\chi_{4,1}$ (g.l <sup>-1</sup> )			Deposited $\delta_{4,1}$ exp			$\Delta_{4,1}$ exp		$w_{d4,1}^*$	$w_{d4,1}$ (m.s <sup>-1</sup> )
		$C_{4,1}$ (g.l <sup>-1</sup> )	sample (g)	sample (g)	sample (g)	(kg.m <sup>-2</sup> .s <sup>-1</sup> )	(kg.m <sup>-2</sup> .s <sup>-1</sup> )				
275	0.0310	0.06	0.0012	2.06E-03	0.4	0.0082	3.69E-05	0.576	0.0179		
231	0.0245	0.15	0.0031	5.16E-03	0.73	0.0149	6.73E-05	0.534	0.0130		
196	0.0192	0.27	0.0056	9.28E-03	1.01	0.0207	9.31E-05	0.521	0.0100		
165	0.0147	1.14	0.0235	3.92E-02	3.05	0.0624	2.81E-04	0.487	0.0072		
137.5	0.0109	2.12	0.0437	7.29E-02	4.93	0.1008	4.55E-04	0.571	0.0062		
115.5	0.0081	4.77	0.0984	1.64E-01	7.34	0.1501	6.77E-04	0.510	0.0041		
98	0.0060	7.6	0.1567	2.61E-01	9.62	0.1967	8.87E-04	0.563	0.0034		
82.5	0.0044	8.7	0.1794	2.99E-01	9.22	0.1885	8.50E-04	0.647	0.0028		
69	0.0031	7.32	0.1510	2.52E-01	6.01	0.1229	5.54E-04	0.701	0.0022		
58	0.0023	4.73	0.0975	1.63E-01	2.88	0.0589	2.86E-04	0.725	0.0016		
49	0.0016	4.13	0.0852	1.42E-01	2.07	0.0423	1.91E-04	0.827	0.0013		
41.5	0.0012	3.1	0.0639	1.07E-01	1.01	0.0207	9.31E-05	0.744	0.0009		
19	0.0003	4.4	0.0907	1.51E-01	0.64	0.0131	5.90E-05	1.559	0.0004		
		48.49		1.67E+00	48.91		4.51E-03				

Size (μm)	$w_a$ (m.s <sup>-1</sup> )	Near-bed $\chi_{4,2}$ (g.l <sup>-1</sup> )			Deposited $\delta_{4,2}$ exp			$\Delta_{4,2}$ exp		$w_{d4,2}^*$	$w_{d4,2}$ (m.s <sup>-1</sup> )
		$C_{4,2}$ (g.l <sup>-1</sup> )	sample (g)	sample (g)	sample (g)	(kg.m <sup>-2</sup> .s <sup>-1</sup> )	(kg.m <sup>-2</sup> .s <sup>-1</sup> )				
275	0.0310	0.06	0.0012	1.84E-03	0.31	0.0063	3.37E-05	0.590	0.0183		
231	0.0245	0.1	0.0020	3.07E-03	0.6	0.0122	6.53E-05	0.869	0.0213		
196	0.0192	0.2	0.0041	6.14E-03	1.08	0.0220	1.17E-04	0.994	0.0191		
165	0.0147	0.83	0.0169	2.55E-02	3.15	0.0642	3.43E-04	0.913	0.0134		
137.5	0.0109	1.92	0.0391	5.89E-02	5.12	0.1043	5.57E-04	0.866	0.0094		
115.5	0.0081	3.92	0.0797	1.20E-01	7.69	0.1567	8.36E-04	0.860	0.0070		
98	0.0060	7.35	0.1495	2.26E-01	10.13	0.2064	1.10E-03	0.810	0.0049		
82.5	0.0044	8.61	0.1751	2.64E-01	9.04	0.1842	9.83E-04	0.847	0.0037		
69	0.0031	7.61	0.1548	2.34E-01	5.86	0.1194	6.37E-04	0.869	0.0027		
58	0.0023	5.21	0.1060	1.60E-01	2.86	0.0583	3.11E-04	0.864	0.0019		
49	0.0016	4.48	0.0911	1.38E-01	1.92	0.0391	2.09E-04	0.935	0.0015		
41.5	0.0012	3.44	0.0700	1.06E-01	0.85	0.0173	9.24E-05	0.745	0.0009		
19	0.0003	5.43	0.1105	1.67E-01	0.46	0.0094	5.00E-05	1.200	0.0003		
		49.16		1.51E+00	49.07		5.34E-03				

Size (μm)	$w_a$ (m.s <sup>-1</sup> )	Near-bed $\chi_5$ (g.l <sup>-1</sup> )			Deposited $\delta_5$ exp			$\Delta_5$ exp		$w_{d5}^*$	$w_{d5}$ (m.s <sup>-1</sup> )
		$C_{56}$ (g.l <sup>-1</sup> )	sample (g)	sample (g)	sample (g)	(kg.m <sup>-2</sup> .s <sup>-1</sup> )	(kg.m <sup>-2</sup> .s <sup>-1</sup> )				
275	0.0310	0.05	0.0010	1.50E-03	0.26	0.0052	2.17E-05	0.467	0.0145		
231	0.0245	0.09	0.0018	2.70E-03	0.54	0.0108	4.51E-05	0.683	0.0167		
196	0.0192	0.16	0.0033	4.80E-03	0.9	0.0181	7.52E-05	0.814	0.0157		
165	0.0147	0.75	0.0153	2.25E-02	2.86	0.0574	2.39E-04	0.721	0.0106		
137.5	0.0109	1.72	0.0350	5.16E-02	4.95	0.0993	4.14E-04	0.734	0.0080		
115.5	0.0081	3.81	0.0776	1.14E-01	7.75	0.1555	6.47E-04	0.701	0.0057		
98	0.0060	7.17	0.1461	2.15E-01	10.33	0.2072	8.63E-04	0.665	0.0040		
82.5	0.0044	8.89	0.1811	2.67E-01	8.79	0.1763	7.34E-04	0.627	0.0028		
69	0.0031	7.63	0.1554	2.29E-01	6.14	0.1232	5.13E-04	0.714	0.0022		
58	0.0023	5.38	0.1096	1.61E-01	3.15	0.0632	2.63E-04	0.724	0.0016		
49	0.0016	4.38	0.0892	1.31E-01	2.16	0.0433	1.80E-04	0.845	0.0014		
41.5	0.0012	3.54	0.0721	1.06E-01	1.16	0.0233	9.69E-05	0.777	0.0009		
19	0.0003	5.52	0.1124	1.66E-01	0.86	0.0173	7.18E-05	1.734	0.0004		
		49.09		1.47E+00	49.85		4.16E-03				

Size ( $\mu\text{m}$ )	$w_s$ ( $\text{m}\cdot\text{s}^{-1}$ )	Near-bed sample (g)	$\chi_r$ ( $\text{g}\cdot\Gamma^{-1}$ )	$C_{sp}$ ( $\text{g}\cdot\Gamma^{-1}$ )	Deposited sample (g)	$\delta_r$ exp	$\Delta_r$ exp ( $\text{kg}\cdot\text{m}^{-2}\cdot\text{s}^{-1}$ )	$w_{d7}^*$	$w_{d7}$ ( $\text{m}\cdot\text{s}^{-1}$ )
275	0.0310	0.03	0.0006	8.63E-04	0.13	0.0026	1.05E-05	0.391	0.0121
231	0.0245	0.06	0.0012	1.73E-03	0.31	0.0063	2.49E-05	0.591	0.0145
196	0.0192	0.15	0.0031	4.31E-03	0.61	0.0124	4.91E-05	0.591	0.0114
165	0.0147	0.73	0.0150	2.10E-02	2.3	0.0466	1.85E-04	0.599	0.0088
137.5	0.0109	1.82	0.0374	5.23E-02	4.67	0.0946	3.76E-04	0.658	0.0072
115.5	0.0081	3.77	0.0774	1.08E-01	7.07	0.1432	5.69E-04	0.649	0.0052
98	0.0060	6.91	0.1418	1.99E-01	10.2	0.2066	8.21E-04	0.685	0.0041
82.5	0.0044	8.91	0.1829	2.56E-01	9.36	0.1896	7.53E-04	0.669	0.0029
69	0.0031	7.33	0.1505	2.11E-01	6.7	0.1357	5.39E-04	0.815	0.0026
58	0.0023	5.6	0.1149	1.61E-01	3.46	0.0701	2.78E-04	0.767	0.0017
49	0.0016	4.19	0.0860	1.21E-01	2.39	0.0484	1.92E-04	0.982	0.0016
41.5	0.0012	3.55	0.0729	1.02E-01	1.26	0.0255	1.01E-04	0.845	0.0010
19	0.0003	5.67	0.1164	1.63E-01	0.91	0.0184	7.32E-05	1.795	0.0004
		48.72		1.40E+00	49.37		3.97E-03		

Appendix 5.1: deposition of particles transported by saltation: computation of the landing angles  $\beta$

L/R is ratio of the distance between two consecutive discs to the disc radius (Figure 5.2)

and  $u_b$  is the near-bed flow velocity ( $m.s^{-1}$ ).

The settling velocity  $w_s$  corresponding to each size fraction of median diameter  $d$  is computed from Cheng (1997). The landing angle  $\beta$  is computed by trial and error, by comparison between the value of the dimensionless deposition velocity  $w_d^*$  obtained from [5.20b] (column " $w_d^*$  eq") and that obtained experimentally (column " $w_d^*$  exp").  $P_d$  is the proportion of depositing particles.

D3

L/R	4
$u_b$ ( $m.s^{-1}$ )	0.29
$v$ ( $m^2.s^{-1}$ )	1.05E-06

$\rho_w$ ( $kg.m^{-3}$ )	1000
$\rho_s$ ( $kg.m^{-3}$ )	2700
$g$ ( $m.s^{-2}$ )	9.8
$\rho_s^*$	1.7

d ( $\mu m$ )	$w_s$ ( $m.s^{-1}$ )	$\beta$ (deg)	$P_d$	$w_d^*$ eq	$w_d^*$ exp
550	0.067	19.1	0.236	0.354	0.359
462.5	0.056	23.4	0.371	0.828	0.833
390	0.047	24.8	0.404	1.163	1.167
327.5	0.038	23.9	0.383	1.301	1.304
275	0.030	21.1	0.306	1.132	1.137
		22.46			

D4

L/R	4
$u_b$ ( $m.s^{-1}$ )	0.28
$v$ ( $m^2/s$ )	1.02E-06

$\rho_w$ ( $kg.m^{-3}$ )	1000
$\rho_s$ ( $kg.m^{-3}$ )	2700
$g$ ( $m.s^{-2}$ )	9.8
$\rho_s^*$	1.7

d ( $\mu m$ )	$w_s$ ( $m.s^{-1}$ )	$\beta$ (deg)	$P_d$	$w_d^*$ eq	$w_d^*$ exp
550	0.067	22.3	0.341	0.585	0.588
462.5	0.056	24.1	0.388	0.865	0.862
390	0.047	23.4	0.371	0.965	0.967
327.5	0.038	24	0.385	1.270	1.263
275	0.030	22.3	0.341	1.297	1.308
		23.22			

D5

L/R	4
$u_b$ ( $m.s^{-1}$ )	0.37
$v$ ( $m^2/s$ )	1.08E-06

$\rho_w$ ( $kg.m^{-3}$ )	1000
$\rho_s$ ( $kg.m^{-3}$ )	2700
$g$ ( $m.s^{-2}$ )	9.8
$\rho_s^*$	1.7

d ( $\mu m$ )	$w_s$ ( $m.s^{-1}$ )	$\beta$ (deg)	$P_d$	$w_d^*$ eq	$w_d^*$ exp
550	0.067	20.4	0.283	0.581	0.581
462.5	0.056	23.7	0.378	1.094	1.089
390	0.047	21.2	0.309	0.952	0.945
327.5	0.038	20.5	0.286	1.047	1.041
275	0.030	18.9	0.228	0.957	0.964
		20.94			

D6

L/R	4
$u_b$ ( $m.s^{-1}$ )	0.49
$v$ ( $m^2/s$ )	1.03E-06

$\rho_w$ ( $kg.m^{-3}$ )	1000
$\rho_s$ ( $kg.m^{-3}$ )	2700
$g$ ( $m.s^{-2}$ )	9.8
$\rho_s^*$	1.7

d ( $\mu m$ )	$w_s$ ( $m.s^{-1}$ )	$\beta$ (deg)	$P_d$	$w_d^*$ eq	$w_d^*$ exp
550	0.067	19.9	0.266	0.704	0.708
462.5	0.056	19.8	0.262	0.823	0.820
390	0.047	18.9	0.228	0.823	0.829
327.5	0.038	18.5	0.212	0.920	0.916
275	0.030	17.5	0.169	0.862	0.871
		18.92			

E2

L/R	4
$u_b$ ( $m.s^{-1}$ )	0.35
$v$ ( $m^2/s$ )	1.05E-06

$\rho_w$ ( $kg.m^{-3}$ )	1000
$\rho_s$ ( $kg.m^{-3}$ )	2700
$g$ ( $m.s^{-2}$ )	9.8
$\rho_s^*$	1.7

d ( $\mu m$ )	$w_s$ ( $m.s^{-1}$ )	$\beta$ (deg)	$P_d$	$w_d^*$ eq	$w_d^*$ exp
550	0.067	23.7	0.378	0.868	0.865
462.5	0.056	22.2	0.338	0.861	0.858
390	0.047	22.6	0.349	1.094	1.095
327.5	0.038	21.1	0.306	1.091	1.082
275	0.030	19.4	0.247	1.009	1.011
		21.8			

E3b

L/R	4
$u_b$ ( $m.s^{-1}$ )	0.27
$v$ ( $m^2/s$ )	1.02E-06

$\rho_w$ ( $kg.m^{-3}$ )	1000
$\rho_s$ ( $kg.m^{-3}$ )	2700
$g$ ( $m.s^{-2}$ )	9.8
$\rho_s^*$	1.7

d ( $\mu m$ )	$w_s$ ( $m.s^{-1}$ )	$\beta$ (deg)	$P_d$	$w_d^*$ eq	$w_d^*$ exp
550	0.067	21.2	0.309	0.483	0.478
462.5	0.056	26	0.430	1.008	1.004
390	0.047	24.4	0.395	1.039	1.031
327.5	0.038	23.6	0.376	1.171	1.168
275	0.030	21.4	0.315	1.103	1.100
		23.32			

E4

L/R	4
$u_b$ ( $m.s^{-1}$ )	0.23
$v$ ( $m^2/s$ )	1.02E-06

$\rho_w$ ( $kg.m^{-3}$ )	1000
$\rho_s$ ( $kg.m^{-3}$ )	2700
$g$ ( $m.s^{-2}$ )	9.8
$\rho_s^*$	1.7

d ( $\mu m$ )	$w_s$ ( $m.s^{-1}$ )	$\beta$ (deg)	$P_d$	$w_d^*$ eq	$w_d^*$ exp
550	0.067	24.9	0.406	0.648	0.642
462.5	0.056	23.6	0.376	0.672	0.680
390	0.047	24.6	0.399	0.904	0.907
327.5	0.038	25.2	0.413	1.182	1.179
275	0.030	23.1	0.363	1.178	1.178
		24.28			

E5

L/R	4
$u_b$ ( $m.s^{-1}$ )	0.4
$v$ ( $m^2/s$ )	1.02E-06

$\rho_w$ ( $kg.m^{-3}$ )	1000
$\rho_s$ ( $kg.m^{-3}$ )	2700
$g$ ( $m.s^{-2}$ )	9.8
$\rho_s^*$	1.7

d ( $\mu m$ )	$w_s$ ( $m.s^{-1}$ )	$\beta$ (deg)	$P_d$	$w_d^*$ eq	$w_d^*$ exp
550	0.067	19	0.232	0.478	0.473
462.5	0.056	19.7	0.258	0.659	0.663
390	0.047	19.2	0.240	0.718	0.713
327.5	0.038	18.8	0.224	0.807	0.808
275	0.030	17.8	0.182	0.775	0.780
		18.9			

## E6

L/R	4
$u_b$ (m.s <sup>-1</sup> )	0.4
$v$ (m <sup>2</sup> /s)	1.02E-06

$\rho_w$ (kg.m <sup>-3</sup> )	1000
$\rho_s$ (kg.m <sup>-3</sup> )	2700
$g$ (m.s <sup>-2</sup> )	9.8
$\rho_s^*$	1.7

d ( $\mu$ m)	$w_s$ (m.s <sup>-1</sup> )	$\beta$ (deg)	$P_d$	$w_d^*$ eq	$w_d^*$ exp
550	0.067	22.5	0.347	0.858	0.851
462.5	0.056	21.4	0.315	0.879	0.886
390	0.047	20.7	0.293	0.951	0.948
327.5	0.038	19.7	0.258	0.978	0.972
275	0.030	18.4	0.208	0.916	0.918
		20.54			

## G2b

L/R	4
$u_b$ (m.s <sup>-1</sup> )	0.26
$v$ (m <sup>2</sup> /s)	1.02E-06

$\rho_w$ (kg.m <sup>-3</sup> )	1000
$\rho_s$ (kg.m <sup>-3</sup> )	2700
$g$ (m.s <sup>-2</sup> )	9.8
$\rho_s^*$	1.7

d ( $\mu$ m)	$w_s$ (m.s <sup>-1</sup> )	$\beta$ (deg)	$P_d$	$w_d^*$ eq	$w_d^*$ exp
550	0.066	21.2	0.309	0.472	0.474
462.5	0.055	24	0.385	0.809	0.807
390	0.046	23.3	0.368	0.903	0.905
327.5	0.037	23.1	0.363	1.089	1.083
275	0.029	21.2	0.309	1.058	1.051
		22.56			

## G4

L/R	4
$u_b$ (m.s <sup>-1</sup> )	0.58
$v$ (m <sup>2</sup> /s)	1.05E-06

$\rho_w$ (kg.m <sup>-3</sup> )	1000
$\rho_s$ (kg.m <sup>-3</sup> )	2700
$g$ (m.s <sup>-2</sup> )	9.8
$\rho_s^*$	1.7

d ( $\mu$ m)	$w_s$ (m.s <sup>-1</sup> )	$\beta$ (deg)	$P_d$	$w_d^*$ eq	$w_d^*$ exp
550	0.066	17.6	0.173	0.483	0.477
462.5	0.055	17.9	0.187	0.634	0.640
390	0.046	17.5	0.169	0.676	0.685
327.5	0.037	17.1	0.150	0.723	0.715
275	0.029	16.6	0.125	0.734	0.727
		17.34			

## G1

L/R	4
$u_b$ (m.s <sup>-1</sup> )	0.33
$v$ (m <sup>2</sup> /s)	1.1E-06

$\rho_w$ (kg.m <sup>-3</sup> )	1000
$\rho_s$ (kg.m <sup>-3</sup> )	2700
$g$ (m.s <sup>-2</sup> )	9.8
$\rho_s^*$	1.7

d ( $\mu$ m)	$w_s$ (m.s <sup>-1</sup> )	$\beta$ (deg)	$P_d$	$w_d^*$ eq	$w_d^*$ exp
550	0.066	22.9	0.358	0.756	0.755
462.5	0.055	21.9	0.330	0.793	0.800
390	0.046	23.7	0.378	1.201	1.192
327.5	0.037	21.2	0.309	1.069	1.078
275	0.029	19.5	0.251	0.997	0.996
		21.84			

## G3

L/R	4
$u_b$ (m.s <sup>-1</sup> )	0.23
$v$ (m <sup>2</sup> /s)	1.05E-06

$\rho_w$ (kg.m <sup>-3</sup> )	1000
$\rho_s$ (kg.m <sup>-3</sup> )	2700
$g$ (m.s <sup>-2</sup> )	9.8
$\rho_s^*$	1.7

d ( $\mu$ m)	$w_s$ (m.s <sup>-1</sup> )	$\beta$ (deg)	$P_d$	$w_d^*$ eq	$w_d^*$ exp
550	0.066	26	0.430	0.731	0.730
462.5	0.055	26.6	0.442	0.922	0.921
390	0.046	25.6	0.421	1.018	1.019
327.5	0.037	26.3	0.436	1.340	1.342
275	0.029	23.4	0.371	1.253	1.254
		25.58			

## G5

L/R	4
$u_b$ (m.s <sup>-1</sup> )	0.53
$v$ (m <sup>2</sup> /s)	1.01E-06

$\rho_w$ (kg.m <sup>-3</sup> )	1000
$\rho_s$ (kg.m <sup>-3</sup> )	2700
$g$ (m.s <sup>-2</sup> )	9.8
$\rho_s^*$	1.7

d ( $\mu$ m)	$w_s$ (m.s <sup>-1</sup> )	$\beta$ (deg)	$P_d$	$w_d^*$ eq	$w_d^*$ exp
550	0.066	18	0.191	0.499	0.505
462.5	0.055	18.8	0.224	0.734	0.723
390	0.046	18.3	0.204	0.783	0.772
327.5	0.037	17.75	0.180	0.826	0.821
275	0.029	17.3	0.159	0.894	0.883
		18.03			

Appendix 5.2: percentage of error between the experimental results and equation [5.27] for experiments with LA-260 and B3-100 sand

The percentage of error e is defined as  $e = \frac{2 \cdot (w_{dexp} - w_{dcalc})}{(w_{dexp} + w_{dcalc})} \cdot 100$

LA-260		Experimental $w_d$														
$d_m$ (mm)	d*	D3	D4	D5	D6	E2	E3b	E4	E5	E6	G1	G2b	G3	G4	G5	
275	7.0236	0.0343	0.0401	0.0287	0.0266	0.0305	0.0338	0.0362	0.0239	0.0281	0.0293	0.0323	0.0379	0.022	0.0272	
231	5.8998	0.0248	0.0276	0.0236	0.0214	0.0228	0.0252	0.0274	0.0194	0.0229	0.0234	0.0256	0.0281	0.0189	0.0231	
181	4.6228	0.0165	0.0166	0.017	0.0161	0.0169	0.0185	0.02	0.0147	0.0174	0.0188	0.0175	0.0208	0.0188	0.0196	
106.5	2.72	0.0055	0.0063	0.0075	0.0092	0.0101	0.0101	0.0095	0.0071	0.0093	0.0095	0.0081	0.0112	0.0069	0.0088	

LA-260		model $w_d$ (equation [5.27])														
$d_m$ (mm)	d*	D3	D4	D5	D6	E2	E3b	E4	E5	E6	G1	G2b	G3	G4	G5	
275	7.0236	0.0329	0.0335	0.0306	0.0282	0.0292	0.0333	0.0357	0.0271	0.032	0.0287	0.0306	0.03	0.0223	0.0281	
231	5.8998	0.0258	0.0262	0.024	0.0222	0.0174	0.0229	0.0261	0.0279	0.0214	0.0258	0.0164	0.0225	0.0239	0.0233	
181	4.6228	0.0182	0.0185	0.0171	0.0158	0.0119	0.0162	0.0185	0.0197	0.0153	0.0191	0.0112	0.016	0.0169	0.0163	
106.5	2.72	0.0086	0.0086	0.0081	0.0076	0.0051	0.0077	0.0087	0.0092	0.0074	0.0101	0.0047	0.0075	0.0079	0.0074	

LA-260		error e														
$d_m$ (mm)		D3	D4	D5	D6	E2	E3b	E4	E5	E6	G1	G2b	G3	G4	G5	avg(exp)
275		4	18	7	6	4	1	1	12	13	2	6	23	2	3	7
231		4	5	2	4	27	10	5	36	7	10	44	22	23	1	14
181		10	11	1	2	35	13	8	29	13	1	44	26	10	18	16
106.5		44	31	8	19	67	27	8	26	23	6	53	39	14	17	27
avg		15	16	4	8	33	13	6	26	14	5	36	28	12	10	16

B3-100		Experimental $w_d$				
$d_m$ (mm)	run	D7	E7	G6	G7	
275		0.0248	0.0177		0.0186	
231		0.0202	0.0156	0.0175	0.018	
196		0.0138	0.0118	0.0124	0.0148	
165		0.0093	0.0087	0.0086	0.0107	
137.5		0.0064	0.0066	0.0063	0.0081	
115.5		0.0051	0.0051	0.005	0.0058	
98		0.0037	0.0036	0.0037	0.0043	
82.5		0.0027	0.0028	0.0029	0.003	
69		0.0021	0.0022	0.0024	0.0024	
58		0.0015	0.0015		0.0018	
49		0.0012	0.0014		0.0013	
41.5		0.0007	0.0009		0.0008	

B3-100		model $w_d$ (equation [5.27])				
$d_m$ (mm)	d*	D7	E7	G6	G7	
275	7.0236	0.0228	0.0215		0.0226	
231	5.8998	0.0174	0.0164	0.0137	0.0172	
196	5.0059	0.0135	0.0127	0.0106	0.0133	
165	4.2141	0.0103	0.0097	0.008	0.0102	
137.5	3.5118	0.0077	0.0072	0.006	0.0076	
115.5	2.9499	0.0058	0.0054	0.0045	0.0057	
98	2.5029	0.0044	0.0041	0.0034	0.0043	
82.5	2.1071	0.0033	0.0031	0.0025	0.0032	
69	1.7623	0.0024	0.0022	0.0018	0.0023	
58	1.4813	0.0018	0.0016		0.0017	
49	1.2515	0.0013	0.0012		0.0012	
41.5	1.0599	0.0009	0.0009		0.0009	

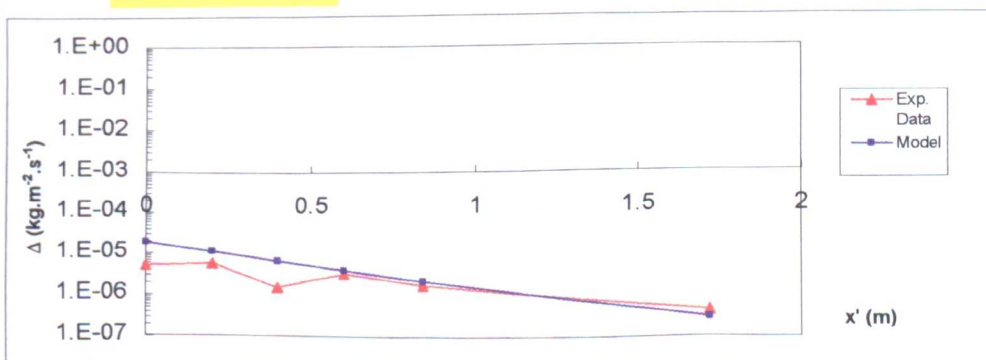
B3-100		error e				
$d_m$ (mm)		D7	E7	G6	G7	avg(exp)
275		8	19		19	16
231		15	5	24	4	12
196		2	8	16	10	9
165		10	11	7	5	8
137.5		19	10	6	7	10
115.5		12	6	12	1	8
98		18	13	10	1	10
82.5		19	8	14	6	12
69		16	1	25	3	11
58		18	10		3	11
49		6	16		7	10
41.5		27	1		7	12
avg		14	9	14	6	11

	A	B	C	D	E	F	G	H	I	
1	Appendix 6: longitudinal distribution of D for a line source: evaluation of ( $r_i$ ) for experiment D3									
2										
3	$u^*$ (m.s <sup>-1</sup> )	0.08		$d_m$ ( $\mu$ m)	$C_{bo}^i$ (g.l <sup>-1</sup> )			X (m)	1.72	
4	$\rho_w$ (kg.m <sup>-3</sup> )	1000		550	0.000184			$\Delta$	0.00090057	
5	$\rho_s$ (kg.m <sup>-3</sup> )	2700		462.5	0.000158			$\Delta$	0.00144441	
6	$v$	1.00E-06		390	0.001969			$\Delta$	0.00133733	
7	$g$ (m.s <sup>-2</sup> )	9.8		327.5	0.013651			$\Delta$	0.00135454	
8	$Q$ (m <sup>3</sup> .s <sup>-1</sup> )	0.041		275	0.095294			$\Delta$	0.00135168	
9	$q$ (m <sup>2</sup> .s <sup>-1</sup> )	0.053		231	0.179824			$\Delta$	0.00135215	
10				181	0.108551			$\Delta$	0.00135207	
11								$\Delta$	0.00135208	
12										
13										
14										
15	$d^i$ (mic)	550	462.5	390	327.5	275	231	181	Overall	
16	$d^{*i}$	14.05	11.81	9.96	8.36	7.02	5.90	4.62		
17	$w_s^i$ (m.s <sup>-1</sup> )	0.068	0.057	0.048	0.039	0.031	0.024	0.017		
18	$l^i$ (m)	0.783	0.932	1.121	1.375	1.716	2.178	3.130		
19	$x'$ (m)	0							Cb	
20	$C_{bo}^i$ (g.l <sup>-1</sup> )	0.00018	0.00016	0.00197	0.01365	0.09529	0.17982	0.10855	0.39962899	
21	$\chi_o^i$	0.00046	0.00039	0.00493	0.03416	0.23845	0.44998	0.27163		
22	$\chi_o^i d^i$ (mic)	0.25	0.18	1.92	11.19	65.58	103.94	49.16		
23	$d_{50}^o$ (mic)								232.23	
24	$d_{50}^{*o}$								5.93	
25	$w_{s0}$ (m.s <sup>-1</sup> )								0.0246	
26	$\phi_o$	0.0343	0.0343	0.0343	0.0343	0.0343	0.0343	0.0343		
27	$w_{d0}^i$ (m.s <sup>-1</sup> )	0.1069	0.0826	0.0641	0.0494	0.0382	0.0295	0.0206	$\Delta$	
28	$\Delta_o^i$ (kg.m <sup>-2</sup> .s)	0.000020	0.000013	0.000126	0.000675	0.003636	0.005301	0.002232	0.01200239	
29	$x'$ (m)	1.72							Cb	
30	$C_b^i$ (g.l <sup>-1</sup> )	2.068E-06	4.916E-06	0.00003	0.00035	0.00495	0.01663	0.02063	0.04259861	
31	$\chi^i$	0.00005	0.00012	0.00074	0.00814	0.11613	0.39050	0.48432		
32	$\chi^i d^i$ (mic)	0.03	0.05	0.29	2.67	31.94	90.21	87.66		
33	$d_{50}$ (mic)								212.84	
34	$d_{50}^{*}$								5.44	
35	$w_s$ (m.s <sup>-1</sup> )								0.0217	
36	$\phi$	0.0127	0.0127	0.0127	0.0127	0.0127	0.0127	0.0127		
37	$w_d^i$ (m.s <sup>-1</sup> )	0.0957	0.0729	0.0556	0.0420	0.0317	0.0239	0.0160	$\Delta$	
38	$\Delta^i$ (kg.m <sup>-2</sup> .s)	1.980E-07	3.581E-07	0.000002	0.000015	0.000157	0.000397	0.000329	0.00090057	
39	$C_b^i$ (g.l <sup>-1</sup> )	3.298E-06	7.389E-06	0.00005	0.00060	0.00815	0.02614	0.02989	0.06484025	
40	$\chi^i$	0.00005	0.00011	0.00084	0.00926	0.12564	0.40308	0.46102		
41	$\chi^i d^i$ (mic)	0.03	0.05	0.33	3.03	34.55	93.11	83.44		
42	$d_{50}$ (mic)								214.55	
43	$d_{50}^{*}$								5.48	
44	$w_s$ (m.s <sup>-1</sup> )								0.0220	
45	$\phi$	0.0151	0.0151	0.0151	0.0151	0.0151	0.0151	0.0151		
46	$w_d^i$ (m.s <sup>-1</sup> )	0.0976	0.0745	0.0570	0.0433	0.0328	0.0248	0.0167	$\Delta$	
47	$\Delta^i$ (kg.m <sup>-2</sup> .s)	3.220E-07	5.504E-07	0.000003	0.000026	0.000267	0.000648	0.000499	0.00144441	
48	$C_b^i$ (g.l <sup>-1</sup> )	3.046E-06	6.897E-06	0.00005	0.00055	0.00750	0.02428	0.02817	0.06055943	
49	$\chi^i$	0.00005	0.00011	0.00082	0.00905	0.12390	0.40092	0.46515		
50	$\chi^i d^i$ (mic)	0.03	0.05	0.32	2.96	34.07	92.61	84.19		
51	$d_{50}$ (mic)								214.24	
52	$d_{50}^{*}$								5.47	
53	$w_s$ (m.s <sup>-1</sup> )								0.0219	
54	$\phi$	0.0147	0.0147	0.0147	0.0147	0.0147	0.0147	0.0147		
55	$w_d^i$ (m.s <sup>-1</sup> )	0.0973	0.0742	0.0568	0.0431	0.0326	0.0246	0.0166	$\Delta$	
56	$\Delta^i$ (kg.m <sup>-2</sup> .s)	2.964E-07	5.119E-07	0.000003	0.000024	0.000245	0.000598	0.000467	0.00133733	

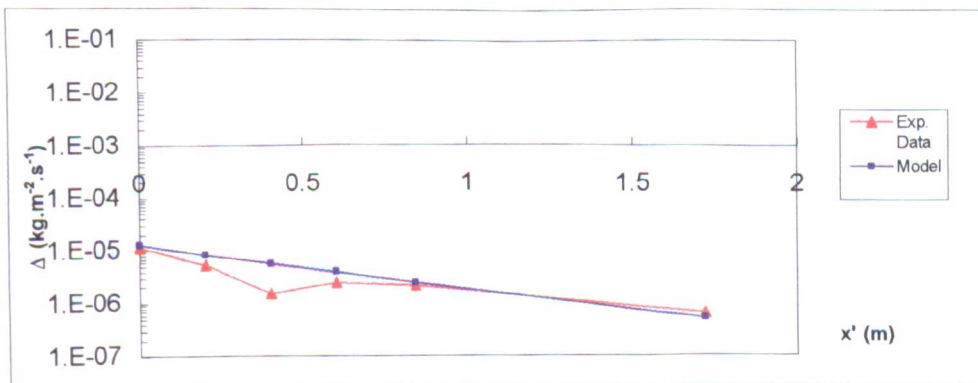
	A	B	C	D	E	F	G	H	I
57	$C_b^1$ (g.l <sup>-1</sup> )	3.086E-06	6.975E-06	0.00005	0.00056	0.00761	0.02458	0.02845	0.06125033
58	$\chi^1$	0.00005	0.00011	0.00082	0.00908	0.12419	0.40127	0.46447	214.29 5.47 0.0219
59	$\chi^{k,d^1}$ (mic)	0.03	0.05	0.32	2.97	34.15	92.69	84.07	
60	$d_{50}$ (mic)								
61	$d^*_{50}$								
62	$w_s$ (m.s <sup>-1</sup> )								
63	$\phi$	0.0148	0.0148	0.0148	0.0148	0.0148	0.0148	0.0148	
64	$w_d^1$ (m.s <sup>-1</sup> )	0.0974	0.0743	0.0568	0.0431	0.0326	0.0247	0.0166	Δ
65	$\Delta^1$ (kg.m <sup>-2</sup> .s)	3.005E-07	5.181E-07	0.000003	0.000024	0.000248	0.000606	0.000472	0.00135454
66	$C_b^1$ (g.l <sup>-1</sup> )	3.079E-06	6.962E-06	0.00005	0.00055	0.00759	0.02453	0.02840	0.06113544
67	$\chi^1$	0.00005	0.00011	0.00082	0.00908	0.12414	0.40121	0.46458	214.28 5.47 0.0219
68	$\chi^{k,d^1}$ (mic)	0.03	0.05	0.32	2.97	34.14	92.68	84.09	
69	$d_{50}$ (mic)								
70	$d^*_{50}$								
71	$w_s$ (m.s <sup>-1</sup> )								
72	$\phi$	0.0147	0.0147	0.0147	0.0147	0.0147	0.0147	0.0147	
73	$w_d^1$ (m.s <sup>-1</sup> )	0.0974	0.0743	0.0568	0.0431	0.0326	0.0247	0.0166	Δ
74	$\Delta^1$ (kg.m <sup>-2</sup> .s)	2.998E-07	5.171E-07	0.000003	0.000024	0.000248	0.000605	0.000471	0.00135168
75	$C_b^1$ (g.l <sup>-1</sup> )	3.081E-06	6.964E-06	0.00005	0.00056	0.00759	0.02454	0.02841	0.06115445
76	$\chi^1$	0.00005	0.00011	0.00082	0.00908	0.12415	0.40122	0.46456	214.28 5.47 0.0219
77	$\chi^{k,d^1}$ (mic)	0.03	0.05	0.32	2.97	34.14	92.68	84.09	
78	$d_{50}$ (mic)								
79	$d^*_{50}$								
80	$w_s$ (m.s <sup>-1</sup> )								
81	$\phi$	0.0147	0.0147	0.0147	0.0147	0.0147	0.0147	0.0147	
82	$w_d^1$ (m.s <sup>-1</sup> )	0.0974	0.0743	0.0568	0.0431	0.0326	0.0247	0.0166	Δ
83	$\Delta^1$ (kg.m <sup>-2</sup> .s)	2.999E-07	5.172E-07	0.000003	0.000024	0.000248	0.000605	0.000472	0.00135215
84	$C_b^1$ (g.l <sup>-1</sup> )	3.080E-06	6.964E-06	0.00005	0.00056	0.00759	0.02454	0.02841	0.0611513
85	$\chi^1$	0.00005	0.00011	0.00082	0.00908	0.12415	0.40122	0.46457	214.28 5.47 0.0219
86	$\chi^{k,d^1}$ (mic)	0.03	0.05	0.32	2.97	34.14	92.68	84.09	
87	$d_{50}$ (mic)								
88	$d^*_{50}$								
89	$w_s$ (m.s <sup>-1</sup> )								
90	$\phi$	0.0147	0.0147	0.0147	0.0147	0.0147	0.0147	0.0147	
91	$w_d^1$ (m.s <sup>-1</sup> )	0.0974	0.0743	0.0568	0.0431	0.0326	0.0247	0.0166	Δ
92	$\Delta^1$ (kg.m <sup>-2</sup> .s)	2.999E-07	5.172E-07	0.000003	0.000024	0.000248	0.000605	0.000472	0.00135207
93	$C_b^1$ (g.l <sup>-1</sup> )	3.080E-06	6.964E-06	0.00005	0.00056	0.00759	0.02454	0.02841	0.06115182
94	$\chi^1$	0.00005	0.00011	0.00082	0.00908	0.12415	0.40122	0.46457	214.28 5.47 0.0219
95	$\chi^{k,d^1}$ (mic)	0.03	0.05	0.32	2.97	34.14	92.68	84.09	
96	$d_{50}$ (mic)								
97	$d^*_{50}$								
98	$w_s$ (m.s <sup>-1</sup> )								
99	$\phi$	0.0147	0.0147	0.0147	0.0147	0.0147	0.0147	0.0147	
100	$w_d^1$ (m.s <sup>-1</sup> )	0.0974	0.0743	0.0568	0.0431	0.0326	0.0247	0.0166	Δ
101	$\Delta^1$ (kg.m <sup>-2</sup> .s)	2.999E-07	5.172E-07	0.000003	0.000024	0.000248	0.000605	0.000472	0.00135208
102									
103									
104									
105									
106									
107									
108									
109									
110									
111									
112									

	A	B	C	D	E	F	G	H	I
113	$\Delta_{exp}$	0	0.2	0.4	0.6	0.84	1.72		
114	550	0.000005	0.000006	0.000002	0.000003	0.000002	4.32E-07		
115	462.5	0.000012	0.000006	0.000002	0.000002	0.000002	0.000001		
116	390	0.000150	0.000065	0.000032	0.000025	0.000012	0.000004		
117	327.5	0.000730	0.000370	0.000187	0.000165	0.000098	0.000028		
118	275	0.004019	0.002565	0.001435	0.001320	0.000864	0.000246		
119	231	0.004798	0.003823	0.002297	0.002277	0.001649	0.000594		
120	181	0.001990	0.001802	0.001112	0.001205	0.000968	0.000496		
121	$\Delta_{model}$	0	0.2	0.4	0.6	0.84	1.72		
122	550	0.000020	0.000012	0.000007	0.000004	0.000002	3.00E-07		
123	462.5	0.000013	0.000009	0.000006	0.000004	0.000002	0.000001		
124	390	0.000126	0.000077	0.000048	0.000030	0.000018	0.000003		
125	327.5	0.000675	0.000435	0.000286	0.000190	0.000119	0.000024		
126	275	0.003636	0.002540	0.001802	0.001296	0.000886	0.000248		
127	231	0.005301	0.003946	0.002979	0.002278	0.001675	0.000605		
128	181	0.002232	0.001795	0.001462	0.001204	0.000965	0.000472		

$\Gamma_{550}$  1.3



$\Gamma_{462.5}$  1.3



$\Gamma_{390}$  2

